ISSN 1849-0751 (On-line)
ISSN 0013-7448 (Print)
UDK 621.31

Journal of Energy

VOLUME 62 Number 1–4 | 2013 Special Issue

ENERGIJA

Journal of Energy

Scientific Professional Journal Of Energy, Electricity, Power Systems

Online ISSN 1849–0751, Print ISSN 0013–7448, VOL 62

Published by

HEP d.d., Ulica grada Vukovara 37, HR–10000 Zagreb

HRO CIGRÉ, Berislavićeva 6, HR–10000 Zagreb

INTRODUCTION

Journal of Energy special issue: Papers from 9th International Conference of the Croatian Nuclear Society "Nuclear Option in Countries with Small and Medium Electricity Grids"

Welcome to this special issue, which is based on selected papers presented at the 9th International Conference of the Croatian Nuclear Society "Nuclear Option in Countries with Small and Medium Electricity Grids", held in Zadar, Croatia, on June 3rd–6th, 2012.

The International Conference was organized by the Croatian Nuclear Society in cooperation with International Atomic Energy Agency (IAEA), Croatian State Office for Nuclear Safety and University of Zagreb, Faculty of Electrical Engineering and Computing. The goal of the Conference was to address the various aspects of the implementation of nuclear energy in the countries with small and medium electricity grids and in power system in general. The conference also focuses on the exchange of experience and co-operation in the fields of the plant operation, nuclear fuel cycle, nuclear safety, radioactive waste management, regulatory practice, liability, and insurance for nuclear damage and environment protection.

The conference was organized in ten oral sessions and one poster session. In three Conference days authors presented 42 papers orally and 11 papers in poster session. 110 participants came from 11 countries representing equipment manufacturers and utilities, universities and research centres, and international and government institutions. Seven invited lectures were held and 53 papers were accepted by international programme committee.

The Conference topics reflect some current emphasis, such as country energy needs, new reactor technologies (especially small reactors), operation and safety of the current nuclear power plants, move of the focus in nuclear safety toward severe accidents and accident management strategies, improvement in nuclear safety, reactor physics and radiation shielding calculation tools and ever increasing requirements for minimization of environmental impact. Impact of Fukushima accident on future of nuclear power and lessons learned from the accident are explicitly covered.

From 53 papers presented at the Conference, 18 papers were accepted for publication in this number of Journal of Energy after having undergone the additional peer–review process. We would like to thank the authors for their contributions and the reviewers who dedicated their valuable time in selecting and reviewing these papers, both during the Conference and during the preparation of this special issue of Journal of Energy. As usual, it was very challenging to collect a balanced overview of the entire Conference. We believe that the papers which were selected for this issue represent some of the best research related to nuclear plant operation, energy planning, development of new reactors and technologies, reactor physics, and radiation shielding. We hope this special issue will provide a valuable insight into different aspects of nuclear and electrical engineering, reactor physics, and nuclear power plants operation, as well as a pleasant and inspiring reading.

Guest Editors

Dubravko Pevec

Davor Grgić

University of Zagreb, Croatia

Journal of Energy
VOLUME 62 Number 1–4 | 2013 Special Issue
journal homepage: http://journalofenergy.com/

Future without Nuclear Energy; is it Feasible, is it Sensible?

Vladimir Knapp, Dubravko Pevec
Faculty of electrical engineering and computing, University of Zagreb
Unska 3, 10000 Zagreb, Croatia
vladimir.knapp@fer.hr, dubravko.pevec@fer.hr

ABSTRACT

Considering the necessity and future role of nuclear energy as relevant to the climate problem, we have focused on the period to the year 2065. For quantification of the required emission reduction we have used IEA WEO 2009 and WEO 2011 data as presented in their Reference strategies predicting emissions with business as usual practices, and WEO 450 Energy strategies which show the time development of allowed emissions consistent with a limit on the global temperature increase of 2 ºC and the peak CO_2 concentration of 450 ppm. By extrapolating these data to the year 2065 we obtain 77.4 GtCO2-eq for Reference emission and 10 GtCO2-eq for WEO 450 strategy allowing emission, resulting in 67.4 GtCO2-eq reduction required to come down to sustainable WEO 450 trajectory. The large contributions to emission reduction from fusion energy and fossil fuel with carbon separation and storage are not likely. Main carbon non-emitting sources assumed in the years up to 2065 are proven technology nuclear fission and renewable sources. In our specified strategy aimed to achieve WEO 450 target we assumed an energy mix including nuclear power build-up in the period 2025-2065 to the level of 3300 GW in 2065. With the resulting nuclear contribution of 25.2 GtCO2 to the total required emission reduction of 67.4 GtCO2, what remains for renewable sources, energy saving and increased efficiency of energy use to contribute are prodigious 42.2 GtCO2-eq. Assuming that energy saving and more efficient energy use will by 2065 effect an annual reduction between 10 to 16 GtCO2-eq, remaining 26.2 to 32.2 GtCO2, respectively 27290 and 33540 TWh would be the task for renewable energy sources. Our estimates about contribution of renewable sources going as far as 2065 are based on EREC prediction for EU and on our extension to world total with EREC and GWEC prediction as a guide. Our high, but still credible estimates of predicted world renewable energy contribution by 2065 come to the similar figures between 29260 and 36180 TWh. However, without nuclear contribution in 2065, renewable energy contribution would have to be doubled, practically impossible task in the time period in consideration. Resulting contributions by renewable sources, probably their upper limits, allow some conclusions about the role of nuclear energy in future decades. By combining highest contributions from energy saving, efficiency increase and other measures to reduce emission, apart from energy production, with highest prediction for renewable sources contribution, we obtain the minimum nuclear energy requirement of about 2190 GW in 2065. This minimum nuclear strategy should be planned and prepared for, unless there is strong evidence that other carbon free energy sources (CCS or fusion) could be developed in time. Expansion of nuclear power by about 1800 GW by 2065 would come from different and already developed industrial sector, which can give its contribution to the energy mix, without obstructing the build-up of renewable sources. It would not be wise to forfeit nuclear contribution at least in the period to 2065, critical for the control of climate change.

1 INTRODUCTION

The future of nuclear energy will be essentially determined by its role in reduction of carbon emission and prevention of associated unacceptable climate changes. In trying to assess the role of nuclear energy in resolving the carbon emission problem we focus on the several next decades when the choice of carbon free energy sources will not include large scale energy production by nuclear fusion or coal power plants with carbon capture and storage (CCS). Starting with generally accepted recommendations by IPCC about carbon emission reductions, the question about the future of nuclear (fission) energy is really the question whether required emission reduction in the next decades can be achieved with renewable sources alone, or the contribution from nuclear power must also be included. First step towards the answer is to quantify the emission reduction target. Present consensus is that global temperature increase be limited to 2 degrees Celsius. This limit was adopted in Copenhagen Accord [1] and in EU energy strategy [2]. Global endorsement reflecting IPCC recommendations was given at the UN climate change conference in Cancun in December 2010 [3, 4]. In order to obtain a quantitative guidance on the carbon emission reduction required to keep global temperature increase below 2 ºC we use the WEO 2009 and subsequent WEO 2011 energy strategy designed to achieve this target by limiting the increase of greenhouse-gases (GHG) concentration below 450 parts per million of CO2-eq. That strategy was presented in the International Energy Agency annual report in 2009, WEO 2009 [5] as WEO 2009 450 Energy Strategy, and further elaborated in WEO 2011[6]. According to the IEA WEO 2011 Reference Scenario, by continuing present trends, global anthropogenic GHG emission from all sectors of human activity would reach 56.5 GtCO2-eq by 2020 and 64.4 GtCO2-eq by 2035, increasing from 47.1 GtCO2-eq in 2009. Continuation of this trend would increase long-term CO2-eq concentration in excess of 1000 ppm and increase average temperature by up to 6 ºC, leading almost certainly to the irreparable damage to the planet. The environmentally sustainable WEO 2011 450 Energy Strategy, in line with the Copenhagen Accord and EU energy policy, aims to stabilize concentration at 450 ppm and limit temperature increase to 2 ºC. In WEO 2009 and later in WEO 2011, strong arguments are presented for this scenario. According to WEO 2009 450 scenario the estimated allowed limits on total GHG emission in 2030 and 2050 would be 37.1 and 21 GtCO2-eq respectively, whilst consistent figures in WEO 2011 450 strategy are 47.1 GtCO2-eq for 2020 and 32.6 for 2035. They are lower than Reference scenario in 2035 by 31.8 GtCO2-eq and in 2050 by as much as 50.4 GtCO2-eq. The time scale appears to be too short for several carbon non-emitting technologies. The CCS technology is in the development stage for future applications, which will have to grow from the present experimental level of million tons per year to the scale of billion tons per year. Many hundreds or even thousands of safe non-leakage storage locations would be required. The future success of applications on such a scale cannot be taken for granted, at least not in next few decades. It could be many years before more definite predictions become possible. No solution can be seen in nuclear fusion, either. Even should the tokamak concept of nuclear fusion develop successfully physically and commercially, which is by no means certain, a significant contribution by nuclear fusion to the world energy production cannot be expected before 2065. This is evident from the dynamics of ITER and the follow-up projects (DEMO) before the first commercial plants could be constructed [7, 8]. Plasma ignition may be achieved at the laser fusion National Ignition Facility of Lawrence Livermore National Laboratory (LLNL) this year or very soon, or in France at Megajoule facility, but the technological problems on the road to commercial power are so formidable that the predictions about energy production cannot be more optimistic [9,10]. As for the solar energy in spite of its large physical potential, it is less ready for large-scale deployment than wind energy. Some authors estimate two or three decades as a time needed to achieve economic competitiveness [11]. However, even when renewable sources of energy, such as wind and solar, become technically and economically ready for large-scale deployment, their intermittent nature of energy production would limit their share in total energy production, barring the development of energy storage at an acceptable cost, not in sight at present. Heat storage can resolve day-night cycle for concentrated solar energy installations in sunny periods, but not in

winter or for several cloudy days. Very large grids connecting wind and solar installations would smooth the variations, but would also remove independence on big systems, perceived as one advantage of renewable energy. Energy field is in transition and the picture depends on how far in the future we look. We have to understand that the rate of change in the field of energy differs from that of, say, communication gadgets which become obsolete in a year. Big energy installations take years to build and operate for decades. Change of energy technology is correspondingly slow process. We consider the period up to the year 2065, critical from the climate point of view, during which large contributions from CCS and fusion are not likely, while a large build-up of nuclear fission energy could be accomplished. In this period substantial contribution is expected from wind and solar energy, although still with economic limitations. Another important point to note is, if the aim is to reduce carbon emissions, as required by 2 ºC increase limit, build-up of carbon free sources should be as fast as possible. Nuclear fission, as developed energy source, can take the main burden while other non-carbon sources are not yet available on a large scale. The selected year 2065 is a present judgment, a compromise between what is desirable and what seems technically feasible, regardless of current limited nuclear plans and present levels of renewable energy sources. Reduced nuclear strategies that would reach a high nuclear share later, by 2080 or as late as 2100, would, of course, provide more time for the development of the technical and political prerequisites for nuclear build-up, but their contribution to the urgent problem of CO_2 emission would be diminished or too late, if we take the IPCC recommendations seriously. The next few years will tell us whether we can afford delays. Climatologists are warning us that we cannot [12, 3, 4]. Optimists generally believe that future is uncertain and that black climate change forecasts are still inadequately researched and even disputed. On the other hand, should the climate situation develop in an alarming way, demanding urgent measures and an earlier contribution of carbon-free energy, the final year of nuclear build-up could be moved back to about the year 2060, or even earlier. It would mean a correspondingly greater challenge to international nuclear industry.

In order to be able to gain some quantitative insight about the necessity and potential of nuclear contribution for achievement of emission reduction in accordance with WEO 2011 450 Energy strategy, we base our discussion on the energy strategy which achieves this aim with an energy production mix inclusive nuclear power [13, 14, 15]. Nuclear share in the mix is determined as a maximum attainable with established light-water nuclear technology, under constraints of consuming presently (2008) estimated uranium resources by 2065, and by abstaining from reprocessing of spent fuel and from introduction of fast breeders at least until that year. These technology and safety constrains on nuclear power are chosen having in mind the political problems associated with nuclear power and nuclear fuel cycle and with the need for public acceptance of nuclear contribution. The point of this exercise was not to propose this particular nuclear strategy, but to see whether under these constraints, which respect public concerns about nuclear technology, nuclear power can still give a substantial reduction of carbon emission. Postponement of fuel reprocessing and plutonium use at least until 2060 would offer the time for development of political institutions and efficient international control measures to prevent nuclear proliferation. As witnessed by Fukushima events, even the technologies with many years of experience can surprise, therefore postponement of introduction of breeder reactors or other not sufficiently proven technologies is advisable, in the interest of nuclear industry and would respond to general public attitude towards nuclear energy.

2 EMISSION REDUCTION TARGETS

The ‘‘Business-as-Usual’’ WEO 2009 Reference Scenario gives the energy-related carbon emission of 40.2 GtCO2 for 2030, and anthropogenic GHG emission of 56.5 GtCO2-eq. The total anthropogenic GHG emission according to the WEO 2009 Reference Scenario in 2050 is 68.4 GtCO2-eq. WEO 2011 Business-as-Usual Reference scenario starts in 2009 with total anthropogenic emission amounting to 47.1 GtCO2-eq and runs few GtCO2 above the WEO 2009

Reference scenario. Predicted emissions for the years 2020 and 2035 are 56.5 and 64.4 GtCO2-eq, respectively. For the years 2050 and 2065, we extrapolate by following general trend and allowing for expected decrease of growth rate. Continuing on the increase of 7.9 GtCO2-eq in the period 2020 to 2035 with increases of 7 and 6 GtCO2-eq in the next two 15 years intervals we obtain 71.4 and 77.4 for the total anthropogenic emission in 2050, respectively in 2065. To obtain the WEO 450 emission limit for the year 2065 we could extrapolate from the WEO 2009 450 total allowed anthropogenic GHG emission of 21 GtCO2-eq in 2050 to the year 2065 continuing with the 2030/50 rate of decline, from 37.1 GtCO2-eq to 21 GtCO2-eq, into the 2050–2065 period. The extrapolated allowed anthropogenic GHG emission for 2065 would then come to 13.7 GtCO2-eq. However, with emission rate for early years in WEO 2011 being higher than predicted in WEO 2009, emissions in the later of WEO 2011 years 2050 should be lower than in WEO 2009 if the integral emission should remain the same. Difference demonstrates the effects of delay in carbon emission mitigation measures. Recent analysis by Meinshausen et al. [16] puts the integral CO2 emission limit to keep the probability of 2 ºC temperature rise below 0.25% at 1000 GtCO2 in the years 2000-2050, consistent with the earlier IPCC limit of 1800 GtCO2 for period 2000-2100 [17]. Any delay in reduction in early years must be compensated with sharper reduction in later years. So the revised values for WEO 450 trajectory for years 2050 and 2065 should be below 21 and 13.7 GtCO2 figures in WEO 2009, close to 19 and 10 GtCO2-eq, which we take as working assumptions. Resulting WEO Reference and WEO 450 trajectories are shown in figure 1. To reduce the emission from the Reference Scenario level of 77.4 GtCO2-eq to the WEO 450 Scenario level of 10 GtCO2-eq, an emission reduction of 67.4 GtCO2 in the year 2065 would be needed. This would be a reduction of 87%. Several countries have already adopted drastic emission cuts as the basis for their energy strategies, at least as a declaration of understanding what should be done. Great Britain is committed to 80% cuts by 2050 relative to 1990 emission.

3 NUCLEAR CONTRIBUTION IN AN ENERGY MIX SCENARIO

We use above considerations of required total reduction from WEO Reference scenario to WEO 450 Scenario to get some quantitative insight on the required non-nuclear contributions. As we determine maximum nuclear contribution under conditions specified below, non-nuclear contribution which follows would be a minimum required to reach WEO 450 requirements. Figure 1 presents two WEO scenarios, reference, “business as usual”, and WEO 450 up to the year 2065. Our specified “maximum” nuclear scenario with a build-up in the years 2025-2065 would reach 3300 GW by 2065. This level of nuclear power would be reached by linear nuclear power build-up starting in the year 2025 and proceeding until 2065. Rate of growth is obtained requiring that uranium resources as estimated in 2008 Red Book [18] be consumed by 2065.

Second constraint defining maximum nuclear strategy is postponing of spent fuel reprocessing, respectively introduction of fast breeders until 2065, at least. Under these constraints maximum linear nuclear growth compatible with prescribed constraints is a constant growth by 71.8 GW/year, and the resulting nuclear power of 3300 GW by 2065 is the maximum attainable under specified constraints. Linear growth was assumed as it gives larger emission reductions in earlier years than exponential growth. With determination and international effort such nuclear build-up could start by 2025. More discussion on that point can be found in [13]. This maximum nuclear contribution, not to be mixed with actual construction rate, serves to determine minimum non-nuclear contribution required to reach the total emission reduction of 67.4 GtCO2-eq by 2065. Lower nuclear growth would imply increased requirements on non-nuclear contributions to carbon emission reduction in order to come down from WEO Reference scenario to the WEO 450 Scenario. Nuclear carbon emission reduction in the year 2065 from operation of 3300 GW amounts to 25.2 GtCO2, assuming that nuclear power plant replace worst emitters, coal power plants. This would be 37.4% of required reduction, leaving remaining 42.2 GtCO2-eq , respectively 62.6% of total reduction required 67.4 GtCO2-eq, to be achieved by energy saving, increased efficiency of

energy use, forestry management, renewable energy sources, and a range of present and future methods and ways to cut carbon emission (Figure 1). Task is so enormous that no reasonable contribution should be neglected.

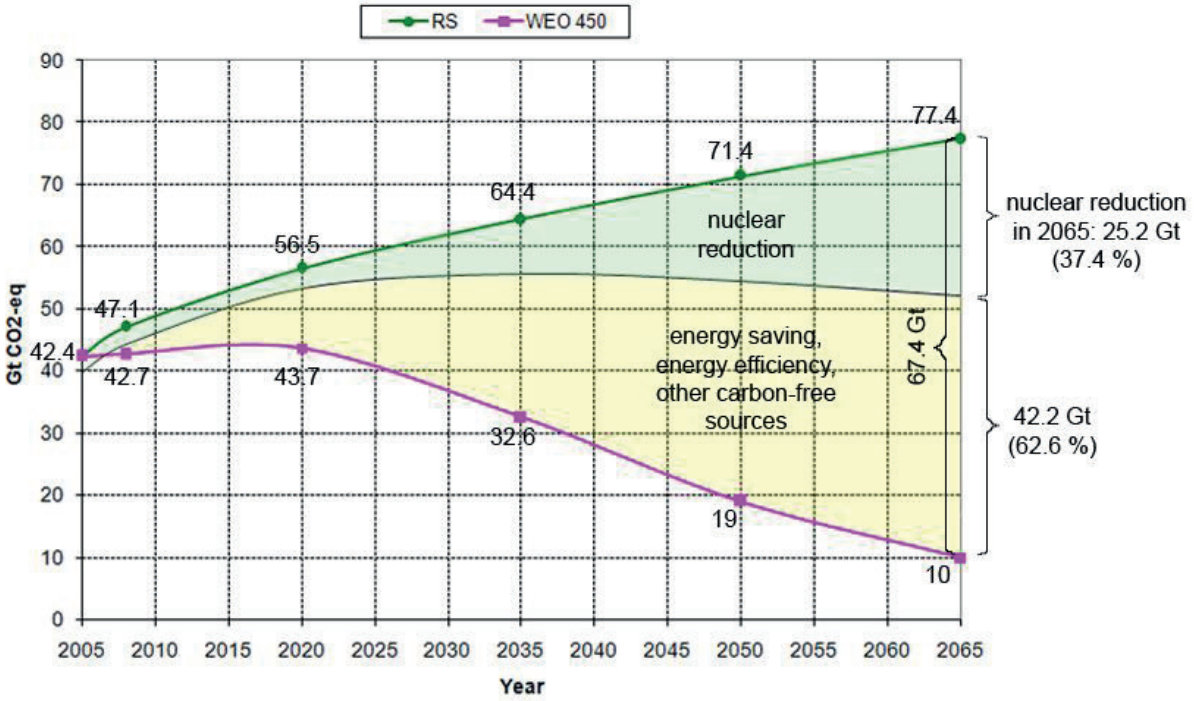

Figure 1: Emission reduction by linear nuclear build-up to 3300 GW in GtCO2-eq. The upper and bottom curve are the total anthropogenic emissions according the WEO 2011 Reference Scenario and the WEO 450 Scenario. The 2065 values were extrapolated from predictions for up to 2050 in WEO 2009 and WEO 2011.

Undoubtedly, with nuclear reduction greater than one-third, reduction of the remaining two thirds would be much easier to achieve. The question we aim to clarify is whether it is possible to forfeit or essentially decrease nuclear contribution and correspondingly increase burden on the non-nuclear sources. For that we have to compare required reductions with the predictions or extrapolations of non-nuclear sources growth. Year 2065 is too distant for a reliable predictions about relatively fast developing renewable sources and many methods of energy saving. Yet, if we want to have some bases for creating comprehensive long term energy strategy with a mix of energy sources we must make some estimates about all of them. Attempting this we face first a difficult problem of quantifying effects of increased efficiency of energy use and of reduced energy use. Progress in this direction is going to take place in all sectors of energy use, industry, housing, transport, in countless small steps and innovations impossible to predict. Many more creative minds are working now on the energy problems than in the past era of cheap energy without climate problem. At present we have to make a guess on how much emission reduction can be expected from improvement of energy efficiency, from energy saving, from reduced deforestation and many other measures, some unknown today, that can reduce carbon emission.

Without sufficient certainty about future development, we shall put our estimate into a wide range between 10 and 16 GtCO2-eq by 2065, respectively between 14.8 % and 23.7 % of the emission reduction required to come down from world anthropogenic emission in WEO Reference scenario to WEO 450 scenario in 2065. This range is supported by estimate for emission abatement by energy use efficiency and saving for the year 2035 as given in WEO 2011, figure 6.4. Emission reduction in 2035 amounts to about 6.4 GtCO2, respectively about 20% of the requirement for reaching WEO 450 trajectory from the anthropogenic emission WEO 2011 reference trajectory. As is recognized, efficiency and saving emission reductions are cost effective and expected to be introduced in early years, whilst new energy generating technologies are expected to dominate in later years. Both trends will act to reduce the share of energy efficiency and saving in emission

reductions in the years after 2035, probably well below 20%, consistent with our selected range for 2065. The required contribution from renewable sources would consequently have to be between 26.2 and 32.2 GtCO2/year in order to sum up to a total non-nuclear share of 42.2 GtCO2-eq.

4 PREDICTIONS OF WIND AND SOLAR ENERGY CONTRIBUTION FOR THE YEAR 2065

Assuming that renewable sources replace the coal power plants the required amounts of 26.2 to 32.2 GtCO2 of annual emission reduction can be expressed as the corresponding amount of renewable electricity, again assuming replacement of coal power plants, (we use figure of 0.96 kg CO_2/kWh for coal plants emission) from 27290 to 33540 TWh/year. These figures are the minimum required. When replacing gas power plants for a given amount of emissions more renewable power would be needed. With global average of wind energy conversion efficiency of 25%, which is probably overestimated, and with 15% for solar installations, we would come to the global average of about 20% for a system of about the same amount of wind and solar power. What will be the real ratio of these two main renewable sources contributions by 2065 depends on future developments, especially of solar materials. From our assumption of about equal contributions we obtain required installed power of these installations between 15500 GW to 19100 GW for 26.2 respectively 32.2 GtCO2 of required emission reduction. How this requirement compares with the predictions on the future developments of renewable sources? Predictions as far in future as 2065 do not exist, although 40 years is a not a long period compared with the working life of a large power station. One reason is that some technologies, such as solar, are still rapidly evolving.

4.1 Renewable sources in EU

For European Union there is a prediction of renewable energy sources (RES) growth prepared by European Renewable Energy Council (EREC) [19] which goes up to 2050. Global prediction for wind energy is given by Global Wind Energy Council up to 2050 [20]. The predictions of RES capacities by EREC up to the year 2050 and our linear extrapolation to the year 2065 are given in Table 1. The contributions of RES to electricity production given by EREC up to the year 2050 and our linear extrapolation to the year 2065 are presented in Table 2. Acronyms, PV and CSP, stand for Photovoltaics and Concentrated Solar Power in both tables, respectively.

Table 1 Predictions of renewable energy capacities (GW) by EREC in the "RE-thinking 2050", forecasts for European Union (2011) up to 2050 with our linear extension to 2065 (last column)

	2007	2020	2030	2050	2065
Wind	56	180	288.5	462	592
Hydro	102	120	148	194	228
PV	4.9	150	397	962	1386
Biomass	20.5	50	58	100	131
Geothermal	1.4	4	21.7	77	118
CSP	0.011	15	43.4	96	135
Ocean		2.5	8.6	65	107
Total RES-Capacity (GW)	185	521.5	965.2	1956	2697

Table 2 EREC: Contribution of renewable sources to electricity production (TWh) to 2050. Figures for 2065 are our linear extrapolation from the 2030-2050 period

	2007	2020	2030	2050	2065
Wind	104	477	833	1552	2091
Hydro	325	384	398	448	485
PV	5.4	180	556	1347	1940
Biomass	102	250	292	496	649
Geothermal	5.8	31	169	601	925
CSP	0.8	43	141	385	568
Ocean		5	18	158	263
Total RES Energy (TWh)	543	1370	2407	4987	6921

As our purpose is to judge the need for nuclear energy we include also the possibility of rapid growth of such renewable sources as wind and solar beyond 2050 up to 2065, in order to see whether in that case renewable energy could be sufficient. By extending EREC predictions exponentially the rapid growth from the period 2030-2050 up to the year 2065 (Table 3) we expect to obtain a very generous upper limit on the renewable energy production capacities in European Union for the year 2065.

Table 3 EREC predictions of total renewable energy capacities in EU until 2050 and exponential extrapolation to the year 2065, installed capacity in GW

Year	2020	2030	2050	2065
RES Capacities (GW)	521.5	965.2	1956	3000

First doubling occurs in 2020/30 period, in 10 years, second doubling in 2030/50 period in 20 years. Our estimate assumes continuing 2030/50 rate with doubling in 2050/70 period, so 3000 GW in 2065 is the result of exponential growth up to 2065. So we proceed with linear extrapolation of 2700 GW and with 3000 GW as the range for the upper limit of extension of EREC predictions for EU up to the year 2065.

4.2 Some technical limits on the wind energy potential in EU

Simple calculation [21] as well as examples of built wind farms (Whitelee wind farm, Scotland, 322 MW peak power on 55 square km, average power 2W/m^2, and London Array, offshore wind farm, 1 GW peak on 245 km^2, average power 1.5 W/m^2) show that, due to physical and technical criteria on a distance between windmills, average power on the wind farms is not above 2 W/m^2. Assuming that in densely populated European Union area about 10% of 4 500 000 km^2 area were covered with wind farms we obtain rough estimates of EU wind power potential. Building wind farms on some 450 000 km^2, i.e. on the 10% of total EU area, and with 2 W/m^2, i.e., $450 \cdot 10^9$ m^2 x 2 W/m^2, we would obtain average wind power of 900 GW. Required installed peak power would be about 3500 GW, at 25% efficiency, as for such mass construction efficiency value of best location cannot be assumed. It should be noted that this technical limit is much higher figure than EREC extrapolation for 2065 which is below 1000 GW of installed power. All the same, is it realistic to see wind power in EU as replacement for nuclear power in the period up to 2065?

Our global strategy assumed construction of 3300 GW of nuclear power by 2065 resulted in 37% reduction of carbon emission required to reach WEO 2009 450 strategy. At present with about 140 nuclear reactors in operation in EU, i.e. approximately one third of world number, one would expect that EU share in future global nuclear expansion be not less than one third. Clearly, in spite of present Fukushima conundrum, international solidarity would ask that main burden of nuclear development for carbon reduction falls on industrialized regions of the world; EU, US, and Far East regions which possess already developed nuclear industries. One would therefore expect from EU a share of at least 1100 GW of the global nuclear program of 3300 GW, on the level of present EU

share in global nuclear power. If we extrapolate exponentially EREC prediction of installed wind power for 2050 of 462 GW to 2065, resulting 900 GW peak would certainly not suffice to replace 1100 GW of nuclear power. With an average to peak power ratio of 25%, additional installed wind power would have to be some 4400 GW in order to replace 1100 GW of nuclear power, almost five times the EREC based (exponential) wind power prediction for 2065. It is also larger than the total wind power estimate for EU should wind farms cover 10% of EU area resulting in average power of about 900 GW and corresponding installed power about 3500 GW.

4.3 Global estimates of wind power

To obtain an idea on the upper limits of the wind power development for the world, we look at the Global Wind Energy Council and Greenpeace 2010 predictions given to the year 2050 [20]. WEC Survey of energy resources [22] does not give predictions for installed capacities in 2050 but discusses conditions which are important for wind power development. Highest prediction by GWEC-Greenpeace for the year 2050, designed as "advanced" variant, is 4.5 times above their "reference prediction" (880 GW), and amounts to 4000 GW of installed wind power. By extrapolating advanced variant with the 2% increase assumed before 2050, we obtain about 5400 GW of installed power in 2065. Even this highest prediction, with optimistic assumption on average energy conversion efficiency (25%), and corresponding annual production of about 14000 TWh, leaves a large space to be covered by other renewable energy sources in order to reach the required renewable energy carbon free energy production between 27290 and 33540 TWh remaining after contributions from 3300 GW of nuclear power and from the energy saving and increased efficiency of energy use, equivalent to 10 to 16 GtCO2-eq of emission reduction. It should be also noted that in case of very high expansion of wind power some material limitations may occur. One of these may be the scarcity of neodymium and dysprosium, rare earth elements needed in production of permanent magnets.

4.4 Solar contribution in EU and globally

According to EREC, again, solar photovoltaic (PV) and Concentrated Solar Power (CSP) installed in EU in 2050 would be some 1000 GW (peak) producing close to 2000 TWh of electricity. If, again, we assume doubling in the years from 2050 to 2070, we reach the figure of about 1500 GW peak in 2065 and the electricity production on the level of 3000 TWh. With capacity factor of 0.8 one GW of nuclear power produces 7 TWh per year, so 3000 TWh could be produced by 430 GW of nuclear power. To estimate the physical limits on solar power in EU we can again use the value for solar energy density for EU region. Taking average solar power per m^2 of 100 W, a figure for Britain which cannot be far from average for EU [21] and energy conversion efficiency of 15% for mass produced solar photovoltaic cells we get the average solar power of 15 W/m^2, much larger than the average wind power. With an area of 9000 m^2 per person in EU and with solar farms on the 10% of total area (which includes buildings, roads, water, arable land etc) we obtain average solar power per person in EU on the level of 15 W/m^2x900 m^2 = 13500 W, and energy production of 324 kWh per day per person. By transforming EU total energy consumption of 1800 Mtoe [23] into equivalent amount in kWh, we obtain the considerably smaller figure (115 kWh/day) for the average of primary energy consumption in 2010. Our physical limit on solar energy production would come to the high figure of about 59 000 TWh/year, while the total energy consumption in 2010 in EU amounted to 21 000 TWh. No doubt, even for relatively densely populated EU theoretical physical potential of solar energy is abundant enough to replace 1/3 of the nuclear reactors (EU share) from the global 3300 GW nuclear strategy shown in figure 1, i.e. 1100 GW which would produce about 8000 TWh/year. Thus, in order to judge what could be real contribution of solar energy in the years to 2065 we must look into economic and technical parameters which limit the production of solar energy. With installed solar power at the end of 2011 reaching 67 GW, solar energy production may reach 100 TWh in 2012. Can solar energy

production be increased by several hundreds times by 2065 in order to replace nuclear contribution of about 26000 TWh (Figure 1) to carbon emission reduction? There is a very rapid increase of solar power from the present low level of solar power but sustained high growth and an increase by a factor of several hundreds in the course of 50 years cannot be taken as granted without consideration of essential developments of solar materials towards higher efficiency and lower costs. If such sustained high growth is to take place then also energy required to produce solar installations should come into consideration. If the installed power is to double in approximately every six years, as implied by growth with a factor of 300 in 50 years, then each operating solar installation should in six years produce at least the amount of energy for production of materials and construction of another installation. Energy balance or yield of an energy installation is expressed with the ratio between lifetime production of energy and the energy needed to produce required materials and construct the installation. For roof mounted solar installations yield would be in the range 5 to 10 depending on the technology and location [24, 25]. At the lower yield limit, applicable for developed northern world regions, and the lifetime of 20 years, 4 years would be needed to cover the energy for materials and construction. Applying this estimate to an expanding solar system with doubling time of five years we see that available net energy will be significantly reduced relative to the nonexpanding system. In our example about two thirds of energy produced would be used to support the expansion of the system. In the period of rapid growth from 5.4 GW in 2005 to 67 GW in 2011 energy balance in growing system was definitely negative. This may not look so in the country which does not produce photovoltaic materials itself, but globally it is even worse if materials come from the country where coal is the main source of energy. The point we wish to make is that however large be the potential of solar energy it cannot be reached in a very short time. An increase by high factor (significantly larger than 1000 in 50 years) would pose a problem at least in the regions of lower yield factors. Another issue is economy. At present solar installations costs, economic burden on EU of building at least 4000 GW peak of solar photovoltaic installations in order to replace 1100 GW of nuclear power would be staggering. Even with the cost per unit peak power at the level of nuclear power, due to efficiency factor not above 0.2, the cost of solar installations per unit produced energy would be about 4 times higher. In production of large amounts of energy economic considerations have been decisive in the past, there is no reason to expect much change in the future. Globally, the theoretical sufficiency of solar energy is even more evident, as EU is not optimal location considering the intensity of solar radiation. However, for many regions where physical conditions for solar energy use are better, economic constraints are stronger, limiting development. Investments from developed industrial countries could help, but this is not an immediate future. Important point in this discussion is that we look at the period up to the year 2065, critical for the climate control. In spite of a large and in the long run abundant potential of solar energy, its contribution in coming decades is limited by economic constraints. With intensive development of solar materials this may change. This will certainly be a very welcome development. However, the known times from scientific discovery to the very large scale applications do not warrant that this will take place in the years up to 2065, early enough to abandon nuclear contribution. As we have noted, there is a physical limit on the rate of growth of solar installations beyond which the effect on carbon emission reduction becomes negative.

4.5 Renewable energy on the world scale

In view of cost disadvantage of renewable sources it can be expected that their large scale deployment will be undertaken largely by the developed industrial countries; EU as leading region, North America, but also by rapidly developing countries such as China and India where conventional fossil sources pose serious problems to environment. However, some relevant well founded predictions, rather than wishful thinking, for world renewable sources do not exist. It is however very important to have some picture about energy scene up to 2065. Large thermal power stations built now may be still operating in sixties. One generation in conventional energy production is much longer than in communication technology, while renewable sources technology

is somewhere in between. We cannot answer the question on the need or not of nuclear power in 2065 without some estimate on the probable or possible contributions from renewable sources. We venture to make a guess on the future of renewable sources fully aware of very large uncertainties. In view of this, our approach is to choose somewhat easier task, to make an upper limit estimate. Should the upper limit contribution from renewable sources turn out to be insufficient for coming down to WEO 450 strategy from the WEO reference strategy, argument will stand for nuclear contribution. To obtain estimate for global contribution of renewable energy we start from EREC (European Renewable Energy Council) predictions for EU and use it as guidance, trusting that their predictions do not underestimate the prospects for renewable energy. For North America we assume approximately equal contribution of renewable sources per capita as in EU; prediction analogous to EREC for North America would then come between 1800 and 2300 GW, figures corresponding to prediction range for EU region of 2700 and 3000 GW, respectively. For Asian region predictions are rather more uncertain. So globally we estimate probable upper limit of world renewable power in 2065 capacities (GW) and contribution to energy production (Table 2) by equating contributions of North America with that of India, and of China with EU. The projection of world RES installed power in the year 2065 is given in Table 4.

Table 4 Projection of world renewable energy installed power in 2065

Present population millions	500	350	1300	1400	3450	7000
Region	EU	North Amer.	India	China	Rest**	World
Estimated renewable power GW	2700-3000*	1800-2300	1800-2300	2700-3000	2000-3000	11000-13600

*prediction range results from linear and exponential extrapolation of EREC values for 2050 to 2065
**main contributors South Korea, Japan, Brazil, Indonesia

In adopting these figures considerations were made of starting positions, population, rate of development, and of awareness of environmental problems. With all that, figures can be only tentative. So far economic science was reasonably good in explaining past events, but rather less successful in predictions. If the world had time to wait, better data would be available. Using the EREC average ratio between installed power and energy production (2.66 TWh/GW) i.e. the same average efficiency, we obtain in the last column a range of estimate for the upper limit of world renewable sources installed power. Corresponding values of annual energy production are 29260 TWh and 36180 TWh.

5 REQUIRED AND PREDICTED RENEWABLE SOURCES PRODUCTION

These figures can be now compared with the required contributions of non nuclear energy sources as shown in Figure 1 in order to reach WE0 450 values of allowed emission. Within the analysis presented in Figure 1 when nuclear contribution of 25.2 GtCO2 is subtracted from the total reduction to WEO 450 trajectory amounting to 67.4 GtCO2-eq we obtain 42.2 GtCO2-eq to be covered by renewable sources, as well as energy efficiency and saving. As elaborated above, impossibility to predict energy saving and increased efficiency is reflected in a wide range for our prediction; from 10 GtCO2-eq to 16 GtCO2-eq of emission reduction in 2065. The reduction which would remain as a task for renewable sources would be, consequently, in the range from 26.2 GtCO2 to 32.2 GtCO2 (Table 5). If these emissions were produced by coal power plants corresponding quantities of energy would be 27290 TWh and 33540 TWh. To replace coal plants this amount of energy would have to be produced by renewable energy sources. It would increase if the thermal power plants included gas plants. However, for our discussion we are interested in a minimum demand on renewable energy required to reach WEO 450 trajectory from the WEO

Reference trajectory in 2065. We see that these values of required contributions from renewable sources correspond reasonably well with the figures for predicted renewable energy production in the range from 29260 to 36180 TWh, especially as we cannot be sure to reach highest emission reduction of 16 GtCO2-eq from the energy efficiency and saving sector, and highest production of 36180 TWh by renewable energy sources.

Table 5 Balance of emission reductions from the WEO 2011 Reference scenario to the WEO 450 strategy

Emission reduction and produced energy from operation of 3300 GW of nuclear power in 2065	25.2 GtCO2 26250 TWh	25.2 GtCO2 26250 TWh
Emission reduction by energy saving and increased efficiency in 2065	10 GtC02-eq	16 GtCO2-eq
Estimated reduction by renewable sources in 2065	32.2 GtCO2	26.2 GtCO2
Required contribution of Renewable sources; corresponding required production in TWh and in average power in GW	33540 TWh 3830 GW	27290 TWh 3120 GW
Renewable sources range estimate of global energy production in TWh, corresponding average power in GW, and emission reduction in GtCO2 for the year 2065	29260-36180 TWh 3340 – 4130 GW 28.1-34.7 GtCO2	29260-36180 TWh 3340 – 4130 GW 28.1-34.7 GtCO2

Total required reduction to reach WEO 450 Strategy trajectory from WEO Reference strategy emission in 2065 amounts to 67.4 GtCO2-eq. (Fig.1). Figures refer to total anthropogenic emissions. Required contribution from renewable sources is obtained by subtraction of nuclear and energy saving and efficiency increase emission reduction from the total, third and fourth row. Two values given in the Table 5 for renewable sources production (last row) are linear and exponential extrapolation of EREC and GWEC data from the year 2050 to 2065 determining a range for predicted upper limit of renewable energy contribution.

Interesting data are the estimates of cumulative carbon emission savings which follow from nuclear build-up to 3300 GW and of savings which would follow from the upper limit RES development. For nuclear case with linear build-up to 3300 GW in the years 2025-2065 for cumulative saving in the period 2015-2065 we obtain about 550 GtCO2. This would be a contribution limited by constraints of using proven conventional nuclear technology and once-through fuel cycle. Estimates for renewable sources in their upper limit, as given in the last row of Table 5, are in the range of 600 GtCO2 for graded (faster growth in the first 20 years) exponential growth to 780 GtCO2 in case of linear growth in the 2015–2065 period. These figures can be compared with figures for cumulative carbon emission saving by renewable energy in SRREN [3] given for the period 2010-2050. Cumulative saving for this period is given in the range 220-560 GtCO2. As our estimate is the upper limit we compare it with SRREN upper limit which extended to 50 years period comes to about 700- 750 GtCO2, again depending on growth rates. This is consistent with our estimate of RES saving in the range of 600-780 GtCO2. This also indicates that our upper limit on the renewable sources contribution by 2065 is not underestimated. Sum of the nuclear and RES emission savings is consistent with limits on cumulative emissions as given in [3] and [16].

6 DISCUSSION

A look at the table 5 gives some quantitative insights about the energy strategy that could by 2065 fulfil the aim of reducing the carbon emission from the unacceptable WEO 2009(2011) Reference strategy down to the WEO 2009(2011) 450 strategy. With nuclear energy contribution

defined by specific constraints and reaching 3300 GW of power by 2065, we obtain the required production of renewable energy by the year 2065. This is important as it can be compared with the predictions for build-up of renewable sources and offers an answer on the role of nuclear power in the same time period. We see that renewable energy predicted production could match the requirement, but only after nuclear power has given its contribution. Smaller nuclear contribution would require increased contribution of renewable energy. Without nuclear contribution production of renewable sources would have to be about doubled, which must be considered completely unrealistic in view of optimistic estimate of their production in 2065.

Whilst these conclusions should be of importance for future structuring of energy plans and strategies, one should be aware of unavoidable limitations and several caveats should be given. The figures presented in Table 5 are, of course not predictions, they are an attempt to guess now about the future 50 years ahead. Nuclear build-up to 3300 GW by 2065 reducing CO_2 emission by 25.2 GtCO2 is a maximum based on the conventional uranium resources known in 2007, with conventional reactor technology and without fuel reprocessing and plutonium recycle. The point of selecting this nuclear strategy was to show what can be achieved with these, in our opinion, very desirable constraints. More detailed discussion on the reality of such nuclear contribution with the constraints imposed is given in our earlier study [13]. It also discusses the fuel sufficiency after 2065. Further details which show that with advanced nuclear technologies of Generation 4 sufficiency of nuclear fuel should not be a problem are given in [13,26]. We could not have the same confidence in predicting the contribution to emission reduction from energy saving, from increased efficiency of energy use and from many other ways, some unknown today, which could reduce carbon emission. In evaluation of nuclear contribution adopted constraints of conventional technology, fuel cycle and uranium resources help predictions, whilst the amount of emission reduction through energy saving and better use of energy will be determined by future developments and innovations. Thus, there is large range from 10 to 16 GtCO2-eq for reductions from that sector. Graphic presentation on Figure 2 should help to offer some further insights about future energy mix. Shadow belt is the range for the high prediction of contribution from renewable sources. Range is determined by linear, respectively exponential extrapolation from 2050 values. Boxes a) and b) depict a situation with lower and upper limit of reduction by energy saving and other ways of reducing emission outside power production sector, respectively.

In estimation of future contribution from renewable sources we adopted high predictions based on European Renewable Energy Council and on Global Wind Energy Council, as shown in box c). From the box c) of the Figure 2 we see that by combining the high production of renewable energy, corresponding to emission saving of 34.7 GtCO2 with the upper value of emission reduction by energy saving of 16 GtCO2-eq, required nuclear contribution would be reduced to 16.7 GtCO2 , respectively to about 2190 GW in terms of installed power in 2065. With maximum contributions from renewable energy and from energy saving, 2190 GW of nuclear power would be needed and sufficient to cover the required reduction of 67.4 GtCO2-eq. However, if with high predictions on contributions from both renewable sources and from energy saving, the need for nuclear contribution still remains, then a very important conclusion about the nuclear energy future follows. That is, 2190 GW of nuclear power seems to be the minimum required to reach the WEO 450 trajectory in 2065. This would require about 1800 GW in addition to present about 380 GW. We pointed out that physical limits exist on the wind energy capacity and on the solar energy rate of growth. Should, hopefully, through intense international efforts high predictions on renewable sources be realized, then together with nuclear contribution with additional 1800 GW and with contributions from energy saving, efficiency increase etc, on the level of up to 16 GtCO2-eq, World could succeed in coming down from WEO 2011 Reference scenario to WEO 450 scenario by 2065. Clearly, only future developments will give more certainty. However, before we have more certainty this analysis tells us that abandoning nuclear contribution would be a risky game with the future of our planet.

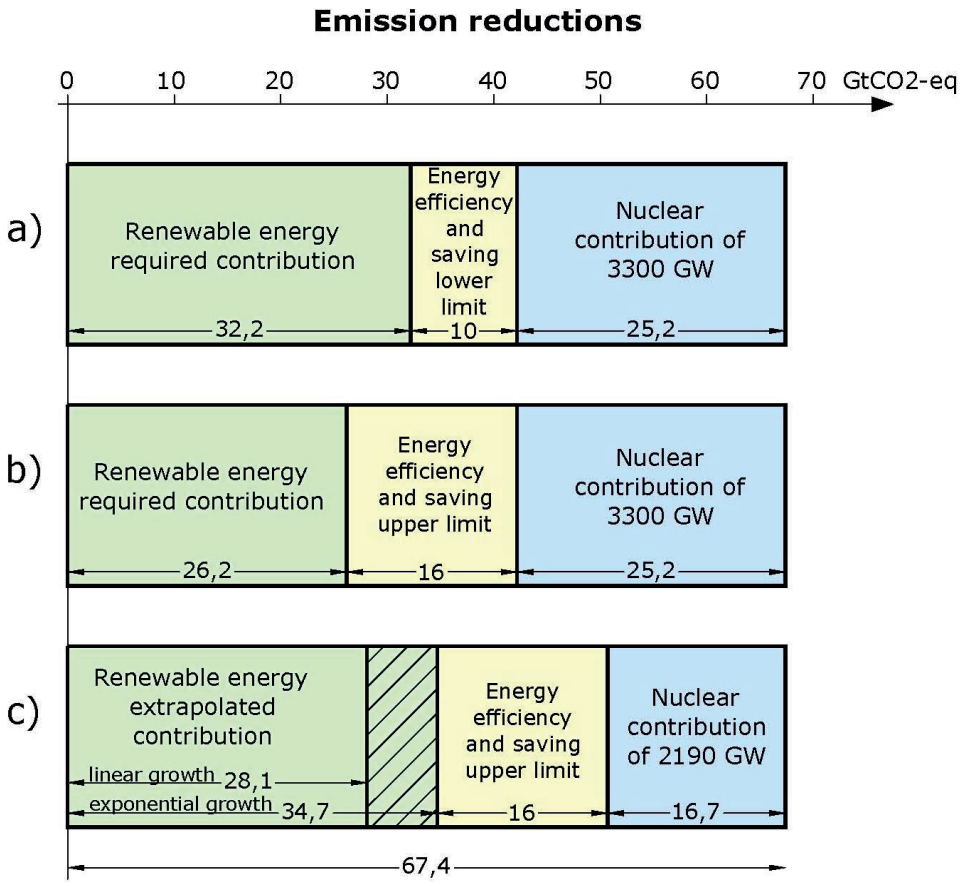

Figure 2: Graphic presentation of contributions to carbon or equivalent emission reduction by 2065

Neither CCS, nor nuclear fusion is likely to give essential contribution before 2065, although it is impossible at present to foresee the role of these technologies in later years. Developments of photovoltaic materials are faster and situation would be different with drastic reduction of their costs. That may or may not happen soon enough. If delayed it may not be possible to benefit fully from it in the period up to 2065. Whilst physical potential of solar energy is undisputed, actual deployment is much lower, limited by economic considerations. Should future developments of solar materials remove economic disadvantages, there would still remain a physical limit on the rate of growth preventing a very rapid build-up of solar power. If we cannot be sure of timely and favourable developments, we must plan for less favourable and the technologies we now have at our disposal. Nuclear technology is one of these. Whilst one can place solar installations in a number of sun-rich countries, nuclear contribution should come primarily from industrialized countries and regions which have industry, knowledge and experience in the field required to build reliable and safe nuclear power plants. This may be one lesson of Fukushima accident. EU is one such region, and is also a region with high intensity of carbon emission. If we accept that climate problem will not be resolved without nuclear energy then EU would fail in its responsibility and in solidarity with the less developed regions of the world by not contributing to carbon emission reduction in the critical period to 2065 with its nuclear energy sector for which EU possesses an outstanding potential and capabilities. With all the unavoidable uncertainties we hope this study offers some guidance for the future energy strategies.

7 SUMMARY

Considering the necessity and future role of nuclear energy as relevant to the climate problem, we have focused on the period to the year 2065. The reasons for this choice are twofold; first, this is a critical period for achieving the essential 80% CO_2 emission reductions and, secondly, this is the period during which large contributions from fusion and carbon separation and storage are not likely. For quantification of the required emission reduction we have used IEA WEO 2009 and WEO 2011 data as presented in their Reference strategies predicting emissions with business as usual practices, and WEO 450 Energy strategies which show the time development of allowed emissions consistent with a limit on the global temperature increase of 2 ºC and the peak CO_2 concentration of 450 ppm. From the 2035 and 2050 values of total anthropogenic CO2eq emissions given in WEO 2011 and WEO 2009 we extrapolated the Reference strategy and WEO 450 strategy to the year 2065. With Reference emission in 2065 reaching 77.4 GtCO2-eq and WEO 450 strategy allowing emission of 10 GtCO2-eq we obtain the reduction required by 2065 amounting to 67.4 GtCO2-eq in order to come down to sustainable WEO 450 trajectory. Main carbon non-emitting sources assumed in the years up to 2065 are proven technology nuclear fission and renewable sources. Shorter period, more desirable from the climate control view, would correspondingly increase technical and economic demands in development of required carbon free energy production capacities. Even with the year 2065 as a compromise there is a giant task facing renewable sources in the mixed energy strategy which includes nuclear power, if by that year total anthropogenic GHG emission is to be reduced to 10 GtCO2–eq. In our specified strategy aimed to achieve WEO 450 target we assumed an energy mix including nuclear power build-up in the period 2025-2065 to the level of 3300 GW in 2065. With the resulting nuclear contribution of 25.2 GtCO2 to the total required reduction down from the WEO 2009 reference strategy amounting to 67.4 GtCO2 in 2065, what remains for renewable sources, energy saving and increased efficiency of energy use to contribute are prodigious 42.2 GtCO2-eq. In the absence of estimates about contribution of renewable sources going as far as 2065, we had to make reasonable guesses trying not to underestimate their possible contributions. Relevant energy policy cannot be deduced by looking only two or three decades in advance when construction and the lifetime of energy installations can be 50 years or more. Our estimates are based on EREC prediction for EU and on our extension to world total with EREC and GWEC prediction as a guide. Resulting contributions by renewable sources, probably their upper limits, allow some conclusions about the role of nuclear energy in future decades. Assuming that energy saving and more efficient energy use will by 2065 effect an annual reduction between 10 to 16 GtCO2-eq, remaining 26.2 to 32.2 GtCO2, respectively 27290 and 33540 TWh would be the task for the renewable energy sources as presented in Table 5 and in Figure 2. Our high, but still credible estimates of predicted world renewable energy contribution by 2065 come to the similar figures between 29260 and 36180 TWh. However, as is evident from Table 5 and Figure 2, even so without nuclear contribution in 2065, renewable energy contribution would have to be doubled, practically impossible task in the time period in consideration and in view of their generous predictions. By combining highest contributions from energy saving, efficiency increase and other measures to reduce emission, apart from energy production, with highest prediction for renewable sources contribution, we obtain the minimum nuclear energy requirement of about 2190 GW in 2065. This minimum nuclear strategy should be planned and prepared for, unless there is strong evidence that other carbon free energy sources (CCS or fusion) could be developed in time. Expansion of nuclear power by about 1800 GW by 2065 would come from different and already developed industrial sector, which can give its contribution to the energy mix, without obstructing the build-up of renewable sources. It would not be wise to forfeit nuclear contribution at least in the period to 2065, critical for the control of climate change.

8 CONCLUSIONS ABOUT THE FUTURE OF NUCLEAR POWER

1. After combining a reasonably largest prediction of carbon emission reduction from the renewable sources (36180 TWh, respectively 34.7 GtCO2 in 2065) with a maximum predicted reduction from energy saving, efficiency increase and other non-energy methods of carbon emission reduction (16 GtCO2-eq in 2065), about 16.7 GtCO2 of further reduction is still missing in order to reach a total of 67.4 GtCO2-eq required to bring in the year 2065 the WEO Reference energy strategy down to the WEO 450 energy strategy limiting the global temperature increase to 2 °C.

2. Gap could be closed by operating about 2190 GW of nuclear power in 2065. In view of the assumed high predictions for renewable energy and for energy saving, this figure should be considered a minimum future need. Plans for about 1800 GW of nuclear power, additional to presently operating about 360 GW should be discussed and coordinated. For political, technical and public reasons, plans should be realized with proven conventional technology and with once through fuel cycle, while the new technologies can be prepared for the years after 2065.

3. Whilst the need for nuclear (fission) power appears to be clear for the period to about 2065, its long term future will be determined by developments of alternatives such as CCS or nuclear fusion. Nuclear future will also depend on whether the period up to 2065, during which conventional nuclear technology without reprocessing can be adequate, will be used for development of political and technical institutions and technologies for the safe use of U238 and Th232 that would make nuclear fission practically inexhaustible source of energy.

REFERENCES

[1] UNFCCC 2009 Copenhagen Accord, UN Framework Conference on Climate Change, Conference of the Parties, Copenhagen, 7–18 December 2009.

[2] EEA (European Economic Area) Report, 2008. Impacts of Europe's changing climate-2008 indicator-based assessment, Joint EEA-JRC-WHO Report.

[3] IPCC, 2011: Summary for Policymakers. In: IPCC Special Report on Renewable Energy Sources and Climate Change Mitigation,[O. Edenhofer, R. Pichs-Madruga, Y. Sokona, K. Seyboth, P. Matschoss, S. Kadner, T. Zwickel, P. Eickemeier, G. Hansen, S. Schlömer, C. von Stechow (eds)], Cambridge University Press, Cambridge, United Kingdom and New York, NY, USA.

[4] UN Climate Change Conference, Cancun, Mexico, 2010

[5] IEA (International Energy Agency), 2009. World Energy Outlook 2009, OECD/IEA Report

[6] IEA (International Energy Agency), 2011. World Energy Outlook 2011, OECD/IEA report

[7] J.Lister, H.Weisen, What will we learn from ITER, Europhysicsnews,36/2, 2005

[8] Nuclear Fusion Status and Prospects, Max Planck Institut fuer Plasmaphysik, September 2011

[9] Lawrence Livermore National Laboratory, The National Ignition Facility (lasers.llnl.gov)

[10] CEA, Le Laser Megajoule (www-lmj.cea.fr)

[11] Zweibel, K., Mason, J., Fthenakis, V., By 2050 solar power could end U.S. dependence on foreign oil and slash greenhouse gas emissions, Scientific American, January 2008.

[12] UN (United Nations) Sigma XI Report, 2007. Confronting climate change, 2007: Avoiding the unmanageable and managing the avoidable. Report prepared by The United Nations Sigma XI Scientific Expert Group on Climate Change for the United Nations Commission on Sustainable Development, February.

[13] Vladimir Knapp, Dubravko Pevec, Mario Matijevic: The potential of fission nuclear power in resolving global climate change under the constraints of nuclear fuel resources and once-through fuel cycles, Energy Policy 38 (2010)

[14] Communication from the Commission to the European Council and European Parliament – An energy policy for Europe{SEC(2007)12}

[15] Brook, B.W., Could fission energy, etc., solve the greenhouse problem? The affirmative case, Energy Policy 42 (2012)

[16] Meinshausen, M., Meinshausen, N., Hare, W., Raper, S.C.B., Frieler, K., Knuitti, R., Frame, D.J., Allen, M.R., Greenhouse gas emission targets for limiting global warming to 2 °C, Nature 458 (2009)

[17] IPCC (Intergovernmental Panel on Climate Change), 2007. Fourth Assessment Report, Synthesis Report.

[18] OECD/NEA-IAEA (Organization for Economic Co-operation and Development/Nuclear Energy Agency – International Atomic Energy Agency), 2008. Uranium 2007: Resources, Production and Demand

[19] EREC, European Renewable Energy Council" The Road to 2050", 2011.

[20] Global Wind Energy Outlook 2010, Greenpeace-GWEC, October 2010.

[21] David McKay: Sustainable energy without hot air, UIT, Cambridge 2009.

[22] WEC World Energy Insight 2011, WEC November 2011, 2010 WEC Survey of Energy Resources.

[23] Information prepared for European Council, Background on energy in EU, 4 February 2011

[24] Richards, B.S and Watt, M.E. (2007). Permanently dispelling a myth of photovoltaics via the adoption of a new net energy indicator, Renewable and Sustainable Energy Reviews, 11(1):162172

[25] Murphy, D.J., and Hall, A.S., Year in review-EROI or energy return on energy invested, Annals of New York Academy of Science 1185(2010), 102-118.

[26] Dubravko Pevec, Vladimir Knapp and Krešimir Trontl, Long Term Sustainability of Nuclear Fuel Resources, Chapter in the book, *Advances in Nuclear Fuel*, InTech, Rijeka 2012

Journal of Energy
VOLUME 62 Number 1–4 | 2013 Special Issue
journal homepage: http://journalofenergy.com/

Nuclear Power as an Option in Electrical Generation Planning for Small Economy and Electricity Grid

Prof.dr.sc. Željko Tomšić
University of Zagreb, Faculty of Electrical Engineering and Computing
Unska 3, 10000 Zagreb, Croatia
zeljko.tomsic@fer.hr

ABSTRACT

Implementing a NPP in countries with relatively small total GDP (small economy) and usually with small electricity grid face two major problems and constrains: the ability to obtain the considerable financial resources required on reasonable terms and to connect large NPP to small electricity grid.

Nuclear generation financing in developing countries involves complex issues that need to be fully understood and dealt with by all the parties involved. Besides conventional approaches for financing power generation projects in developing countries, recently some alternative approaches for mobilizing financial resources are developed.

The safe and economic operation of a nuclear power plant (NPP) requires the plant to be connected to an electrical grid system that has adequate capacity for exporting the power from the NPP, and for providing a reliable electrical supply to the NPP for safe start-up, operation and normal or emergency shut-down of the plant. Connection of any large new power plant to the electrical grid system in a country may require significant modification and strengthening of the grid system, but for NPPs there may be added requirements to the structure of the grid system and the way it is controlled and maintained to ensure adequate reliability.

Paper shows the comparative assesment of NPP adn differrent base load technologies as an option in electrical generation planning for small economy and electricity grid

1 INTRODUCTION

Energy in general and electricity in particular, is essential for economic and social development, prosperity, health and security of citizens: GDP is also closely related to energy consumption/cost/quality of supply. Countries must meet its rising energy demand without environmental damage, reducing harmful emissions and securing a stable and sustainable energy supply, and without excessive price or availability fluctuations. The many energy sector currently faces three major challenges: ensuring security of energy supply; reducing greenhouse gases (GHG) emissions and maintaining economic competitiveness by keeping energy prices at an affordable level. Making decisions on the future energy mix will depend on national goals and priorities, on exploration for fossil resources, on the development of clean coal and carbon capture and storage technologies, on improving the performance and cost of renewables, energy efficiency or placing greater reliance on imports. The only base load generation option available today, with low carbon emissions comparable to nuclear power (NPP) is large hydropower, but its contribution in meeting the energy demand in many cases cannot be much greater than that at present as most of its potential as already been exploited. NPP do not emit greenhouse gases. Already, due to low cost fuel and improved efficiency, nuclear plants once built can be less expensive to operate. Thus, even in a marketplace that does not credit its virtues, nuclear power is increasingly competitive. Putting a tag on harmful emissions would quickly make nuclear power the cheapest option as well as the

Ž. Tomšić, Nuclear Power as an Option in Electrical Generation Planning for Small Economy and Electricity Grid, Journal of Energy, vol. 62 Number 1–4 (2013) Special Issue, p. 19–32

cleanest for generating increasing energy in the global scale. New NPPs could make an important contribution, to meeting needs for low carbon electricity generation and energy security in this period and beyond to 2050. Many countries are and will face a great deal of uncertainty about energy supplies over the next couple of decades. But there are also uncertainties relating to future fossil fuel and carbon prices; the speed at which we can achieve greater energy efficiency and therefore likely levels of energy demand here and globally; the speed, direction and future economics of development in the renewable sector; and the technical feasibility and costs associated with applying carbon capture and storage technologies to electricity generation on a commercial scale. Faced with these uncertainties we need diversity and flexibility in the energy mix and a policy framework that opens up the full range of low carbon options. The best way to achieve secure energy supplies is by encouraging a diversified mix of generating technologies. Giving energy companies the option of investing in new NPP lowers the costs and risks associated with achieving our energy goals to tackle climate change and ensure energy security.

Making the decision to embark upon a nuclear power program is a major undertaking for any country. Such a decision involves careful planning, as well as a long-term commitment to the nuclear power program. It is significant commitment in terms of time and resources (both human and financial). The process involves the development of a nuclear power project within the overall national program; consequently, the host government must consider both the NPP and the supporting infrastructure for the NPP. Such infrastructure must include legal, regulatory, technological, human resources, and industrial support.

The experience of the NPP projects already implemented showed that a major requirement for, and constraint to, the development of NPP projects in developing countries is the ability to obtain the considerable financial resources required on reasonable terms. As nuclear generation financing in developing countries involves complex issues that need to be fully understood and dealt with by all the parties involved. The financing of such projects presents a critical problem not only because of the very large amount of financing needed, but also because of the relatively low creditworthiness of country as perceived by various lending organizations. Consideration should be given to the principal characteristics specific to nuclear power projects, as well as to the overall complexities of such projects and how these complexities affect their financing. It is essential that every effort be made by all parties involved in the development of a nuclear power project to reduce the uncertainties linked to such large investments and long project times, in order to improve the overall climate for the financing of these projects. In order to successfully finance a nuclear power project, it is essential for the government/utility to prepare a thorough financial analysis, together with an economic analysis, for evaluating the feasibility of the project.

Today the question is which approach can be used to finance nuclear power plants to be compatible with current utility and financial market conditions and specially in small economy. The economics of nuclear power depend on national or even local conditions, including the costs of capital, labour and materials, the regulatory environment, and the availability and costs of alternative generating technologies. Increasingly, the economics of new nuclear power plants can, depending on location and alternatives, compare favourably with non-nuclear alternatives. The overall comparison also depends on values assigned to possible external costs, such as air pollution, greenhouse gas emissions, import dependence, cost uncertainties and the comparative risks of different alternatives. Also deeper understanding of the risks involved in project finance and risks evolution over time is important for both practitioners and policymakers. In particular, further research in this area might help in the implementation of risk sensitive capital requirements providing market participants with the incentives for a prudent and, at the same time, efficient allocation of resources across asset classes. This is particularly relevant, given the predominant role of internationally active banks in project finance and the fundamental contribution of project finance to economic growth, especially in emerging economies.

Now also should be studied how the risks specific to a nuclear power investment in liberalised markets can be mitigated, how they can be allocated to the different stakeholders, and which financial arrangements are consistent with the alternative allocations of the construction and

operating risks. Under the former regulated utility regime and regulatory arrangements, many of the risks associated with power plant construction costs, operating performance, fuel price changes, and other factors were borne by consumers rather than investors. The current context for new nuclear build in power markets is significantly different with producers bearing much of the risks unless some are transferred onto other stakeholders through long term contracts and/or innovative financing arrangements.

1.1 Specificities of the Nuclear Industry

The decision of a country to embark on a nuclear power program entails a long-term commitment to the peaceful, safe, and secure use of nuclear technology, based on a sustainable organizational, regulatory, social, technological, and economic infrastructure.

The global financial system has recently experienced its worst crisis for several decades, with a number of major banks having failed or requiring large-scale government support. This is having a significant near-term impact on the ability to raise commercial finance for any purpose, including large-scale infrastructure like NPP. Significant risk transfers from plant investors onto governments, consumers, and for the first new reactors, onto vendors are likely to be needed to make nuclear power attractive to investors in liberalised markets.

Special features of nuclear power projects with respect to finance are: High capital cost, long construction period, Long term return on investment, Long term government commitment and public support (Plan, build, operate, decommission, waste management; Need to ensure funds for operation, maintenance, decommissioning and waste management) , Underpinning technical and human resource; Commercial risks (Credit rating of sponsor, Market, Competition, Schedule, Utility risk) , Economic risks (Inflation, Interest rates, Exchange rates, Political risks, Force majeure, Change in law); Government participation is seen as vital for a first unit in respect of non-design related ‘first of a kind’ issues (such as: First experience of regulatory process, Site preparation, Local supply chain and labour issues)

2 OVERVIEW OF CLASSICAL CONTRACTUAL AND OWNERSHIP APPROACHES FOR FIRST NPP

Looking at prior and current development of NPPs, development of NPP program has occurred either through sovereign-based structures or through corporate-based structures. This development history is one of leadership by public entities in a regulatory environment that enabled transfer of the significant development costs to an allocated customer base. Traditionally has been that owner/operator of the NPP was either government owned and/or regulated through the dedicated rate based that it serviced. As markets have liberalized, there is less opportunity to cover development costs through the rate base. Instead, potential NPPs need to be assessed on the strength of the underlying economics of the project within a competitive market structure.

Based on prior NPP development, project models have favoured the presence of a national or regional utility that has served as the owner/operator. Such owner/operator, either on the strength of its own balance sheet or through the support of sovereign funds, has provided the equity component for these NPPs, with debt financing (both commercial lending and Export Credit Agency financing) also based on balance sheet metrics and/or sovereign guarantees.

Historically, nuclear power development occurred either as part of a national power program that has been led by the host government or by national or regional utility companies that has been able to recover project costs through a regulated rate base.

2.1 Sovereign Model

In the case of the sovereign model, funding is provided through, or guaranteed by, sovereign sources, and ownership and operation of the NPP is through a government-owned utility [1]. Nuclear development is part of a national program, often evidenced by a national energy policy.

The strength of the sovereign model is that the program has the demonstrated support of the host government, with the ultimate credit behind the project being a sovereign credit. The critical aspect of the sovereign model is the underlying financing strength of the sovereign, either as financier or guarantor, to support the costs for the nuclear power program.

2.2 Utility Balance Sheet Model

In the absence of direct involvement of the sovereign, NPPs have been developed by utility companies, utilizing classic balance sheet financing for the nuclear power plants [1] . A national or regional utility serves as the developer of the project, financing the project based on the strength of the utility's balance sheet. Under historical models, such utilities operated within regulated power markets, thereby having the ability to recover project costs through a regulated rated of return.

By having a dedicated market for the power and a fixed rate of return (which was established by law), the regulated utility was able to assume project development risks and absorb cost overruns, recognizing that the project costs would ultimately get passed through to the rate base.

However, as electricity markets have been liberalized in many countries, the ability to structure rate-based projects has been minimized. Furthermore, given the multi-billion dollar cost to develop a NPP project involving in the range of 1100 – 1700 MWe, many utilities might not be large enough to assume the costs of one or more projects without placing the company at risk.

While long-term power purchase agreements could provide a substitute for the regulated rate-base approach. Without the ability to assure long-term off-take at pre-determined pricing, the utility might not be willing to develop a project and rely on market pricing to provide the expected rate of return on the investment.

2.3 Contracting new NPP

Distinct from the issue of ownership is the method by which the project will be delivered. Three main approaches have been used. In each case, the owner finances the project [1].

First, the owner can acquire the nuclear unit under an engineering, procurement, and construction (EPC) contracting approach, whereby the owner enters into a contract with a major engineering and construction firm that will deliver both the NSSS technology and construct the facility (also know as a "turnkey" approach). Under this approach, the owner monitors the project, but the owner is looking to the EPC Contractor to deliver the project under the terms of the EPC contract.

Second, the owner can divide the procurement based on the three main elements of the plant: the nuclear island, the turbine island, and the balance of plant. Under this split-package approach, also possibly mixing foreign delivery (nuclear island) with domestic delivery (balance of plant and, perhaps, turbine island).

Third, the owner can serve as architect-engineer, whereby it enters into a myriad of contracts for various services (engineering, design and construction) and equipment. Under this approach, the owner must have the internal capability to integrate this multi-faceted contracting approach. It is probably not an approach that could be employed by an owner looking to develop its first NPP.

2.4 Description of alternative new contracting models - BOO/BOOT

As possible new concept for developing NPP project can be Build-Own-Operate (BOO) or a Build-Own-Operate-Transfer (BOOT) structure. The host government first makes a determination that a non-government entity will develop the infrastructure project. BOO and BOOT models have been used successfully in a variety of infrastructure projects, a BOO(T) structure had not been attempted in the nuclear sector. Under such structures, the Developer is responsible for bringing together project development capabilities, to include: Technology; Engineering, Procurement, and Construction; Fuel Supply; Operations; and Financing.

Very simply, the BOO(T) structure places the responsibility for "bringing the project to market" on the Developer.

3 HIGH FINANCING COSTS FOR NEW NUCLEAR CONSTRUCTION

Factors contributing to high financing costs for new nuclear construction are: interest rate that includes a risk premium; credit rating of utility; inability to pre-charge rate payers without backlash; duration of project; cash on hand; risk premiums charged by banks.

Utilities are subjected to paying an interest rate that includes a risk premium for loans to build new nuclear power plants. Banks argue that the uncertainty associated with new nuclear construction warrants a higher interest rate than market rate. The uncertainty banks are referring to is whether or not the nuclear power plant will ever be completed, and if it is, whether or not the plant will receive an operating license from the nuclear regulator. These risk factors allow the banks to make a case that the interest rate on loans for new nuclear construction should be several percentage points higher than market rates because the utility company may never get the cash flow benefit from the project should it not obtain an operating license or the construction is not completed. Every business has a different credit rating and banks charge businesses with a lower credit rating a higher interest rate than businesses with higher credit ratings and each company's individual credit rating will affect the interest rate they obtain on the loan(s) from the bank(s).

Every utility company will choose a different financing structure to fund new nuclear construction. Since financing costs are such a large proportion of the total construction cost of new NPPs, it is wise to fund as much of the project as possible through pre-charges and cash on hand.

4 HOW TO FINANCE NEW NUCLEAR BUILD IN LIBERALISED MARKETS

Under the former regulated utility regime and regulatory arrangements, many of the risks associated with power plant construction costs, operating performance, fuel price changes, and other factors were borne by consumers rather than investors. The current context for new nuclear build in power markets is significantly different with producers bearing much of the risks unless some are transferred onto other stakeholders through long term contracts and/or innovative financing arrangements.

A project for potential new nuclear power plant in liberalised markets will face a number of hurdles associated with the specificities of the technology and the legacy of past experiences. Nuclear power suffers indeed from some specific risks: the regulatory risk associated with the instability of safety regulations and design licensing; the policy risk where electoral cycles could undermine the commitment to nuclear power and the development of nuclear waste disposal facilities; and the construction and operation risks associated with the necessary re-learning of the technology. Besides, the large size of a nuclear project and the capital intensity of the technology make it relatively more sensitive to some critical market risks such as the electricity price and volume risks.

The contractual and financing choices for new nuclear build in typical market cases can be:

- The decentralised market is based on a project finance approach. The critical factors enabling such financing structure are the federal loan guarantees, federal tax credits, and long term fixed price contracts with credible counterparts;
- The Nordic market, wherein the Finnish TVO project to build an EPR uses an hybrid financing approach. The project relies on two special arrangements: a turnkey contract by which the constructor bears a large part of the construction and performance risks, and the financing by a consumers' consortium whose members will in return pay electricity at cost-price over the life of the plant;
- The imperfectly reformed market, wherein the project is managed and lead by the large size and vertically integrated historical incumbent, using a corporate financing approach;
- Finally, the case of oligopolistic markets of mid-size vertical companies or of small markets dominated by incumbent companies developers and their potential lenders in such markets would likely seek to share costs and risks by e.g. investing in a producers consortium, and would search to have some market risks transferred onto the state.

In these cases there remain many critical factors specific to each country's industrial and regulatory environment, there is no optimal "once-for-all" contractual and financing arrangement for investing in nuclear in liberalised markets.

In the perspective of project financing of new nuclear plants, loan guarantees by government and power purchase agreements at fixed price for almost all the off-take power will likely be required. Turnkey contract for the FoAK reactors could also provide a guarantee during the construction phase, followed by refinancing for the plant operation phase. Nuclear build in liberalised markets is going to bring some new light on some critical issues associated with the maturing of electricity markets.

Improving prospects for financing means understanding financing risks, establishing ownership and effecting mitigation and there may be no financial 'silver bullet': Nuclear perceptions and realities also impact on financing.

5 ELECTRICITY GRID AND NPP UNIT CAPACITY

Considering that the nuclear power plant will be integrated into the national electrical power grid and into the local and -wider regional environment, the selection of the station capacity should take into account the implications of the necessity to strengthen the electrical connections to the other nodal points of the electric grid, to the neighbouring countries, and of the necessary legal and commercial agreements with those countries.

The size of a nuclear unit in this context refers to the maximum electrical power that it can deliver to the transmission system. Partly driven by economies of scale, there has been a steady increase in the size of new nuclear units, so the designs of nuclear units that are currently available from international nuclear plant vendors are large, generally greater than 1,000 MW.

Consequently, a first nuclear unit built today is almost certainly going to be the largest single generating unit in the system to which it is connected. This may represent an issue if the system is relatively small such as:

- The need to control the large and rapid changes in frequency, voltage and power flow that will occur after a trip of the nuclear unit or if a fault in the transmission system disconnects the nuclear unit
- The need to have sufficient generation to meet electricity demand during periods that the nuclear unit is shut down, whether for planned maintenance or following a fault or unplanned trip
- From the point of view of the NPP, the need to ensure that a trip of a nuclear unit will not cause a loss of offsite power to the NPP, and the voltage and frequency of the offsite supply will remain within the acceptable range.

If the current or future electricity demand of the country is too small, and there is not a reasonable prospect of developing strong grid connections to neighbouring countries, then a conclusion of a feasibility study of the introduction of nuclear power in country could be that the country is not able to consider nuclear power until smaller nuclear units become available.

5.1 NPP and Electricity Generation Planning

The first step in working on generation plan is to collect, summarize and review all relevant information on the present state of power generation capacity [8]. Power system expansion planning involves analyzing, evaluating and recommending what new facilities and equipment must be added to the power system in order to replace worn-out facilities and equipment and to meet changing demand for electricity. Planning the expansion of the generation component of a power system has to be carried out taking into account two other major components of the system – transmission and distribution.

The most important concept in a definition of the energy planning process is that its ultimate purpose is to provide information to decision-makers.

Power generation plan can be successfully completed only if necessary inputs coming from Electricity demand analysis and from certain parts of other energy sector analysis are adequately provided. The obtained results will serve as one of the inputs for transmission and distribution, as well as for environmental impact analysis.

The goal of electric power systems expansion planning is to determine the optimal pattern of system expansion to meet the electricity requirements over a given period. Computer assisted modelling forms are the core of the approach to energy analysis and planning. Energy planners or policy analysts design future development trajectories of the principal drivers of the energy system 20 to 50 years into the future, and by using the energy planning tools, derive profiles of energy service demands and optimal supply mixes. Critical policy and investment aspects of different energy strategies can be defined, undesirable consequences can be identified, and the most cost effective approach to meeting future energy needs can be determined.

The Wien Automatic Simulation Planning Package (WASP) [9] helps to find the economically optimum expansion plan for a power generating system for up to 30 years, within constraints specified by the planner. The model evaluates many combinations of candidate generation projects to obtain the least-cost expansion plan (optimal solution) for a given period. The outputs of WASP include the alternative expansion plans and their Present Value (NPV) costs, annual financing requirements and summary reports. WASP is a cost minimization tool whose objective function is to generate the power planning expansion plan with the lowest present worth cost for the planning period.

WASP is designed to find the economically optimal long-term generation expansion policy for an electric utility system within user-specified constraints by utilizing several mathematical tools: probabilistic simulation, linear programming and dynamic programming. The optimum is evaluated in terms of minimum discounted total costs. Each possible sequence of power units added to the system (expansion plan or expansion policy) meeting the constraints is evaluated by means of a cost function (the objective function) that is composed of: Capital investment costs, Salvage value of investment costs, Fuel costs, Fuel inventory costs, Non-fuel operation and maintenance costs, Cost of the energy not served. WASP was successfully used as a planning tool in many Generation Investment Studies.

5.2 Example of introducing NPP in small electricity grid

The uptake of Nuclear power technology has been growing over time across different countries and regions. Various countries without existing nuclear power technology in their power systems have expressed interest in investing in initial nuclear power projects, while developed countries with existing nuclear plants have been expanding their capacities. Design and development of nuclear reactors is a major undertaking, which requires significant technical and financial resources. In recent decades the nuclear power industry has managed to improve the output of existing nuclear power plants quite dramatically. The net capacity of recently reviewed nuclear reactors in a joint 2010 study by the International Energy Agency (IEA) and the OECD Nuclear Energy Agency (NEA) [2], finds that nuclear reactors ranges from 954 MWe in the Slovak Republic to 1,650 MWe in the Netherlands, with the largest site to be constructed in China consisting of 4 units of 1,000 MWe each, (OECD, 2010). Owing to differences in country-specific financial, technical and regulatory boundary conditions, overnight costs for the new nuclear power plants currently under consideration in the OECD area vary substantially across the countries, ranging from as low as 1,556 USD/kWe in Korea (noting the generally low construction costs in that country, as well as its recent experience in building new reactors) to as high as 5,863 USD/kWe in Switzerland, with a standard deviation of 1 338 USD/kWe, median of 4,102 USD/kWe and mean of 4,055 USD/kWe. Table 1 provides an overview of nuclear generation costs for different technologies used in various countries [2].

The OECD 2010 study [10] assumption for the average lifetime load factor for calculating the levelized costs of nuclear generation is 85%. The load factor is an important performance indicator

measuring the ratio of net electrical energy produced during the lifetime of the plant to the maximum possible electricity that could be produced at continuous operation. In 2008, globally, the weighted average load factor reported for PWRs (a total of 265 reactors) was 82.27%, for BWRs (total of 94 reactors) it was 73.83%, with larger reactors (>600 MWe) exhibiting on average a 2% higher load factor than smaller reactors.

Table 1 Nuclear generation costs for different technologies used in various countries [2]

COUNTRY	NUCLEAR TECHNOLOGY	USD/kWe
Belgium	EPR-1600	5,383
Czech Republic	Pressurised Water Reactor (PWR)	5,858
France	EPR	3,860
Germany	PWR	4,102
Hungary	PWR	5,198
Japan	Advanced Boiling Water Reactor (ABWR)	3,009
Korea	Optimised Power Reactor (OPR-1000)	1,876
	APR-1400	1,556
Netherlands	PWR	5,105
Slovak Republic	WER	4,261
Switzerland	PWR	5,863
	PWR	4,043
United States	Adv Gen III+	3,382
Brazil	PWR Siemens/Areva	3,798
China	Chinese Pressurised Reactor (CPR-1000)	1,763
	CPR-1000	1,748
	AP-1000	2,302
Russia	WER-1150	2,933

The decommissioning costs of the nuclear power plants reviewed in this study have also been included in the levelized costs calculation. Where no country-specific cost figure was provided, a generic study assumption of 15% of the overnight cost has been applied to calculate the costs incurred during all the management and technical actions associated with ceasing operation of a nuclear installation and its subsequent dismantling to obtain its removal from regulatory control. In particular, the fact that for nuclear power plants decommissioning costs are due after 60 years of operation and are discounted back to the commissioning date, makes the net present value of decommissioning in 2015 close to zero, even when applying lower discount rates or assuming much higher decommissioning costs.

5.2.1 Long term plan - Screening curves of power plants

The screening curve technique is an approximate method that captures major tradeoffs between capital costs, operating costs and utilization levels for various types of generating capacity in the system. The screening curve method expresses the total annualized electricity production cost for a generating unit, including all capital and operating expenses, as a function of the unit capacity factor. This approach is especially useful for quick comparative analyses of relative costs of different electricity generation technologies. Figure 1 shows the screening curves for the reference discount rate (10%) scenario in our example. The results of the screening curve analysis indicate that the Nuclear and coal are suitable for base load operation.

In Screening of Candidate Plans fuel prices for thermal generation unit cost was: Crude Oil Price = 100 US$/bbl, Coal Price = 120 US$/tonne, Natural Gas = 10.1 US$/GJ [3-7].

The screening curves show the yearly cost of one firm kilowatt according to the load factor of the power plant and can show ranking of candidate projects. For a given load factor, we obtain the levelized cost of energy (LCOE) related to this load factor.

The candidates are categorized according to the type of supply they are designed for; either base load or peak load. Figure 1 show the screening curves for the discount rate 10%. The screening curves shows that nuclear plant are the most economically attractive for capacity factor higher than 43% in base case of 10% discount rate. In the case of 7% discount rate this is the case even for capacity factor for nuclear more than 36% and in the case of 12% discount rate this is the case for capacity factor for nuclear more than 50. As a conclusion, this means that the expansion plan designed by the WASP model will first resort to nuclear resources as far as possible. The capacity needed in addition to nuclear should be supplied by coal, natural gas and gas oil.

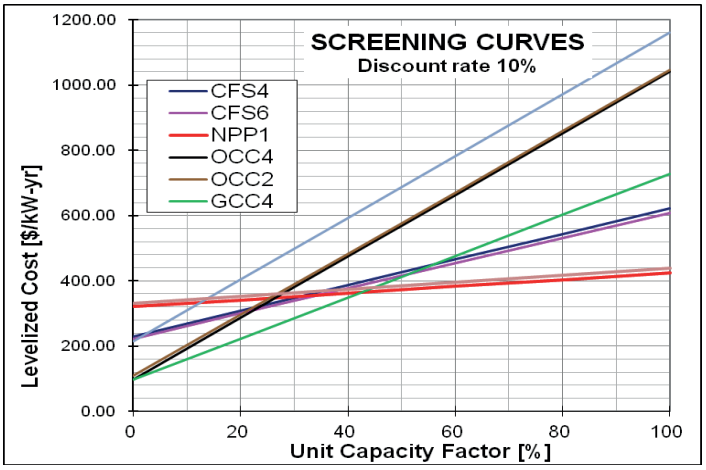

Figure 1 Screening of candidates at 10% discount rate

5.2.2 Long -term optimization: WASP Least Cost Expansion Plan Example

The objective of analysis in our example was is to analyze possible long-term development options of the small electric power system in the period for 30 years and to analyze possible introduction of nuclear power plant in relative near future. The analysis involved systems planning studies for the least-cost generation expansion planning. Very well-known and widely accepted computer model were used in the analysis: the WASP-IV model for the optimization of long-term system development [9].

In Least Cost Expansion Plan candidate generation resources considered in the system expansion plan include, hydro, coal, oil-fired, natural gas and nuclear power plants. The load forecast covers a period of 30 years. It sets out the following in Base Case Scenarios from year 1 to year 30 total increase of peak load in MW is around 19 GW (from 1 300 MW in year 1 to 20 600 MW in year 30) - Figure 2. During whole study period Load factor is 65 %.

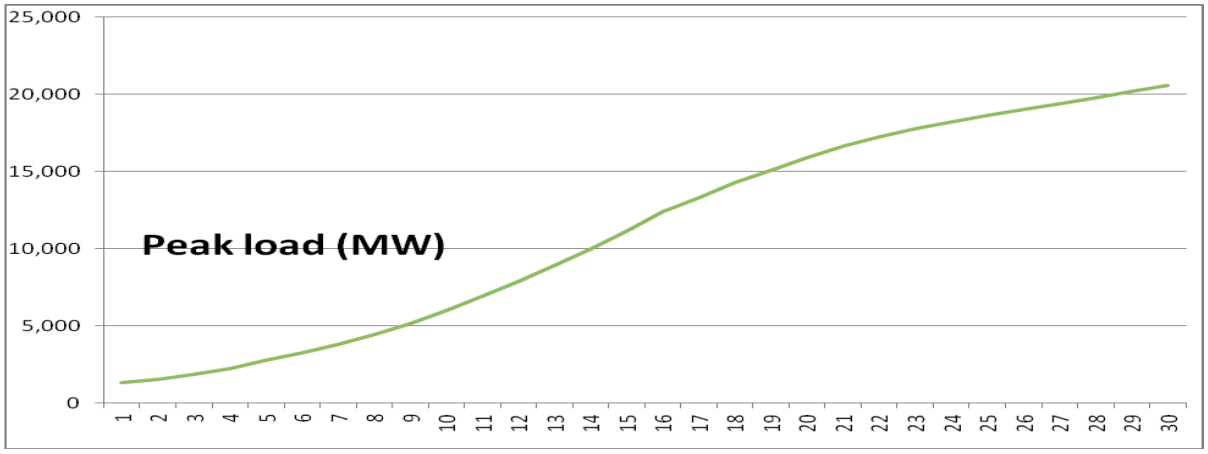

Figure 2 Peak load for whole study period

The candidate plats were: steam coal plants, nuclear power plants, gas oil combined cycle plants and natural gas combine cycle plants. For candidate thermal power plants were selected

following plants with net capacity (nuclear plant 600 MW just in some cases): Steam Coal plant 400 MW, Steam Coal plant 600 MW, Nuclear Power Plant 1000 MW, Gas oil combined cycle 470 MW, Gas oil combined cycle 210 MW, Natural gas combine cycle 450 MW, *Nuclear Power Plant 600 MW*.

For whole study period were used next fuel costs: Heavy fuel oil 4.3 US$/GJ, Gas Oil 15.2 US$/GJ, Diesel Oil 15.2 US$/GJ, Crude 16.1 US$/GJ, Imported coal 4.2 US$/GJ, HFO - future candidate 11.3 US$/GJ, Nuclear fuel 0.65 US$/GJ, Natural gas 10.1 US$/GJ [3-7]. LOLP-loss of load probability was 0.27% (1 day in year) from year 7. All costs were expressed in U.S. dollars. The discount rate applied for the present worth analysis was 10%, No real cost escalation was assumed for the fuels. The sinking fund depreciation method was used to calculate the salvage value of candidate plants committed during the study period. The economic loading order of existing and candidate generating units was used in all analyzed scenarios. The upper and lower values of the planning reserve margin were specified exceeding the peak load from 15% to 45%, in order to simulate every possible system configuration that can adequately meet the system demand and reliability constraints. Sensitivity studies were performed for different LOLP values, and the cases with no LOLP constraints were also examined. The energy-not-served (ENS) cost for the Base Case analysis was estimated at 1.00 $/kWh.

There were some constraints applied in all WASP simulations because to get realistic picture for candidate NPP 1000 MW: the first NPP is open in year 8 and, additional NPP as candidate in year 14, 19, 23 and 26; possible to add one natural gas combine cycle (NGCC) plant in year 16, 17, 20, 23, 26 and 29. In some cases there were two nuclear power plants as candidate NPP 1000 MW and 600 MW.

Figure 3 shows system load and WASP optimal solution for whole study period of 30 years in Base Case conditions. Figure 4 shows total capacity added in each year for whole study period. Figure 5 shows total capacity added in NPP in each year for whole study period.

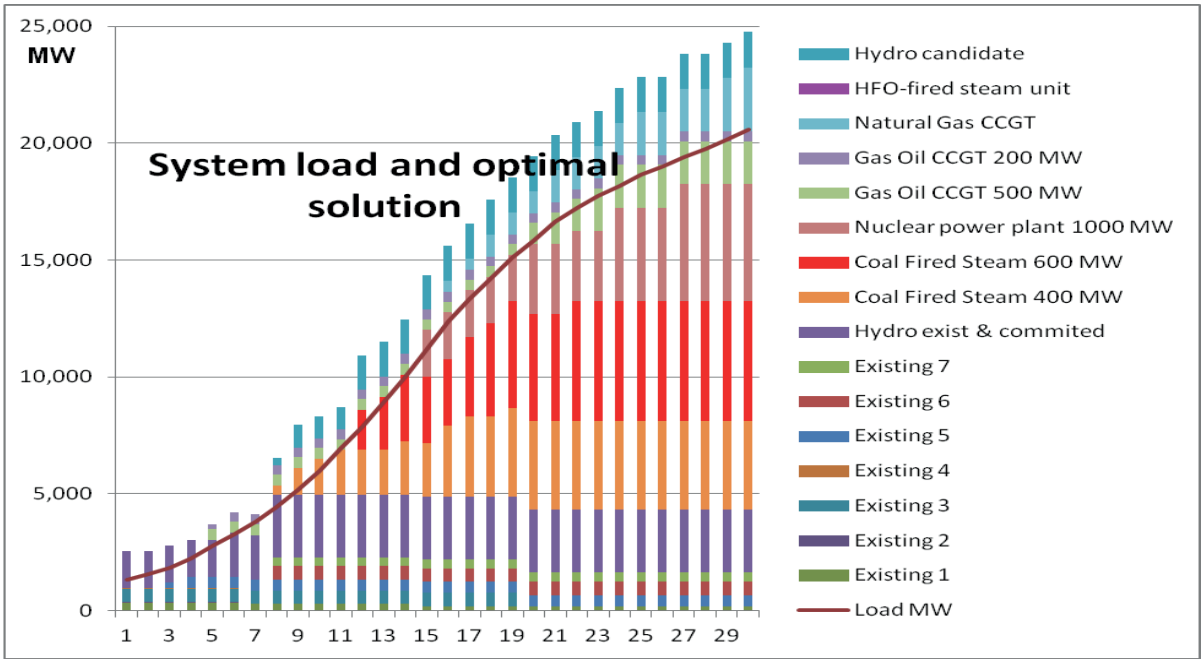

Figure 3 System load and WASP optimal solution for whole study period for 30 years in Base Case conditions

Some sensitivity analysis was done for some cases that have limitations on coal power plants: Limitations on coal new plants about total 3 000 MW for whole study period; Limitations on coal 1 plant in 2 year and total 3000 MW for whole study period; Limitations on coal new plants about total 3000 MW; no NGCC for whole study period; Limitations on coal 1 plant in 2 year and total

3000 MW; no NGCC for whole study period; Limitations on coal new plants, no new coal plants until 2024.

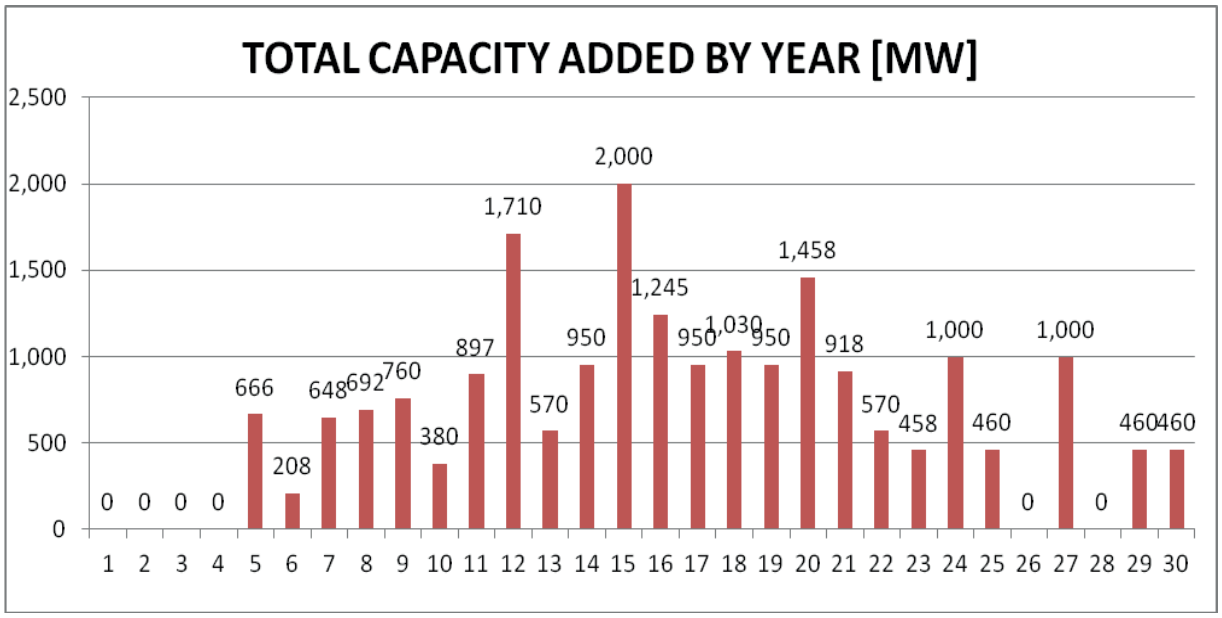

Figure 4 Total capacity added by year [MW] - BASE Case (MED)

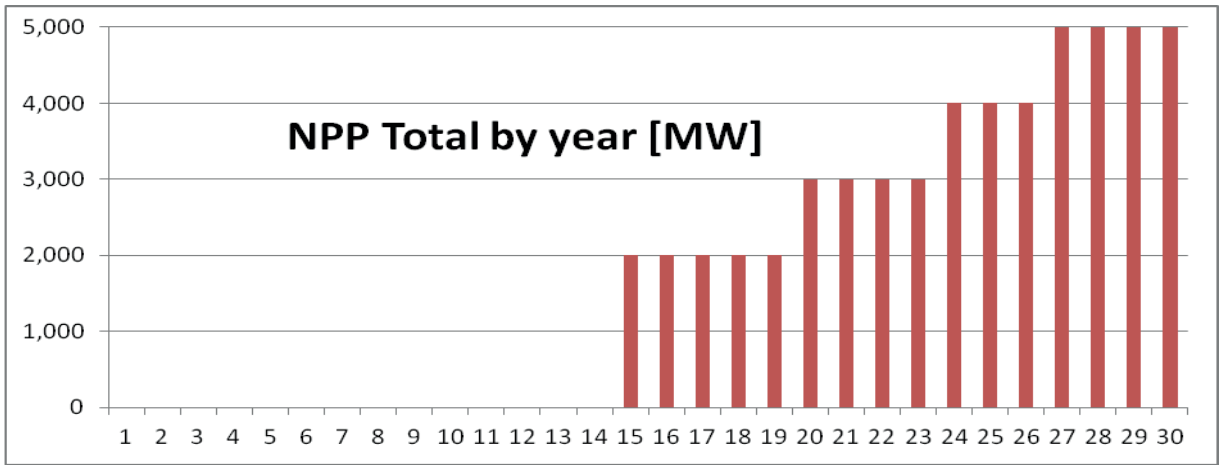

Figure 5 Total installed capacity in NPP by year [MW] - BASE Case (MED)

5.2.3 Some conclusions and comments from analysed example

Results from Base Case Scenarios in our example show:

- main competition for base power production is between nuclear and coal power plants
- in case that only candidate NPP is 1000 MW the first year of operation for the first unit is year 14
- in all cases after year 14 all five candidates NPP 1000 MW are selected in optimal solution at the end of study period
- in case that candidates NPP are 1000 MW and 600 MW the first year of operation for the first unit for 600 MW is year 9 for discount rate of 10% and 12% and year 8 in the case of 7%.
- in case that candidates NPP are 1000 MW and 600 MW the first year of operation for the first unit for 1000 MW is year 13
- in case that candidates NPP are 1000 MW and 600 MW the objective function and total costs of operation are less than in case when only candidate is NPP 1000 MW.

Conclusions from Base Case Scenarios under different constrains:

- in case of constraints on coal (new coal plants about total 3000 MW): the introduction of the first unit for 1000 MW NPP is year 12 (in base case is year 14)

- in case of constraints on coal construction of one plant in 2 year and total new plants 3000 MW: the introduction of the first unit for 1000 MW NPP is year 10 (in base case is year 14)
- in case of constraints on new coal plants about total 3000 MW: no natural gas plants-NGCC, the introduction of the first unit for 1000 MW NPP is year 12 (in base case is year 14)
- in case of constraints on coal construction of one plant in 2 year and total new plants 3000 MW: no natural gas plants-NGCC the introduction of the first unit for 1000 MW NPP is year 10 (in base case is year 14)
- in case of constraints on coal new plants about total 3000 MW and in case that candidates NPP are 1000 MW and 600 MW: the first year of operation for the first unit for 1000 MW is year 13, for 600 MW is year 9
- in case of constraints of forced the first 1000 MW NPP in year 9, the objective function is higher than in base case but not too much just less than 1%.

Results from Sensitivity on investment cost for NPP in Base Case Scenarios (NPP investment for values: 1700 – 4000 USD/kW) show:

- in optimal solution for base condition the first new 1000 MW NPP in year 14
- for NPP 1000 MW investment cost between 1700 and 1880 USD/kW the first new 1000 MW NPP in optimal solution is in year 11
- for NPP 1000 MW investment cost between 1890 and 3005 USD/kW the first new 1000 MW NPP in optimal solution is in year 14 and optimal solution is same like in base case
- for NPP 1000 MW investment cost between 3010 and 3400 USD/kW the first new 1000 MW NPP in optimal solution is in year 16
- for NPP 1000 MW investment cost above 3500 USD/kW there is no 1000 MW NPP in optimal solution

From this analysis can be seen that investment cost of 1000 MW NPP can influence optimal solution and this parameter is one of the most important in decision for introduction of nuclear option and must be define as soon as possible to make good decision for possible construction of nuclear power plants.

Results from Sensitivity on Constraints on coal new plants, different number of candidates until year 12 in Base Case Scenarios shows:

- number and year of introduction new coal candidate plant influence optimal solution regarding introduction of 1000 MW NPP
- if only two new coal plants are as candidate until 11 (after that 4 coal plants are candidates) the first 1000 MW NPP is in optimal solution in year 10
- any limitation to new coal plats until 12 introduce the first NPP is in optimal solution in year 10/11
- this analysis shows that policy regarding introduction of new coal plants should be carefully defined and this decision highly influence optimal solution for introduction of nuclear power plant 1000 MW

Results from sensitivity on increase base case investment costs for Coal Power Plants (increase for 100 to 700 USD/kW) in Base Case Scenarios:

- increase of base case investment costs for candidate coal power plants from 100 to 390 USD/kW do not influence optimal solution regarding 1000 MW NPP
- increase of base case investment costs for candidate coal power plants from 400 to 700 USD/kW has small influence to optimal solution regarding 1000 MW NPP and just introduce 1000 MW NPP one year earlier from 14 to 13.
- this analysis shows that investment cost of new coal plants does not too much influence optimal solution regarding introduction of nuclear power plant 1000 MW and that main factor in selecting new candidate power plant until year 14 is install capacity of candidate plant.

In almost all cases when candidate NPP was 1000 MW the first 1000 MW NPP in optimal solution was selected by model in year 14 and later in the year when it is next additional NPP available.

In cases when candidates NPP were 1000 MW and 600 MW the first NPP were selected by model mostly in year 10 or in some cases year before.

These are logical solutions for Least Cost Power Development Plan done by WASP programme because there is large capacity additions of committed thermal plants in year 6 and if we look to graph for system load in all cases and compare with existing installed capacity plus committed plants it can be seen that is no space for addition of large unit 1000 MW. In that cases program select coal power plants until there is enough large new demand.

Even nuclear power plant is selected by programme relatively late, screening curves show that nuclear is very competitive and in the cases with unit of 600 MW it is the best options. But the problem is in case of small load in our example and also because continues relative high growth (but still in absolute term low) and model is taking smaller unit to fill the gap and there is difficult to find place for large unit. Because of that after year 14 nuclear 1000 MW become the best options and model wants even more than five NPP.

Under the characteristics as selected for the study nuclear is competitive in simple comparison but in real power system it is not always optimal solution for small power system in case of large NPP units.

Results, under conditions defined in study, is very robust and changes in discount rate, investment cost of coal plant (should be more than 3000 USD/kW what is unrealistic) etc. do not change results. Finally, main conclusion from example is that nuclear option is economically feasible (even the best option) but in very small system that can be problematic for large unit of 1000 MW.

6 CONCLUSIONS ABOUT NPP FINANCING IN SMALL GRID

It is clear that strong and consistent government support is an essential prerequisite for initiating or expanding any nuclear power programme, as part of a long-term national energy strategy. Otherwise investors will be open to the risks of sudden policy shifts as governments change, potentially jeopardising their investment. Specifically, governments need to put in place an efficient regulatory framework, which allows appropriate opportunities for public involvement but allows clear and definite decision making within a reasonable timescale. Additional legal frameworks dealing with liability issues, radioactive waste management and decommissioning are also necessary.

Electricity market risks can be mitigated by long-term agreements with large consumers or electricity distributors. In some cases, direct involvement of such consumers in the structure of the project may be an attractive option.

Corporate finance is the most likely generally applicable model for new NPPs. Large, financially strong utilities will be best able to finance new NPPs especially if they are vertically integrated. They will be able to attract loans as required, backed by their existing assets. In countries where such utilities do not exist, the need for direct government support to share in the construction risks is likely to be all the greater. It appears that there is very little likelihood in the foreseeable future to finance a new NPP by using non-recourse or “project” financing (i.e. using only the NPP project itself as collateral).

It is important to note that the financing of an NPP need not remain static over its lifetime, and in particular that refinancing is likely to be possible once the plant has successfully entered operation. At that stage, with construction risks removed and with the plant expected to generate steady revenues over several decades, an NPP could be an attractive investment opportunity for investors with a long term perspective.

The important question examined in developing NPP project is which approach can be used to finance nuclear power plants to be compatible with current utility and financial market conditions and specially in country with small economy. Also deeper understanding of the risks involved in project finance and risks evolution over time is important for both practitioners and policymakers. In particular, further research in this area might help in the implementation of risk sensitive capital requirements providing market participants with the incentives for a prudent and, at the same time, efficient allocation of resources across asset classes.

Main competition for base power production is between nuclear and coal power plants

From analysis of presented example can be seen that investment cost of 1000 MW NPP can influence optimal solution and this parameter is one of the most important in decision for introduction of NPP and must be define as soon as possible to make good decision for possible construction of nuclear power plants. This analysis shows that investment cost of new coal plants (in reasonable range) does not too much influence optimal solution regarding introduction of NPP and that main factor in selecting new candidate power plant is install capacity of candidate plant in time when load is still small.

Even nuclear power plant is selected by programme relatively late; screening curves show that nuclear is very competitive. But the problem is in case of small load in our example and also because continues relative high growth (but still in absolute term low) there is need for new capacity optimal solution is taking smaller unit to fill the gap and there is difficult to find place for large NPP unit.

Under the characteristics as selected for the study nuclear is competitive in simple comparison (screening of candidates) but in real power system it is not always optimal solution for small power system in case of large NPP units. Conclusion from presented example is that nuclear option is economically feasible (even can be the best option) but in very small system that can be problematic for large unit of 1000 MW.

In developing NPP project should be identified the special circumstances for financing nuclear power project in relatively small economy.

REFERENCES

[1] INTERATIONAL ATOMIC ENERGY AGENCY, Draft report on Alternative Contracting and Ownership Practices for NPP, 2012

[2] INTERNATIONAL ENERGY AGENCY & NUCLEAR ENERGY AGENCY ORGANISATION FOR ECONOMIC CO-OPERATION AND DEVELOPMENT: Projected Costs of Generating Electricity, 2010 Edition

[3] Worldbank: Commodity Prices and Price Forecast in Current US Dollars, http://www.worldbank.org

[4] World Bank: COMMODITY PRICE DATA, 1818 H Street, N.W. , Development Prospects Group, Washington, D.C. 20433 U.S.A, http://www.worldbank.org/prospects/commodities

[5] World Bank: Commodity Markets Review, Number 119, 9 December 2011, www.worldbank.org/prospects/commodities

[6] JRC Institute for Energy: Coal of the Future (Supply Prospects for Thermal Coal By 2030-2050), Prepared for the European Commission – DG JRC Institute for Energy by Energy Edge Limited, February 2007

[7] World Energy Council: Performance of Generating Plant: New Metrics for Industry in Transition, World Energy Council *For sustainable energy.* Published 2010 by: World Energy Council, Regency House 1-4 Warwick Street London W1B 5LT United Kingdom

[8] INTERATIONAL ATOMIC ENERGY AGENCY, Expansion Planning for Electrical Generating Systems: A Guidebook, Technical Report Series, TRS 241, IAEA, Vienna (1988).

[9] INTERATIONAL ATOMIC ENERGY AGENCY, Wien Automatic System Planning (WASP) Package: A Computer Code for Power Generating System Expansion Planning, Version WASP-IV with User Interface

[10] Projected Costs of Generating Electricity, OECD, (2010)

Journal of Energy

VOLUME 62 Number 1–4 | 2013 Special Issue

journal homepage: http://journalofenergy.com/

Aging of Power Cables in Nuclear Power Plant due to Influence of Local Temperature Conditions

Irena Jakić
Hrvatska elektroprivreda d.d., Sustainable Development and Quality Management Department
Ulica grada Vukovara 37, 10000 Zagreb, Croatia
irena.jakic@hep.hr

Nenad Debrecin
Faculty of Electrical Engineering and Computing, University of Zagreb
Unska 3, 10000 Zagreb, Croatia
nenad.debrecin@fer.hr

ABSTRACT

A significant number of operating nuclear power plants (NPP) is approaching the end of the initially estimated design life. Considering that plants are stable and competitive, it may be possible to extend design lives to 60 years (perhaps even longer).

Before expending life time, ageing in NPPs must be effectively managed to ensure the availability of design functions throughout the plant service life. From the safety perspective, this means controlling ageing degradation and wear-out within acceptable safety limits so that adequate safety margins remain, i.e. integrity and functional capability in excess of normal operating requirements.

Even though cables are not active component, they are vital components in NPPs since they link the system components with instruments and control equipment used to monitor and control the plant. Consequently, the functionality of the cable necessary for nuclear safety is necessity for ensuring the functionality of equipment relevant to nuclear safety.

Since the cable ageing have been recognized as potential threat to safe operation of NPP, this paper deals with cable ageing aimed at identifying effects of aging and to determine whether the degradation caused by aging is within the stipulated tolerance limits. Also, it analyses the impact of ambient temperature changes on the cable ageing comparing to a qualified life. For an illustration, Arrhenius's model was used to calculate cable ageing in hot spot with the increased local temperature.

1 INTRODUCTION

Currently, there are 436 nuclear reactors in the world with a total of 370.5 MW of installed capacity in operation. The largest number of reactors started in 1970 and most of those had designed life expectancy of 30-40 years. These plants are approaching the end of the initial estimated life span, while working well and competitive. Therefore, there is interest in extending their time of exploitation. The reasons are primarily economic since the costs to extend the lifetime are minor compared with the capital costs of any replacement plants.

However, it is necessary to determine whether aging of the exposed components, structures and systems nuclear power plant can meet its intended design function in the case extending the life of exploitation. Aging equipment can be defined as a continuous, time-dependent degradation of the material. For nuclear power plant, operating conditions are difficult security requirements of the

I. Jakić, N. Debrecin, Aging of Power Cables in Nuclear Power Plant due to Influence of Local Temperature Conditions, Journal of Energy, vol. 62 Number 1–4 (2013) Special Issue, p. 33–44

accident situations. Equipment important to nuclear safety must be functional both in normal and anticipated transient operating conditions and in accident conditions that are caused by the events defined by the project (for example, loss of coolant, LOCA). Generally, the cables themselves are not active safety equipment; cables transmit signals for indication, control and management commands or energy to the equipment that performs a security function. Consequently, the functionality of the cables necessary for nuclear safety is to ensure functionality of the equipment relevant to nuclear safety. Functionality of cable is defined by continuous cable operations to maintain proper operation of equipment important to nuclear safety. This means that the cable must remain operational and accidental conditions of the end of its qualified life.

One of the major causes of cable aging is temperature; therefore, by monitoring the ambient temperature and understanding of the aging mechanisms, cable aging can be assessed and preventive action is possible.

This paper analyses the aging effect due to elevated ambient temperature and its influence on cable qualified life. For an illustration, Arrhenius's model was used to evaluate changes in the cable qualified life in relation to environmental conditions.

2 AGING OF CABLES

Cables inside the containment building of NPP are exposed to various environmental conditions of which the most important factors are temperature and ionizing radiation. The electrical cables in NPPs are also used over very long periods of time, which can typically reach 40 to 50 years. The three basic factors for ageing are therefore present and will cause ageing of the polymeric materials of the cables. The consequences of this ageing on the required functional capability of cables need to be considered.

Aging is defined as the gradual degradation of the physical characteristics that occur due to passage of time or work in conditions that may reduce the reliability or functionality. It turned out that the aging of the cable depends on the aging of electrical insulation, therefore the main object of interest electrical insulation. External jacket is not considered subject to aging assessment, since it is considered that the physical protection on primary isolation, although our situation is actually sheathed cables can be used as an indicator of primary isolation. Even more so, because the cable sheath is usually made of a material that is slightly lower than the basic properties of insulation, so they are visible on it before the negative environmental impacts (if any).

The external jacket and the insulating materials are formulated organic compounds. They are made of a basic polymer (a macromolecular chain obtained by multiple replications of a unitary monomer) or co-polymer and of additives which provide the material with specific properties. These additives are mainly protective agents (anti-oxidants, thermal stabilizers and fire retardants), mineral fillers, plasticizers, oil (used to aid manufacture of the material), pigments etc. Some complex compounds may contain up to ten or fifteen different constituents. Variations in formulation can affect both the activation energy and rate of thermal ageing and the maximum dose for radiation ageing.

3 CABLE SPECIFICATION AND ANALYSIS DOMAIN

One of the common reasons for decreasing the cable lifetime in nuclear power plants is the possibility of exposure to elevated temperature due to a fracture of fluid transfer system. Such event, analysed here, is the fracture of blow-down system (BDS) pipe which is above 6.3 kV power cable.

3.1 Cable specification

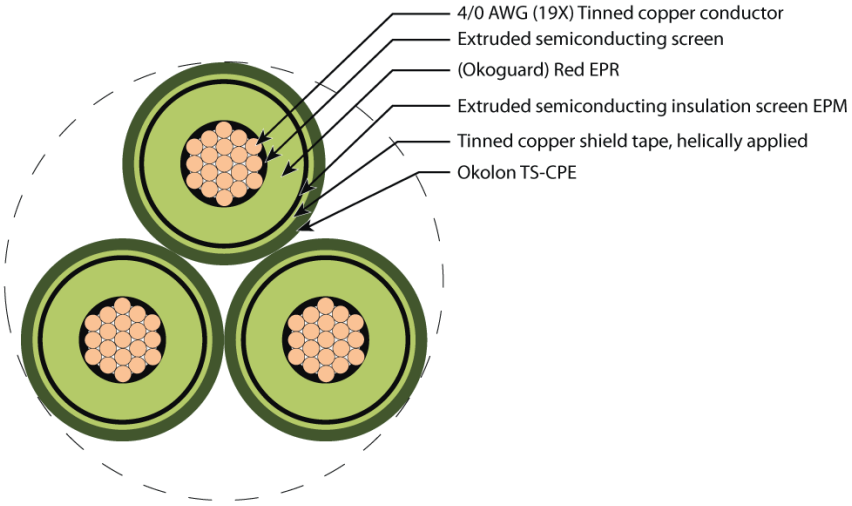

Figure 1 Cable configuration

Table 1Cable specification

Manufacturer	The Okonite Company
Voltage level	10 kV (6,3 kV)
Conductor	4/0 AWG (19X) Tinned copper conductor
Conductor screen	Extruded semiconducting screen
Insulation	Red EPR
Separator	Extruded semiconducting insulation screen EPM
Insulation screen	Tinned copper shield tape, helically applied
Separator	Tape
Jacket	TS-CPE

3.2 Analysis domain

The choice of the spot (IB-21) was based on the result from previous analysis (*Gothic* model developed to determine the environmental parameters) which showed the greatest impact on the ambient temperature increase.

Inside the room, two volumes were identified in the immediate vicinity of pipeline. Additionally, the subvolume (IB-21) includes a power cable. (Such a discretization was made to get better determination of the local conditions.)

For the purpose of analysis, dominant influence of mass transfer after opening the door to turbine building was examined. (The influence of heat transfer to the environment is limited.) All relevant concrete structures (walls, floor and ceiling) were part of the model. The equipment inside the premises was excluded. Thermal coefficient is defined assuming heat transfer by natural convection, depending on the orientation and type of surface and condensation on the surface. Thermal structure representing cable was added to the model. It was used pipe-type structure where the pipe wall is composite, consisting of an inner layer and the copper equivalent thickness of the outer insulation material. The copper is possible to have or not a source of heat due to ohmic heating. Additionally, surface of the cable can radiate heat, in exchange with the surface of BDS pipe. That impact is small on the total heating of the cable. Also, it can be significant for the local conditions (and for the formation of the overall temperature in the area of IB-21) in steady state.

First step in this analysis is calculation of the mass and energy content of the released fluid. For this purpose, simplified BDS model is added to the existing *RELAP5* model. It is assumed that total cut of the BDS pipeline (pipeline is 10m long and its outer diameter is 3in. (76.2mm)) which is

isolated manually after 1800s. Insulation of the pipeline is neglected in the calculation to gain a greater temperature rise. Figure 2 shows the mass flow of water and steam after the cut.

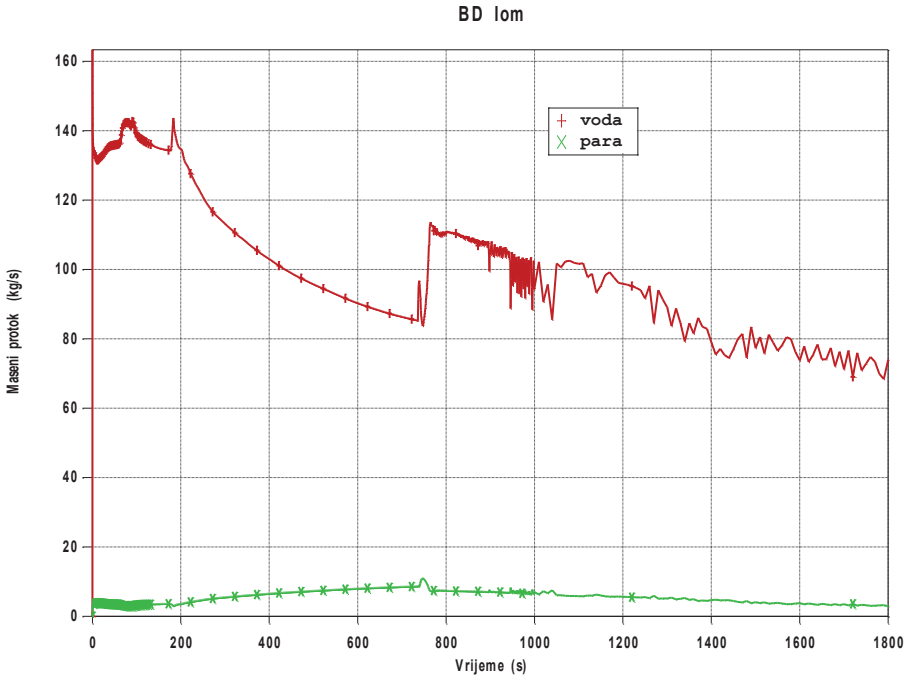

Figure 2 Mass flow (water and steam)

These data are used as boundary conditions to define disorder in the *Gothic* model. Assumed initial parameters of the premises are 40˚C and 60% relative humidity, at atmospheric pressure. The maximum design temperature in these areas was used as the ambient temperature when selecting equipment for installation in the room (hence the scaling and qualification of electrical cables).

Two scenarios were analysed, operating and non-operating cable. The calculation was carried out for over two days which is approximately the time during which environmental conditions should return to normal without any additionally treatment related to ventilation.

Short-term increase of the air temperature (Figure 3) has no effect on cable heating and insulation aging, but can lead to immediate failure of the cable if the temperature is too high and continues long time. The maximum ambient temperature is about 150˚C (Figure 4). The design temperature used to determine the maximum power load cable is 40˚C.

Visible is the difference in the cable temperature depending on whether there is an internal heat source (operating cable) or the cable is only heated due to pipeline fracture (non-operating cable).

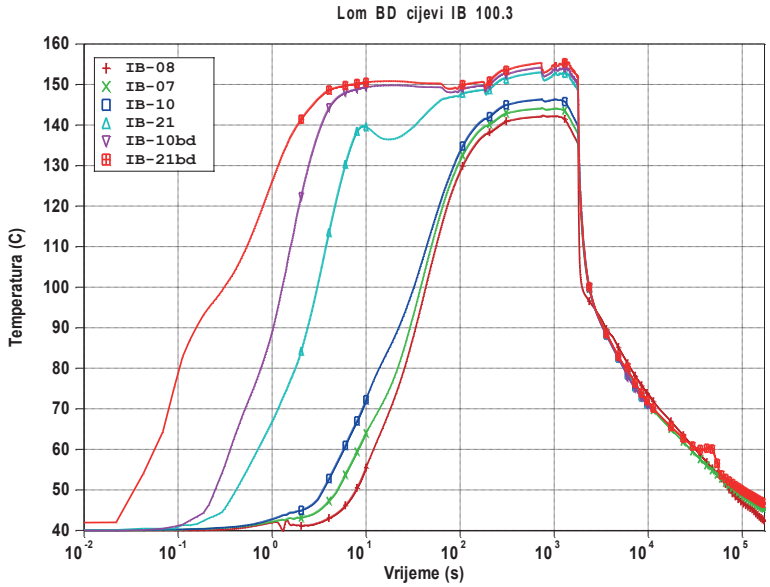

Figure 3 Distribution of the air temperature during BDS pipeline fracture

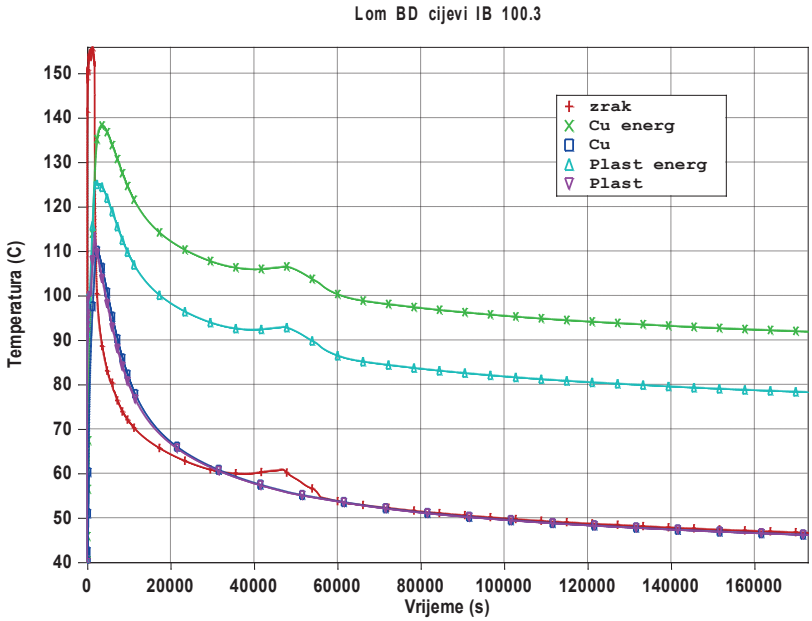

Figure 4 Distribution of the cable temperature (conductor and insulation)

4 CALCULATION OF CABLE HEATING

First step was the analysis of the steady-state conditions for which *ALGOR* (program for Finite element method, FEM) was used. In this model, cable is divided in four sectors to facilitate the assignment of boundary conditions which take into account the different convective heat transfer and spatially dependent radiate heat transfer from the pipeline.

Since the thickness of the copper shield, about 0.13 mm, the average length of the final element is set on 0.1 mm. The area is covered with a homogeneous quadrilateral mesh of linear elements using an automatic mesh generator. The total number of nodes is 84.934, and the total number of finite elements is 84.362.

Steady-state linear analysis was performed (ambient temperature was set on default value, 40°C and convective heat transfer coefficient from the surface was 6W/m^{2}K; only resistive losses of the conductor were taken into account). Results are shown Figure 5

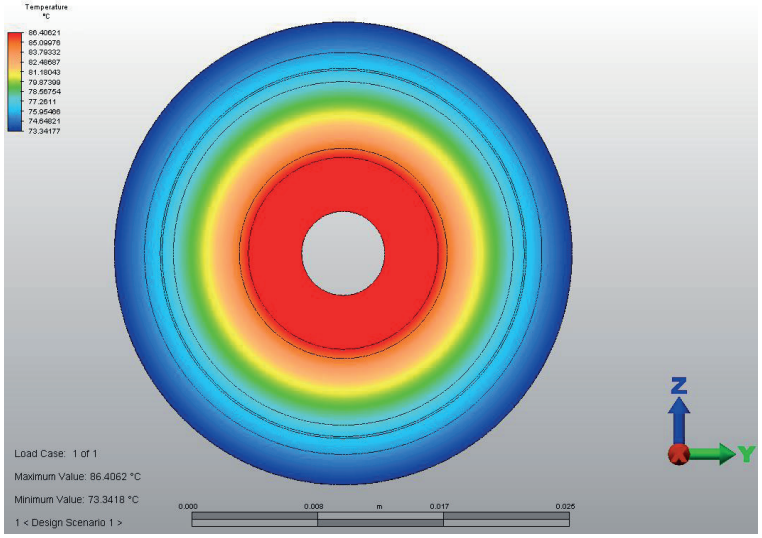

Figure 5 Distribution of operating cable temperature, nominal current

Obtained temperature distribution is completely symmetric and can be obtained by 1D calculation. In reality, the three cables in specific configuration do not have the same cooling conditions, nor individual conductor do not have equal convective heat transfer from the upper and lower surfaces. As an illustration, Figure 6 shows the temperature distribution in the cable where the heat transfer coefficient convection in the upper half of the 6W/m^{2}K, and the one with the lower half is 3W/m^{2}K (this situation corresponds to the cable laid on the poorly conducting surface).

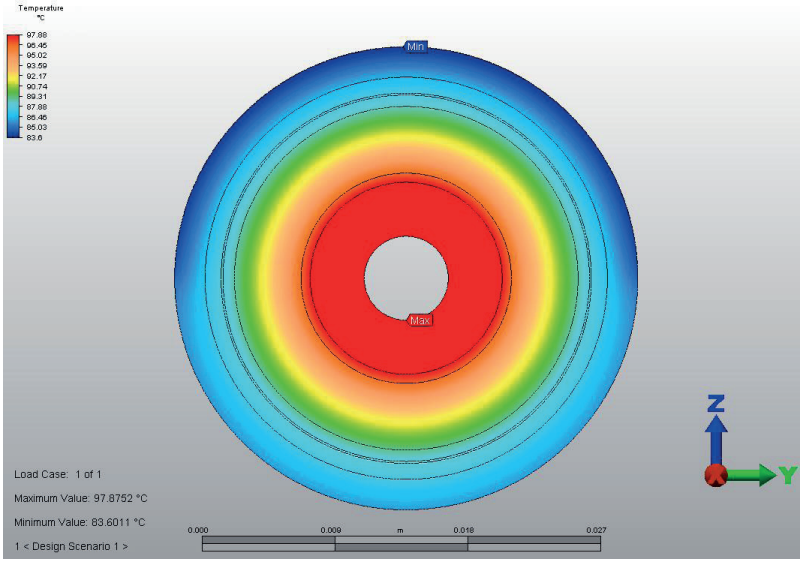

Figure 6 Distribution of operating cable temperature, nominal current where lower part of the cable has lower heat transfer coefficient

In order to conservatively estimate the possible radiate cable heating due to BDS tube above it, it was assumed that the tube has no insulation and outside diameter temperature is constant 260°C. The problem is due to transfer heat very nonlinear. The formula gives the heat transferred from the pipe, and the visible surface.

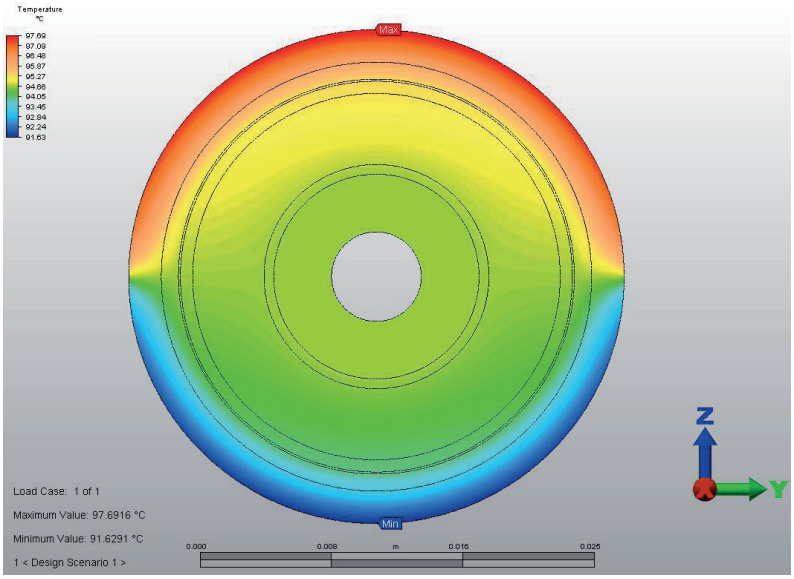

Figure 7 Distribution of non-operating, upper-placed cable temperature

5 ARRHENIUS'S MODEL

Once the actual temperature conditions and possible deviations from design conditions are established, we analyse impact it has on the design life of the cable.

Arrhenius's law (Eq. 1) is often used as a physical model for lifetime prediction during thermal ageing. It assumes that the rate of the thermal ageing mechanism decreases with the inverse of the temperature, such that the rate constant k can be described by the following equation:

$$R = Ce^{-E_a/kT} \tag{1}$$

C – Constant,
k – Boltzmann constant [8,617343·10^{-5} eV/K],
E_a – Activation energy [eV],
T – Absolute temperature [K].

Based on probability theory, middle time to failure is defined as shown in Eq.

$$MTTF = \int_0^\infty t \cdot f_\tau(t)\,dt \tag{1}$$

and if using Arrhenius's law, middle time to failure is

$$MTTF = \tau = \left[A \cdot \exp\left(-\Phi/kT\right)\right]^{-1} \tag{2}$$

The Equations (2) is usually used for correlation of two different lifetime, depending on different temperatures

$$\frac{MTTF_1}{MTTF_2} = \frac{t_1}{t_2} = e^{\left[\frac{\Phi}{k}\left(\frac{1}{T_1}-\frac{1}{T_2}\right)\right]} \tag{3}$$

If we understand relations that exposure of the material with an activation energy Φ temperature T_2 during the time t_2 has degrading effect equivalent to the exposure to the temperature T_1 over time t_1, we can estimate the impact of a history of exposure to the temperature to changes of the lifetime of a designed temperature. It should be noted that the Arrhenius law can be applied only to the slow and long-term degradation processes that do not involve exposure to extreme conditions

that can cause immediate failure. Nevertheless, form of the above equation can be used to split continuous time interval t_2 down to smaller intervals and in this way can be approximately taken into account exposure to fluctuating temperatures. The relation enables the reduction of each individual impact on the reference temperature. Incorporating a simple application in the programming language Fortran 90, can load an arbitrary time dependence of temperature or can be manually entered to simulate an operational history. Program, by seeking file name with the time dependence of temperature, read a free format and automatically determine the size of the required fields. In addition, it is necessary to enter the temperature for which the initially designated lifetime is and the whole calculation will be reduced to the calculation of equivalent effect. The activation energy needs to be entered and measuring temperature unit must be set (C, K or F). The program converts temperature into absolute temperature [K]. It is important that the time dependence temperature and design temperature are the same units since they are transformed in the same way the absolute temperature.

Program find the average temperature for every two consecutive time points and calculate the cable lifetime as if the cable is exposed to constant high temperature within that time step. Arrhenius's relation is used to determine the equivalent time that would cause the same degradation temperature at the designed temperature for the actual time interval t_2 and temperature T_2.

Equivalent time is saved in the first output file as a function of real time. Then total exposure time equivalent to the transient and the time that would produce the same effect on the design temperature. Remaining lifetime is designed lifetime for given temperature reduced for the equivalent time for designed temperature in that time interval. Shortening life expectancy is given as the difference of the equivalent time and real time spent the time-dependent temperature. The program actually calculates equivalent exposure time on designed temperature for each real time of exposure to specific temperature.

If the equivalent time is greater than the real-time it means that the actual temperature conditions are worse than the design and that we need a longer exposure to the design temperature to achieve the same adverse effect. Usually, we know the qualified lifetime of the designed temperature and determine the appropriate period of time at a different temperature. Here, we know the actual time spent on an actual historical temperature and calculate the equivalent of time spent on the design temperature.

6 RESULTS

The program was tested for three simple constant temperature profiles. In the first case, the cable worked 40 years at 90˚C and it is also the projected lifespan of the cable insulation and the design temperature. In the second case, the cable was exposed to a temperature of 100˚C for 40 years and the third case, the cable was exposed to a temperature of 80˚C for 40 years. The first history of the project corresponds to the situation, and the equivalent time is no different from the actual exposure time and the curve is inclined at 45˚. In the second case when the cable is exposed to temperatures greater than designed and equivalent time grows faster (steeper than 45˚). For the cable operating for 40 years at 100˚C, calculated equivalent time is 111 years of design temperatures. (Figure 8, Figure 9 and Figure 10)

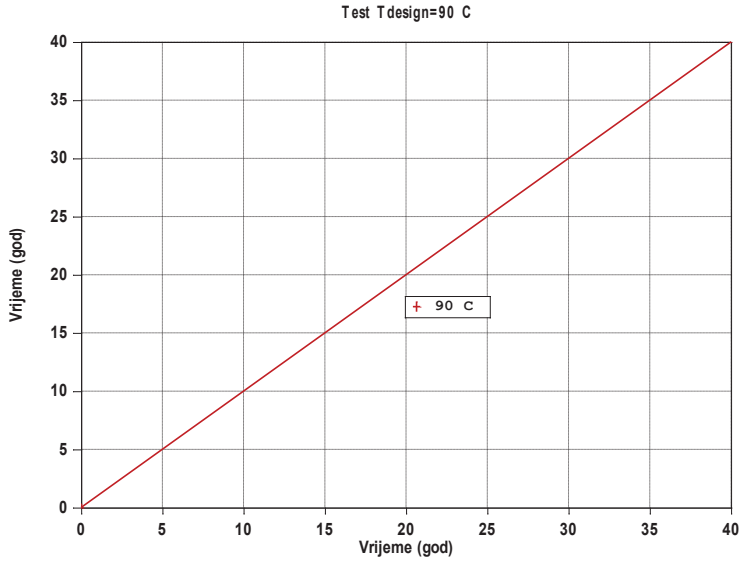

Figure 8 Equivalent time of exposure to designed temperature

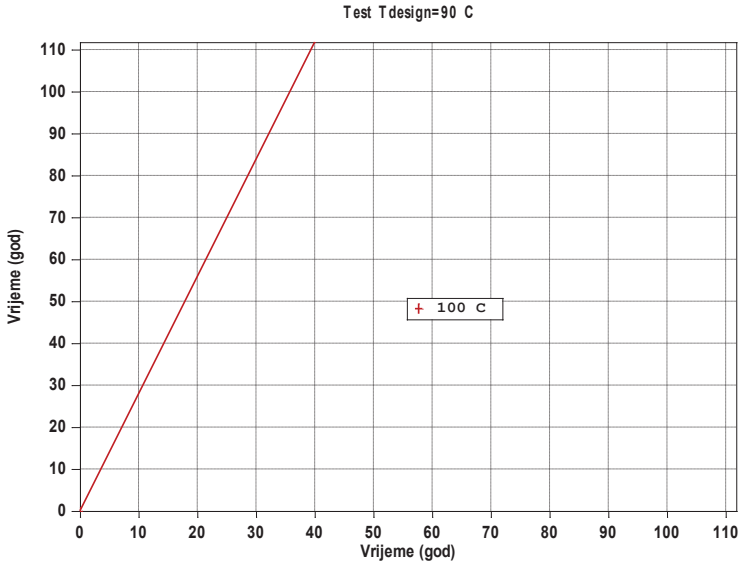

Figure 9 Equivalent time of exposure to temperature higher then designed

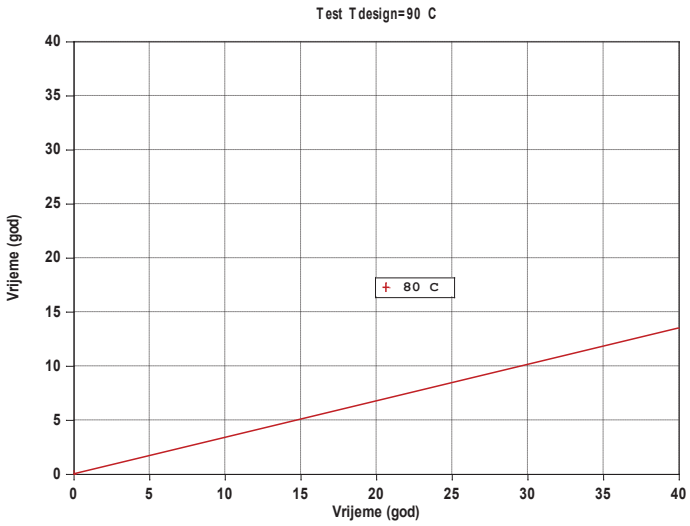

Figure 10 Equivalent time of exposure to temperature lower then designed

I. Jakić, N. Debrecin, Aging of Power Cables in Nuclear Power Plant due to Influence of Local Temperature Conditions, Journal of Energy, vol. 62 Number 1–4 (2013) Special Issue, p. 33–44

Arrhenius program was implemented to assess the effects of cable heating during the BDS pipeline fracture on qualified lifetime.

In Figure 11, the three historical profiles of temperature are shown (previously calculated by *Gothic*) that are used to assess the effects of aging. Profile marked with a temperature of Cu is scenario of cable in operation during BD fracture. The other two profiles are temperatures of the cable jacket in operating and non-operating state during the same transient. The reference temperature in all cases is 90˚C as the temperature of cable in continuous operation and as such is supposed to be used for defining the life span.

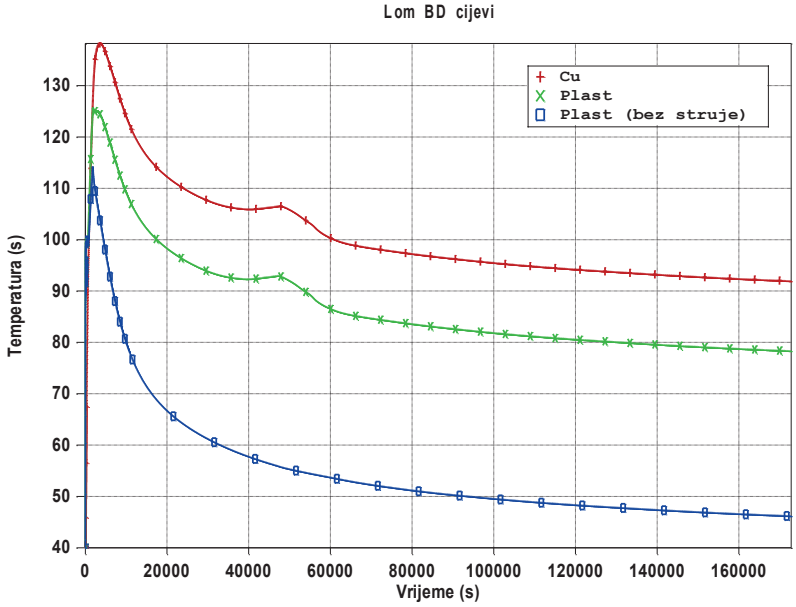

Figure 11 Cable temperatures for different scenarios

In Figure 12 shows the equivalent time of exposure to the designed temperature for the three considered profiles of temperature that can cause aging.

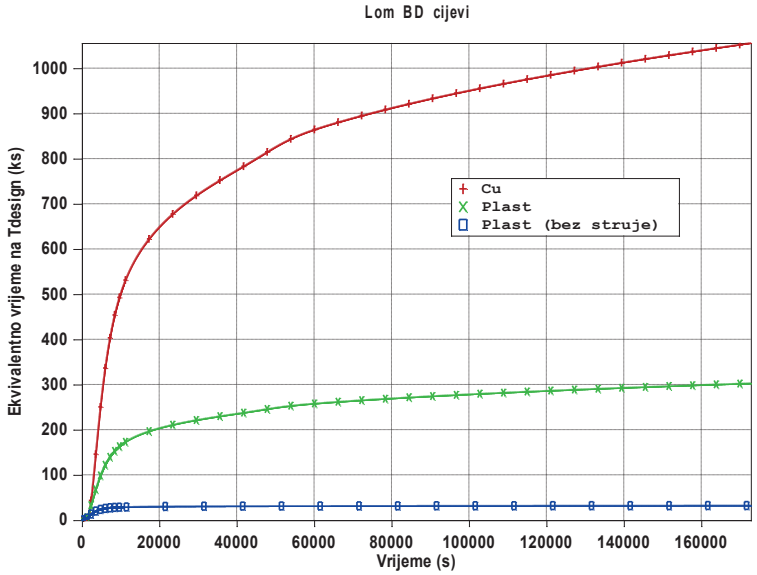

Figure 12 Equivalent time of exposure to cable temperature for different cases

Figure 13 shows shortening of cable lifetime compared to qualified life on designed temperature and Figure 14 presents data relatively, in percentage of qualified lifetime. Negative values correspond to extension of time and indications are that the cable is loaded less.

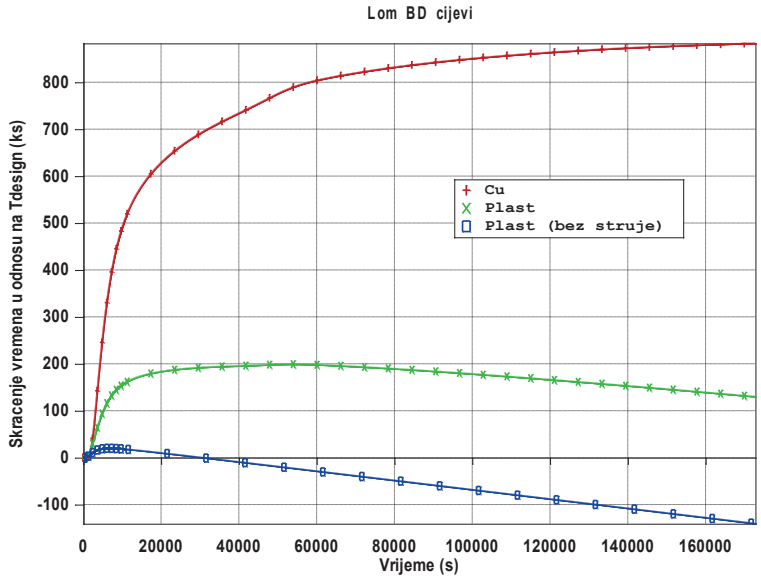

Figure 13 Lifespan changed due to increased cable temperature

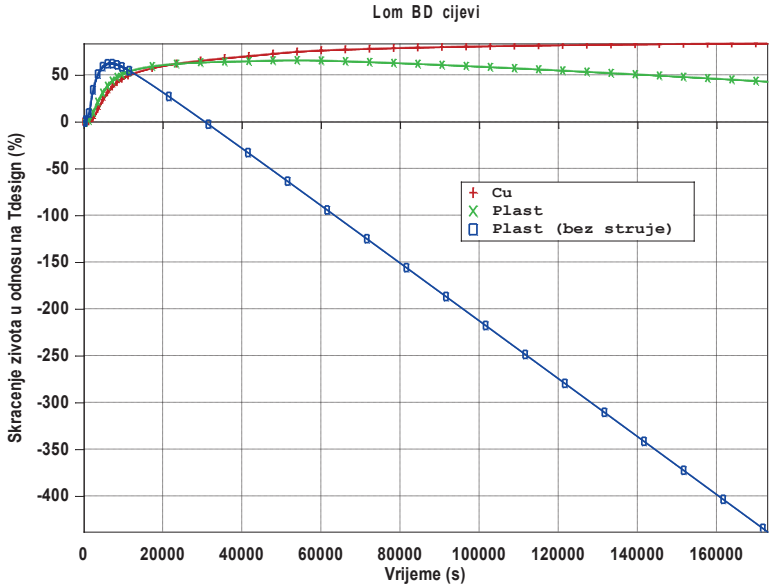

Figure 14 Lifespan changed due to increased cable temperature, relative

The meaning of the application is determination of the equivalent time of exposure to design temperature. The difference of the equivalent and real-time is the shortening of life span because the cable has spent more time on the design temperature than the actual length of exposure. In this case, cable was exposed to adverse environmental conditions for relatively short period of time.

If we were able to define the time dependence of the temperature of isolation from the moment of putting cable into operation until the present time, the described procedure could calculate the proper time spent on the design temperature. If obtained time subtract from qualified life, we would get the remaining time of the cable, on designed temperature.

7 CONCLUSION

Evaluation of cable aging is an important nuclear safety indicator and therefore, it is justified to analyse various potential events or situations that may reduce the lifespan of the energy cable.

Calculation described can be used to determine the local temperature in the steady state and the temperature rise during an unplanned event. Obtained results were input data for the estimation of effects on life expectancy using a simple model based on the Arrhenius equation. Scenarios for calculation were combination of events (normal operation and fracture of a BDS pipeline) for the different initial conditions of the cable (operating and non-operating cable).

The results show that the cable is functional for the entire projected life in all proposed combinations, except in the case of pipe fracture during operating cable. Given the role and function of the cable (cable supply safety pumps and is not expected to work in normal operation), respectively, cable load is very low, it can be concluded that it is not probable to lose the functionality of this cable. However, it should be checked if radiate heat exchange with BDS pipe can cause damage or reduce its effective life. Although the simplifications were introduced in the analysis and assumptions, it was not expected to have a significant impact on the final results.

From a security standpoint, it is useful to analyse possible hot spots and/or transient states with significant impact on worsening the environmental conditions.

REFERENCES

[1] International Atomic Energy Agency, “Procedures for Conducting Common Cause Failure Analysis in Probabilistic Safety Assessment”, IAEA-TECDOC-648, 1992

[2] International Atomic Energy Agency, “Management of ageing of I&C equipment in nuclear power plants”, IAEA-TECDOC-1147, Vienna, 2000.

[3] International Atomic Energy Agency, “Assessment and management of ageing of major nuclear power plant components important to safety: in-containment instrumentation and control cables”, volume I & II, IAEA-TECDOC-1188, Vienna, 2000.

[4] Electric Power Research Institute, “Aging Management Guideline for Commercial Nuclear Power Plants – Electrical Cable and Terminations”, EPRI, 1996.

[5] Electric Power Research Institute, “Power Plant practices to Ensure Cable Operability”, EPRI Report Summary, 1992.

[6] Electric Power Research Institute, “A Review of Equipment Aging Theory and Technology”, EPRI NP-1558, Final Report, 1980.

[7] United States Nuclear Regulatory Commission, “Essential Elements of an Electric Cable Condition Monitoring Program”, NUREG/CR-7000, USNRC, 2009.

[8] Institute of Electrical and Electronics Engineers, “IEEE Guide for Assessing, Monitoring and Mitigating Aging effects on Class 1E Equipment used in Nuclear Power Generating Stations”, IEEE Std 1205-2000

[9] Institute of Electrical and Electronics Engineers, “IEEE Standard for Qualifying Class 1E Electric Cables and Field Splices for Nuclear Power Generating Stations”, IEEE Std 383™-2003 (Revision of IEEE Std 383-1974)

Journal of Energy

VOLUME 62 Number 1–4 | 2013 Special Issue

journal homepage: http://journalofenergy.com/

Use Of Micro-Void Content Growth Rates To Validate And Add Value To Electrical Insulation Tan-Delta Aging Testing

David A Horvath, PE and Greg M Hostetter, CAPM
Tetra Tech Advent
PO Box 555, Ann Arbor, MI 48106-0555, USA
david.horvath@tetratech.com, greg.hostetter@tetratech.com

ABSTRACT

Our research as well as others has shown that micro-void content in electric insulation polymers grows in a way that can be correlated to the degree of aging. Specific results of our experiments combined with research by others have led us to conclude that a promising technique for predicting remaining life in electric cable insulation, based on micro-void content and proximity to void limiting parameters, can be developed.

This approach involves use of acoustic or optical microscopy to establish an estimate of void content in polymers by determining micro-void sizes and density. Separate research is used to establish limiting values for percent void content correlating to material failure. The mode of failure varies depending on the applied voltage regime. For example, at medium and high voltage levels, partial discharge detection can be considered indicative of pending end of life. Whereas for low voltage regimes, brittleness to the point of cracking susceptibility would allow the potential for moisture ingress and shorting and can be considered end of life. It has been separately shown that void growth rate is a function of temperature and radiation dose rate both during normal and nuclear accident conditions and is predictable based on the known polymer chemical degradation equations, which produce gaseous products in the form of oxygen, water vapor, carbon dioxide, and carbon monoxide.

Thus if end of life void content is known, the degree of void content growth occurring during a design basis accident is properly accounted for, and void content growth rates during normal temperature and radiation conditions are considered, then remaining life in electrical insulation can be accurately predicted. In recent years, several techniques have been proposed to assess electrical insulation aging. One of the more promising approaches for use with medium voltage cable is the tan-delta technique. This paper will demonstrate how the mirco-void content approach can be used to validate other techniques such as tan-delta and add additional meaning and value not otherwise available from tan-delta alone.

1 INTRODUCTION

Electric cable is an important component of nuclear power plants because of its unique ability and need to convey power as well as signals for instrumentation and control. If a nuclear power plant is intended to function beyond its license term of typically 40 years, it becomes necessary for critical components to be assessed or monitored for deleterious aging effects. Such critical components include electric cable used in safety-related and other essential applications such as power generation, fire protection, accident monitoring, and plant security. With regard to aging of electric cable, nuclear power stations have many unique considerations such as:

- tens of thousands of installed cable making complete replacement impractical,
- many areas inaccessible for inspection or testing for periods of time of 18 months or more,

D. A. Horvath, G. M Hostetter, Use Of Micro–Void Content Growth Rates To Validate And Add Value To Electrical Insulation Tan–Delta Aging Testing, Journal of Energy, vol. 62 Number 1–4 (2013) Special Issue, p. 45–53

- multiple cable manufacturers representing diverse insulation system jacket and dielectric material combinations, and
- concurrent temperature and radiation aging during the plant's normal life license term.

In addition, for a limited number of essential equipment cables, continued operability is required during a harsh environment assumed to occur at the end of the plant's license term. This harsh environment (an accelerated aging period) is postulated to be caused by a design basis event such as a major steam system pipe break and can produce elevated levels of temperature, pressure, radiation dose, humidity, and possibly even chemical spray.

The weak limiting subcomponent of electric cable is its dielectric insulation. Thus it is desirable to be able to monitor aging degradation of electrical insulation while allowing margin (remaining life) for some accelerated aging to occur during a postulated design basis event.

In this paper we will describe how electric cable insulation health may be characterized in terms of micro-void content and consider how such micro-voids may be detected based on an update of our earlier research. [1, 2, 3, and 4] Then the micro-void content approach is used to validate or supplement how tan-delta assesses cable insulation aging and can assist in a theoretical way to predict remaining life of electrical insulation.

2 ELECTRICAL INSULATION "HEALTH" AND REMAINING LIFE AS A FUNCTION OF MICRO-VOID CONTENT

2.1 What is End of Life for Electrical Insulation?

As with most industrial facilities, nuclear stations contain power, instrumentation, and control cables. The end of life for a power cable (normally energized at or near rated voltage and at an appreciable amount of electric current) would typically be based on preventing significant partial discharge to the point where reliable current carrying functionality is affected.

End of life for instrument and control cable is based on preventing excessive leakage current such that instrument accuracy or controlled equipment operation is detrimentally affected. Such conditions can occur when the insulation becomes hard or brittle and subject to cracking and moisture ingress during a postulated design basis event.

In both cases, margin to end of life must be confirmed for the license term (40 years in the US but shorter and/or longer time frames exist in some other countries). This paper will focus on medium voltage power cable assessments but similar approaches can be used to assess proximity to embrittlement in ways similar to how margin to prevent unacceptable partial discharge is outlined below.

2.2 Void Content as an Indicator of Insulation "Health"

Discharges within cavities (voids) in solid insulating systems has long been associated with gradual degradation and eventual dielectric failure. Studies by the C. Laurent and C. Mayoux of Laboratoire de Genie Electrique [5] have shown that gas-filled cavities (or voids) can originate in a wide range of solid dielectric systems through many mechanisms including differential thermal expansion, incomplete impregnation or excessive mechanical stress, or improper process control. Such cavities can originate during the manufacturing process or over a lifetime of operation as a result of environmental and operational stresses. Progressive deterioration caused by discharges in gas filled cavities has long been known to be a major factor limiting the life of cables. [6]

Voids will grow in size and the void density will increase as a function of energy absorption (heat, radiation dose, electrical field induced stress, etc.). The insulation's polymer structure consists of long, intertwined molecular combinations of carbon, hydrogen, and oxygen atoms. When the polymer absorbs energy while in the proximity of oxygen or ozone, radicals and various gases are produced. The resulting chemical reaction products include carbon dioxide, carbon monoxide, water vapor, and other volatile gaseous molecules. Some or many of these gaseous

reaction products will create new void sites or accumulate in nearby voids contributing to an increase in density and size in a manner which will, therefore, be a function of the cable's insulation aging degradation rate.

It is also possible that voids would additionally be formed from physical rearrangements of the molecules due to crystallization from aging. The voids distributed throughout the insulation structure will increase in size and the polymer structure of the material will weaken. The result is that the net or equivalent amount of insulation between the separated conductors decreases. A point will be reached at which partial discharge and/or voltage breakdown between nearby conductors of high potential can occur.

As the void content increases with age, the equivalent remaining thickness of the insulation reduces to a point where a breakdown (discharge) can occur. The limiting equivalent remaining insulation thickness that is just large enough to prevent breakdown can then be determined. By modeling the void growth from service condition factors (including post-nuclear accident harsh environment effects), the remaining life can be accurately predicted. It will be necessary to determine by experimental test at what void content (for a given insulation material) end of life occurs.

For a given temperature, the production rate for each single gas molecule product should be approximately constant. Using the ideal gas law, the rate of increase in the volume occupied by that gas (assumed to accumulate in the voids) will be directly proportional to the gas molecule production rate, which is a constant for a given temperature. Therefore:

$$dV/_{dt} = K \tag{1}$$

$$dV = Kdt \tag{2}$$

$$V(t) = Vo + Kt \tag{3}$$

Where:

V = Volume occupied by voids
t = Time
K = experimentally determined constant
Vo = Volume at t = 0

If the voids are modeled as approximately spherical and the void size increase effect dominates over the density increase effect as expected then:

$$V(t) = \frac{4}{3}\pi r^3 n \text{ , then} \tag{4}$$

$$Vo + Kt = \frac{4}{3}\pi r^3 n \tag{5}$$

$$r = [3(vo + Kt)/4\pi n]^{1/3} \tag{6}$$

Where:

n = number of voids
r = equivalent radius of each void.

Therefore, the size of the voids will approximately follow the cubic root of the elapsed time which perhaps explains the long life, in general, of electric insulation. This relationship assumes no pressure build-up in the voids and no leakage of gases from the insulation medium. These two

considerations would further reduce the void size increase rate but allows the above relationship to be conservatively high for modeling purposes. This approximation is also simplistic in that it does not account for the accelerated growth, which occurs near end of life from space charge build-up and self- heating effects. [7]

As a first-order approximation, it is expected that the gaseous production rate will be a linear function of temperature, which allows a determination of void size growth rate for different elevated temperatures. It is expected that early in life, void density will increase and then level off as a sufficient number of gas collection sites are created. After a certain point, long before the onset of any degradation of concern, the dominant factor will be void size growth.

More accurate computer modeling can be accomplished by considering multiple gaseous production reactions and gaseous loss rates and by calibrating via use of experimental test results.

Research by C. Dang et al [8] and A.C. Gjaerde [9] summarize advantages and disadvantages of current aging models including theories, multifactor effects and validating data. Relationships deduced from these aging models include a decrease in insulation life when:

- applied electric field goes up,
- applied electric field frequency goes up,
- increased exposure time to moisture,
- increased residual stresses (thermal, electric, mechanical),

Also, for increased exposure to moisture, the applied voltage to cause breakdown decreases. Each of these relationships can be correlated with increasing void content and computer modeled with the aid of experimental calibration.

3 VOID CONTENT MONITORING AND CORRELATION TO REMAINING LIFE

3.1 Void Detection

Previous research results [1] have confirmed successful void detection and imaging of electric insulation void size and density using dissected samples and imaged using either an optical or electron microscope. Figures 1 and 2 provide two views of micro-voids of various sizes (0.3 to 12 microns) within aged polyethylene electric cable insulation.

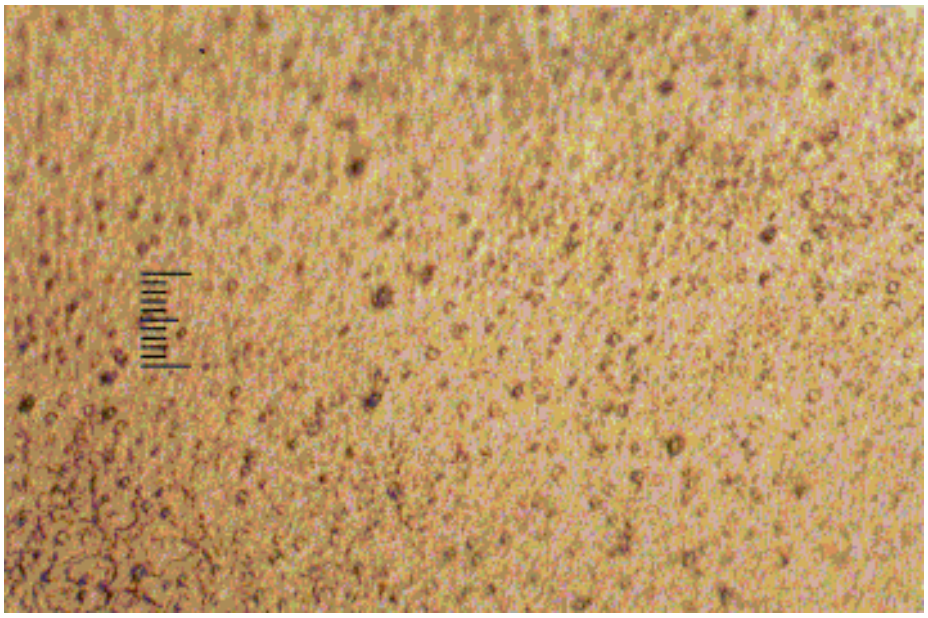

Figure 1: Sample 1 (Aged Polyethylene) Using an Optical Microscope at 500X

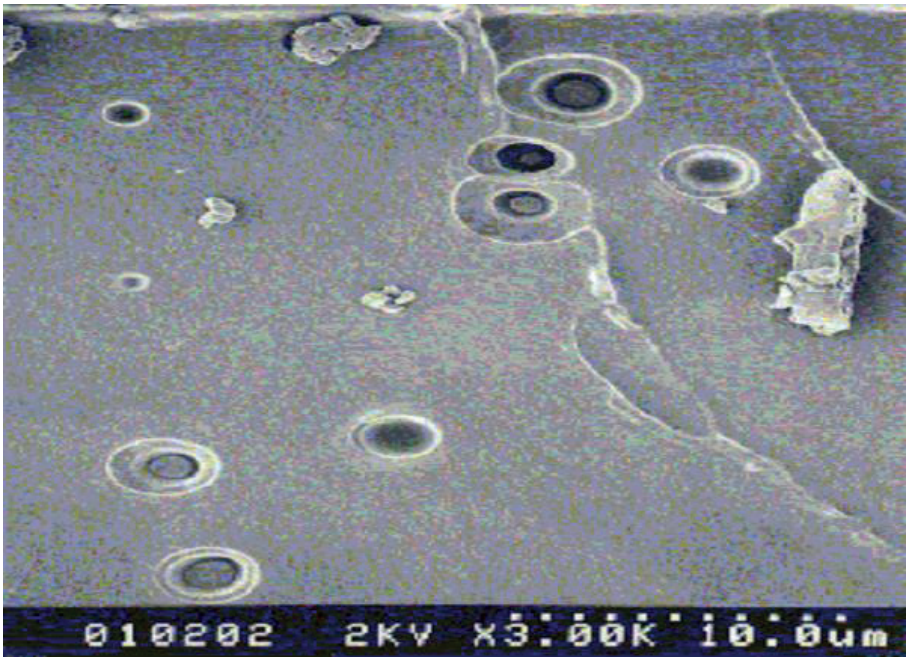

Figure 2: Sample 1 (Aged Polyethylene) Using a Scanning Electron Microscope at 3000X

Use of acoustic microscopy was also investigated and found to be another valuable tool although it would require prior calibration by other means such as by comparison to a sample dissected and viewed using an optical or electron microscope.

The principle of acoustic microscopy is that sound waves reflect at interfaces of material density decreases such as from solid polymer to a gaseous void site. The sharper the discontinuity in density, the stronger the reflected wave. Sonoscan, Inc. of Chicago, Illinois, USA volunteered use of its C-Mode Scanning Acoustic Microscope (C-SAM) Series D6000 for this research. This C-SAM operates at 10 to 100 MHz, which was found to provide the desired resolution. The C-SAM through adjustment of the observed time interval of the reflected wave was found to be capable of filtering out reflections from the cable's jacket material. Therefore, images of the electric insulation's internal void characteristics were readily apparent. Figures 3 and 4 provide two sample views of electric insulation using acoustic microscopy. Figure 3 is a prepared (dissected) sample view. Figure 4 is a view of a jacketed cable as it would appear if monitored in the field (in situ).

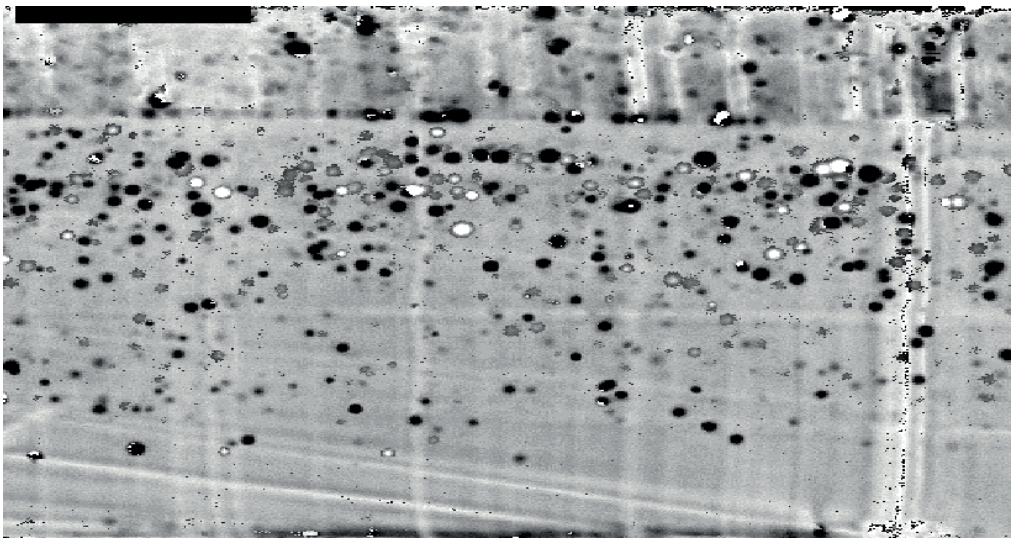

Figure 3: Aged Polyethylene Viewed with C SAM at 50 MHz.
In this inverted image the voids are dark spots.

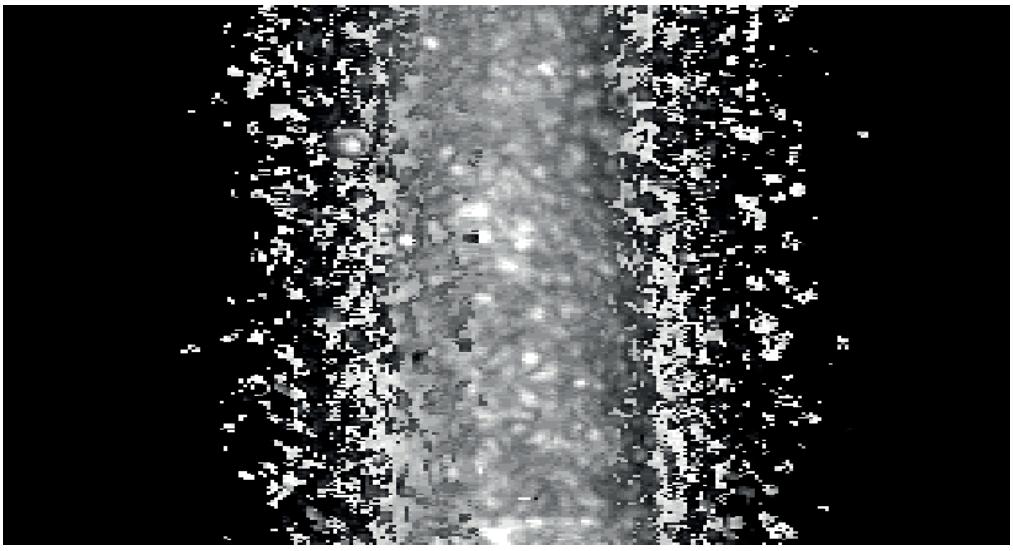

Figure 4: Aged Ethylene Propylene Viewed with C SAM at 15 MHz.
The bright spots are reflected void formations

3.2 Void Correlation to Remaining Life

As stated earlier, void size and density are indicative of remaining life through comparison to end of life criteria values. Such a correlation can be performed as shown in Figure 5 and described below.

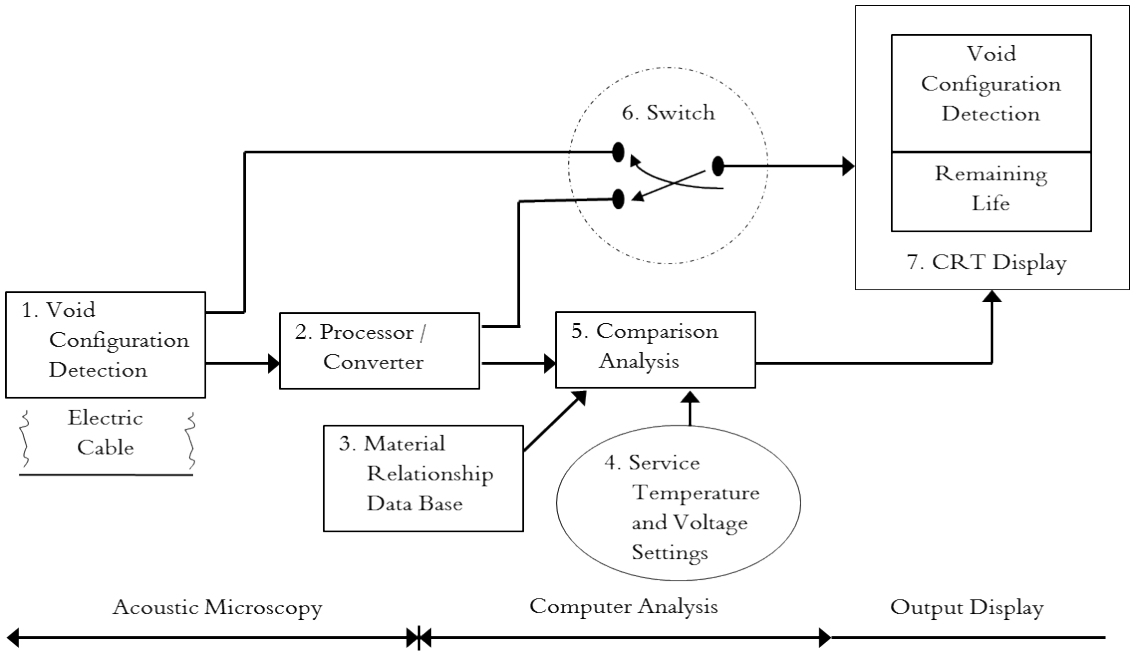

Figure 5: Electrical Insulation Life Determination Using Acoustic Microscopy and Computer Aided Void Content Analysis

Note that this technique requires no baseline or trending. It is not necessary to know past void history. Only the present level of proximity or margin to limiting void parameters is required to establish remaining life.

Void content information is detected (1) using an Acoustic Transducer (1) and sent to a Switch (6) as well as to a Processor / Converter (2). The Processor / Converter allows a conversion to a digital signal which is analyzed and converted to an equivalent insulation medium of uniform

void size and density (homogeneous dispersion throughout the insulation medium). Equivalent is defined as the same (or somewhat more limiting in terms of) susceptibility for production of an electrical partial discharge path across the electrical insulation medium under design potential conditions. This equivalent void size and density configuration is provided as one input to the comparison analysis device (5). An analog output signal representative of this "equivalent configuration" could also be made available for display (7) via switch (6).

Using void characteristics and partial discharge failure prediction techniques, relationships for service temperature and limiting void size and density corresponding to the appropriate failure criterion are available for various insulation materials [from data base (3)] as the second input to the comparison analysis performed by device (5).

Desired future service temperature and design voltage conditions are set in via setting (4). Inputs from (2), (3), and (4) are used to determine remaining life in device (5) by first determining the margin between actual equivalent void configuration and the limiting (impending failure) configuration and then calculating void growth rate, which is a function of temperature and material type. The output is a numerical or temperature dependent signal, which is sent to the display monitor (7) such that either remaining life for a given temperature or a graph of remaining life vs. temperature can be displayed.

The Display Switch (6) allows monitoring on device (7) of either a "raw" (unprocessed) reflected signal representative of the actual void configuration within the insulation medium or the equivalent void configuration.

This display device (7) is envisioned to be the display screen on a laptop computer. The upper portion of the display will show an image of the insulation medium's void configuration (processed or unprocessed). The lower portion will provide the remaining life result (for a specified temperature or as a function of temperature).

4 COMPARISON TO TAN-DELTA METHOD

4.1 Tan-Delta Testing Approach

Tan-delta testing [10] has proven promising in recent years for assessing the integrity of medium voltage cables even when such cables are buried or otherwise inaccessible. The process does, however, require that the cable be de-energized and, except for a ground connection, the remaining conductors are disconnected. Tan-delta testing consists of applying a test voltage at a very low frequency (VLF) near or above the rated voltage to a pair of conductors, one of which is grounded and then measuring the dissipation factor. The VLF is typically between 0.01 to 1 Hz.

The dissipation factor is the ratio of the resistive component of the insulation impedance between the conductors being tested and the capacitive resonance portion. The capacitive resonance portion is inversely proportional to the test frequency and equivalent capacitance. This quantity is also the tangent of the angle (delta) between the tested insulation leakage current and an ideal leakage current where the cable conductors act like a perfect capacitor with infinite resistance. When a cable is new with no defects, it behaves almost like a perfect capacitor and tan-delta is almost zero.

As the cable insulation ages, the resistive component of impedance decreases and the corresponding resistive current through the insulation is lower. It has also been found that for a given sample cable age and test frequency, the resistive component decreases with applied voltage (whereas the capacitive resonance component remains relatively constant). Therefore, for an aged cable as applied voltage is increased, a decrease in tan-delta (the ratio of resistance to capacitive resonance) will be detected and can be monitored or trended.

It follows that the lower the VLF used for testing, the more sensitive the test and more accurate and useful will be the resulting tan-delta value.

4.2 Comparison, Validation, and Remaining Life

The results of tan-delta testing of aged medium voltage cable can be explained and validated when considering the role of micro-void content. As discussed earlier, as polymers age, micro-void content increases. The micro-void content increase results in an increase in measurable insulation leakage current.

Previously [4] we had predicted that the existence of micro-voids in insulation increases the energy storage ability of the electric field created between adjacent conductors subjected to a test voltage at or near rated conditions. Since capacitance is a measure of the ability to store energy in an electric field, the size and density of the voids would affect the equivalent capacitance of the dielectric and, therefore, also affect insulation leakage current.

High void content would cause high equivalent capacitive effects resulting in increased leakage current. However, results of extensive tan-delta testing in recent years has demonstrated that this increased capacitance effect is minor when compared to the reduced equivalent resistance paths created between the conductors by the micro-voids.

The micro-voids contain gases, which are easily ionized when subjected to an electric potential. This ionization reduces the effective thickness of the insulation correspondingly and raises the resistive component of the leakage current.

At the present time, many nuclear utility plant owners are baseline testing and monitoring trends resulting from data collected by tan-delta testing. Depending on the number of cables, this amount of testing can be both time consuming and costly with no end in sight. However, as demonstrated above, the results of a one-time tan-delta test is, in theory, correlatable to micro-void content. If the insulation material and environmental stressors are known as discussed in Sections 2.2 and 3.2, a slight variation of the Figure 5 process can be used to predict remaining life. The one drawback is the need to create the material data base for the various insulation types. At the present time an extensive number of cable insulation samples exist from throughout the industry representing various degrees of aging and can be tested to establish the needed parameters for the future benefit of all nuclear plant owners and possibly also other industries.

5 FUTURE WORK

It is desirable that future research efforts should include and prioritize the development of a comprehensive material data-base, which would characterize both micro-void growth rates for various environmental stressors and micro-void content representative of end of life for low, medium, and high voltage cable insulation. This work should be done for the most widely used polymer materials (PE, EPR, and SiR) to start with and can be expanded at a future time if needed. It may even be possible to show that material content and formulations are secondary effects to aging processes for most materials when compared to the more dominating effect of void content.

Over the last decade, research funding in the US for techniques to monitor and assess electric cable insulation aging has been limited to a small number of approaches such as the indenter, oxidation induction time, and tan-delta all of which have their limitations. Now that a better understanding exists of the way in which polymers age through void content increases, it is considered prudent to expand future research in directions more universally useful and adaptable.

6 CONCLUSIONS

Micro-void content within electric cable insulation is an important precursor to deleterious aging effects. Such micro-void content is theoretically correlatable to results of tan-delta testing and to a prediction of remaining life as a function of environmental stressors (such as temperature, radiation dose, and applied voltage) and insulation material. Future research efforts will demonstrate the necessary relationships and help to develop the parameters needed for a predictive lifetime polymer material data base.

REFERENCES

[1] SM Avila and DA Horvath, "Microscopic Void Detection as a Prelude to Predicting Remaining Life in Electric Cable Insulation", *Proceedings of International Topical Meeting on Nuclear Plant Instrumentation, Controls, and Human Machine Interface Technologies (NPIC & HMIT)*, November 2000

[2] DA Horvath, DC Wood, and MJ Wylie, "Microscopic Void Characterization for Assessing Aging of Electric cable Insulation Used in Nuclear Power Stations", *Proceedings of IEEE Conference on Electrical Insulation and Dielectric Phenomena (CEIDP)*, October 2000

[3] DA Horvath and DC Martin, "Preliminary results of electric insulation void content growth from simulated exposure to a nuclear power plant's high energy line break event", *Proceedings of IEEE Conference on Electrical Insulation and Dielectric Phenomena (CEIDP)*, October 2001

[4] DA Horvath and RL Steinman, "Relationship of electric insulation void content with electric cable normalized capacitance", *Proceedings of IEEE Conference on Electrical Insulation and Dielectric Phenomena (CEIDP)*, October 2001

[5] C. Mayoux, "Aging of Polymeric Insulating Materials in Power Cables", *IEEE Transaction on Dielectrics and Electrical Insulation*, Vol 4, December 1997, pp 665-673

[6] C. Mayoux and C. Laurent, "Contribution of Partial Discharges to Electrical Breakdown of Solid Insulating Materials", *IEEE Transaction on Dielectrics and Electrical Insulation*, Vol 2, August 1995, pp 641-652

[7] Y. Zhang, J. Lewiner, and C. Alquie, "Evidence of Strong Correlation Between Space-Charge Buildup and Breakdown in Cable Insulation", *IEEE Transaction on Dielectrics and Electrical Insulation*, Vol 3, December 1996, pp 778-783

[8] C. Dang, J.-L. Parpal, and J.-P. Crine, "Electrical Aging of Extruded Dielectric Cables: Review of Existing Theories and Data", *IEEE Transactions on Dielectrics and Electrical Insulation*, Vol 3, April 1996, pp 237-247

[9] A.C. Gjaerde, "Multifactor Ageing Models - Origin and Similarities", *IEEE Electrical Insulation Magazine*, Vol 6, January/February 1997, pp 6-13

[10] IEEE Std 400.2-2004 "IEEE Guide for Field Testing of Shielded Power Cable Systems Using Very Low Frequency (VLF)"

Journal of Energy
VOLUME 62 Number 1–4 | 2013 Special Issue
journal homepage: http://journalofenergy.com/

Analysis of Rod Withdrawal at Power (RWAP) Accident using ATHLET Mod 2.2 Cycle A and RELAP5/mod 3.3 Codes

Vesna Benčik, Nikola Čavlina, Davor Grgić
Faculty of Electrical Engineering and Computing, University of Zagreb
Unska 3, 10000 Zagreb, Croatia
vesna.bencik@fer.hr, nikola.cavlina@fer.hr, davor.grgic@fer.hr

ABSTRACT

The system code ATHLET (Analysis of THermal-hydraulics of Leaks and Transients) is being developed by the Gesellschaft für Anlagen-und Reaktorsicherheit (GRS) mbH in Garching, Germany. In the paper, an overview of activities performed at Faculty of Electrical Engineering and Computing (FER), University of Zagreb, in application of system code ATHLET in transient analyses for NPP Krško (NEK) is presented. Newly, the NEK input deck for the released ATHLET version (Mod 2.2 Cycle A) has been developed. For that purpose, the NEK data base that has been developed and maintained at FER for the last two decades primarily for development of standard input deck for RELAP5 code was used. The ATHLET model has been validated by analyzing the Rod Withdrawal At Power (RWAP) accident at nominal power. The results for steady state calculation as well as RWAP transient were assessed against the analysis performed by RELAP5/mod 3.3 code. In both ATHLET and RELAP5 calculation, the RWAP accident was simulated by constant reactivity insertion rate equal to 2.4 pcm/sec. For ATHLET analysis, two fluid dynamic options were tested for the primary side: a) base case analysis with 5 conservation equations and mixture level model and b) two-fluid model with separate conservation equations for liquid and vapour phases for all the volumes except for the pressurizer where 5 equations+mixture level model was retained. The Steam Generators (SGs) were built using basic ATHLET elements together with the dedicated separator model. For RELAP5/mod 3.3 analysis, a standard option with thermal and mechanical non-equilibrium (6 equations) was used. The results of the steady state calculation for the ATHLET model have shown a very good agreement with RELAP5 calculation. In the transient analysis very small differences for the main physical parameters between ATHLET and RELAP5 as well as between the two ATHLET models were obtained.

1 INTRODUCTION

The system code ATHLET, ref. [4] is being developed by the GRS for the analysis of anticipated and abnormal plant transients as well as of the whole spectrum of Loss of Coolant Accidents (LOCAs) in light water reactors. The code consists of several basic modules, e.g., Thermo-fluiddynamics (TFD), Heat Transfer and Heat Conduction (HECU), Neutron Kinetics (NEUKIN) and General Control Simulation Module (GCSM). The GCSM is a block oriented simulation language for modelling of balance of plant (BOP) systems and actions, e.g., the plant control systems, trip logic, as well as the interaction between thermal-hydraulics and BOP.

In 1996, the NPP Krško input deck for ATHLET Mod 1.1 Cycle C has been developed at FER. The input deck was tested by analyzing the realistic plant event 'Main Steam Isolation Valve Closure' and the results were assessed against the measured data, ref. [5]. The input deck was established before plant modernization that took place in 2000 and included the power uprate and SG replacement. The released ATHLET version (Mod 2.2 Cycle A) is now being available at FER.

V. Benčik, N. Čavlina, D. Grgić, Analysis of Rod Withdrawal at Power (RWAP) Accident using ATHLET Mod 2.2 Cycle A and RELAP5/mod 3.3 Codes, Journal of Energy, vol. 62 Number 1–4 (2013) Special Issue, p. 54–67

Accordingly, the NEK input deck for ATHLET Mod 2.2 Cycle A has been developed. A completely new input deck has been created taking into account the large number of changes due to power uprate and SG replacement as well as taking advantage of developmental work on NEK data base performed at FER. The new NEK input deck for ATHLET code has been tested by analyzing the RWAP accident and the results were assessed against the analysis performed by RELAP5/mod 3.3 code.

The RWAP accident is caused by a continuous uncontrolled Rod Cluster Control Assembly (RCCA) bank withdrawal while reactor is at power. The RWAP accident can be either Departure from Nucleate Boiling (DNB) ratio or overpower limiting accident depending on initial power and reactivity insertion rate. The automatic rod control system is assumed unavailable, thus the only negative reactivity is due to Doppler and moderator feedback. Due to positive total reactivity and nuclear power increase, the core heat flux as well as transferred heat in the steam generators (SGs) rise, too. Since the steam flow to the turbine and the extracted power from the SGs remain constant, the unbalance between produced and extracted heat is established. Consequently, the secondary side pressure and primary side temperature continue to increase until either reactor trip terminates the power production or SG relief or safety valves open thus increasing the heat removal. Unless terminated by manual or automatic action, the power mismatch between primary and secondary side and the resultant coolant temperature rise could eventually result in DNB ratio and/or fuel centreline melt. In order to avoid core damage, the reactor protection system is designed to automatically terminate the transient before the DNB ratio falls below the limit value, or the fuel rod power density limit (kW/m) is reached. Depending on the initial power level and the reactivity insertion rate, the reactor protection system will actuate any of the following reactor trips: a) Power range high neutron flux, b) Power range high positive neutron flux rate, c) Overtemperature ΔT (OTΔT), d) Overpower ΔT (OPΔT), e) High pressurizer pressure, f) High pressurizer water level and g) Manual reactor trip.

The steady state was calculated for 1000 seconds for both ATHLET and RELAP5 analysis. Thereupon, the RWAP accident was simulated for 200 seconds by constant reactivity insertion rate equal to 2.4 pcm/sec.

2 CALCULATIONAL MODEL FOR NPP KRŠKO

For RELAP5/mod 3.3 calculation, the NPP Krško nodalization developed at FER, [1], [2] and [3] has been used. Here, only a brief description of the RELAP5 nodalization is provided since it has already been described in a number of papers; e.g., recently in ref. [6]. The standard RELAP5/mod 3.3 model comprises the Resistance Temperature Detector (RTD) bypass lines thus enabling the accurate representation of Narrow Range (NR) temperature measurement at the plant. However, since the NPP Krško is considering the replacing of the RTD bypass manifold system with fast-response thermowell-mounted (TW) RTDs, the latter (TW RTD) configuration was assumed in this analysis. The RTD bypass lines were removed from the model while the TW RTD temperature measurement was modeled by imposing the measurement delay and filter on calculated loop temperatures. After removing the RTD bypass lines, the RELAP5 model has 469 thermal-hydraulic nodes, 497 junctions, 378 heat structures (with 2107 mesh points), and 691 control variables, with 199 variable and 208 logical trips, respectively.

As a basis for ATHLET model, the NEK data base that has been used for development of the RELAP5 model was used. In Figure 1, a part of ATHLET nodalization for NPP Krško is presented. Due to complexity, only components of the first loop are shown; i.e., the reactor pressure vessel and the first coolant loop (hot and cold leg, reactor coolant pump and steam generator primary and secondary side) and the pressurizer. The NPP Krško model for ATHLET code has 108 Thermo-Fluiddynamic Objects (TFOs) containing 497 control volumes (CVs), 340 junctions, 355 heat slabs (with 1407 mesh points) and 398 GCSM signals. Contrary to RELAP5 model, the ATHLET nodalization does not contain the detailed models for a number of systems so far; e.g., the safety

injection system and steam generator feedwater (main and auxiliary) system. For the rest of the plant, the same approach with rather comprehensive description of the plant components was applied in ATHLET model, too. The reactor pressure vessel (RPV) is represented with 18 TFOs. In particular, the lower plenum is divided into four TFOs; the reactor core (type PIPE simulating 1 coolant channel consists of 12 CVs) represents the active core (from bottom to the top of active fuel) and, parallel to the core with the same length; the empty RCCA guide tubes inside core are represented with GUIDET; the region between baffle and barrel is represented with BUFFBPSS; TFOs UPCORE1 and UPCORE2 represent the core region above top of active fuel; the RCCA guide thimbles (connecting core outlet and the upper head) is represented with volume RCCBPSS; TFOs UPPL1 and UPPL2 form the upper plenum and TFOs UPHEAD1 and UPHEAD2 represent upper head; the bypass flow path from upper head is introduced by connecting the UPPHEAD2 with upper downcomer (UPDCM) that is connected to the RPV inlet (TFO RVIN); the cold legs 1 and 2 ends are connected to RVIN that is further led to lower downcomer first part (LWDCM1) which is connected to the rest of the downcomer (PIPE LWDCM2 having 14 CVs) that is finally connected to the lower plenum (TFO LWPL2); the hot leg's (HOTLEG1, HOTLEG2) inlets are connected to the upper plenum (UPPL1); the bypass flow path between the lower downcomer (LWDCM2) and TFO BUFFBPSS is also considered. The pressurizer is connected to the hot leg 1 via surge line whereas the both cold legs are connected to the top of the pressurizer via pressurizer spray lines. The pressurizer has been built using the standard ATHLET elements (TFOs, Heat Conduction Objects -HCOs and GCSM signals). Realistic models for pressurizer relief and safety valves with loop seal have been developed.

For modeling of the steam generator, the flexible U-tube SG model built out of standard ATHLET elements together with the dedicated separator model were used. Contrary to RELAP5 model, the detailed models for steam generator main and auxiliary feedwater with realistic control valves are not included in the ATHLET model. Instead, the Single Junction Pipes (SJP) with FILL components are used (B-FWINL1 and AUXFW1 in Figure 1). The steam lines are modeled with their physical lengths (the lengths are different for loop 1 and 2). Also, each steam line is equipped with 1 SG PORV and 5 safety valves that discharge into containment (modeled as time dependent volume). The steam lines are connected via respective main steam isolation valves to the steam header line (STML1T). The steam header line is further connected via the control valve to the turbine that is modeled as time dependent volume thus representing the boundary condition on the secondary side. The simple steam dump model was applied with SJP flow calculated in the steam dump GCSM control block. The ATHLET Mod 2.2 Cycle A offers the possibility of choosing between two different models for the simulation of fluid-dynamics: 1) 5-equation model, with separate conservation equations for liquid and vapour mass and energy, and a mixture momentum equation, and including a mixture level tracking capability, and 2) two-fluid model – 6 conservation equations, with separate conservation equations for liquid and vapour mass, energy, and momentum (without mixture level tracking capability). In the analysis presented in this paper two fluid dynamic options have been tested for the TFOs on the primary side: a) base case analysis with 5 conservation equations+mixture level option (IARTO=1 in input) and b) two-fluid model (IARTO=2) with separate conservation equations for liquid and vapor mass, energy and momentum (without mixture level tracking capability) for all the volumes except for the pressurizer where 5 equations+mixture level option was chosen. On the secondary side, only 5 equations + mixture level model was applied. This is the only available option for dedicated separator model (SG1SEP), which on the other side requires the mixture level model that is not allowed in six equation model for the associated volumes to the separator (downcomer and steam dome).

For nuclear heat generation the point kinetics model was selected. The Cycle 24 Beginning Of Life (BOL) data prepared for RELAP5 point kinetics input were adapted for ATHLET model. Both Doppler and moderator density feedback were taken into account. The detailed models of reactor protection as well as plant control systems have been modeled using GCSM module. They include: 1) Reactor protection system, 2) Turbine trip logic, 3) Pressurizer pressure and level control system, 4) Steam generator level control system and 5) Steam dump system.

The initial conditions for RWAP analysis were obtained after 1000 sec steady state calculation for both ATHLET and RELAP5 code. The results of the steady state calculation at nominal power are summarized in Table 1. The 1000 sec steady state calculation took 218 and 117 sec CPU time for RELAP5 and ATHLET code, respectively. Thereby, the maximum time step chosen for steady state calculation was 0.1 sec for RELAP5 and 0.5 sec for ATHLET, respectively.

Table 1 Initial conditions for RWAP analysis (results after 1000 seconds of steady state calculation)

Parameter	Unit	ATHLET	RELAP5
Reactor power	MW	1994	1994
SG power	MW	1001.23/1001.89	996.56/1002.5
Pressurizer pressure	MPa	15.5125	15.5126
SG steam dome pressure	MPa	6.43/6.43	6.42/6.4
RCS average temperature	K	578.16/578.15	578.15/578.056
RCS volumetric flow	m^3/s	6.26/6.26	6.26/6.26
SG steam mass flow rate	kg/s	545.94/543.25	541.28/544.41
SG feedwater mass flow rate	kg/s	545.94/543.25	541.28/544.42
Feedwater enthalpy	kJ/kg	942	943
SG circulation ratio	-	3.73/3.74	3.74/3.72
Pressurizer level	%	55.6	55.7
SG level	%	69.3/69.3	69.3/69.3

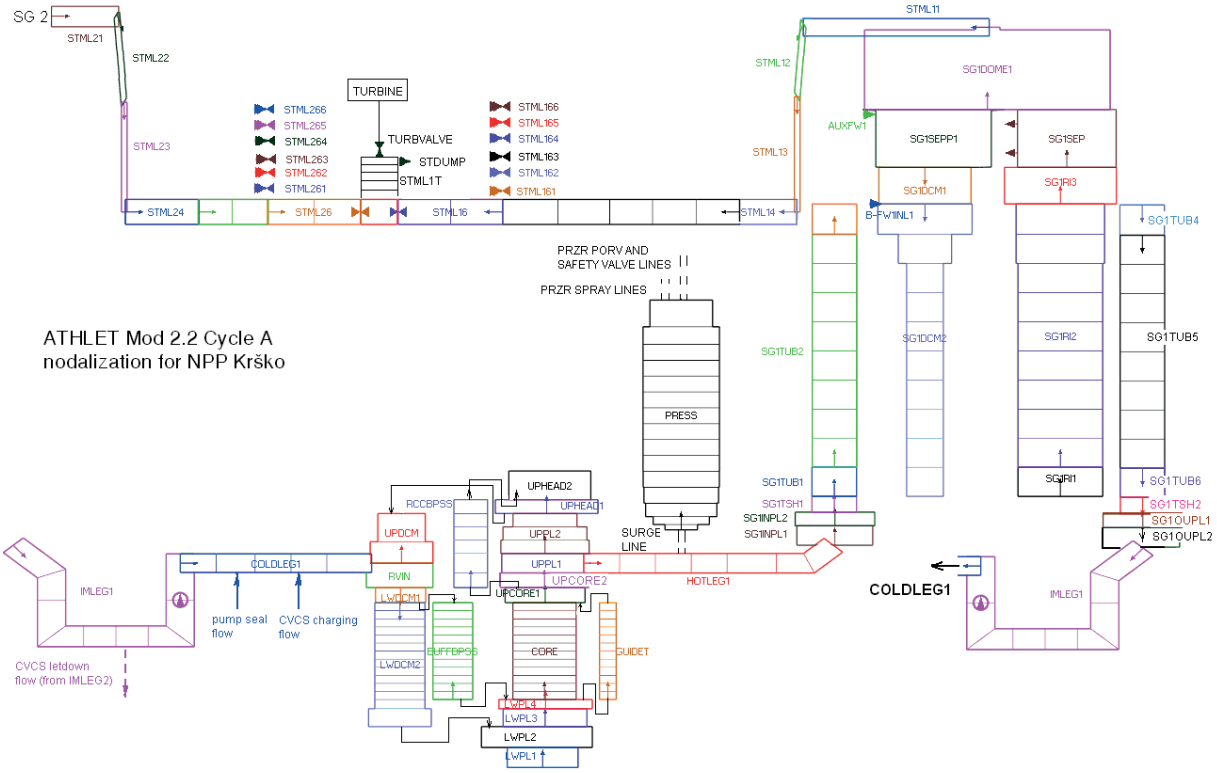

V. Benčik, N. Čavlina, D. Grgić, Analysis of Rod Withdrawal at Power (RWAP) Accident using ATHLET Mod 2.2 Cycle A and RELAP5/mod 3.3 Codes, Journal of Energy, vol. 62 Number 1–4 (2013) Special Issue, p. 54–67

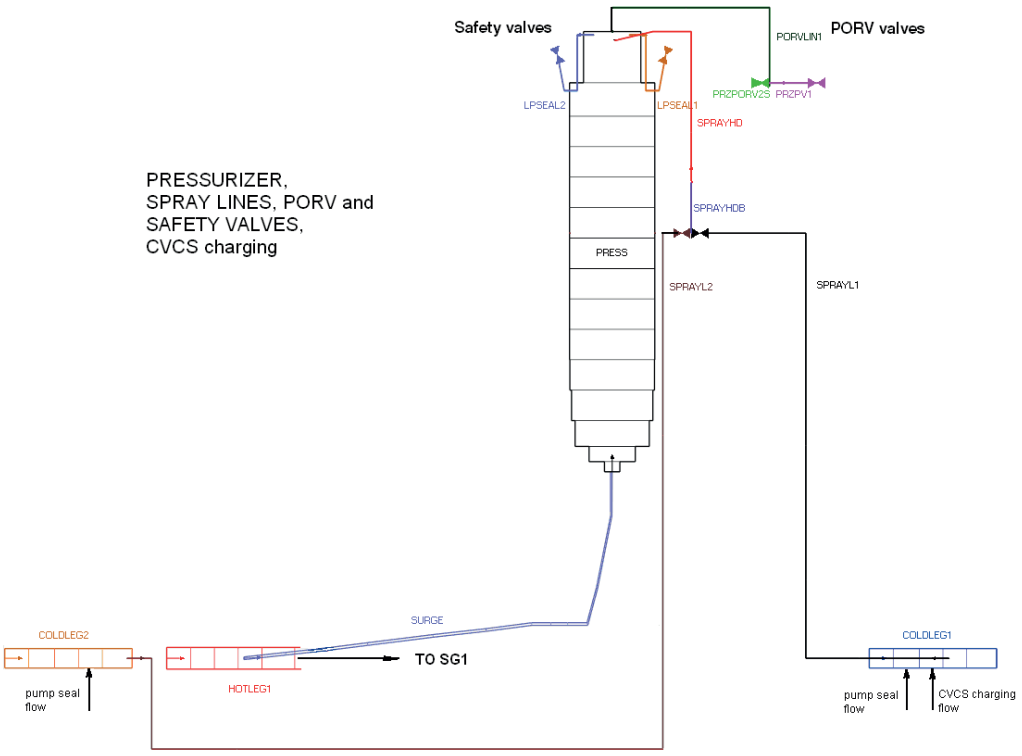

Figure 1: ATHLET Mod 2.2 Cycle A nodalization of NPP Krško

2.1 Reactor Trip Functions during RWAP

In order to avoid core damage because of RWAP, reactor protection system will actuate any of the following reactor trips: a) Power range high neutron flux, b) Power range high positive neutron flux rate, c) Overtemperature ΔT (OTΔT), d) Overpower ΔT (OPΔT), e) High pressurizer pressure, f) High pressurizer water level and g) Manual reactor trip. At fast reactivity insertion rates, a steep nuclear power rise will result in actuation of high neutron flux or high neutron flux rate trip (trips a) and b)) before the RCS temperatures rise significantly to actuate trips c) through f). The nuclear power increase rate is being reduced during the transient due to negative reactivity feedback (Doppler and moderator density). For slow reactivity insertion rates, the increase of core heat power and moderator temperature may significantly reduce the increase rate of nuclear power. Nuclear power may even start to decrease while the coolant temperatures are still increasing. Such scenario may prolong the transient and result in a significant increase of coolant temperature thus compromising the margin to DNBR.

In order to protect the reactor from excessive core heat power increase and low DNBR, the OPΔT and OTΔT are generated. Thereby, for larger reactivity insertion rate, the OPΔT trip is expected to be actuated before the OTΔT trip. In this paper, the relatively slow reactivity insertion rate (2.4 pcm/sec) was analyzed and the OTΔT trip is actuated first.

At the plant, the setpoint for OTΔT trip is continuously calculated by solving the following equation:

$$OT\Delta T_{setp} = \Delta T_0 \left[K_1 - K_2 \left(\frac{1+\tau_1 s}{1+\tau_2 s} \right) \left(T_{avg} \frac{1}{1+\tau_7 s} - T_{avg}^0 \right) + K_3 \left(P - P_0 \right) - f\left(\Delta\Phi \right) \right] \quad (1)$$

Where:

$OT\Delta T_{setp}$ - Overtemperature ΔT setpoint

V. Benčik, N. Čavlina, D. Grgić, Analysis of Rod Withdrawal at Power (RWAP) Accident using ATHLET Mod 2.2 Cycle A and RELAP5/mod 3.3 Codes, Journal of Energy, vol. 62 Number 1–4 (2013) Special Issue, p. 54–67

ΔT_0 - Indicated ΔT at nominal thermal power

T_{avg}, T_{avg}^0 - Measured and indicated loop average temperature at nominal thermal power

P, P_0 - Measured and nominal pressurizer pressure

K_1 - Setpoint bias

K_2, K_3 - Constants based on the effect of temperature (K_2) and pressure (K_3) on the DNB limits

τ_1, τ_2 - Time constants (s) of dynamic signal compensators (lead-lag)

τ_7 - Time constant (s) of dynamic signal compensator (lag)

s - Laplace transform variable (s^{-1})

$f(\Delta\Phi)$ - A function of the neutron flux difference between the upper and the lower long ion chambers (DNBR is lower for non-uniform axial power distribution and for power shifted in the upper part of the core).

The calculated $OT\Delta T_{setp}$ is compared with two sets of loop temperature difference measurements (ΔT) per loop. The OTΔT reactor trip function will trip the reactor on coincidence of two out of four signals satisfying the condition below:

$$OT\Delta T_{setp} \leq \Delta T ,$$

where ΔT is the compensated lead-lag ($\frac{1+\tau_4 s}{1+\tau_5 s}$) signal of the measured difference between the indicated hot and cold leg temperatures (as determined by RTD thermowell instrumentation). The model is implemented in NPP Krško nodalization for both RELAP5 and ATHLET codes.

3 TRANSIENT RESULTS

The transient was initiated after 1000 sec steady state calculation by inserting the positive reactivity at a constant rate (2.4 pcm/sec). The main events for ATHLET and RELAP5 calculation are summarized in Table 2, and the results for main physical parameters are presented in Figure 2 through Figure 16. The insertion of positive reactivity, Figure 2, leads to an increase of nuclear power, Figure 3, that results in the core heat flux increase, that lags slightly behind the nuclear power, Figure 4. The fuel as well as coolant temperature increase result in addition of negative reactivity due to negative Doppler and moderator density reactivity coefficient. However, since the automatic rod control system is not credited, the total reactivity is positive and nuclear power increases further until reactor scram actuation. The power transferred from primary to secondary side in the steam generators, Figure 5, increases, too, due to primary temperature increase, Figure 6, whereas on the secondary side, the pressure rises, Figure 9, due to increased heat. Since the steam flow to the turbine, Figure 10, is limited to its nominal value, the extracted heat to the turbine remains constant. Due to imbalance between the added and extracted heat, the secondary pressure rises further, which increases the imbalance between core heat power and SG power thus yielding to primary side heat-up. The RCS temperature increase causes coolant expansion and pressurizer level increase, Figure 14, that results in pressurizer pressure increase, Figure 8. The pressurizer pressure control actuates the pressurizer spray valves opening, Figure 15, while the pressurizer relief valves did not open during power increase, Figure 16. The RCS pressure is maintained at the constant value slightly above the setpoint value (15.51 MPa). Thus, the RCS temperature increase is the major cause of OTΔT setpoint decrease (the second term in Eq. (1)), Figure 7. The initial fast increase of the nuclear power and core heat power subsides due to negative reactivity feedback and the compensated measured temperature difference ΔT, Figure 7, that is an indicator of the core heat power follows that trend. On the other side, the RCS temperature continues to rise even faster due

to increased difference between produced and removed heat. With RCS pressure at constant value, the RCS temperature rise has the decisive influence on decreasing the setpoint for OTΔT trip. It has also the major influence on actuation of OTDT trip since the compensated measured ΔT rises at a slow rate. It is important to note that the reactor protection functions OPΔT and OTΔT depend on RCS temperature measurement that has a delay related to the actual temperature as it is shown in Figure 6. In all three analyzed cases (ATHLET-base case-5 equations, ATHLET-6 equations, RELAP5), the OTDT trip signal in the first loop trips the reactor. The difference in a time of the generation of reactor trip among the analyzed cases is very little (The largest difference (1.1 sec) was obtained for ATHLET-6 equations and RELAP5). The maximum nuclear power in all analyzed cases (maximum value=2109.8 MW (105.8 % of nominal) obtained for RELAP calculation) was well below reactor trip setpoint (109 %). Negative reactivity insertion following the reactor scram shuts down the reactor and the heat produced in the core decreases. On the secondary side, turbine trip is actuated on reactor trip, Figure 10. The steam dump valves open, Figure 11, with RCS average temperature setpoint at no-load value and with 50 % of the maximum capacity for plant trip mode operation. Due to the fact that at a time of reactor trip the temperatures and accumulated heat in the primary circuit were higher than nominal, the cooldown to no-load conditions was extended when compared with the trip at nominal power. In the time period between 100 and 120 sec, the cooldown process was even stopped as it can be observed on SG power, Figure 5 as well as on RCS temperature, Figure 6 and SG pressure, Figure 9. Despite the steam dump operation the secondary pressure rises significantly above the final no-load value. However, the SG pressure did not exceed the setpoint for SG relief and safety valves. Finally, due to prolonged steam dump operation with high steam flow the RCS cooldown continued and RCS temperatures as well as SG pressure decreased with the trend of achieving their target no-load values.

Following the turbine trip and sudden pressure increase, the SG level shrinkage occurs due to rapid condensation, Figure 13. The main feedwater, Figure 12, is isolated in all three calculations on signal: low RCS average temperature & reactor trip, and the auxiliary feedwater is actuated 5 seconds thereafter. Upon turbine trip, the coolant additional heat-up with expansion into the pressurizer and subsequent pressurizer pressure increase result. The pressurizer relief valve no. 1 opens for a very short time, Figure 16. Immediately thereafter, the reduction of coolant temperature and of specific volume causes the outsurge from the pressurizer and pressurizer pressure drop, Figure 14 and Figure 8. Consequently, the pressurizer spray valves close, Figure 15.

In general, a very good agreement for the relevant physical parameters was obtained between the analyzed cases. There is a certain agreement between the analyzed cases for the period before reactor trip. After reactor trip, the first differences appear as summarized below.

- First, the instant pressurizer pressure increase after reactor and turbine trip is different between the ATHLET (both 5 and 6 equations) and RELAP5 calculation. It is obvious that the resulting insurge into the pressurizer and the pressurizer pressure increase were larger in RELAP5 than in ATHLET calculation. Consequently, in the RELAP5 calculation, the pressurizer pressure control system responded with the higher pressurizer relief valves flow. However, the differences are very small and do not have influence on the global trends.
- A part of the observed differences in the steam generator behaviour can be attributed to a) less detailed model of main feedwater system in ATHLET model so far (modelled only with FILL component) when compared with a detailed RELAP5 model (with the model of piping and realistic main feedwater valve) and b) Time of the reactor trip. Later trip results in larger amount of accumulated heat and greater maximum secondary pressure. However, the time of the reactor trip is only slightly different between the analyzed cases and therefore it cannot explain the major differences between ATHLET and RELAP5 SG behaviour.
- The interaction of control systems (in the analyzed transient, the SG level control and steam dump, in particular) with the inherent system behaviour can impede the identification of the actual causes of the observed differences between the two codes (ATHLET vs. RELAP5).

• There are two differences between the two models for ATHLET calculation (5 vs. 6 equations). First, there is a small difference in the time of reactor trip which may be caused by very small differences in the variables affecting the OTΔT setpoint value. The second discrepancy between the two ATHLET models appears at approx. 120 seconds after transient begin when during the outsurge, the small difference in pressurizer level as well as pressurizer pressure was established.

Table 2 Time table of events – RWAP, 2.4 pcm/sec

Event	ATHLET (base case - 5 equations)	ATHLET (6 equations)	RELAP5
Reactor trip setpoint reached	67.5 sec (OTDT trip in loop 1)	67.0 sec (OTDT trip in loop 1)	68.1 sec (OTDT trip in loop 1)
Rods begin to drop	68.5 sec (1 sec delay)	68.0 sec (1 sec delay)	69.1 sec (1 sec delay)
Turbine trip	68.5 sec (on reactor trip)	68.0 sec (on reactor trip)	69.1 sec (on reactor trip)
Main feedwater isolation	96.8 sec (on signal: low Tavg & reactor trip), 7 sec closure time	96.0 sec (on signal: low Tavg & reactor trip), 7 sec closure time	98.1 sec (on signal: low Tavg & reactor trip), 7 sec closure time
Auxiliary feedwater actuation	101.8 (on MFW isolation, 5 sec delay)	101.0 (on MFW isolation, 5 sec delay)	103.1 (on MFW isolation, 5 sec delay)
Maximum nuclear power	2107.5 MW (68.5 sec)	2107.2 MW (68.0 sec)	2109.8 MW (69.1 sec)
Maximum core heat power	2102.3 MW (68.7 sec)	2102.0 MW (68.2 sec)	2104.6 MW (69.2 sec)
Maximum RCS average temperature	581.9 K (69.7 sec)	581.8 K (69.1 sec)	581.9 K (70.2 sec)

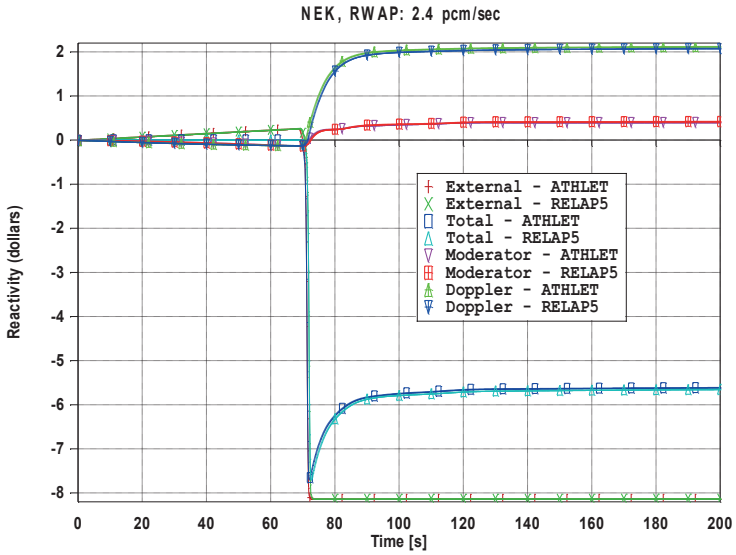

Figure 2: Reactivity (ATHLET – 5 equations)

V. Benčik, N. Čavlina, D. Grgić, Analysis of Rod Withdrawal at Power (RWAP) Accident using ATHLET Mod 2.2 Cycle A and RELAP5/mod 3.3 Codes, Journal of Energy, vol. 62 Number 1–4 (2013) Special Issue, p. 54–67

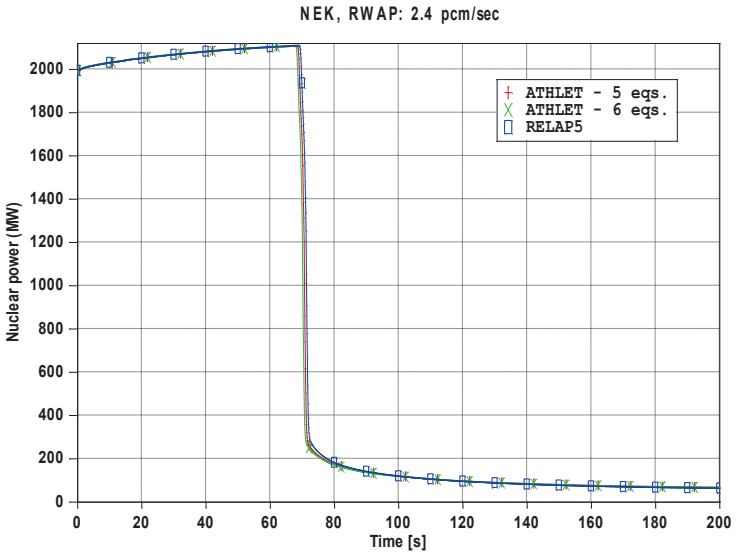

Figure 3: Nuclear power

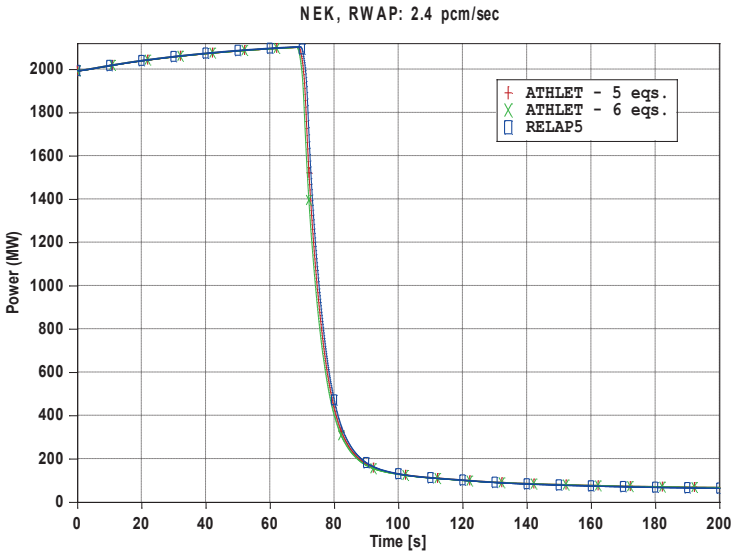

Figure 4: Core heat power

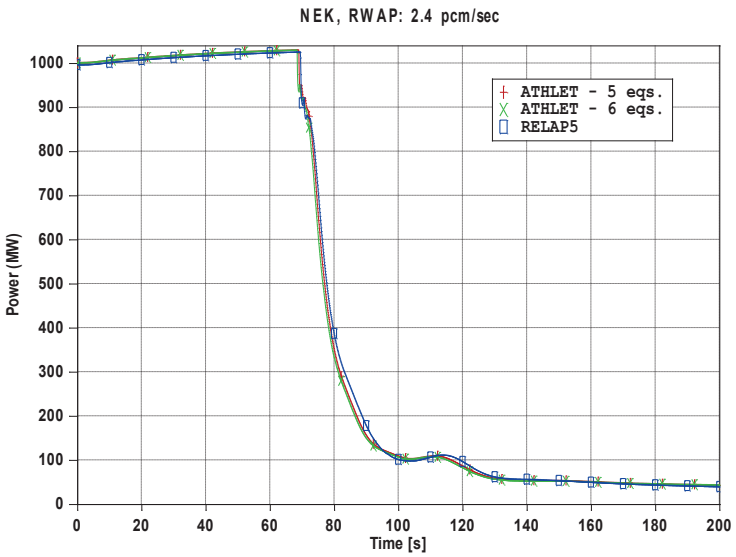

Figure 5: SG 1 power

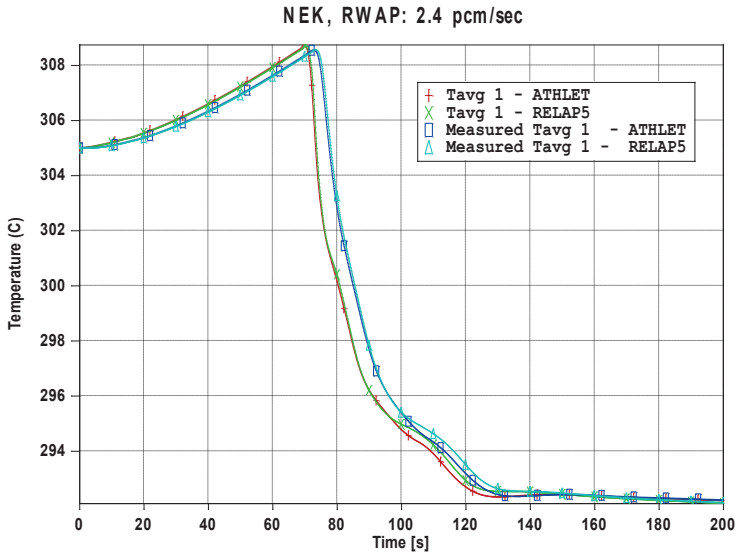

Figure 6: RCS average temperature – loop 1 (ATHLET – 5 equations)

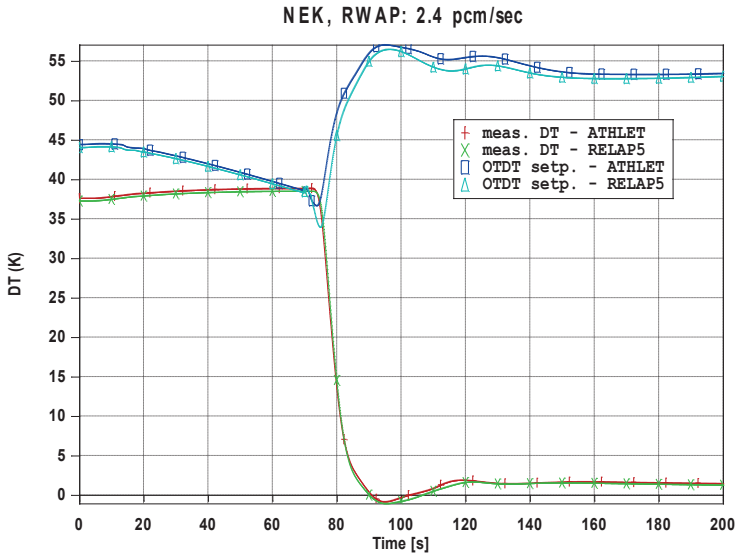

Figure 7: Measured DT and OTΔT setpoint (loop 1, ATHLET – 5 equations)

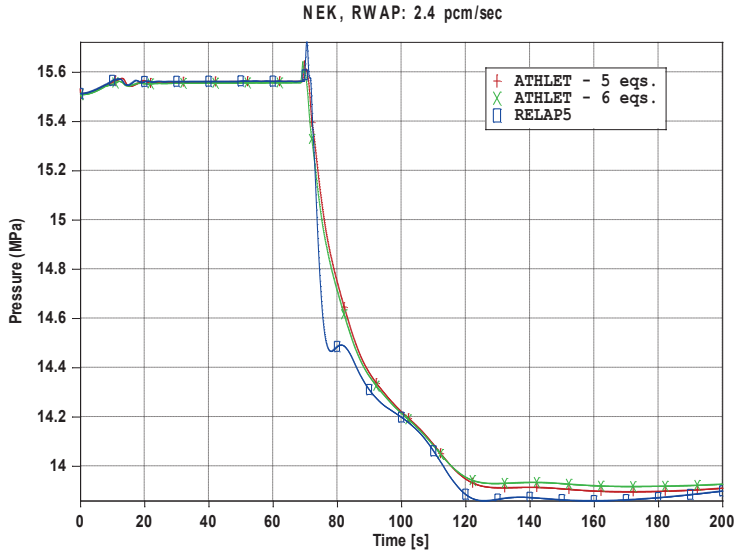

Figure 8: Pressurizer pressure

V. Benčik, N. Čavlina, D. Grgić, Analysis of Rod Withdrawal at Power (RWAP) Accident using ATHLET Mod 2.2 Cycle A and RELAP5/mod 3.3 Codes, Journal of Energy, vol. 62 Number 1–4 (2013) Special Issue, p. 54–67

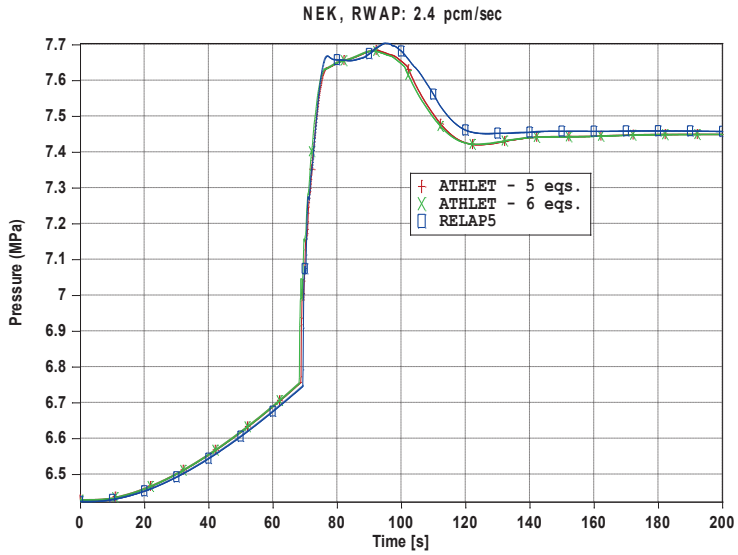

Figure 9: SG 1 steam dome pressure

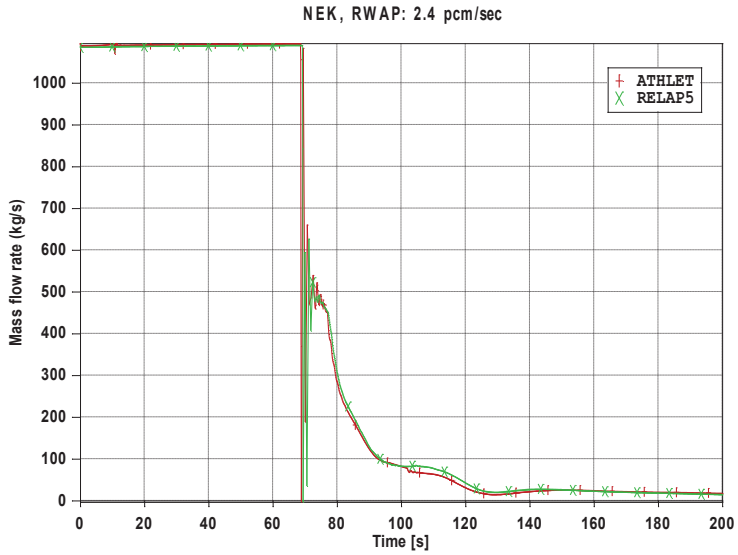

Figure 10: Total steam mass flow rate (ATHLET - 5 equations)

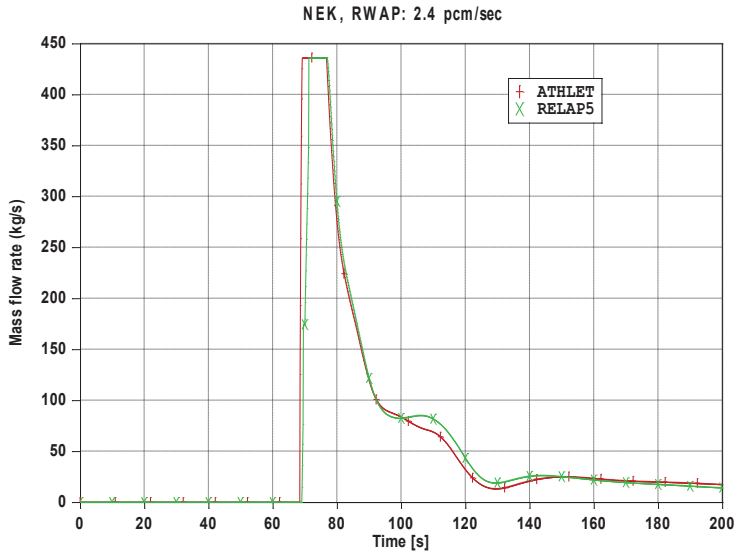

Figure 11: Steam dump mass flow rate (ATHLET - 5 equations)

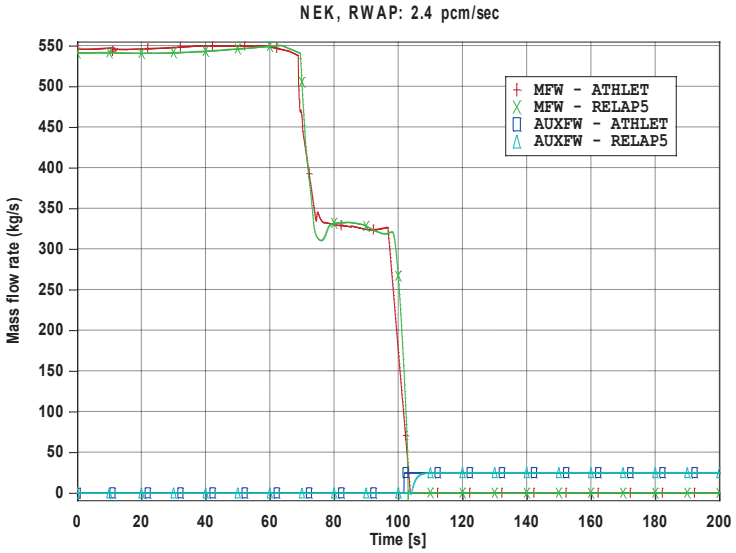

Figure 12: SG 1 main feedwater and auxiliary feedwater mass flow rate (ATHLET – 5 equations)

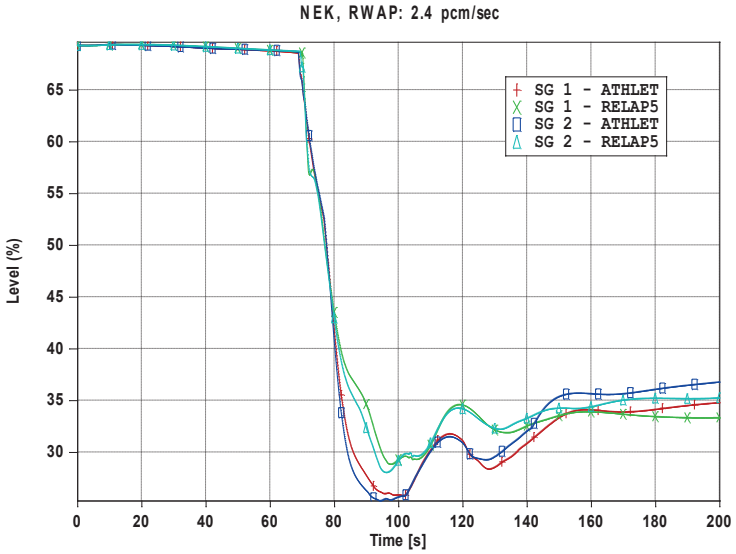

Figure 13: SG level (ATHLET – 5 equations)

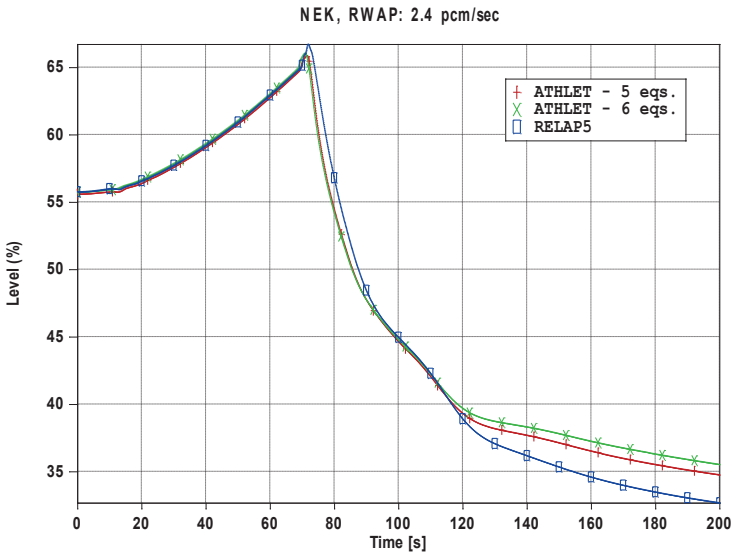

Figure 14: Pressurizer level

V. Benčik, N. Čavlina, D. Grgić, Analysis of Rod Withdrawal at Power (RWAP) Accident using ATHLET Mod 2.2 Cycle A and RELAP5/mod 3.3 Codes, Journal of Energy, vol. 62 Number 1–4 (2013) Special Issue, p. 54–67

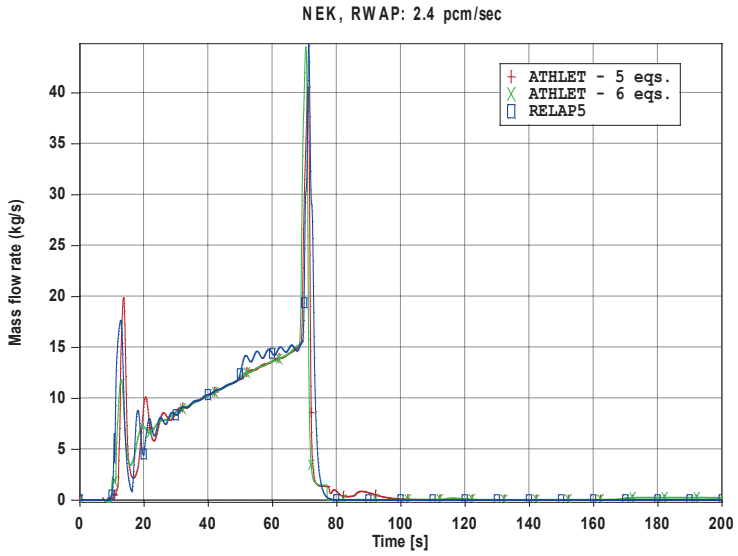

Figure 15: Pressurizer spray mass flow rate

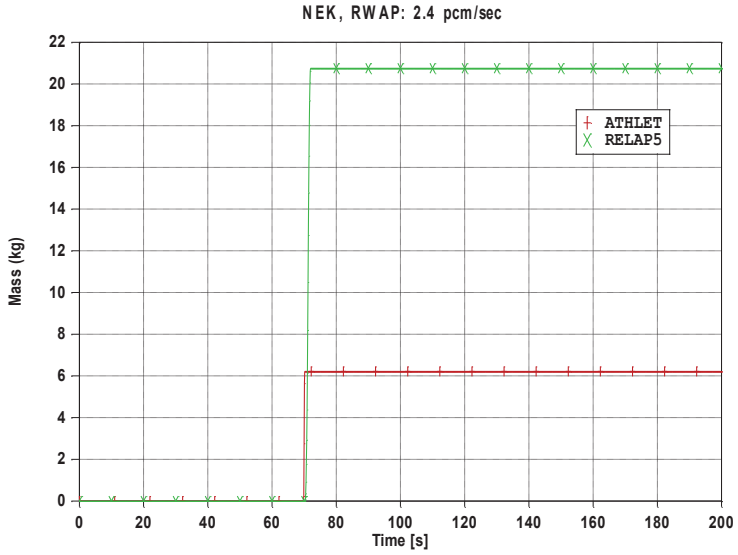

Figure 16: Integral of pressurizer relief and safety valves mass flow rate (ATHLET – 5 equations)

4 CONCLUSION

The ATHLET Mod 2.2 Cycle A model for NPP Krško has been developed. For that purpose, the NEK data base that has been used at FER for development and maintenance of the RELAP5 model for NPP Krško was applied. The ATHLET model was tested by analyzing the RWAP accident initiated after 1000 seconds steady state calculation. The results of both steady state calculation and RWAP transient analysis were assessed against the analysis performed by RELAP5/mod 3.3 code.

For ATHLET analysis, two fluid dynamic options were tested for the primary side: a) base case analysis with 5 conservation equations and mixture level model and b) two-fluid model with separate conservation equations for liquid and vapour phases (6 equations) and the 5 equations+mixture level model for pressurizer. For both cases, 5 equations model was selected for the secondary side. For RELAP5/mod 3.3 analysis, the standard 6 equation model was used. Following conclusions can be drawn from the presented analyses:

- The steady state calculation has been performed for 1000 seconds for both ATHLET and RELAP5. A very good agreement for relevant physical parameters between the two codes was obtained.
- In the transient analysis all three analyses have shown the same trends and the differences for the main physical parameters are very small. First noticeable differences between the analyzed cases appear after reactor and turbine trip. The differences between RELAP5 and ATHLET models (both 5 and 6 equations) are larger than the differences between the two ATHLET models (5 vs. 6 equations).
- The major differences between RELAP5 and ATHLET calculation are related to steam generator behaviour after reactor and turbine trip. One part of the observed differences may be attributed to the differences in the main feedwater model (simplified model in ATHLET compared with the detailed RELAP5 model). In addition, the interaction of control systems (e.g., SG level control and steam dump) with inherent system behaviour can amplify the already existing differences between the two models and impede the identification of the actual causes of the observed discrepancies.
- The observed differences for the time of the reactor trip and slightly different pressurizer behaviour between the two ATHLET models (5 vs. 6 equations) can be attributed to small differences in pressurizer surge line as well as spray line flow.

ACKNOWLEDGMENTS

The work presented in this paper has been performed within cooperation agreement between the Faculty of Electrical Engineering and the Gesellschaft für Anlagen-und Reaktorsicherheit (GRS). The authors wish to acknowledge the GRS for their willingness to provide the released version of the ATHLET code (ATHLET Mod 2.2 Cycle A) for use at FER.

REFERENCES

[1] RELAP5/mod3.3 Users Manual, The RELAP Code Development Team, NUREG/CE-5535/Rev 1, Information Systems Laboratories, Inc., Rockville-Maryland, Idaho Falls-Idaho, January 2002.

[2] NEK RELAP5/MOD3.3 Nodalization Notebook, NEK ESD-TR-01/09, (FER-ZVNE/SA/DA-TR04/08-1), Krško 2009.

[3] NEK RELAP5/MOD3.3 Steady State Qualification Report, NEK ESD-TR-02/09, (FER-ZVNE/SA/DA-TR05/08-1), Krško 2009.

[4] G. Lerchl, H. Austregesilo, ATHLET Mod 2.2 Cycle A User's Manual, Gesellschaft für Anlagen-und Reaktorsicherheit (GRS) mbH, July 2009.

[5] V. Benčik, A. Höld, "Analysis of Transients and Accidents with the System Code ATHLET for the Krško Nuclear Power Plant, Proc. Int. Conf. Nuclear Option in Countries with Small and Medium Electricity Grid, Opatija, October 7-9, 1996, 202-209, ISBN 953-96132-4-8.

[6] D. Grgić, V. Benčik, S. Šadek, N. Čavlina, "RELAP5 Modeling of PWR Reactor RTD Bypass", Proc. of the 8th Int. Conf. on Nuclear Option in Countries with Small and Medium Electricity Grids, Dubrovnik, Croatia, May 16-20, 2010, S6-68.

[7] D. Grgić, V. Benčik, N. Čavlina, S. Šadek, "Coupled Code Calculation of Rod Withdrawal at Power Accident", Proc. Int. Conf. Nuclear Energy for New Europe 2011, Bovec, Slovenia, September 12-15, 2011, 817.

Journal of Energy

VOLUME 62 Number 1–4 | 2013 Special Issue

journal homepage: http://journalofenergy.com/

Nuclear Fuel Modelling During Power Ramp

Federico Cantini, Martina Adorni, Francesco D'Auria
GRNSPG, San Piero a Grado Nuclear Research Group, University of Pisa
Via Livornese 1291, San Piero a Grado (PI), Italy
f.cantini@ ing.unipi.it, m.adorni@ing.unipi.it, f.dauria@ing.unipi.it

ABSTRACT

Fuel rods operating for several years in a LWR can experience fuel-cladding gap closure as a result of the phenomena due to temperature and irradiation. Local power increase induces circumferential stresses in the cladding as a result of the different expansion in the cladding and the pellet. In presence of corrosive fission products (i.e. Iodine) and beyond specific stress threshold and level of burnup, cracks may grow-up from the internal to the external cladding surface, causing fuel rod failure. The phenomenon, known as pellet cladding interaction-stress corrosion cracking PCI/SCC, or PCI, has been identified as a problem since the 70's.

The PWR Super-Ramp experiment (part of OECD/NEA "International Fuel Performance Experiments (IFPE) database") twenty eight fuel rods behaviour has been simulated using TRANSURANUS code version "v1m1j11". Two sets ("Reference" and "Improved") of suitable input decks modelling the fuel rods, based on the available literature are used to run the simulations. Focus is given to the main phenomena which are involved or may influence the cladding failure. Systematic comparison of the code results with the experimental data are performed for the parameters relevant for the PCI phenomenon. Sensitivity calculations on fission gas release models implemented in TRANSURANUS code are also performed in order to address the impact on the results.

The results show the ability of TRANSURANUS version "v1m1j11" in conservatively predicting the rods failure due to PCI in PWR fuel and Zircaloy-4 cladding. Increased availability of experimental data would help to perform a deeper analysis.

1 INTRODUCTION

Stress corrosion cracking (SCC) can induce Pellet-cladding interaction (PCI) failures [1][2], which might occur in presence of local power increase. The relevance of PCI in nuclear technology is connected with the prevention of fuel failures due to SCC, involving the loss of integrity of the first and second barriers during normal, off normal and accident conditions.

TRANSURANUS [3][4][5] is a computer program for the thermal and mechanical analysis of fuel rods in nuclear reactors .The TRANSURANUS code consists of a clearly defined mechanical–mathematical framework into which physical models can easily be incorporated. The mechanical–mathematical concept consists of a superposition of a one-dimensional radial and axial description (the so called quasi two-dimensional or 1½-D model). The code was specifically designed for the analysis of a whole rod.

The aim of the study is to verify the ability of TRANSURANUS code version v1m1j11 in simulating the PCI phenomenon and predicting the cladding failure.

The experimental data used for the TRANSURANUS evaluation are part of the Studvisk PWR Super-ramp project. It address the behavior of 28 PWR rods subjected to power ramp at burnup range between 28 and 45 MWd/kgU.

2 PWR SUPER-RAMP

In the PWR Super-Ramp project, 28 fuel rods were ramp tested in order to contribute to the understanding of the PCI (Pellet Cladding Interaction) failure mechanism under power ramp condition[1]. Fuel rods were provided by two manufacturers: 19 by KraftWerk Union AG/Combustion Engineering (KWU/CE) and 9 by Westinghouse (W).

The KWU fuel rods (length about 300mm) were irradiated in the Obrigheim (Germany) power reactor, having a 2655mm core active length. The rods are divided in 4 groups. In Table 1 the main properties of the groups are summarized.

Table 1 KraftWerk Union AG/Combustion Engineering (KWU/CE) rods groups.

Group name	Number of rods	Rod type	Nominal burnup (MWd/KgU)
PK1	5	Standard rods	35
PK2	5	Standard rods	44
PK4	4	Standard rods plus Gd2O3 (4%)	33
PK6	5	Remedy rods. Large grain	36

The W rods (length about 980mm) in the Mol (Belgium) BR-3 reactor, having a 1000mm active core length. The rods are divided in 2 groups. In Table 2 the main properties of the groups are summarized.

Table 2 Westinghouse (W) rods groups.

Group name	Number of rods	Rod type	Nominal burnup (MWd/KgU)
PW3	5	Standard rods	30
PW5	4	Remedy rods, annular pellets	32

All the 28 rods were power ramped at the Studsvik R2 research reactor using suitable experimental rig to simulate PWR conditions. The power ramp test include the following steps:

- 24 hours long preconditioning phase at 25KW/m;
- Power ramp at a constant rate ranging between 150 and 600 KW/(mh) until the power reaches the preselected ramp terminal level (RTL);
- Holding phase at RTL held for about 12 hours or until the rod failure.

Ramping data are reported in Table 3.

Table 3 Rods ramping data.

Rod group	Rod label	Conditioning terminal level (W/m)	Conditioning holding time (h)	Ramp terminal level (W/m)	Ramp rate (W/mh)	Hold time at RTL (minutes)
PK1	PK1/1	25	24	41.5	540	720
	PK1/2	25	24	44	480	720
	PK1/3	25	24	47.5	510	720
	PK1/4	25	24	47.5	570	720
	PK1/S	25	24	42	360	720
PK2	PK2/1	25	24	41	510	720
	PK2/2	25	24	46	570	720
	PK3/3	25	24	49	510	720
	PK2/4	25	24	44	510	1
	PK2/S	25	24	44	510	720
PK4	PK4/1	25	24	39	480	720
	PK4/2	25	24	44.5	510	720

	PK4/3	25	24	50.5	660	720
	PK4/S	25	26	43	510	720
PK6	PK6/1	25	24	45	540	55
	PK6/2	25	24	40	540	720
	PK6/3	25	24	43	540	720
	PK6/4	25	24	44	600	60
	PK6/S	25	24	41	600	720
PW3	PW3/1	25	24	40	600	22
	PW3/4	25	24	37.7	540	12
	PW3/S	25	24	40.5	600	17
PW5	PW5/1	25	24	42.7	540	118
	PW5/2	25	23	40.3	540	26
	PW5/3	25	24	38.2	540	38
	PW5/4	25	24	38	510	72

The rods failed are 9 out of 28: PK6/1, PK6/4 and all the PW rods.

3 TRANSURANUS MODELS

3.1 Input decks

TRANSURANUS models developed in [8] have been used for the validation of version v1m1j11 of the code. The models were developed according to the original experimental data[6] for the 19 KWU rods and for the 9 W rods. Two sets of input decks have been developed in [7] and [8]: "Reference" and "improved".

The models selected in the "Reference" set are generally the ones standard for the transient to be simulated. Only the active part of the fuel is accounted for the simulation. For the reference calculations, the nominal geometrical values were used when available, the measured values are considered when nominal values are not specified (gas plenum length). The input deck of each rod within KWU group differs from the others in:

- boundary conditions: burnup, linear heat rate, ramp terminal level, cladding temperature histories;
- geometry: pellet diameter, cladding inner and outer diameter, gas plenum length;
- physical proprieties: enrichment, UO_2 grain size (PK6 rods are of large grain size), gadolinium content (PK4 rods contain Gadolinium), porosity.

The input deck of each rod within W group differs from the others in:

- boundary conditions: burnup, linear heat rate, ramp terminal level, ramp rate, clad temperature histories;
- geometry: pellet diameter, cladding inner and outer diameter, gas plenum length, kind of pellet standard (PW3 are standard while PW5 are annular);
- physical proprieties: enrichment, UO_2 grain size, porosity.

The KWU rods differ from W rods principally in:

- base irradiation performed into two different reactors.

fuel rods height: W rods are about three times longer than KWU rods.

The main properties of the rods are reported in Table 4.

Table 4 Main properties of fuel rods

Group label	Rod Label	Gas plenum length (mm)	Clad outer diam. (mm)	Clad Inner diam. (mm)	Pellet outer diam. (mm)	Pellet inner diam. (mm)	Clad grain size (µm)	UO2 grain size (µm)	Gd_2O_3 content (w%)	U235 enrich. (w%)
PK1	**PK1/1**	32.0	10.76	9.31	9.110	0	10.5	6	0	3.2
	PK1/2	32.2								
	PK1/3	32.4								
	PK1/4	32.3								
	PK1/S	32.1								
PK2	**PK2/1**	32.6	10.75	9.28	9.138	0	9.5	5.5	0	3.21
	PK2/2	33.0								
	PK2/3	32.5								
	PK2/4	32.6								
	PK2/S	32.8								
PK4	**PK4/1**	32.4	10.77	9.28	9.113	0	9.5	5.5	$4.09^{+/-}_{0.05}$	3.19
	PK4/2	32.8								
	PK4/3	32.4								
	PK4/S	32.8								
PK6	**PK6/1**	33.1	10.74	9.29	9.144	0	12.0	22	0	2.985
	PK6/2	32.5								
	PK6/3	33.0								
	PK6/4	33.0								
	PK6/S	32.9								
PW3	**PW3/1**	117.78	9.51	8.35	8.19	0		10.5	0	8.26
	PW3/2	119.32								
	PW3/3	118.66								
	PW3/4	104.90								
	PW3/S	116.48								
PW5	**PW5/1**	120.94	9.51	8.35	8.19	2.17		16.9	0	5.74
	PW5/2	121.36								
	PW5/3	121.48								
	PW5/4	121.88								

KWU rods have been modelled using 3 axial slices, while W rods have been modelled using 6 axial slices. The lengths of the slices are reported in Table 5 and Table 6.

Table 5 KWU rods axial slices

Group label	Slice 1 Height [mm]	Slice 2 Height [mm]	Slice 3 Height [mm]
PK1 PK2 PK4	104	80	128
PK6	90	80	145

Table 6 W rods axial slices

Rod label	Slice 1 Height [mm]	Slice 2 Height [mm]	Slice 3 Height [mm]	Slice 4 Height [mm]	Slice 5 Height [mm]	Slice 6 Height [mm]
PW3/1	169	169	13	209	209	209
PW3/4	171	171	13	211	211	211
PW3/S	170	170	14	209	209	209
PW5 group	169	169	14	208	208	208

The "Improved" set is based on the results obtained from the sensitivity analyses performed in [8]. An "improved" input-deck may be necessary to take into account the different designs and irradiation conditions among the six groups (PK1, PK2, PK4, PK6, PW3, PW5). Differences in design, material, fabrication procedure and base irradiation history may influence the rod behavior during ramping and the achieved rod data[1]. It must be mentioned that the gap geometry, the grain size, the cladding tensile and rupture stresses are characteristics of each group as well as the rod lengths and the active lengths of the NPP cores used for the base irradiation

3.2 Boundary conditions

The following boundary conditions have been implemented in order to allow the TRANSURANUS simulation both in base irradiation and ramp test:

- Linear heat rates (LHR) at 3 (KWU rods) or 6 (W rods) axial position;
- Cladding temperature histories at the same axial position;
- Neutron fast flux (one average value for each irradiation cycle);
- Coolant pressure (one value).

The rate of increase and decrease between different constant LHR spans has been selected as 6 KW/(mh). The power ramps have been derived from original experimental data [6] and from data available in [1]. **Error! Reference source not found.** shows, as an example, the LHR for the rod PK1/S during base irradiation (left) and power ramp (right).

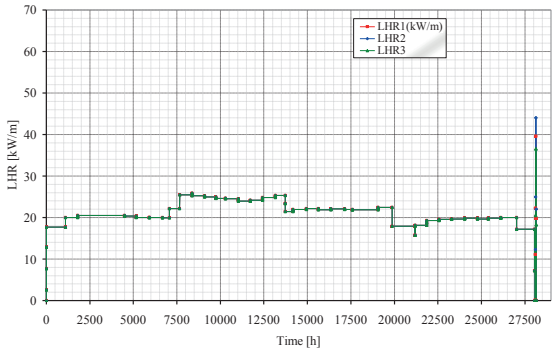

Figure 1: Rod PK1/S – LHR for base irradiation.

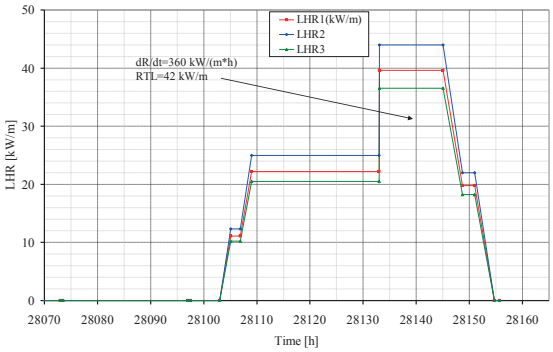

Figure 2: Rod PK1/S – LHR for power ramp (right).

3.3 Fission Gas Release sensitivity analysis

The objective of the sensitivity analysis is to verify the influence of the FGR models on the failure predictions. The "Reference" calculations are performed with Fgrmod 6 to treat intragranular bubbles gas behavior. It uses the URGAS algorithm with the diffusion coefficients of Hj. Matzke (thermal) and a constant athermal diffusion coefficient; the sensitivities concern:

- Fgrmod 4: URGAS algorithm with the diffusion coefficients of Hj. Matzke (thermal) and athermal diffusion coefficient according to data of R. White.
- Fgrmod 9: URGAS algorithm with diffusion coefficients of T. Turnbull.

The "Reference" model that considers intergranular gas bubbles behavior is igrbdm 3, the new model to treat the grain boundary FGR during power ramps. Three sensitivities are performed with the "Reference" model for intragranular behavior (Fgrmod 6) and setting the intergranular behavior to:

- Igrbdm 0: Fission gas behavior at grain boundaries not treated
- Igrbdm 1: Simple grain boundary fission gas behavior model (standard option)
- Igrbdm 2: Simple grain boundary fission gas behavior model

The solving algorithm used in the "Reference" simulation is Idifsolv 0: diffusion equation is solved by the URGAS-algorithm. The analyses are performed with the "Reference" models for intragranular and intergranular behaviors (Fgrmod 6, Igrbdm3 respectively) and changing the solving algorithm to:

- Idifsolv 6: Diffusion equation is solved by the FORMAS-algorithm with 6 exponential terms.

4 RESULTS

4.1 Cladding diameter change

Measurements related to the cladding creep down are provided by the PWR Super-Ramp Project database [6]. The maximum cladding diameter decrease (max creep down) is calculated as the greatest difference between several measures of the diameter prior to irradiation (PTI) and prior to ramp (PTR) at room temperature (20 C°) and atmospheric pressure. The same parameter is calculates using "reference" TANSURANUS simulation data and compared to the experimental in Figure 2. A systematic under-prediction of the experimental data can be observed.

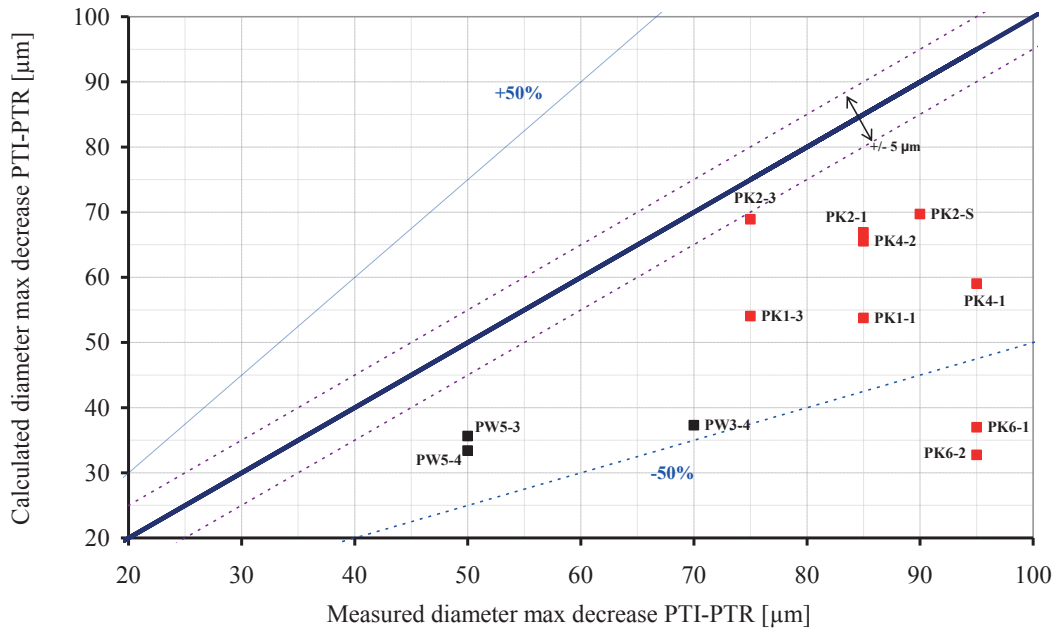

Figure 2: Cladding diameter change, base irradiation.
Comparison between experimental data and simulation.

Analogously, the maximum diameter increase is calculated from several diameter measurements performed prior to ramp (PTR) and after the ramp (AR) at room temperature and atmospheric pressure. Experimental measures are provided between ridges and at the ridges edges. Since TRANSURANUS is not able to simulate ridges, the experimental between ridges are used. Comparison between experimental and calculated data ("Reference") are shown in Figure 3

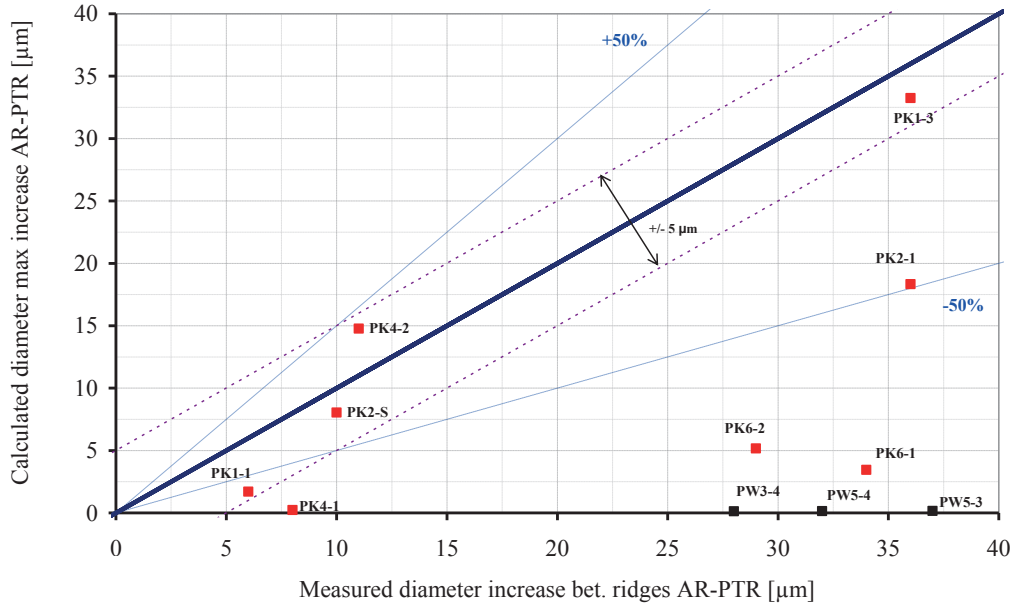

Figure 3: Cladding diameter change, ramp test.
Comparison between experimental data and simulation

4.2 Cladding outer corrosion

The comparison between the experimental data and the "Reference" TRANSURANUS simulation are reported in Figure 4

The KWU rods show highest values of cladding corrosion layer thickness. The simulation suggests that these rods reach the break-away point. The selected model is the EPRI standard model. The results under-estimation is about 50%, except PK2/4 and PK6/3, where greater errors are observed.

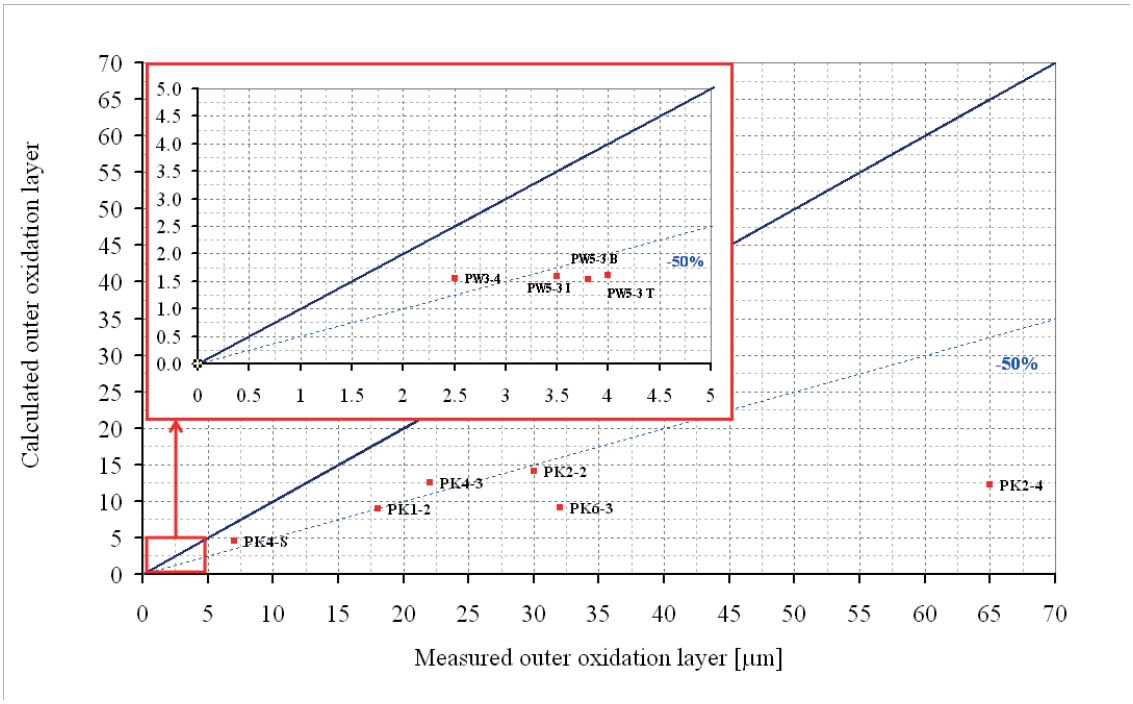

Figure 4: Cladding corrosion. Comparison between experimental data and simulation

4.3 Fission gas release

The comparison between the experimental data and the "Reference" TRANSURANUS simulation are reported in Figure 5.

Different predictions are observed:

- PK1 group results over predicted; the range of FGR is between 5 and 25%.
- PK2 group is generally slightly under predicted with the exception of PK2/S rod, this rod was ramped at a temperature 50° C lesser than the others. In this case, the range of FGR spreads between 10 up to 45 % (simulation and experiment).
- PK4 group results slightly under predicted with the exception of rod PK4/S that shows the worst under prediction (about -60%). The range of FGR is embedded in 10-30% (experiment and simulation)
- PK6 and PW3 groups highlight low values of FGR (less than 10%) both in the experiment and calculation. The trend is generally under predicted.

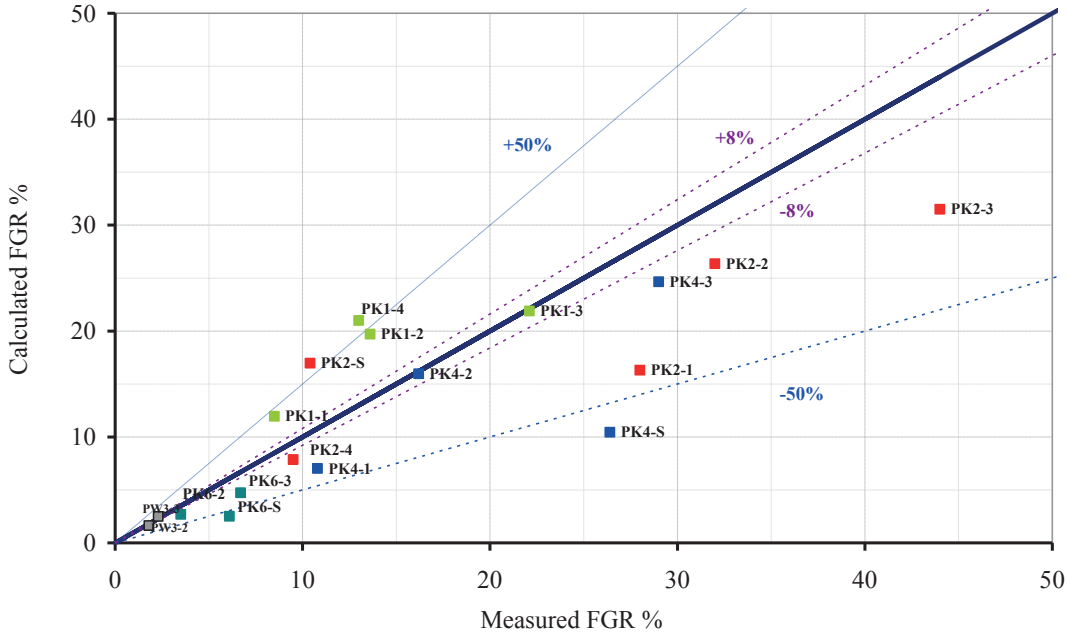

Figure 5: Fission gas release. Comparison between experimental data and simulation

4.4 Failure prediction

The TRANSURANUS failures predictions are summarized and compared with experimental data in Table 7. In the "Reference" calculation, the KWU rods are conservatively predicted even if the failures number is over-estimated, while the W rods are incorrectly predicted not-failed.

Table 7: Failure prediction. Comparison between experimental data and simulation

Rod group	Rod Label	Measured Burnup [MWd/kgU]	EXP F/NF	TU Reference F/NF	TU Improved F/NF
PK1	PK1-1	35.4	NF	NF	NF
	PK1-2	35.6	NF	F	NF
	PK1-3	35.2	NF	F	NF
	PK1-4	33.1	NF	NF	NF
	PK1-S	34.4	NF	NF	NF
PK2	PK2-1	45.2	NF	F	F
	PK2-2	45.1	NF	F	F
	PK2-3	44.6	NF	F	F
	PK2-4	41.4	NF	F	F
	PK2-S	43.4	NF	F	NF
PK4	PK4-1	33.7	NF	NF	NF
	PK4-2	33.8	NF	F	NF
	PK4-3	33.6	NF	F	NF
	PK4-S	32.5	NF	NF	NF
PK6	PK6-1	36.7	F	F	F
	PK6-2	36.8	NF	F	F
	PK6-3	36.5	NF	F	F
	PK6-4	33.6	F	F	F
	PK6-S	35.9	NF	F	F
PW3	PW3-1	38.1	F	NF	F
	PW3-4	36.6	F	NF	NF
	PW3-S	35.1	F	NF	F
PW5	PW5-1	40.5	F	NF	F
	PW5-2	39.9	F	NF	F
	PW5-3	41.4	F	NF	F
	PW5-4	39.2	F	NF	F

The “Improved” calculation corrects the results of 5 KWU rods without introducing false negatives (failed rods predicted not-failed). The W rods are now correctly predicted except PW3/4.

4.5 Fission gas release sensitivity analysis

The results of three different models for the intragranular bubbles gas behavior are plotted in Figure 6. The sensitivities highlight an increase of the calculated FGR comparatively with the reference case. The model Fgrmod4 better represents the behavior of PK2 and PK4 groups (PK1 result over predicted, PK6 and PW3 that have low FGR are predicted as in the reference). Model Fgrmod9 largely over predicts the FGR.

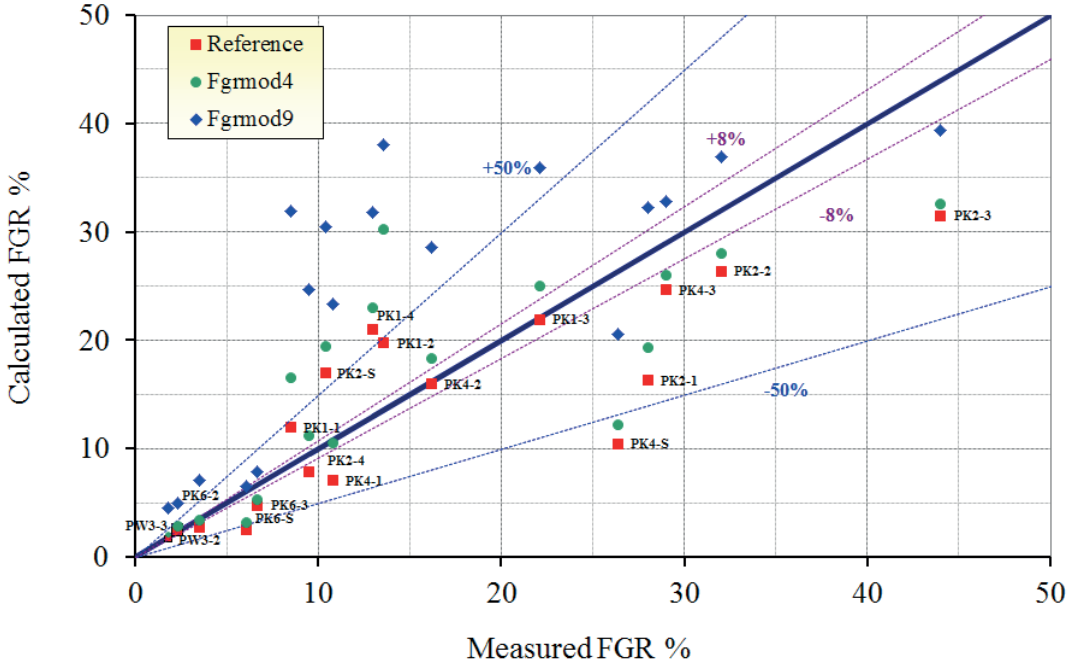

Figure 6: Fission gas release, intragranular behaviour models.
Comparison between experimental data and simulation

The results of four different models for the intergranular bubbles gas behavior are plotted in Figure 7. With the exception of the Igrbdm0 that assumes FGR without grain boundaries trapping in the other cases the predictions are lower compared to the reference one. Igrbdm 1 and Igrbdm 2 seem better represent the FGR of group PK1 while make worst the predictions in the other cases.

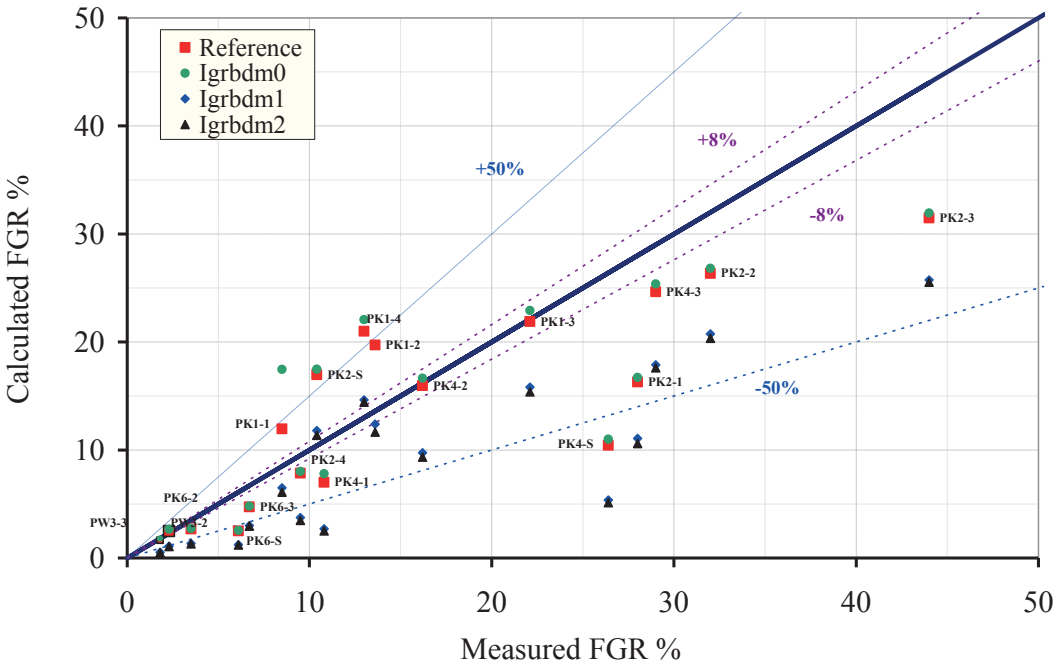

Figure 7: Fission gas release, intergranular behaviour models.
Comparison between experimental data and simulation

Best estimate predictions can be reached choosing different models, the result obtained are presented in Figure 8.

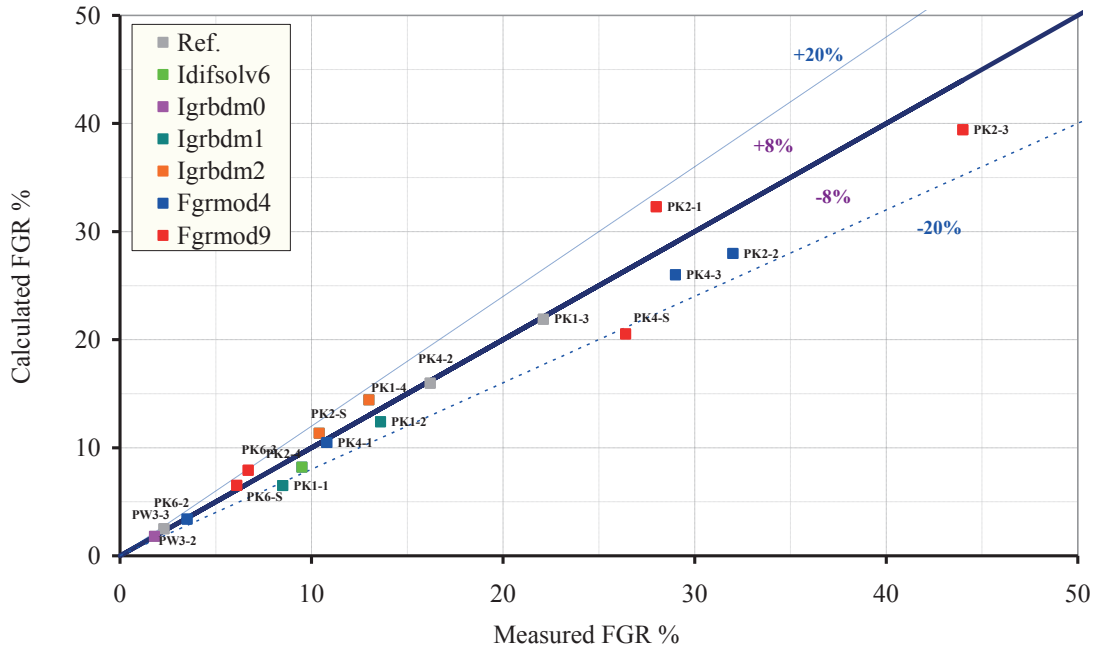

Figure 8: Fission gas release, best estimate results.
Comparison between experimental data and simulation

The different models seem to be not significant in term of failure prediction. Some model predicts the correct not failures of one rod (PK1/2). Results are summarized in Table 8.

Table 8 Failure prediction. FGR sensitivity analysis.

Rod group	Rod Label	Measured Burnup [MWd/kgU]	EXP F/NF	TU Ref. F/NF	TU Idifsolv6 F/NF	TU Igrdbm0 F/NF	TU Igrbdm1 F/NF	TU Igrbdm2 F/NF	TU Fgrmod4 F/NF	TU Fgrmod9 F/NF
PK1	PK1-1	35.4	**NF**	NF	NF	NF	NF	NF	NF	NF
	PK1-2	35.6	**NF**	**F**	NF	**F**	NF	NF	**F**	**F**
	PK1-3	35.2	**NF**	**F**	**F**	**F**	**F**	**F**	**F**	NF
	PK1-4	33.1	**NF**	NF	NF	NF	NF	NF	NF	NF
	PK1-S	34.4	**NF**	NF	NF	NF	NF	NF	NF	NF
PK2	PK2-1	45.2	**NF**	**F**	**F**	**F**	**F**	**F**	**F**	**F**
	PK2-2	45.1	**NF**	**F**	**F**	**F**	**F**	**F**	**F**	**F**
	PK2-3	44.6	**NF**	**F**	**F**	**F**	**F**	**F**	**F**	**F**
	PK2-4	41.4	**NF**	**F**	**F**	**F**	**F**	**F**	**F**	**F**
	PK2-S	43.4	**NF**	**F**	**F**	**F**	**F**	**F**	**F**	**F**
PK4	PK4-1	33.7	**NF**	NF	NF	NF	NF	NF	NF	NF
	PK4-2	33.8	**NF**	**F**	**F**	**F**	**F**	**F**	**F**	**F**
	PK4-3	33.6	**NF**	**F**	**F**	**F**	**F**	**F**	**F**	**F**
	PK4-S	32.5	**NF**	NF	NF	NF	NF	NF	NF	NF
PK6	PK6-1	36.7	**F**	F	F	F	F	F	F	F
	PK6-2	36.8	**NF**	**F**	**F**	**F**	**F**	**F**	**F**	**F**
	PK6-3	36.5	**NF**	**F**	**F**	**F**	**F**	**F**	**F**	**F**
	PK6-4	33.6	**F**	F	F	F	F	F	F	F
	PK6-S	35.9	**NF**	**F**	**F**	**F**	**F**	**F**	**F**	**F**
PW3	PW3-1	38.1	**F**	**NF**	**NF**	**NF**	**NF**	**NF**	**NF**	**NF**
	PW3-4	36.6	**F**	**NF**	**NF**	**NF**	**NF**	**NF**	**NF**	**NF**
	PW3-S	35.1	**F**	**NF**	**NF**	**NF**	**NF**	**NF**	**NF**	**NF**
PW5	PW5-1	40.5	**F**	**NF**	**NF**	**NF**	**NF**	**NF**	**NF**	**NF**
	PW5-2	39.9	**F**	**NF**	**NF**	**NF**	**NF**	**NF**	**NF**	**NF**
	PW5-3	41.4	**F**	**NF**	**NF**	**NF**	**NF**	**NF**	**NF**	**NF**
	PW5-4	39.2	**F**	**NF**	**NF**	**NF**	**NF**	**NF**	**NF**	**NF**

5 CONCLUSIONS

The ability of TRANSURANUS code version v1m1j11 in simulating the PCI phenomenon and predicting the cladding failure has been evaluated using the Studvisk PWR Super-Ramp data.

The simulation of 19 KWU rods shows a general under-prediction of the creepdown during the base irradiation and the diameter increase during power ramp. It is worth noting that the observed differences can be in part explained with the intrinsic limitation in TRANSURANUS geometric modelling: one-dimensional, plane and axisymmetric schematization characterized by plain strain condition, inability to model local geometry variation (i.e. ridges). A general under-prediction of the outer cladding oxidation is also observed. The prediction of the failure is correct for 7 out of 19 rods (Reference input decks). Improved input decks reach a correct prediction of 12 out of 19 rods All the errors are conservative.

The analysis of the W rods shows good results with the “improved” input decks, when an axial shape of the neutron fast flux is considered. & out of 7 rods are correctly predicted.

REFERENCES

[1] H.Bailly, D. Menessier, C. Prunier, “The nuclear fuel of pressurized water reactors and fast neutron reactors”, Collection du Commissariat a l’Energie Atomique, Lavoisier Pub., Intercept, Paris, Andover 1999.

[2] OECD/CSNI/PWG2 Task Force, “Fuel safety criteria technical review”, OECD/NEA/CSNI/R(99)25, Paris, 2000

[3] K. Lassmann, “TRANSURANUS: a fuel rod analysis code ready for use”, Journal of Nuclear Material 188 (1992) 295-302.

[4] P. Van Uffelen, “Modeling of Nuclear Fuel Behavior”, Publications Office, JRC Publications, Report EUR 22321 EN, European Commission, 2006.

[5] K. Lassmann., A. Schubert, P. Van Uffelen, Cs. Gyory, J. van de Laar, “Transuranus Handbook” Version “v1m1j11”, EC, JRC, ITU, 2011.

[6] S. Djurle, et al., “The Super-Ramp Project, Final report of the Super-Ramp project”, STIR-32, Studsvik AB Atomenergi, Studsvik, Sweden, 1984.

[7] D. Rozzia, M. Adorni, A. Del Nevo, F. D’Auria, “Capabilities of TRANSURANUS Code in Simulating Power Ramp Tests from the IFPE Database”, Nuclear Engineering and Design Vol. 241, p. 1078-1086, 2011

[8] D.Rozzia, M.Adorni, A.Del Nevo, F. D’Auria. “Capabilities of Transuranus code in simulating power ramp tests from the IFPE database: PWR super-ramp experiment,” FUMEX III report, 2010.

Journal of Energy
VOLUME 62 Number 1–4 | 2013 Special Issue
journal homepage: http://journalofenergy.com/

Identification of Limiting Case Between DBA and SBDBA (CL Break Area Sensitivity): A New Model for the Boron Injection System

R. Gonzalez, A. Petruzzi, F. D'Auria
San Piero a Grado Nuclear Research Group (GRNSPG)
University of Pisa
Via Livornese 1291-56122 - San Piero a Grado – Pisa - ITALY
r.gonzalez@ing.unipi.it, a.petruzzi@ing.unipi.it

O. Mazzantini
Nucleo-electrica Argentina Sociedad Anonima (NA-SA)
Buenos Aires, ARGENTINA
mazzantini@na-sa.com.ar

ABSTRACT

Atucha-2 is a Siemens-designed PHWR reactor under construction in the Republic of Argentina. Its geometrical complexity and (e.g., oblique Control Rods, Positive Void coefficient) required a developed and validated complex three dimensional (3D) neutron kinetics (NK) coupled thermal hydraulic (TH) model. Reactor shut-down is obtained by oblique CRs and, during accidental conditions, by an emergency shut-down system (JDJ) injecting a highly concentrated boron solution (boron clouds) in the moderator tank, the boron clouds reconstruction is obtained using a CFD (CFX) code calculation. A complete LBLOCA calculation implies the application of the RELAP5-3D© system code. Within the framework of the third Agreement "NA-SA – University of Pisa" a new RELAP5-3D control system for the boron injection system was developed and implemented in the validated coupled RELAP5-3D/NESTLE model of the Atucha 2 NPP. The aim of this activity is to find out the limiting case (maximum break area size) for the Peak Cladding Temperature for LOCAs under fixed boundary conditions.

1 INTRODUCTION

This document reports the information about RELAP5-3D©/NESTLE (thermal hydraulic/neutron kinetics) coupled codes transients analysis, from 0.1A up to the limiting case, Loss of Coolant Accident (LOCA) Cold Leg 2 (CL2) Break for the Atucha-2 PHWR, adopting the model for the CNA-II developed at University of Pisa [[1]], [[2]], [[3]]. The transient analysis was performed for the first twenty seconds.

The aim of this work is to characterize, through a qualified evaluation model, the range of break areas in which the DBA criteria are fulfilled with conservative criteria (n+2) for Safety Injection System (JND) together with the performance of the Boron Injection System (JDJ), that is assuming one lance in maintenance and the failure of another one for the boron injection. The boron clouds reconstruction was obtained using a CFD (CFX) code calculation.

R. Gonzalez, A. Petruzzi, F. D'Auria, O. Mazzantini, Identification of Limiting Case Between DBA and SBDBA (CL Break Area Sensitivity): A New Model for the Boron Injection System, Journal of Energy, vol. 62 Number 1–4 (2013) Special Issue, p. 81–92

Because of the addition of fluid transportation of RELAP5-3D a new boron injection control system was developed to maintain the real boron distribution, given by the CFD calculation, inside the moderator tank.

These activities were performed in the framework of the agreement "UNIPI/GRNSPG – NASA No. 3" for the completion of the Atucha-2 NPP.

All analyses of the LBLOCA are performed adopting the 280ch nodalization model for the CNA-II, developed at the GRNSPG of the University of Pisa, for calculating the Total Peak Power (TPP) and Peak Cladding Temperatures (PCT).

2 THE 3D MODERATOR TANK

The moderator is working also as a solvent for boric acid, which is injected for fast shutdown of the reactor by the boron injection system in the event that adequate shutdown reactivity is not ensured by the control rods

A 3D TH cylindrical model, corresponding to the RELAP5/3D nodalization of CNA-2 reactor developed at UNIPI, was considered.

A sketch of the RELAP5/3D nodalization of the moderator tank is shown in Figure 1.

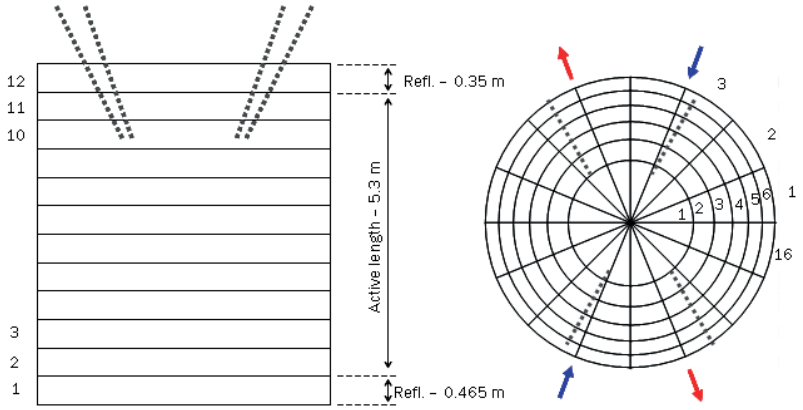

Figure 1: 3D moderator tank

The discretization has the following sub-divisions:

- 6 radial;
- 16 azimuthal (22.5° step);
- 12 axial (1st and 12th level corresponding to the reflector, and the 2nd to 11th corresponding to the active length of the core).

The total number of volumes (macro-cells) is 1152 (6x16x12).

The radial spacing is non-uniform but all macro-cells of the active part have approximately the same volume. The diameter of the moderator tank is 6.79 m. The axial spacing in the active length core is 0.53 m, while bottom and top reflectors are 0.465 m and 0.35 m respectively.

A sketch of the RELAP5 3D TH nodalization of the moderator tank and its coupling with the hexagonal NK nodes is given in Figure 2. The Boron injection lances are represented by the arrows: blue arrows are the working lances, black arrows are the NOT working lances.

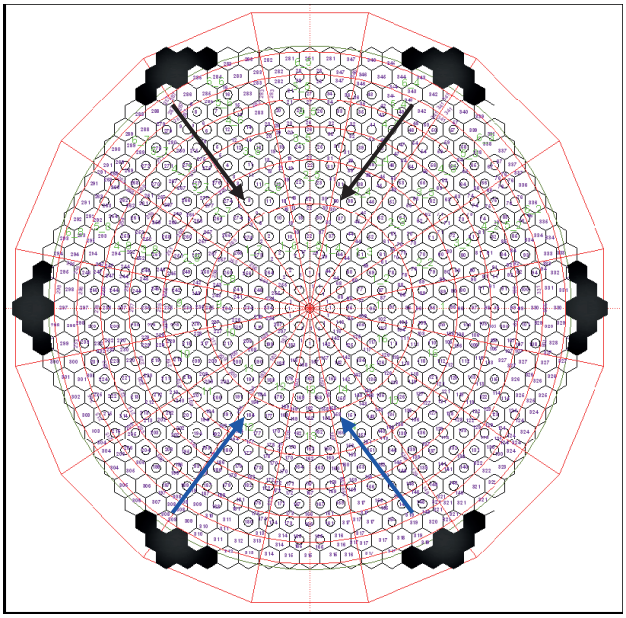

Figure 2: 3D moderator tank

3 JDJ SYSTEM

The information provided in the present section is extracted from the NA-SA report Ref. [[4]]. In addition, a thorough description of the boron injection system is also available on UNIPI report Ref. [[5]].

The emergency boron injection system, also referred to as “JDJ” in German reports, is a backup system for the fast shutdown of CNA-2 reactor, in addition to the control rods. The boron injection, powered by pressurized air, is meant to be actuated whenever the intervention of control rods is not sufficiently fast to shutdown the reactor.

The boron injection system, sketched in Figure 3, consists in four injecting lines, each including the following parts:

- One air tank
- One fast acting valve
- Two boron solution tanks
- One rupture membrane
- One injecting lance
- Pipelines connecting the above components

R. Gonzalez, A. Petruzzi, F. D’Auria, O. Mazzantini, Identification of Limiting Case Between DBA and SBDBA (CL Break Area Sensitivity): A New Model for the Boron Injection System, Journal of Energy, vol. 62 Number 1–4 (2013) Special Issue, p. 81–92

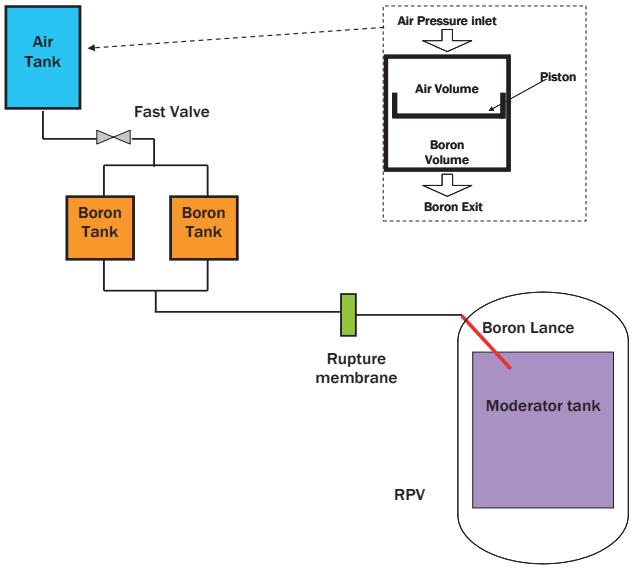

Figure 3: Boron injection system

The air tank is partly filled with highly pressurized air (200 bar) and partly with borated water, the two fluids being kept separated by a piston. The air tank is connected to the two boron solution tanks, which are arranged in parallel. Namely the "boron solution" is a solution of D_3BO_3 in heavy water, with a concentration of **7000 ppm** (1 ppm = 1 g boron per 1000 kg water), according to Ref. [[6]].

A fast-acting valve is located on the pipeline connecting the air tank with the boron tanks; in normal conditions the valve is closed, and separates the high pressure region (air tank) from the rest of the circuit, which is kept at low pressure (1 atm); during accidental events requiring the intervention of the boron injection system, a signal causes the valve to open and the whole system to be pressurized.

A pipeline connects the boron tanks to the RPV. However a rupture membrane is placed on such pipeline, with the purposes of separating the high pressure ambient (RPV) from the low pressure one (boron tanks) during normal operation. When the intervention of the injection system is requested, the pressurization of the injecting circuit causes the rupture membrane to break, thus allowing the borated solution to rapidly flow towards the RPV. Obviously some time is needed for the pressurization, which causes a delay in the intervention of the injection system.

The pipeline ends with the injection lance, which begins at the RPV closure head, passes throughout the upper plenum (UP) and finally enters the moderator tank (MT), allowing the borated solution to be efficiently diffused within the moderator.

4 CFD/RELAP5-3D BORON INJECTION SYSTEM

A procedure was developed by UNIPI for the coupling of the CFD analysis for the boron injection into the moderator with the Neutron Kinetics analysis.

The procedure consists of the following steps:

1. Data extraction from CFD results. The boron concentration calculated with the CFD, for several selected time instants and for each control volume of the computational grid, is extracted into text files in table format;
2. CFD data processing. Special routines read and process the above results. Given a particular discretization of the moderator domain into "macro-cells" (i.e. the 3D-NK mesh), the routines calculate time dependent mass of boron contained in each macro-cell, and output the related boron mass time history.

Further details on the two steps above are provided in the following [[7]].

After the application of the Visual Basic routine "CNA2_CFD2NK" developed specifically for this NK nodalization, the time history of the boron mass contained in each of 1152 macro-cells was output as a text file. The output of such data processing constitutes the information to be transferred to NK analyst. For more details see [[7]].

4.1 Boundary Conditions for CFD Simulation

The boundary conditions were provided by NASA. A RELAP5-3D model was used to simulate the JDJ system behavior during a 2A LOCA and to predict the boron injection flowrate and timing. NASA simulations were performed referring to the latest update of the JDJ system design.

The CFD simulation was performed using heavy water as a working fluid, but keeping the same flowrate as obtained by NASA with light water. Later, an *a posteriori* analysis showed that the selection of working fluid affects the flowrate magnitude by less than 5 % and that the resulting error in terms of injection delay (to reach the moderator tank) is in the order of 10 ms.

Therefore it was decided not to perform a new CFD simulation with a "corrected" flow-rate.

The CFD simulation requires the flowrate to be specified at the lance inlet. The total delay of between the LOCA and the first drop in the moderator tank (sum of electronic delay, valve opening, piston pressure, etc…), was calculated. For more information see [[8]].

4.2 New RELAP5-3D boron injection control

The shapes and the dynamics of the boron clouds were calculated by detailed CFD calculation performed by the CFX code (Moretti et.al., 2010). The evolution of the boron concentration of the clouds was then reconstructed in the 3D TH moderator tank, using an automatic routine and several time-dependent junctions.

In these calculations has been utilized 134 RELAP-time dependent junctions model guided by a boron injection system control that allows us to follow the same distribution of the CFD calculation.

In Figure 4 is showed a scheme of the RELAP5-3D boron insertion control: RELAP5-3D read the CFD data and follows exactly, by inserting and extracting boron, the same concentration of boron calculated by CFX. In Figure 5 is showed one moderator volume utilized for the injection through the time dependent junctions. The boron injection starts at t sec and finish a T s when the total amount of boron contained in all the boron tanks is inside the core moderator tank. The boron injection follows exactly the CFD distribution until X sec ($t<X<T$) then we continue whit a linear injection until the boron tanks are empty (time=T). In the white box (that is a zoom of the first instant of the transient) can be seen how the RELAP5 code (blue line) is following the CFD signal (green line), i.e. RELAP5 keep the quantity of boron inserted equal to that of the CFD. Figure 6 and Figure 7 shows, for two moderator volumes, that boron distribution is kept equal in CFD and in

RELAP5, the first cntrlvar is the boron quantity contained in CFD macro-volumes the second cntrlvar is the boron quantity contained in RELAP5 moderator volumes. After T s the right line of first cntrlvar is not working (the boron control system is off).

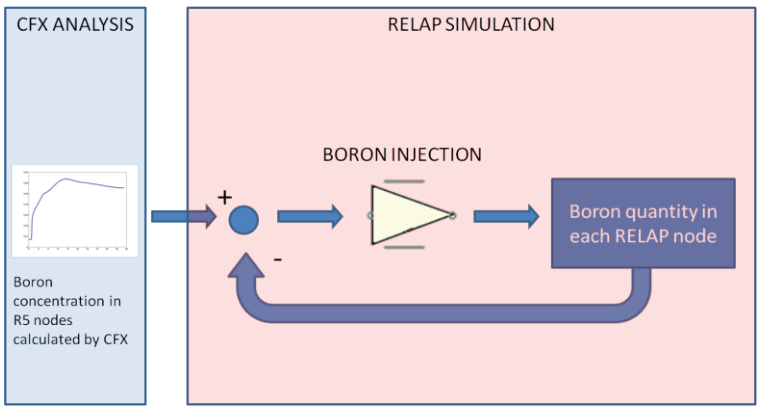

Figure 4: Scheme of the model utilized in RELAP5-3D© for the Boron Injection in the Moderator Tank

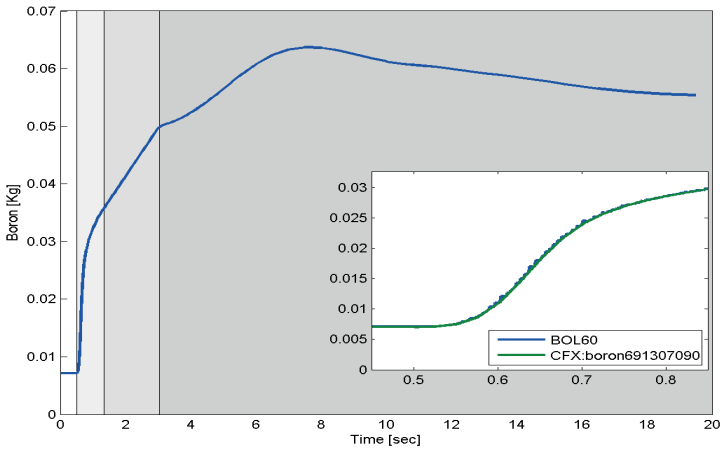

Figure 5: Boron injection in RELAP5-3D© for one moderator volume

R. Gonzalez, A. Petruzzi, F. D'Auria, O. Mazzantini, Identification of Limiting Case Between DBA and SBDBA (CL Break Area Sensitivity): A New Model for the Boron Injection System, Journal of Energy, vol. 62 Number 1–4 (2013) Special Issue, p. 81–92

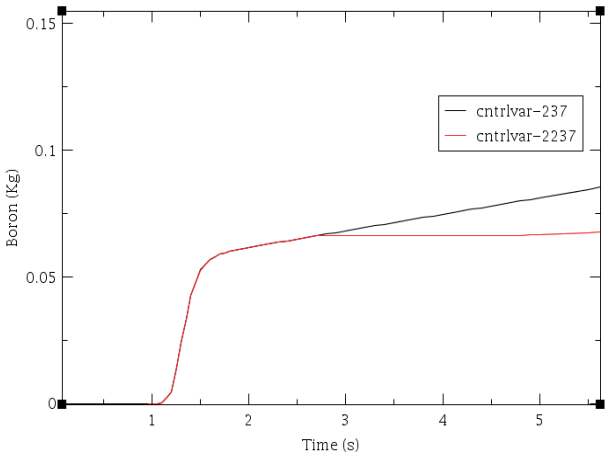

Figure 6: Boron injection in RELAP5-3D© follow CFD data for one moderator volumes. Cntrlvar 237=Boron in CFD macro-volumes, Cntrlvar 2237=Boron in RELAP5 moderator volumes (located in R=1, θ=4 and Z=6. After T s the implementation (black line) of first cntrlvar is not working .

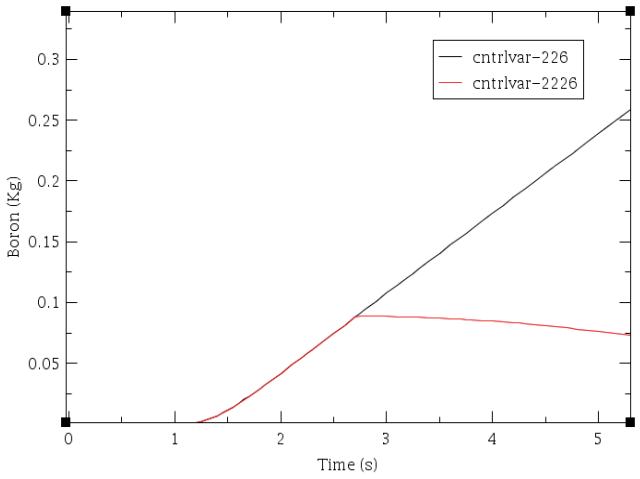

Figure 7: Boron injection in RELAP5-3D© follow CFD data for one moderator volumes. Cntrlvar 226=Boron in CFD macro-volumes, Cntrlvar 2226=Boron in RELAP5 moderator volumes (located in R=1, θ=2 and Z=9). After T s the implementation (black line) of first cntrlvar is not working.

5 CALCULATIONS RESULTS

5.1 Initial and Boundary Conditions

Information about the boundary and initial conditions, the imposed scenario and the main parameters' trends are reported hereafter.

As a common feature of the adopted approach, all the analyses are performed starting from nominal conditions, corresponding to 100% power condition (see [[9]], [[10]]). The core status is burnup equilibrium core (BEQ).

The boundary conditions and imposed events for this scenario are selected according to [[11]] and are reported in Table I and Table II.

The transient is initiated by the instantaneous opening of the break in the CL2 (i.e., 10^{-3} seconds, first time step of the transient). The break is assumed between the Reactor Pressure Vessel (RPV) nozzle and the CL2. Boron injection in the moderator tank by the JDJ emergency system starts at t seconds from the beginning of the transient and terminates at T seconds, even if it follow the CFD data only until X. The time of X seconds is not enough to inject all the boron mass present in the JDJ tanks so we inject constantly until T s the rest of the boron to reach the total amount of boron disposable inside the tanks. This procedure was adopted because of the limited number of time dependent junctions disposables due to the limit in the number of cards for the hydraulics components that can be used in RELAP5/3D. No CR scram intervention was assumed.

Table 1 Initial and Boundary conditions

Condition	Unit	Value
Break opening time	S	1.0e-3
CR position	% of insertion	G10: 94 G20: 67 G30: 24.5 S10: 4.29 Sh.Off: All Rods Out
Reactor Power	MW	2160

Table 2 Initial and Boundary conditions

No.	Event	Time(s)/System	Note
1	Accident start	0.0	Break opening RPV nozzle of CL2
2	Operator action	N/A	
3	Signal for the actuation of the Emergency Boron Injection System	0.0	

The values of the boundary conditions assumed in the calculations before the LB-LOCA transient are the results of the steady-state calculation performed with the nodalization 16-6 (see [[10]]).

All cases: Large Break LOCA at the nozzle connecting CL and RPV (SBDBA, realistic):

- Two boron lances active (first drop of borated boron reaches the core active region at t s after the start of transient).
- Core condition: equilibrium burn-up.

5.2 Calculated Results

An initial comparison was done between CFX (CFD) and RELAP5-3D/NESTLE calculations on boron distribution to verify the validity of the described model [[8]].

The main targets of this work can be synthesized as: a) Peak Cladding Temperature (PCT) for LOCAs, b) Normalized Maximum Total (core) Power Peak (TPP), c) Core Power, d) Clad Temperatures for each break area.

Results for the boron injection model, comparison between RELAP5/3D and CFD, and the main transient results are reported hereafter from Figure 9 to Figure 13. Figure 8 shows the channels that reaches the maximum clad temperatures. Comparison between RELAP/3D and CFD integral boron mass injected are shown in Figure 9 (plots are shifted in the time axis to avoid the RELAP5 and CFD differences in times calculations). Some results for limiting case from calculations for each break area are provided in Figure 12 and Figure 13.

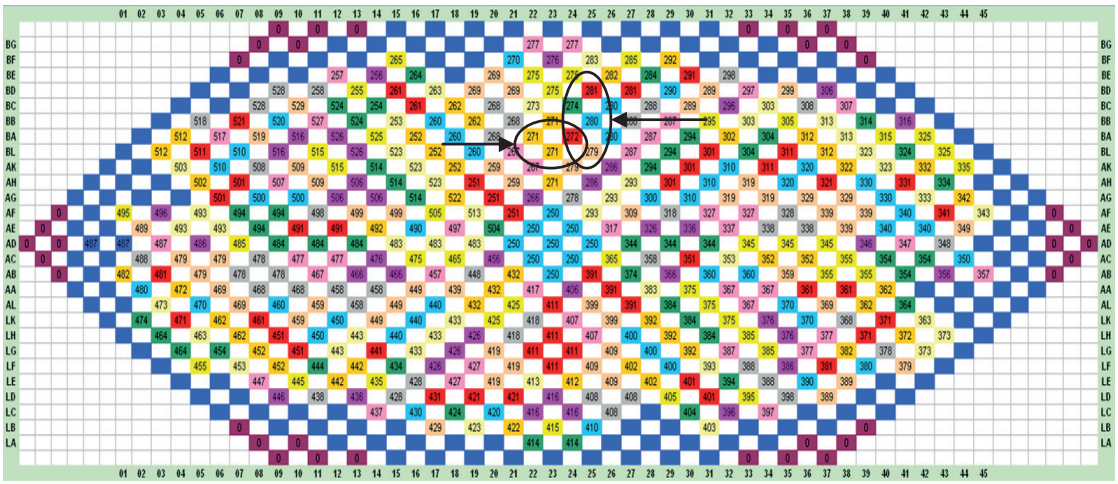

Figure 8: Map for the identification of the hotter channel.

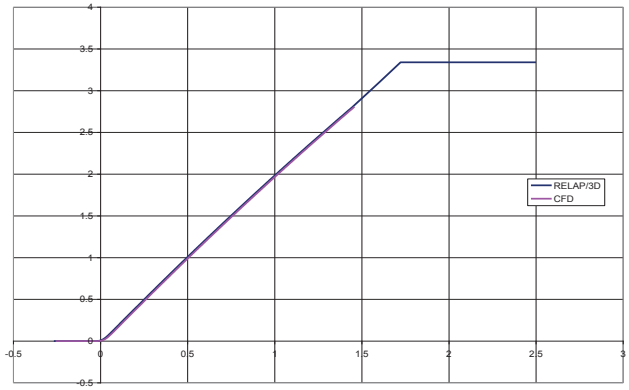

Figure 9: Comparison between RELAP/3D and CFD integral boron mass injected from the first drop in the moderator tank.

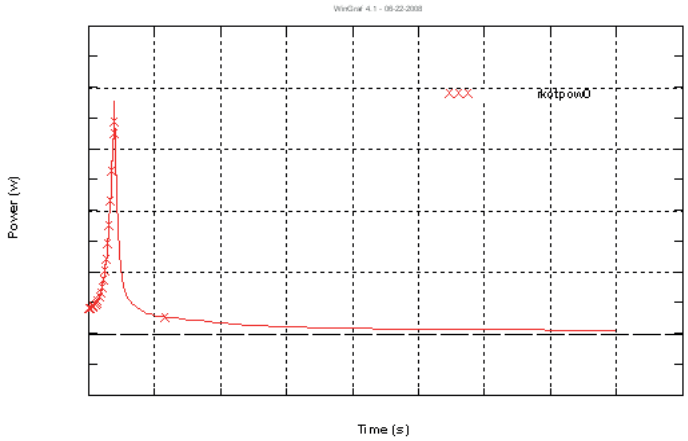

Figure 10: An example of power behavior during the transient

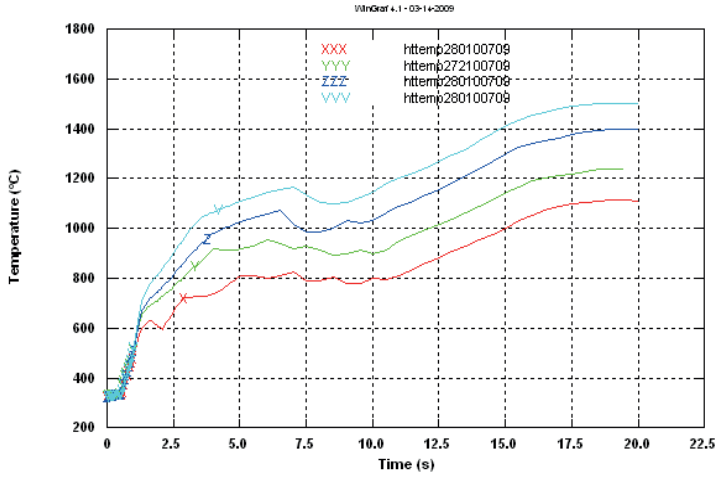

Figure 11: Trend of the clad temperatures in time for some different increasing break areas in LOCAs

R. Gonzalez, A. Petruzzi, F. D'Auria, O. Mazzantini, Identification of Limiting Case Between DBA and SBDBA (CL Break Area Sensitivity): A New Model for the Boron Injection System, Journal of Energy, vol. 62 Number 1–4 (2013) Special Issue, p. 81–92

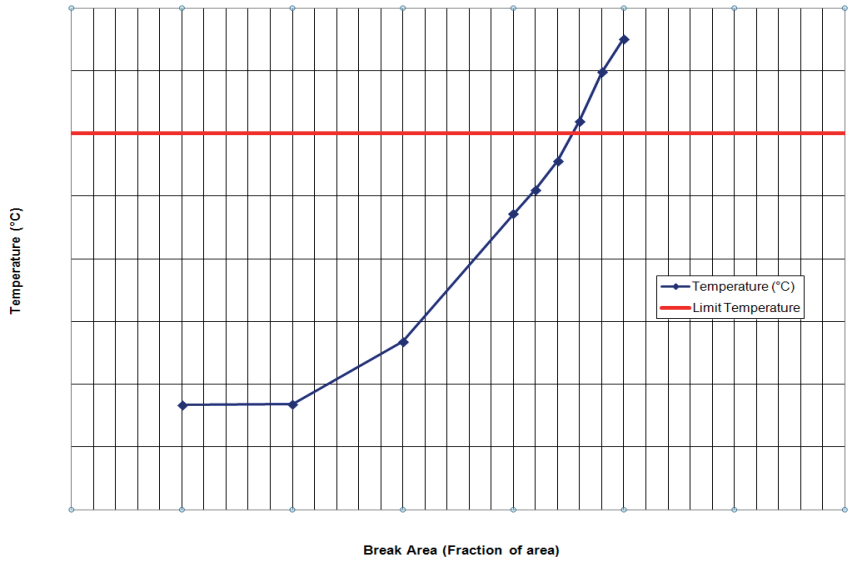

Figure 12: PCT for different break areas

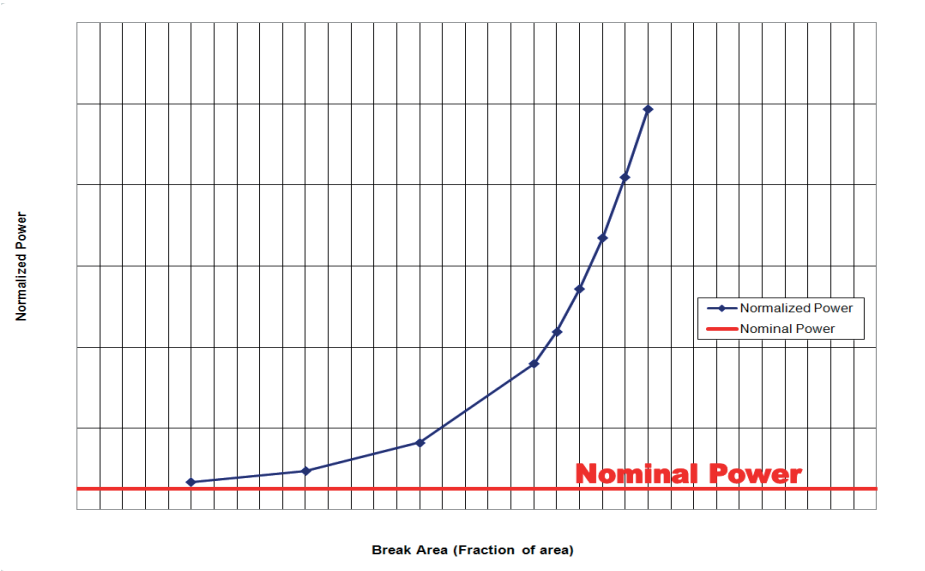

Figure 13: Maximum Normalized Power for all break areas

6 CONCLUSIONS

This document reports the model and the calculations results of RELAP5-3D©/NESTLE (thermal-hydraulic/3D NK coupled codes) of transients analysis, from 0.1A up to the limiting case, LOCAs CL2 Break for the Atucha-2 PHWR, adopting the model for the CNA-II developed at University of Pisa.

Data was adapted to RELAP5-3D/NESTLE after CFD (CFX) calculations by different ad hoc programs.

R. Gonzalez, A. Petruzzi, F. D'Auria, O. Mazzantini, Identification of Limiting Case Between DBA and SBDBA (CL Break Area Sensitivity): A New Model for the Boron Injection System, Journal of Energy, vol. 62 Number 1–4 (2013) Special Issue, p. 81–92

An initial comparison was done between CFD (CFX) and RELAP5-3D/NESTLE calculations on boron distribution to verify the validity of the described model: results showed a perfect agreement between CFD and RELAP calculations.

A new boron injection control system was showed.

The main targets of this work can be synthesized as: a) Peak Cladding Temperature (PCT) for LOCA, b) Normalized Maximum Total (core) Power Peak (TPP), c) Core Power and Normalized Core Power, d) Clad temperatures for claddings that reach the maximum temperatures for each break area.

REFERENCES

[1] RELAP5/Mod3 Code Manual, Volume I: *Code Structure, System Models, And Solution Methods,* INEEL-EXT-98-00834, vers. 2.4

[2] M. Cherubini, *"Upgrading the RELAP5 to RELAP-3D©",* SIR-1.3, Pisa, 30 June 2007**.**

[3] D. Araneo, A. Del Nevo, W. Giannotti, F.Moretti, C.Paris, "*Documentation for Platform Software Development and Qualification,* Task E1/Subtask E1.3 [R8], 31 july 2010.

[4] G. Salom, CNA II: "Modelo Hidraulico Del Sistema De Inyeccion De Boro De Emergencia", NASA Technical Report, 2007.

[5] A. Bousbia Salah, W. Giannotti, M. Cherubini, F. Mascari, M. Adorni, Preliminary RELAP5 "*Results of the Dead time connected with the CNA II Fast Boron Injection System (JDJ) activation*", TH-14, September 2007.

[6] Personal communication with Oscar Mazzantini, NA-SA

[7] F.Moretti**,** *"CFD Simulation of Fast Boron Injection in Case of 2 A LOCA with 2 injection lances",* Notes on Task A3.9 Sub-Task XXX, Task E1/Subtask E1.3 [R8], 28 October 2010.

[8] *D. Araneo, A. Del Nevo, W. Giannotti, F.Moretti, C.Paris,* "*Documentation for Platform Software Development and Qualification",* Task E1/Subtask E1.3 [R8], 31 july 2010

[9] C. Parisi, *"Identification and characterization of a relevant core status",* SIR-2.1, rev. 0, 23 March 2007.

[10] C.Parisi, *"Achievement of the three-dimensional neutron kinetics coupled thermal-hydraulics steady state for Atucha -II "* SIR-2.3, rev. 0, 7 july 2007.

[11] Bordihn, "*Initial and boundary conditions for Accident analyses*" KWU NAT/1195/011, Erlangen, 24.02.95.

Journal of Energy
VOLUME 62 Number 1–4 | 2013 Special Issue
journal homepage: http://journalofenergy.com/

BETHSY 9.1b test calculation with TRACE using 3D vessel component

Andrej Prošek, Ovidiu-Adrian Berar
Jožef Stefan Institute
Jamova cesta 39, SI-1000 Ljubljana, Slovenia
andrej.prosek@ijs.si, adrian.berar@ijs.si

ABSTRACT

Recently, several advanced multidimensional computational tools for simulating reactor system behavior during real and hypothetical transient scenarios were developed. One of such advanced, best-estimate reactor systems codes is TRAC/RELAP Advanced Computational Engine (TRACE), developed by the U.S. Nuclear Regulatory Commission. The advanced TRACE comes with a graphical user interface called SNAP (Symbolic Nuclear Analysis Package). It is intended for pre- and post-processing, running codes, RELAP5 to TRACE input deck conversion, input deck database generation etc. The TRACE code is still not fully development and it will have all the capabilities of RELAP5.

The purpose of the present study was therefore to assess the 3D capability of the TRACE on BETHSY 9.1b test. The TRACE input deck was semi-converted (using SNAP and manual corrections) from the RELAP5 input deck. The 3D fluid dynamics within reactor vessel was modeled and compared to 1D fluid dynamics. The TRACE 3D calculation was compared both to TRACE 1D calculation and RELAP5 calculation. Namely, the geometry used in TRACE is basically the same, what gives very good basis for the comparison of the codes. The only exception is 3D reactor vessel model in case of TRACE 3D calculation. The TRACE V5.0 Patch 1 and RELAP5/MOD3.3 Patch 4 were used for calculations. The BETHSY 9.1b test (International Standard Problem no. 27 or ISP-27) was 5.08 cm equivalent diameter cold leg break without high pressure safety injection and with delayed ultimate procedure. BETHSY facility was a 3-loop replica of a 900 MWe FRAMATOME pressurized water reactor.

In general, all presented code calculations were in good agreement with the BETHSY 9.1b test. The TRACE 1D calculation results are comparable to RELAP5 calculated results. For some parameters they are better, this is mostly due to better tuning of the break flow, what influences timing of the transient. When comparing TRACE 1D and TRACE 3D calculation, the latter is slightly better. One reason for comparable results is already good agreement of 1D calculations and there was not much space to further improve the results. The other reason may be that in the facility the phenomena were mostly one dimensional (for example, external downcomer was used for reactor vessel modeling). However, when 3D behavior of the heater rod temperatures was investigated, the advantage of three dimensional treatment was clearly demonstrated.

1 INTRODUCTION

Recently, several advanced multidimensional computational tools for simulating reactor system behavior during real and hypothetical transient scenarios were developed. The TRAC/RELAP Advanced Computational Engine (TRACE) [1] is the latest in a series of advanced, best-estimate reactor systems codes developed by the U.S. Nuclear Regulatory Commission. The advanced TRACE comes with a graphical user interface called SNAP (Symbolic Nuclear Analysis Package) [2]. It is intended for pre- and post-processing, running codes, RELAP5 to TRACE input deck conversion, input deck database generation etc.

A. Prošek, O. Adrian Berar, BETHSY 9.1b test calculation with TRACE using 3D vessel component, Journal of Energy, vol. 62 Number 1–4 (2013) Special Issue,
p. 93–103

The TRACE code is still not fully development and it will have all the capabilities of RELAP5. In addition, it has 3D capability for vessel components, while U.S. NRC RELAP5 is one dimensional code. The developers stated that TRACE has superior capabilities and accuracy for most applications compared to RELAP5. The comparison between RELAP5 and TRACE code with 1D vessel model has already been done [3]. The TRACE 1D calculation results for main safety parameters were as good as or better than the RELAP5 calculated results. The aim of this study is to assess the 3D capability of the TRACE on BETHSY 9.1b test. The TRACE input deck, which was semi-converted (using SNAP and manual corrections) from the legacy RELAP5 input deck, was used as starting point [3]. The reactor vessel was modeled manually. This means that the geometry except the reactor vessel and renodalization done for TRACE is basically the same for RELAP5, TRACE 1D and TRACE 3D model, what gives very good basis for the comparison of the codes.

2 METHODS

The BETHSY 9.1b test (International Standard Problem no. 27 or ISP-27) was 5.08 cm equivalent diameter cold leg break without high pressure safety injection and with delayed ultimate procedure. BETHSY facility was a 3-loop replica of a 900 MWe Framatome pressurized water reactor. For calculations the RELAP5/MOD3.3 Patch 4 [5] and TRACE V5.0 Patch 1 [1] were used. For better presentation of the calculated physical phenomena and processes, animation masks using SNAP were developed for displaying results obtained by RELAP5 and TRACE.

In the following subsections the BETHSY facility and test scenario are described first. Then the RELAP5 and TRACE input models are described. At the end the RELAP5 and TRACE thermal-hydraulic computer codes and SNAP tool are described briefly.

2.1 BETHSY facility

BETHSY was an integral test facility, which was designed to simulate most pressurized water reactor accidents of interest, study accident management procedures and validate the computer codes. The schematic of the BETHSY facility, created by SNAP, is shown in Figure 1. The BETHSY facility was a scaled down model of three loop Framatome (now AREVA NC) nuclear power plant with the thermal power 2775 MW. Volume, mass flow and power were scaled to 1:96.9, while the elevations and the pressures of the primary and secondary system were preserved [6]. The core power has been limited to approximately 10% of nominal value, i.e. 3 MW. This means that the power was limited to the decay heat level and the transients without reactor trip could not be simulated. The design pressure on the primary side was 17.2 MPa and on the secondary side 8 MPa. There were 428 electrically heated rods, which could reach 1273 K. Like in the reference reactor, the BETHSY facility had three identical loops, each equipped with a main coolant pump and an active steam generator. Every primary and secondary side engineered safety system was simulated. This included high and low pressure safety injection systems, accumulators (one per loop), pressurizer spray and relief circuits, auxiliary feedwater system and steam dumps to the atmosphere and to the condenser.

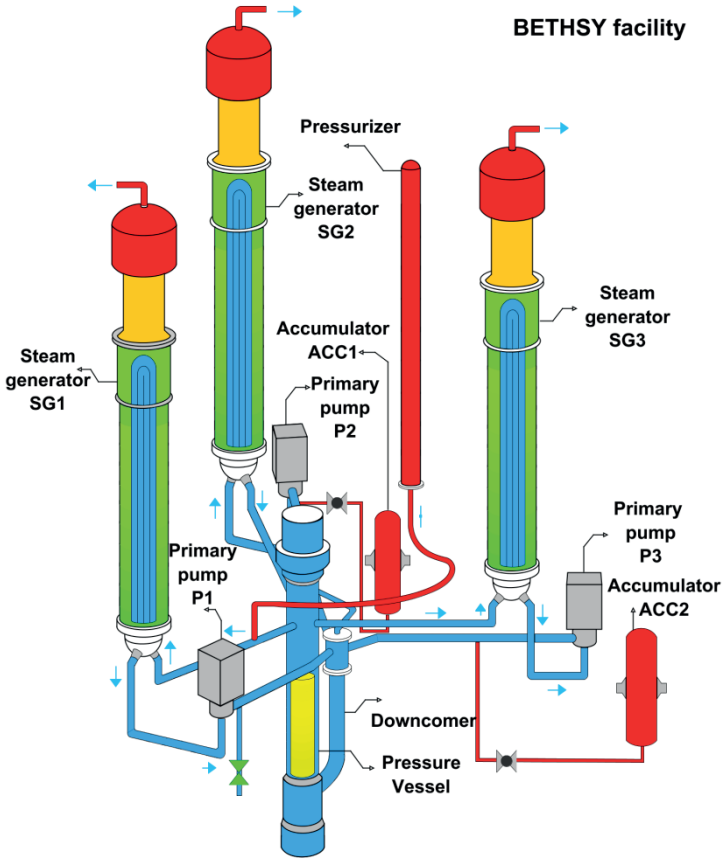

Figure 1: Schematic of the BETHSY facility

2.2 BETHSY 9.1b test description

The BETHSY 9.1.b test was a scaled 5.08 cm cold leg break without high pressure safety injection (HPSI) and with delayed operator action for secondary system depressurization [7]. This transient leads to a large core uncovery and fuel heat-up, requiring the implementation of an ultimate procedure. The scenario of the test started at 10% nominal power. At time 0 s the break was opened. The scram signal was obtained when pressurizer pressure dropped below 13.1 MPa, delayed for 17 s. The safety injection (SI) signal was triggered at 11.9 MPa. However, high pressure safety injection, turbine bypass and main feedwater were assumed to be off. Thirty seconds after SI signal the auxiliary feedwater started. Three hundred seconds after SI signal the reactor coolant pump started to coast down. When the maximum core cladding temperature reaches 723 K, the ultimate procedure was started, i.e. full opening of three steam dumps to atmosphere. Accumulators were available in the intact loops only. They started to inject when pressurizer pressure dropped below 4.2 MPa and were isolated at pressurizer pressure 1.5 MPa. The low pressure safety injection system started at pressurizer pressure 0.91 MPa and injected in the two intact loops. When stable residual heat removal system operating condition prevail (core outlet fluid temperature < 450 K, primary pressure < 2.5 MPa, saturation margin > 20 K), the transient was terminated.

2.3 RELAP5 input model

At the time of participation to ISP-27 the RELAP5/MOD2 input model was developed and initialized according to the specified data. Each of the three coolant loops is represented explicitly without taking into account the small asymmetry between the loops. This model was further adapted to higher versions of RELAP5 computer code [4]. The final RELAP5/MOD3.3 input model

A. Prošek, O. Adrian Berar, BETHSY 9.1b test calculation with TRACE using 3D vessel component, Journal of Energy, vol. 62 Number 1–4 (2013) Special Issue,
p. 93–103

consists from 398 volumes, 408 junctions and 402 heat structures. The hydrodynamic view was generated by SNAP from RELAP5 input model in ASCII and then arranged manually using Model Editor of SNAP as shown in Figure 2.

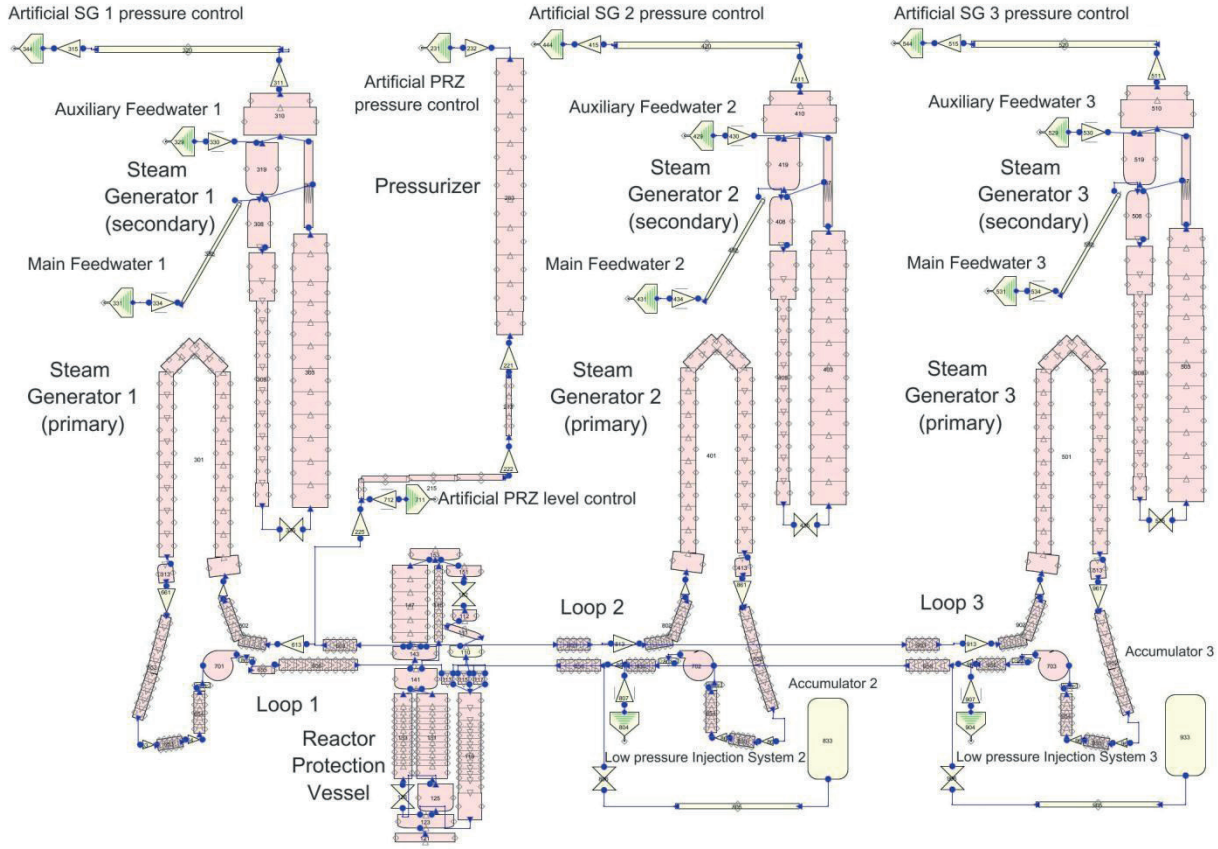

Figure 2: RELAP5/MOD3.3 nodalization of BETHSY facility

2.4 TRACE input models

The TRACE input model was first converted from RELAP5/MOD3.3 input model described in Section 2.3, and is shown in Figure 2. The converted nodalization for 1D TRACE input is similar to the RELAP5 nodalization, except for the few later corrections. The components are mostly preserved. There are 157 hydraulic components and 57 heat structures. The converted input model needed several manual corrections, adaptations of components and introduction of components needed for transient. For further details about TRACE 1D nodalization the reader can refer to reference [3].

The TRACE 1D input model was the basis for the TRACE 3D input model. To get TRACE 3D input model the three dimensional pressure vessel was created using TRACE vessel component. In addition, the external downcomer was slightly modified. The adaptations were done manually using SNAP. The TRACE nodalization of BETHSY facility using 3D vessel is shown in Figure 3. The model consists of 146 hydraulic components and 73 heat structures. The vessel component consists of 31 axial levels, 5 radial rings and 3 azimuthal sectors. The number of hydraulic components in 3D model is decreased compared to 1D model because vessel represents one component. The number of heat structures is increased in 3D model compared to 1D model, because heat structure cannot be shared by radial rings and azimuthal sectors. The core region consists of 12 axial levels, 2 radial rings and 3 azimuthal sectors. Each azimuthal sector within each ring has its own heat structure representing heater rod. This gives in total six heat structures, which can be seen from Figure 3 (on the top of pressure vessel).

A. Prošek, O. Adrian Berar, BETHSY 9.1b test calculation with TRACE using 3D vessel component, Journal of Energy, vol. 62 Number 1–4 (2013) Special Issue,
p. 93–103

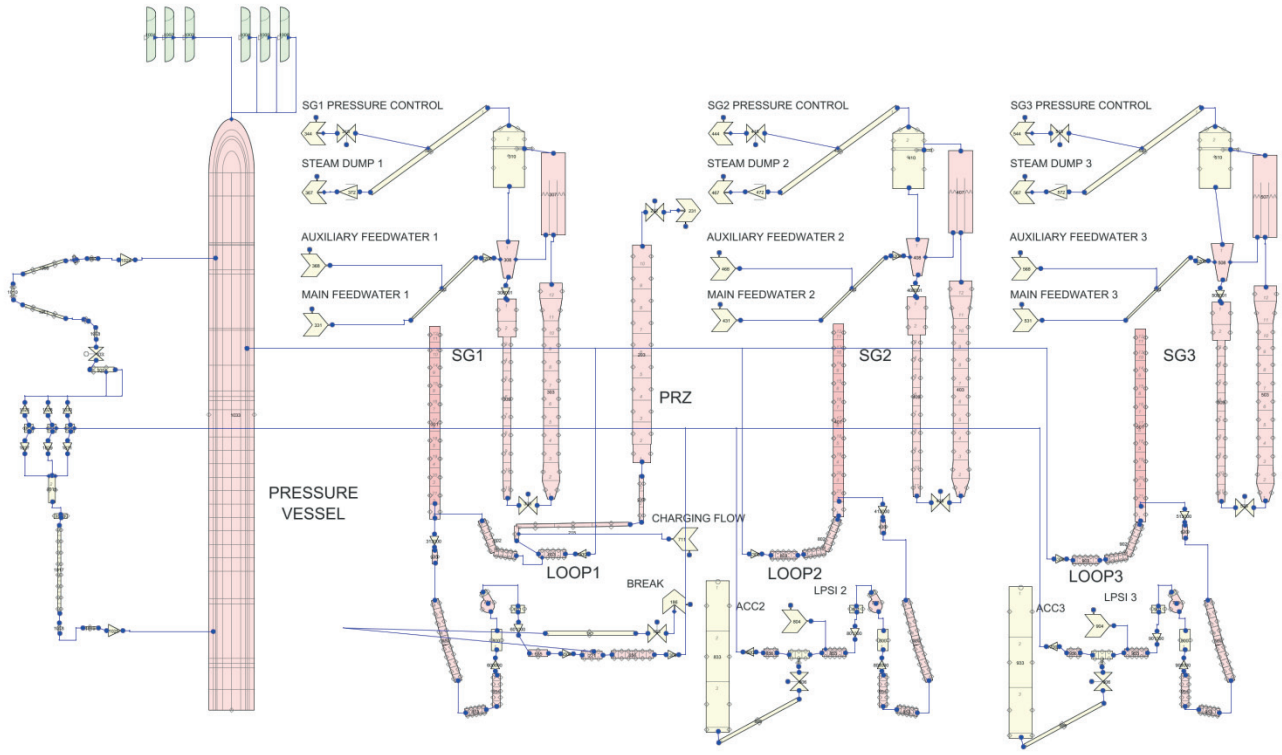

Figure 3: TRACE 3D nodalization of BETHSY facility

2.5 RELAP5, TRACE and SNAP computer codes description

The basic RELAP5 thermal-hydraulic model uses six equations: two mass conservation equations, two momentum conservation equations and two energy conservation equations. Closure of the field equations is provided through the use of constitutive relations and correlations. Since the release of RELAP5/MOD2 in 1985 the code was continuously improved and extended. New models were included like zirconium-water reaction model, level tracking model, thermal stratification model, counter-current flow limiting correlation etc. Several improvements to existing models were also done, for example Henry-Fauske and Moody choking flow models, new correlations for interfacial friction, modified reflood model and new critical heat flux correlation for rod bundles. Finally, user conveniences have been added for code execution on a variety of systems. The latest version is RELAP5/MOD3.3 Patch 04, released in 2010. For more details on RELAP5 the reader can refer to [5].

TRACE was combined from four main systems codes (TRAC-P, TRAC-B, RELAP5 and RAMONA), which were developed under U.S. NRC to perform safety analyses of loss-of-coolant accidents and operational transients, and other accident scenarios in pressurized light-water reactors and boiling light-water reactors. TRACE can also model phenomena occurring in experimental facilities designed to simulate transients in reactor systems. TRACE includes models for multidimensional two-phase flow, nonequilibrium thermo-dynamics, generalized heat transfer, reflood, level tracking, reactor kinetics and passive systems. A component-based approach is used to modeling a reactor system. There is no built-in limit for the number of components or volumes that can be modeled; the size of a problem is theoretically limited only by the available computer memory. There are also heat structures, and components for boundary condition and break. For more details on TRACE the reader can refer to [1].

SNAP [2] consists of a suite of integrated applications designed to simplify the process of performing engineering analysis. SNAP is intended for creating and editing input for engineering analysis codes and it has functionality for submitting, monitoring, and interacting with the codes. SNAP currently support the CONTAIN, COBRA, FRAPCON-3, MELCOR, PARCS, RADTRAD,

A. Prošek, O. Adrian Berar, BETHSY 9.1b test calculation with TRACE using 3D vessel component, Journal of Energy, vol. 62 Number 1–4 (2013) Special Issue,
p. 93–103

RELAP5 and TRACE analysis codes. Each code is supported by a separate plug-in. SNAP's interactive and post-processing capabilities are predominately realized within its animation displays. Within such a display, the results of a calculation may be animated in a variety of ways. An animation display retrieves data from the server and represents it visually in some fashion. The data can be from an actively running calculation, a completed calculation, external data, etc.

3 RESULTS

3.1 BETHSY 9.1b transient simulations

Three calculations of BETHSY 9.1b test were performed and compared to experimental data. The first one was RELAP5 calculation performed by latest RELAP5/MOD3.3 Patch 4 computer code. With TRACE V5.0 Patch 1 two calculations were performed, TRACE 1D with one dimensional pressure vessel and TRACE 3D with three dimensional pressure vessel. Both steady-state and transient calculations were performed. With steady-state calculations the desired initial and boundary conditions were set. The results of calculations are shown in Figures 4 through 8.

Table 1 shows initial and boundary conditions for BETHSY 9.1b test. The RELAP5 model was initialized to cold leg temperature; therefore the secondary pressure is not exactly matched. The difference comes from the geometry and the code models. The steam generator levels and masses were matched to average measured values. The pressurizer pressure and level were also matched to average measured values. The core power was input value. In the experiment the electrical trace heating system was installed of the power of 107.5 kW and was operating till ultimate procedure start. In the calculations the heat losses were modeled only after the electrical heat system was off. Before ultimate procedure start there were no heat losses, what is equal to experiment which compensates the heat losses by electrical heat system.

The TRACE input model was converted before the RELAP5 input model was finely initialized to the values in Table 1. Therefore TRACE 1D input model has practically the same values of initial and boundary conditions as the RELAP5 input model. The exceptions are steam generator level and mass. We performed TRACE 1D calculation with already verified restart input model after conversion. The TRACE 3D model, which was built on TRACE 1D model, was initialized with the artificial controllers. This resulted in better match for cold leg temperature, downcomer mass flow rate and steam generator level. In general, the agreement of initial and boundary conditions is good for all calculations.

Table 1 Comparison of initial conditions for BETHSY 9.1b test

Parameter	Measured	RELAP5	TRACE 1D	TRACE 3D
core thermal power	2864 ± 30 kW	2864 kW	2864 kW	2864 kW
cold leg temperature (per loop)	559.9 ± 0.5 K	559.9 K (core inlet)	559.4 K (core inlet)	559.9 K (core inlet)
downcomer mass flow rate	150.0 ± 5.0 kg/s	155.2 kg/s	155.2 kg/s	150.6 kg/s
reactor coolant pump speed (per loop)	2940 ± 30 rpm	2970 rpm	2970 rpm	2940 rpm
pressurizer pressure	15.51 ± 0.09 MPa	15.51 MPa	15.51 MPa	15.51 MPa
pressurizer level	4.08 ± 0.1 m	4.08 m	4.08 m	4.08 m
reactor coolant system mass	1960 kg	1948 kg	1948 kg	1948 kg
secondary side pressure (per SG)	6.91 ± 0.04 MPa	6.77 MPa	6.77 MPa	6.75 MPa
steam generator level (per SG)	13.45 ± 0.05 m	13.41 m	13.18 m	13.45 m
feedwater temperature	491.1 ± 2.0 K	491.0 K	491.0 K	491.0 K
secondary coolant mass (per SG)	820 ± 30 kg	820 kg	804 kg	800 kg

The main sequence of events is shown in Table 2. As can be seen the RELAP5 calculation using standard BETHSY input model is in a better agreement with the experiment in the initial phase than TRACE 1D calculation using converted model, while in the later part the TRACE 1D model was better than RELAP5. The timing for TRACE 3D calculation is in a good agreement

during the whole transient time. The time sequence of events mostly depends on the break flow. For RELAP5 original Ransom-Trapp break flow model the values of 0.8, 1.0 and 1.1 were used for subcooled, two phase and superheated discharge coefficients, respectively. For TRACE 1D break model the values of 1.0 and 1.1 were used for subcooled and two phase discharge coefficients, respectively. For TRACE 3D break model the value of 0.9 was used for subcooled and two phase discharge coefficient. The values of break discharge coefficients for TRACE calculations were selected after some sensitivity studies and the wish was to use the values as close as possible to the default values. However, decreasing of discharge coefficients delays the ultimate procedure initiation. Our goal was to as closely as possible to match the start of ultimate heat procedure, as this greatly influence primary pressure, which further determines the actuation of accumulators and low pressure injection system.

Table 2 Main sequence of events for BETHSY 9.1b test

Events	Time (s)			
	Measured	RELAP5	TRACE 1D	TRACE 3D
Break opening	0	0	0	0
Scram signal (13.1 MPa)	41	31	21	28
Safety injection signal (11.9 MPa)	50	54	35	51
Core power decay start (17 s after scram)	58	48	38	45
Auxiliary feedwater on (30 s after SI signal)	82	84	65	83
Pump coastdown start (300 s after SI signal)	356	354	335	353
End of pump coastdown	971	969	950	970
Start of the first core level depletion	1830	2020	1820	N.A.
Start of second core uncovery	2180	2130	2183	2091
Ultimate procedure initiation	2562	2508	2573	2614
Accumulator injection starts (4.2 MPa)	2962	2880	2930	2974
Primary mass inventory is minimum	2970	2880	2932	2976
Maximum core clad heatup	3053	3009	3002	2997
Accumulator isolation (1.5 MPa)	3831	3865	3957	3833
Low pressure injection system start (0.91 MPa)	5177	5235	5330	5075

In Figures 4 to 8 are shown the main variables. The break mass flow affects the core water inventory and heat transfer. The heat removal from the core determines the time when the maximum heater rod temperature reaches the setpoint to initiate ultimate procedure (i.e., 723 K). Ultimate procedure actions drive the primary system response, through depressurization the secondary system. Finally, primary pressure determines actuation and closure of accumulators and start of low pressure injection system.

In Figure 4 the break flow and integrated break mass flow are shown. None of the calculations perfectly match the break flow (see Figure 4(left)). In the first part of transient the TRACE 1D and TRACE 3D calculation are similar. However in the second part of transient TRACE 3D calculation better agrees with the measurement than TRACE 1D calculation. Also, no spikes in break flow are present in TRACE 3D calculation as in the case of TRACE 1D calculation. In general the agreement is satisfactory as shown in Figure 4(right). TRACE 1D and RELAP5 integrated break flows are practically the same until accumulator injection, while TRACE 3D is a bit lower. During accumulator injection TRACE 1D and TRACE 3D are better than RELAP5, while during low pressure injection period the slightly higher secondary pressure calculated by TRACE 1D causes lower injection flow and therefore also lower break flow than RELAP5, while TRACE 3D slightly underpredict the secondary pressure, resulting in higher break flow. The pressurizer and steam generator no. 1 pressure are shown in Figure 5. Due to selected break discharge coefficients the timing of pressure drop of pressurizer pressure (Figure 5(left) is better for TRACE calculations than for RELAP5 calculation. On the other hand, the steam generator no. 1 pressure is better predicted by TRACE in the first part, while in the second part the RELAP5 was closer to the measured

values. In the period before ultimate procedure initiation the pressure in all calculations is constant, because in the experiment the pressure was controlled to be constant at 6.91 MPa.

In Figure 6 are shown core inlet and outlet temperature. For core inlet temperature shown in Figure 6(left) the best agreement with measured data was obtained for TRACE 3D calculation and for the core outlet temperature shown in Figure 6(left) for TRACE 1D calculation. The calculated temperatures of core outlet temperature are liquid temperature, while measured value is two-phase mixture temperature.

The maximum heater rod temperature and accumulator pressure are shown in Figure 7. The heater rods start to heatup when the core starts to uncover, as it is shown in Figure 7(left). TRACE 3D calculation has very good timing, while the peak cladding temperature is overpredicted, while in the case of TRACE 1D is underpredicted. For quenching the rod the primary depressurization was needed to enable accumulator injection. Figure 7(right) shows the accumulator pressure drop due to discharging. TRACE 3D calculation is in the best agreement with the experimental data. During accumulator injection the core level recovers. After accumulator injection is terminated, the primary system mass (see Figure 8(left)) start to decrease again until the low pressure injection starts as shown in Figure 8(right). Due to the slightly higher primary pressure prediction in TRACE 1D calculation the injection started a bit later and the injected flow is also lower. Finally, Figure 9 shows cross-over leg no. 1 downflow and upflow side differential pressure. None of the calculations perfectly agree with experimental data, being TRACE 1D in the best qualitative agreement.

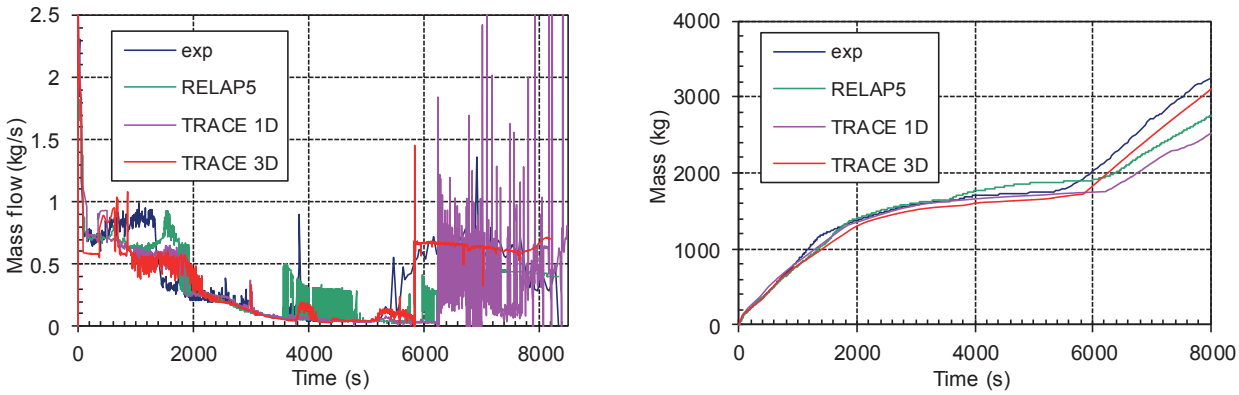

Figure 4: Break mass flow (left) and integrated break mass flow (right)

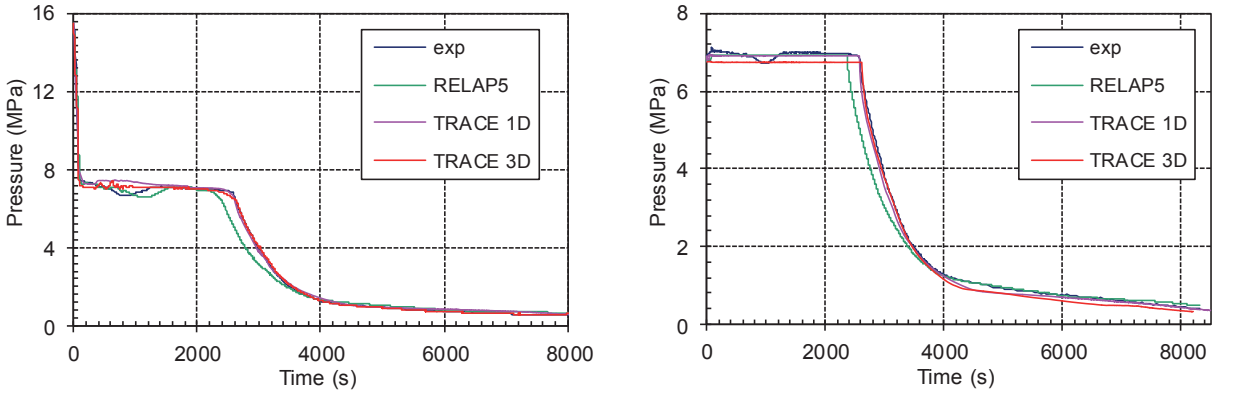

Figure 5: Pressurizer pressure (left) and steam generator no. 1 pressure (right)

A. Prošek, O. Adrian Berar, BETHSY 9.1b test calculation with TRACE using 3D vessel component, Journal of Energy, vol. 62 Number 1–4 (2013) Special Issue,
p. 93–103

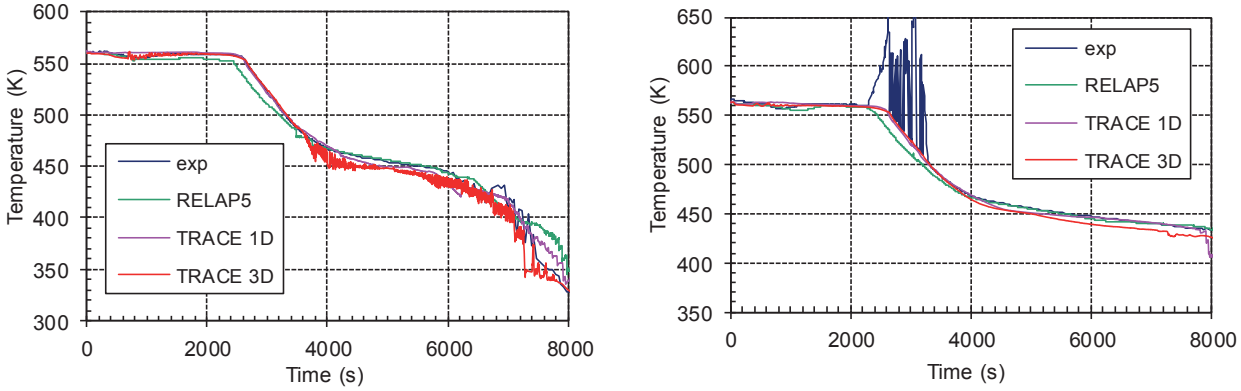

Figure 6: Core inlet (left) and outlet (right) temperature

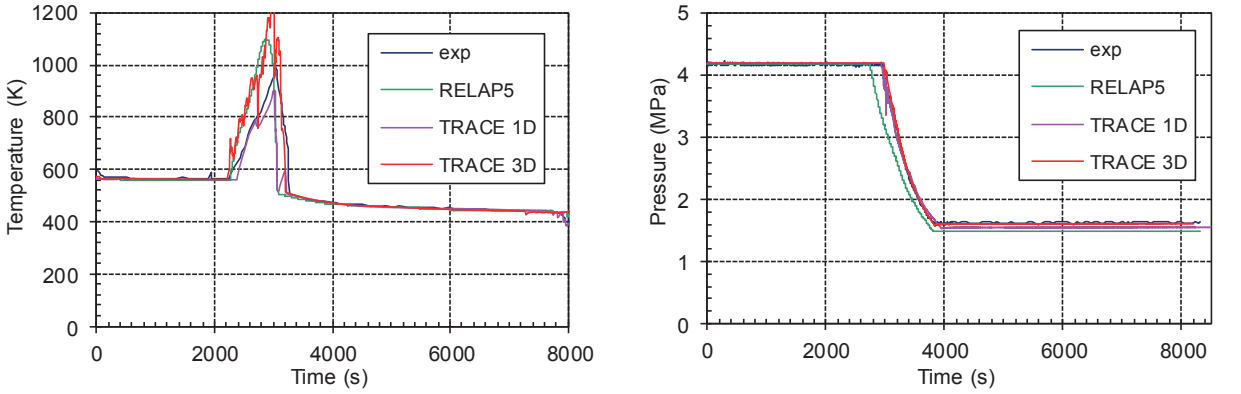

Figure 7: Maximum heater rod surface temperature (left) and accumulator pressure (right)

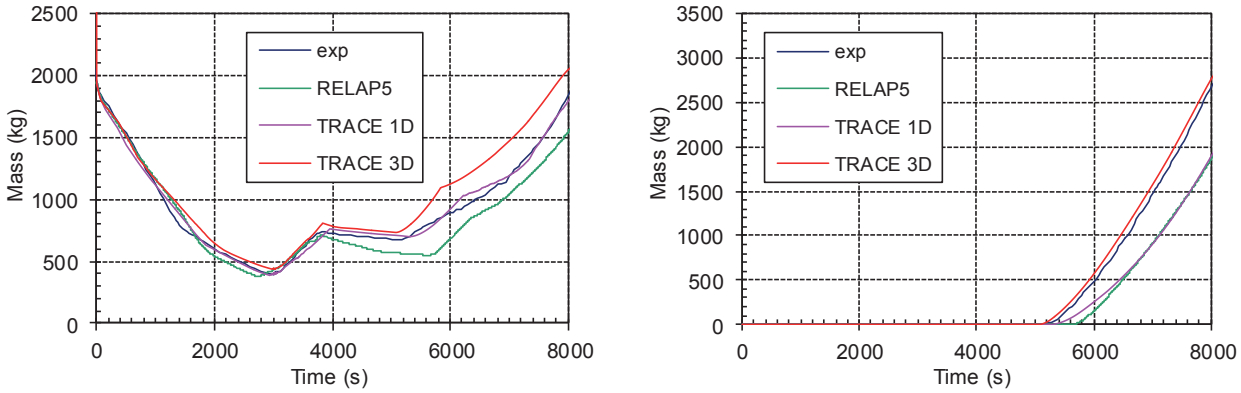

Figure 8: Primary mass inventory (left) and integrated low pressure injection system mass (right)

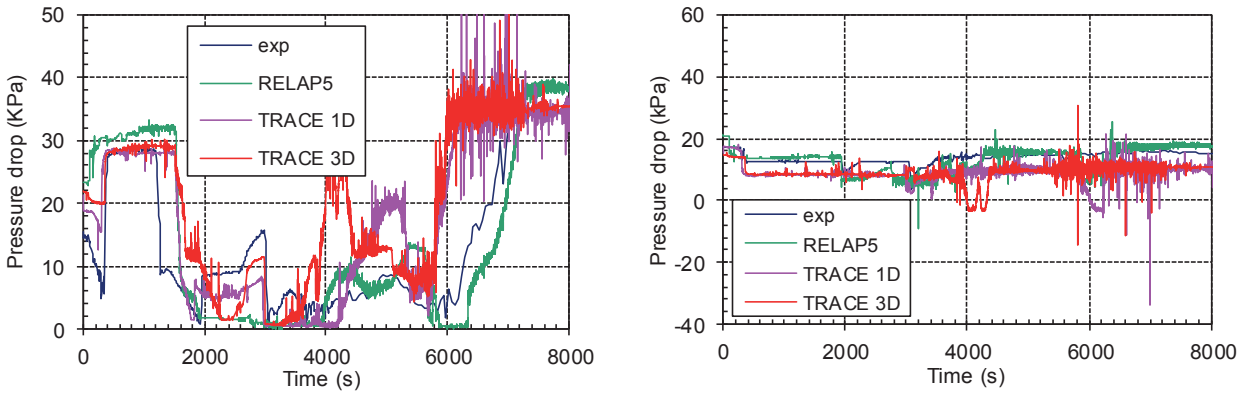

Figure 9: Cross-over leg no. 1 downflow (left) and upflow (right) side differential pressure

A. Prošek, O. Adrian Berar, BETHSY 9.1b test calculation with TRACE using 3D vessel component, Journal of Energy, vol. 62 Number 1–4 (2013) Special Issue,
p. 93–103

3.2 Discussion

The results show that in general the RELAP5 and TRACE 1D calculation are comparable, being TRACE 1D slightly better. One reason may be that in the facility the phenomena were mostly one dimensional. For RELAP5 calculations performed by different versions [4] it has been shown, when the same input deck has been used used, that the results obtained by RELAP5/MOD2 code were comparable to the results obtained by the latest RELAP5/MOD3.3 Patch 4 code. This study showed that converted TRACE input model required some adaptations, before correct timing of events was obtained. The difficulties were especially by BRANCH components of RELAP5 which were not properly converted by SNAP (normally to PIPE components). Such PIPE components in TRACE had to be replaced by TEE components manually (e.g. break location, accumulator injection location, steam generators). It was proved that through SNAP conversions some 90% of conversion is done and that manual corrections are unavoidable. Nevertheless, steady state calculation can be pretty quickly achieved by automatic SNAP conversion and BRANCH components converted to TRACE do not cause difficulties.

Introducing 3D vessel component for pressure vessel requires manual work. It was shown that further improvement was obtained for some variables. Nevertheless, the heater rod temperatures were very high and this should be investigated in the future. One difficulty was, that by setting the flow area fraction in the vessel, the desired core bypass flow could not be achieved. Therefore the core bypass area fraction was set to zero, i.e. no bypass flow was modeled. Also, the maximum heater temperature depends very much on the break discharge coefficients. For example, the change of two phase discharge coefficient from 0.90 to 0.85 the maximum temperature was few hundreds K lower, what requires some further investigation. Nevertheless, the 3D core modeling qualitatively matches the experimental temperatures as shown in Figure 10. The outer core temperatures were higher than the inner core temperatures. Also, it should be noted that the given measured temperatures are from inner part of the core and that quantitative agreement of inner ring heater rod temperatures is satisfactory. This clearly demonstrates the benefits of 3D modeling.

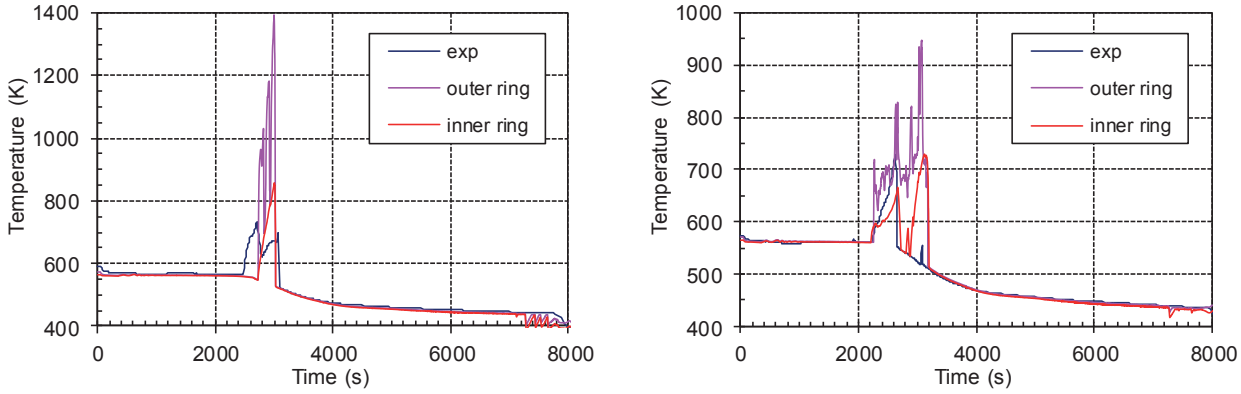

Figure 10: Comparison between TRACE 3D calculation and experimental data for heater rod surface temperature in the middle (left) and at the top of the core (right)

4 CONCLUSION

The BETHSY 9.1b test, which is 5.08 cm equivalent diameter cold leg break without high pressure safety injection and with delayed ultimate procedure, was simulated by RELAP5/MOD3.3 Patch 4 and TRACE V5.0 Patch 1 computer codes. The TRACE 1D input model was obtained by SNAP conversion of RELAP5 input model and several specific adaptations. The TRACE 3D pressure vessel model was build manually. In general, all presented code calculations were in good agreement with the BETHSY 9.1b test data. The TRACE 1D calculation results are comparable to RELAP5 calculated results, being TRACE 1D slightly better. Finally, the TRACE 3D calculation is slightly better than TRACE 1D calculation. One

reason is that the results are comparable because of already good agreement of RELAP5 calculation and the TRACE calculation using converted input model from REALP5 input model. The other reason may be that in the facility the phenomena were mostly one dimensional (for example, external downcomer was used for reactor vessel modeling). However, when 3D behavior of the heater rod temperatures was investigated, the advantage of three dimensional treatment was clearly demonstrated.

REFERENCES

[1] U. S. Nuclear Regulatory Commission, TRACE V5.0 User Manual, Division of Risk Assessment and Special Projects, Office of Nuclear Regulatory Research, Washington, DC.

[2] APT, Symbolic Nuclear Analysis Package (SNAP), User's Manual. Report, Applied Programming Technology (APT), Inc., February 2011.

[3] A. Prošek, O.A. Berar, "Analysis of small-break loss-of-coolant accident test 9.1b at BETHSY facility with TRACE and RELAP5", Proceedings of ICAPP 2011, International Congress on Advances in Nuclear Power Plants, Nice, France, May 2-6, 2011.

[4] A. Prošek, RELAP5 Calculations of Bethsy 9.1b Test, Science and Technology of Nuclear Installations Volume 2012, Article ID 238090, 11 pages, doi:10.1155/2012/238090.

[5] USNRC, "RELAP5/MOD3.3 code manual", Patch 04, Vols. 1 to 8, Information Systems Laboratories, Inc., Rockville, Maryland, Idaho Falls, Idaho, prepared for USNRC, 2010.

[6] CEA, "BETHSY, General Description", Note SETh/LES/90-97, CEA (Commissariat à l'énergie atomique et aux énergies alternatives), Grenoble, France, April 1990.

[7] T. Chataing, P. Clement, "2" Cold Leg Break without HPSI and with Delayed Ultimate Procedure", Note SETh/LES/90-104, CEA (Commissariat à l'énergie atomique et aux énergies alternatives), Grenoble, France, June 1990.

Journal of Energy

VOLUME 62 Number 1–4 | 2013 Special Issue

journal homepage: http://journalofenergy.com/

Risk Impact of Maintenance and Other Activities with Regard to Plant Areas

Ivan Vrbanić, Ivica Bašić
APoSS d.o.o.
Repovec 23B, HR-49210 Zabok, Croatia
ivan.vrbanic@zg.t-com.hr, basic.ivica@kr.t-com.hr

ABSTRACT

In all operating modes of a nuclear power plant a lot of activities take place, including maintenance, surveillance testing and plant modifications. Some of these activities can impose temporary increase in risk level, as they may change the status of equipment important to plant safety. Such risk increases are usually controlled by risk monitoring, which considers changes in risk due to changes in the status (e.g. availability) of plant systems and functions. Risk monitors are, in many cases, designed and operated to be system-oriented (or function-oriented), as they focus on "measuring" the risk associated with different system configurations (from where comes the often used term "configuration risk management").

On the other hand, components of plant systems are placed in various locations and at various floors (elevations) of plant buildings. Piping, as well as cabling, is routed through one or more buildings. Equipment performing different functions is, sometimes, located near each other due to architectural limitations. Where required, barriers are applied in order to ensure physical separation and independency. Due to these reasons, a particular plant area (compartment, room, part of a large room,…) can contain a variety of mechanical, electrical and / or other equipment with different safety implications. As well as system components, plant areas are also related to each other, with different degrees of relative importance. Since activities performed in different plant areas can imply changes, actual or potential, in the status of associated equipment, structures and / or barriers, there is also a need that risk monitoring considers the area-oriented aspects, beside considering those which are system-oriented or function-oriented.

Risk impact of an activity taking place in a particular plant area can be considered in terms of changes (potential or actual) to its three components: 1) likelihood of initiators which can be triggered by equipment in the area (but which are not mitigated by any of the equipment in the same area); 2) mitigating capability regarding the initiators which are not triggered in this area; 3) likelihood of initiators triggered in this area and mitigating capability regarding the same initiators. Activity in a particular plant area may be related to none or to any combination of the three risk impact components. Normally, risk impact under 3) is limited by the architectural engineering principles (because it may become very large risk contributor). However, it may be present in some residual form and it cannot be excluded (as demonstrated by area-related risk studies performed in the past, such as internal fire and internal flooding analyses).

With activity taking place in a particular area, the relevant importance of any other plant area (and, hence, potential risk impact of any activity that may be planned to go on at the same time) is then considered in terms of, respectively: 1) whether it contains the equipment relevant for mitigation of initiators that can be triggered in the considered area; 2) whether it includes the potential for triggering an initiator which is mitigated by the equipment located in the considered area; 3) whether it contains the relevant mitigation equipment or include the potential for relevant initiators.

I. Vrbanić, I. Bašić, Risk Impact of Maintenance and Other Activities with Regard to Plant Areas, Journal of Energy, vol. 62 Number 1–4 (2013) Special Issue,
p. 104–112

The paper discusses these and other related issues and describes some basic concepts for the area-oriented risk management.

1 INTRODUCTION

In all operating modes of a nuclear power plant a lot of activities take place, including maintenance, surveillance testing, temporary and permanent design plant modifications performed when plant is in operation. Some of these activities can impose temporary increase in risk level even if they are not directly performed on the important to safety (ITS) systems, structures and / or components (SSCs), as they may change their status. Such risk increases are usually controlled by risk monitoring, which considers changes in risk due to changes in the status (e.g. availability) of plant systems and functions. Risk monitors (e.g. [1]) are, in many cases, designed and operated to be system-oriented (or function-oriented), as they focus on "measuring" the risk associated with different system configurations (from where comes the often used term "configuration risk management"). Many times, risk monitors do not recognize the non safety equipment or monitor activities related to them.

In this article we discuss a simplified approach which can be used for the initial stages of scheduling of the activities, which considers also plant areas where they would take place. It can be based on the principles such as those established in the US NRC's Significance Determination Process (SDP), [2] and [3] which is used to obtain a risk characterization in terms of an order of magnitude (OOM).

Generally, risk impact associated with implementation of activities relates to two major aspects: Increase in the likelihood of relevant initiators (I) and reduction in the plant mitigation capability in the case that an initiator occurs (M).

2 RISK MODEL

Risk model consists of five elements. The first three of them are, basically, the three elements of the SDP model ([2] and [3]) for functionally oriented risk significance, in terms of an OOM. The elements 4 and 5 represent a characterization of plant areas and activities, respectively.

Element 1: Initiators and their frequencies. The element represents a list of all relevant initiator categories (internal and external) with corresponding frequencies characterized in terms of an OOM.

Element 2: Systems and initiators dependency matrix. The matrix relates supporting systems to supported systems. Furthermore, it relates all relevant systems to initiators (i.e. for a particular system, the initiator categories are identified which require the considered system for mitigation).

Element 3: Event sequences logic. For each initiator category, a list of accident sequences is provided in the form $I_x M_{xi} = I_x M_{xi1} M_{xi2} \cdots$, where "$i$" denotes i^{th} core damage sequence for initiator category "x". Terms M_{xi1}, M_{xi2},… represent the nominal mitigation capabilities of functions which need to fail in order that considered sequence ends with core damage (or radioactivity release). In the simplified approach, these nominal mitigation capabilities are characterized in terms of an OOM (i.e. corresponding failure probabilities are expressed as, e.g. 0.1, 0.01, 0.001,…). Term I_x is initiator category from Element 1. The event sequences can be derived on the basis of simplified event trees from the plant specific PRA.

Element 4: Characterization of plant areas. Plant areas can be defined on the basis of (or, at least, an initial point can be) the PRA for the area events such as internal fires or internal floods. For each area, an inventory of equipment is established which is then related to the initiator categories I_x and mitigation functions M_{xi} . It is pointed that considerations shall also include forced shutdown and categories which may have been screened out during the fire PRA, flood PRA, etc., if presence of the activities changes the underlying screening reasoning. Characterization shall also include connections to the adjacent areas (e.g. fire doors).

I. Vrbanić, I. Bašić, Risk Impact of Maintenance and Other Activities with Regard to Plant Areas, Journal of Energy, vol. 62 Number 1–4 (2013) Special Issue,
p. 104–112

Element 5: Definition and characterization of categories / types of activities. In this element, for the classes of activities such as maintenance, surveillance test, etc., generic activity categories are defined such as "visual inspection", "pump lubricant sampling / exchange", "complete overhaul",… Each generic activity is characterized regarding its potential impact on initiator categories I_x and mitigation function capabilities M_{xi} . The impact is considered in terms of "by a factor" and "by an OOM". Here, both these terms should be interpreted in the sense of the mentioned SDP principles, e.g.:

- Impact "by a factor" would mean that change is of the same order as nominal value. The absolute conditional value remains within the same OOM.
- Impact "by an OOM" would mean that absolute conditional value is changed by an OOM.

Several (e.g. two or three) successive impacts "by a factor" in the same sequence would imply an impact "by an OOM". (For example, if considered set of activities has "by a factor" impact on the initiator likelihood and, also, "by a factor" impact on one of the required mitigation functions in the sequence, the overall impact may be considered to be "by an OOM". Similarly, if considered activities have "by a factor" impact on two or three required mitigation functions in the particular sequence, the overall impact may be considered to be "by an OOM". More specific rules can be defined for particular application.) Examples of activity impact characterization may include:

- Activity such as "welding" can increase a nominal likelihood of fire in the area by a factor or OOM.
- Manipulations with heavy pieces in the vicinity of an electric cabinet can cause damage or a loss of power to/from the cabinet. If the cabinet is related to certain initiator category (e.g. loss of support system or reactor trip), the activity can imply an increase in the initiator frequency by a factor or by an order of magnitude. (Example: temporary use of small cranes and associated chains or / and testing trolley.)
- Activity using a temporary sealing material on a valve which can impact the movement of a valve or even obstruct flow through a valve body.
- Activity at the "high energy" lines and valves which can impact environment conditions in certain areas and ITS equipment located there (harsh environment with pressure, temperature and humidity above design values.)
- Activity using the nitrogen to temporary freeze the water in the pipe due to the necessary corrective measures. The pipe can remain plugged if the time window for deicing has not passed or ice move downstream and potentially jeopardize active components in the line (e.g. pumps, valves,..)
- Activity requires that system train is isolated and put out of service. Therefore, the train is unavailable. (For a system with multiple redundant trains this would imply a decrease in mitigation capability by an OOM.)
- Activity requires temporary bypassing of the control and instrumentation signal. Effect is the same as above.
- Activity requires temporary opening of the fire doors or temporary removal of fire barrier. In such a case, for certain initiator categories (e.g. fire, an impact may need to be extended to other areas.

The activities also need to be characterized in terms of their duration which can, again, be done in terms of OOM (e.g. 1 hr, 10 hrs, 100 hrs… or similar scheme).

3 RISK ASSESSMENT

The risk assessment process is depicted in Figure 1. It would consist of the following general steps:

- Based on the macro-plan, select a desired set of activities and put them into desired time frames. Characterize time frames in terms of OOM (1 hr, 10 hr, 100 hr,…). Each time frame would correspond to a specific area / system configuration (parallel activities).
- Estimate risk impact of initial activities plan. For each time frame:
  - Relate the activities to equipment / systems and areas: use Element 2 to propagate supporting systems to all others; use Element 4 to to map the equipment to areas.
  - Identify implicated initiator categories: use Element 2 to identify the initiators with reduced mitigation capability; use Element 4 to identify initiators with increased frequency. (Note that both aspects may apply).
  - Identify affected event sequences from Element 3. For each, estimate the risk significance ΔR_x by applying generic characterization from Element 5 to the activities involved:

$$\Delta R_x = I_x M_x T \tag{1}$$

Term T represents the time frame duration, while I_x and M_x are initiator frequency and mitigation capabilities involved in the sequence x:

$$I_x = I_{nx} F_{Ix} \tag{2}$$

$$M_{xi} = \prod_{xi} \left(\frac{M_{nxi}}{F_{xi}} \right) = \left(\frac{M_{nxi1}}{F_{xi1}} \right) \left(\frac{M_{nxi2}}{F_{xi2}} \right) \ldots \tag{3}$$

Here, index "n" refers to the nominal initiator frequency (Element 1) or the nominal mitigation function capability (Element 3). The terms (factors) F_{Ix} and F_{xi} generally represent an impact of undergoing activities on the initiator likelihood and mitigation capabilities, respectively. They are used to increase the initiator likelihood or to decrease the mitigation capability (or both). The above term ΔR_x is meant to represent an increase of the risk from the considered sequence, relatively to its nominal value. Therefore, the terms F_{Ix} and F_{xi} can, generally, be OOM(s) or 1.0 (if activity has no impact or an impact is only "by a factor"; in the latter case, the impact, by definition, remains within the same OOM), depending on the characterization of the set of activities.

  - Estimate total risk impact for the time frame as

$$\Delta R = \sum_x \Delta R_x \tag{4}$$

Here, the $\sum_x$ shall not be interpreted as an algebraic sum but, rather, as combining the contributions from sequences with differrent OOM risk significances (e.g. a "counting rule" in the mentioned US NRC's SDP process).

- The above process should be repeated for all defined time frames.

I. Vrbanić, I. Bašić, Risk Impact of Maintenance and Other Activities with Regard to Plant Areas, Journal of Energy, vol. 62 Number 1–4 (2013) Special Issue,
p. 104–112

- Estimate risk reduction potential (RRP)for the involved activities / areas: e.g. reset all initiator frequencies and mitigation capabilities implicated by particular activity / area to their nominal values and re-estimate risk impact.
- Estimate risk increase potential (RIP) for other areas: e.g. increase I_x and/or decrease M_x values associated with an area by an OOM and re-estimate risk impact.
- Depending on the initial risk impact, two different types of further actions may be taken:
    - Reduce the risk impact. This may be done by removing from the schedule the activities or areas with largest RRP.
    - Expand the scope of the activities. This may be done by introducing additional activities to the other areas with lowest RIP.

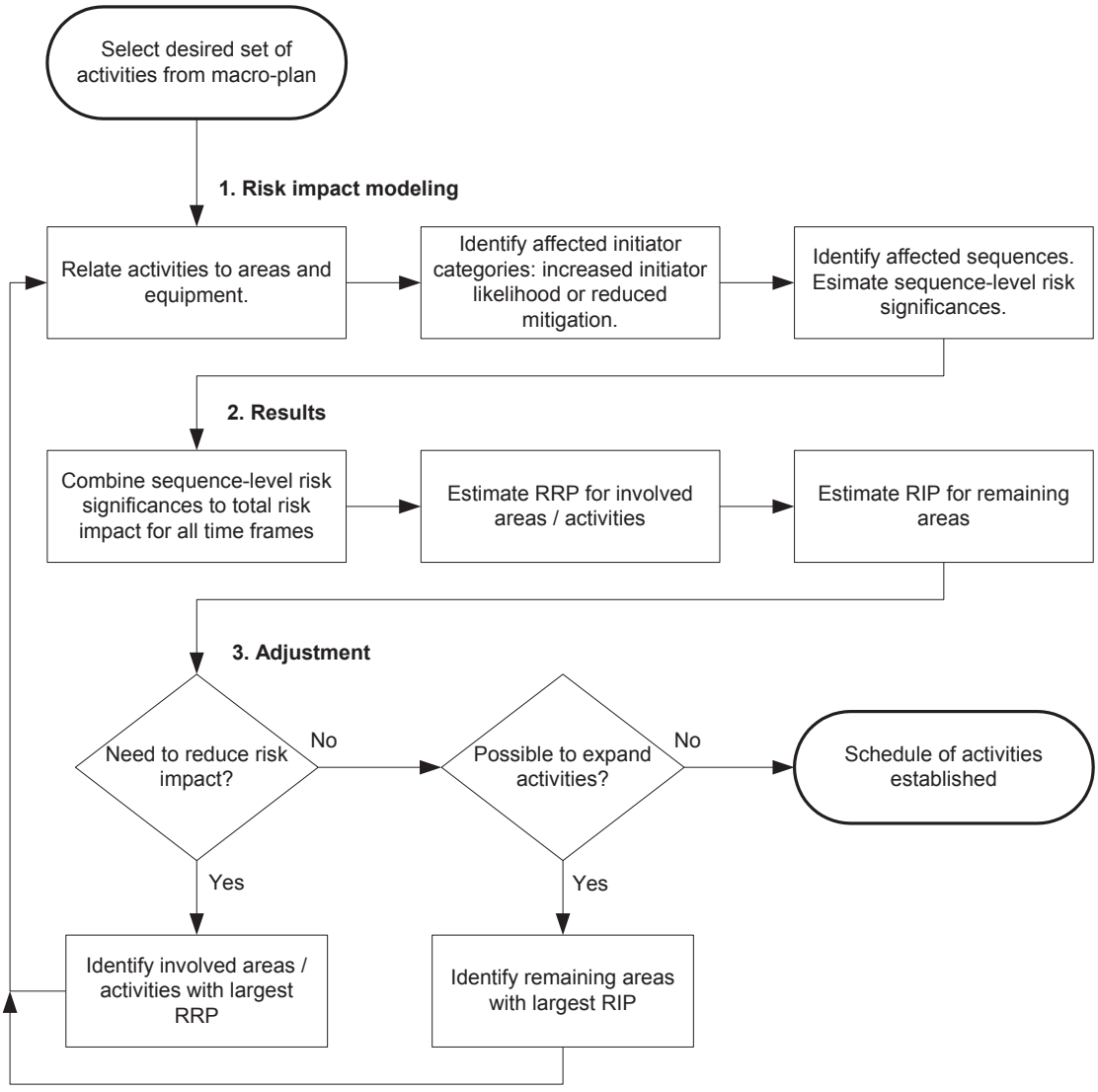

Figure 1: Simplified Risk Assessment Flow Chart

I. Vrbanić, I. Bašić, Risk Impact of Maintenance and Other Activities with Regard to Plant Areas, Journal of Energy, vol. 62 Number 1–4 (2013) Special Issue,
p. 104–112

4 SOME EXAMPLES

4.1 Risk from Transient Followed by a Loss of Secondary Heat Sink

In many cases, the risk from the ongoing online activities is related to the risk from induced reactor trip. The most important safety function following a reactor trip in a PWR plant is the secondary side heat sink.

Table 1 provides an OOM characterization of the baseline core damage risk from the accident sequence with reactor trip followed by a total loss of secondary heat sink, for a PWR plant with two loops (two steam generators (SG)). In such a sequence, assuming the total loss of Emergency Feedwater (EFW), the operators would be instructed by Emergency Operating Procedures to establish the secondary heat sink (keep the SG level) by means of Main Feedwater (MFW). If this function also fails, the operators are instructed by the procedures to initiate primary feed and bleed. Quantitative terms from Table 1 are based on the considerations from US NRC SDP documents [2] and [3]. They come from the considerations which include:

- Train-level credit for a motor operated system train, in OOM terms, is 10^{-02};
- Train-level credit for a turbine driven system train, in OOM terms, is 10^{-01};
- Multi train credit, in OOM terms, is M_{TR} x CCF, where M_{TR} is a single train-level level credit and CCF a common cause failure probability. In terms of OOM, the CCF is characterized as 0.1 ("generic" beta factor). Therefore, in the case of multi train motor driven system, the mitigation credit is 10^{-03}.

Table 1: Baseline OOM Risk Summary for the Sequence with Reactor Trip Followed by a Loss of Secondary Heat Sink

Initiator	Baseline Mitigation Credit			
	Emergency Feedwater	Main Feedwater	Primary Feed and Bleed	Time Frame
Buildings / plant locations where related activities take place include (Note1):				
TB, IB, CB …	IB,…	TB, IB,…	CB, AB, IB…	
In terms of OOM, reactor trip frequency can be characterized as: $I = 1\ yr^{-1}$	Assuming the configuration of two motor driven pumps, each per one SG, and one turbine driven pump for both SGs, the mitigation capability can be summarized as: $M_{MDP} = 10^{-03}$ $M_{TDP} = 10^{-01}$ $M_{EFW} =$ $= M_{MDP}$ x $M_{TDP} =$ $= 10^{-04}$	MFW is a multi train system. M_{MFW} is considered to be at 10^{-03}. The mitigation capability is driven by human action (to establish the heat sink from MFW), which is considered to be in the range of 10^{-02} to 10^{-01}. Assume, for this example: $M_{MFW} = M_{HA} = 10^{-01}$	Both, feed and bleed functions are considered to have multi train mitigation credit and the credit for the overall function is driven by operator action, which is considered to be at OOM of 10^{-01}: $M_{FB} = M_{HA} = 10^{-01}$	Baseline risk can be considered in the long time frame, such as time between two outages, i.e. of the order of 1 year: $T = 1\ yr$
Baseline risk from the considered accident sequence is then characterized as:				

I. Vrbanić, I. Bašić, Risk Impact of Maintenance and Other Activities with Regard to Plant Areas, Journal of Energy, vol. 62 Number 1–4 (2013) Special Issue,
p. 104–112

$$R = I \times \left(M_{EFW} \times M_{MFW} \times M_{FB}\right) \times T = 1(yr^{-1}) \times 10^{-04} \times 10^{-01} \times 10^{-01} \times 1(yr) = 10^{-06}$$

Notes:

1. Note that related activities could take place in other buildings and locations, when considering associated supporting systems and, for example, cable routing. (The acronyms used in the above example stand for: TB = Turbine Building; IB = Intermediate Building; AB = Auxiliary Building, CB = Control Building.)

The characterization given in Table 1 results with OOM estimate of baseline risk from the considered accident sequence of 10^{-06}. This is, indeed, the range of expected CDF contribution from this type of sequence, as can be confirmed by the plant-specific PRA models for the nuclear power plants of this type. For the purpose of plant area-oriented risk impact considerations, this very simple example already provides certain insights.

The activities which require formal declaration of safety system train being out-of-service (OOS) are not so much of interest here since they normally raise awareness of both plant maintenance crew and operators due to entering the Limiting Conditions for Operation (LCO). Those activities can also, very effectively, be addressed by the "conventional" system-oriented risk monitors. Of more interest are the activities which, although not requiring the declaration of formal OOS condition, can still imply the reduced availability or reliability of considered systems. From the above simple risk model for the considered accident sequences the following can be readily seen:

- Presence of "non-OOS activity" which implies an impact "by a factor" (as discussed earlier) on the initiator likelihood (i.e. an activity with some residual potential to induce a reactor trip) during a time frame of several days (i.e. 0.01 yr in the OOM scheme) does not imply relevant risk impact: $\Delta R = 0.01 \times R = 10^{-08}$.
- Even a presence of such activity during several weeks or a month, cumulatively, over a year (i.e. duration of 0.1 yr in the OOM scheme) would not imply significant risk impact: $\Delta R = 0.1 \times R = 10^{-07}$.
- However, presence of "non-OOS activity" with stronger potential to induce an initiator, considered to have an impact "by an OOM" (as discussed above) rather then "by a factor", through several weeks or a month (0.1 yr) over a year could have a moderate risk significance: $\Delta R = 0.1 \times 10 \times R = 10^{-06}$
- Single AOT event for EFW pump, being of duration up to 0.01 yr (e.g. three days) is not an event with relevant risk impact ($\Delta R = 10^{-08}$ as shown above), as long as operability of remaining pumps is out of question. However, combined with multiple activities with potential for inducing a reactor trip it can become risk significant (depending, also, on the confirmed status of remaining pumps.)
- Special category represents the activities with potential for inducing a trip of MFW or Condensate System and, consequentially a Turbine and Reactor trip. The nominal OOM initiator likelihood, from PRAs and SDP ([2], [3]), for the initiator category "reactor trip with MFW unavailable" is 0.1 /yr. From Table 1, the remaining nominal mitigation credit is $M_{EFW} \times M_{FB} = 10^{-05}$. Therefore, if there is an activity with an "impact by an OOM" (i.e. $\times 10$) on this initiator, concurrent with AOT of single EFW pump, then the combined risk impact is: $\left(10 \times 0.1/yr\right) \times \frac{10^{-5}}{10} \times 0.01yr = 10^{-06}$, which is considered to be in the range of a moderate risk significance.

(In the SDP scheme, [2], [3], the instances with impact between 10^{-06} and 10^{-05} are considered to have low to moderate risk significance; impact between 10^{-05} and 10^{-04} is considered to have

substantial risk significance; finally, impact larger than 10^{-04} is considered to have high risk significance.)

4.2 Risk from Station Blackout

Certain combinations of activities can have an impact on the risk from Station Blackout (SBO). Very simple risk model for SBO sequence can be established as follows (once again, the use is made of considerations from the SDP documents [2] and [3]):

- OOM initiator likelihood for Loss of Offsite Power: $I = 10^{-02}$ /yr
- Mitigation credit for Emergency Diesel Generators (multi train system): $M_{EDG} = 10^{-03}$
- Heat sink by EFW TDP and power recovery before depletion of batteries: $M_{REC} = 10^{-01}$
- From the above, the overall mitigation credit for SBO: $M_{SBO} = 10^{-04}$.

This simplistic SBO risk model yields the SBO contribution to CDF at the OOM of 10^{-06} per year, which can be confirmed by plant specific PRAs for this type of the plant.

As an example: any activity with "impact by an OOM" on the LOOP likelihood (e.g. switchyard related activities) concurrent with an AOT (the OOM of 0.01 yr) associated with a single EDG would produce the risk significance of: $\Delta R = \left(10 \times 10^{-2} \text{ /yr}\right) \times \frac{10^{-04}}{10} \times 0.01 \text{ yr} = 10^{-06}$. This is considered to be in the range of moderate risk.

4.3 Risk from Induced LOCA

Many times the perception is that online plant activities are not relevant for the risk from LOCA (i.e. their risk relevance is related to the risk from transients). This is not completely true. When an activity has a potential to induce a reactor trip this also means that it has a potential for producing a pressure transient caused by a plant trip, which can challenge the pressurizer relief or even safety valves and eventually, if any of challenged valves sticks open, induce a LOCA event (which may or may not be isolable).

Therefore, certain activities in plant areas such as TB or IB when combined with AOTs or certain activities in the AB related to the reliability / availability of ECCS can prove to be risk significant.

5 CONCLUDING REMARKS

The above process can be made more sophisticated and automated by the use of PRA or a risk monitor. The PRA elements such as initiators and basic events would be related to plant areas and then, instead of simplified OOM estimate, the conditional risk related to plant areas would be re-quantified in detailed manner. However, special attention would still need to be paid to the screened out sequences and areas in the PRA, as well as to the equipment not represented in the model. Also, the impact of activities would still, probably, be characterized in terms of "by a factor" or "by an OOM". The simplified OOM approach discussed above can be taken as a first step in a detailed process based on the risk monitor or, for example, to address the residual risk from the screened out areas / sequences or equipment, i.e. those not shown in the PRA used as a basis for the risk monitor.

However, it is emphasized here that the point of this paper is not on a quantitative risk estimate for ongoing activities and plant areas, in a mathematical sense. Rather, the point is that the principles outlined above can be, in a relatively simple and straightforward manner, used to produce a risk map of plant areas. That is, a cross-referential map can be developed which would for each plant area and associated set of activities point to those other areas / activities which have

significant risk implications, when combined with the considered area / activities. Such a map can be used in macro and micro scheduling of the proposed activities.

In this way, a concept of a "protected train", which is used in many plants, can be enhanced by a concept of "protected areas".

REFERENCES

[1] Risk Monitors, The State of the Art in Their Development and Use at Nuclear Power Plants, Produced on behalf of IAEA and OECD NEA WG Risk, NEA/CSNI/R(2004)20, OECD, 2004

[2] US NRC Inspection Manual, Chapter 0308, Attachment 3 "Technical Basis for Significance Determination Process 10/16/06" with Appendices

[3] US NRC Inspection Manual, Chapter 0609, "Significance Determination Process 06/02/11" with Appendices

Journal of Energy
VOLUME 62 Number 1–4 | 2013 Special Issue
journal homepage: http://journalofenergy.com/

Liquid-salt-cooled Reactor Start-up with Natural Circulation

Emilien Gros, Bojan Petrovic
Georgia Institute of Technology, Nuclear and Radiological Engineering
770 State Street, NW, Atlanta, GA 30332-0745, USA
emilien.gros@gatech.edu, bojan.petrovic@gatech.edu

Davor Grgic
University of Zagreb, School of Electrical Engineering
Unska 3, 10000 Zagreb, Croatia
davor.grgic@fer.hr

ABSTRACT

The Liquid-Salt-Cooled Very High-Temperature Reactor (LS-VHTR) was modeled using the neutronics analysis code SCALE6.0 and the thermal-hydraulics and kinetics modeling code RELAP5-3D with objective to devise, analyze, and evaluate the feasibility and stability of a start-up procedure for this reactor using natural circulation of the coolant and under the Loss Of Offsite Power (LOOP) conditions.

This Generation IV reactor design has been initially developed by Oak Ridge National Laboratory and studied by researchers worldwide for almost a decade. While neutronics and thermal-hydraulics analyses have been previously performed to show the performance of the reactor during normal operation and for shutdown scenarios, no study has heretofore been published to examine the active or passive start-up of the reactor.

The fuel temperature (Doppler) and coolant density coefficient of reactivity of the LS-VHTR were examined using the CSAS6 module of the SCALE6.0 code. Negative Doppler and coolant density feedback coefficients were calculated.

Two initial RELAP5 simulations were performed to obtain the steady-state conditions of the model and to predict the changes of the thermal-hydraulic parameters during the shutdown of the reactor. Next, a series of step reactivity additions to the core were simulated to determine how much reactivity can be inserted without jeopardizing the safety and stability of the core. Finally, a start-up procedure was developed, and the restart of the reactor with natural convection of the coolant was simulated. The results of the simulations demonstrated the potential for natural circulation start-up of the LS-VHTR.

1 INTRODUCTION

The Liquid-Salt-Cooled Very High-Temperature Reactor (LS-VHTR) is one of the six concepts of Generation IV reactors [1]. It has conceptually many promising features and combines several new technology assets such as: the use of the TRiISOtopic (TRISO) fuel particles, high operating temperature (> 750°C), Brayton power conversion cycle, and a low pressure liquid-salt coolant. Also, it was designed with several safety features enabling passive decay heat removal: the Reactor Vessel Auxiliary Cooling System (RVACS), the Direct Reactor Auxiliary Cooling System (DRACS), and the Pool Reactor Auxiliary Cooling System (PRACS). These systems offer the capability of passively (no external power needed) removing the decay heat from the core after a shutdown. The LS-VHTR project goal is to provide an advanced design which offers the potential

for higher power output, improved efficiency of electricity production and safety, and higher operating temperatures leading to a significant reduction in plant capital costs, as well as its use in high-temperature process heat applications.

Regulations for current nuclear power plants demand that a nuclear power plant have redundant safety features, including two connections to the electrical grid. In case of a loss of offsite power (LOOP), during a blackout for instance, the plant loses these connections, and may have to be tripped for safety reasons. After a power outage, since nuclear power plants require re-establishing the two connections and a large amount of energy to be started-up, they are usually the last power stations to be brought back on-line, leading to significant economic losses.

This paper evaluates the feasibility and stability of a start-up process for the LS-VHTR with natural circulation of the coolant. This novel concept for the start-up of a nuclear plant of LS-VHTR type would enable the restart of the plant under LOOP conditions, which would then help to restore the grid.

Limited experience related to start-up and operation under natural circulation of the coolant comes from the Dodewaard nuclear power plant, that was operated in the Netherlands until 1997, with a net output of 55 MWe [2], and from the passively safe generation III+ reactor ESBWR (Economic Simplified Boiling Water Reactor) designed by GE Hitachi Nuclear Energy that is waiting for final design certification [3]. However, the Dodewaard reactor and the ESBWR are Boiling Water Reactors (BWRs), thus physics phenomena are different than in the LS-VHTR.

2 LSCR SUMMARY

The LS-VHTR represents a unique merging of several design features. In this chapter, the specifics of the design chosen are presented.

2.1 Configuration, fuel element, fuel assembly and fuel core design

A functional diagram of the LS-VHTR layout is shown in Figure 1. The core and the primary heat exchanger are located in a large pool containing a buffer salt. The heat generated by the fuel is removed by a liquid-salt coolant flowing upwards through the core. This fluid flows in a primary loop through the primary heat exchanger, where heat is transferred to an intermediate loop containing another salt. The primary loop is closed and immersed in the buffer salt tank. The salt in the secondary loop conveys heat to a second heat exchanger, where helium flowing in a third loop is heated. This helium, once heated, flows through turbines in order to produce electricity. Alternatively, supercritical CO_2 or supercritical steam may be used.

The core is 12 m tall, and is composed of 8 m of active fuel, a lower plenum, lower reflector, upper reflector, and upper plenum of 1 m height each. The core diameter (including fuel assemblies and outer reflector blocks) is 9.2 m.

The LS-VHTR uses TRISO (TRiISOtopic) fuel particles, which were developed for use in various high temperature reactor concepts. It consists of a fuel kernel made of uranium oxycarbide (UCO) or uranium dioxide (UO_2), surrounded by four different layers of carbon and silicon carbide.

The prismatic block fuel assembly option is considered in this study. A single fuel block is shown in Figure 2. It has a flat-to-flat dimension of 36 cm, is 79.3 cm high, and is made of graphite. One fuel block contains 216 fuel channels (1.27 cm diameter) and 108 coolant channels (0.953 cm diameter). The fuel and coolant channels are arranged in a triangular array.

The reactor core layout is shown in Figure 2. The core has a diameter of 9 m. It consists of 265 fuel assemblies arranged so that they form a fuel region surrounded by four rows of reflector blocks. The latter have the same dimensions as the fuel blocks, and are composed of graphite.

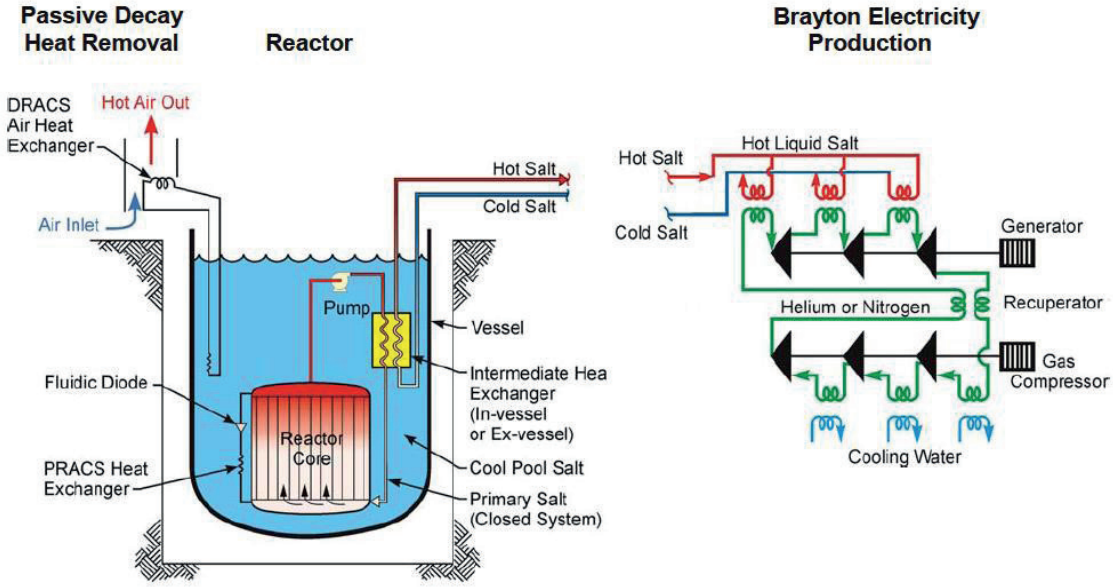

Figure 1: Configuration of the LS-VHTR plant [4]

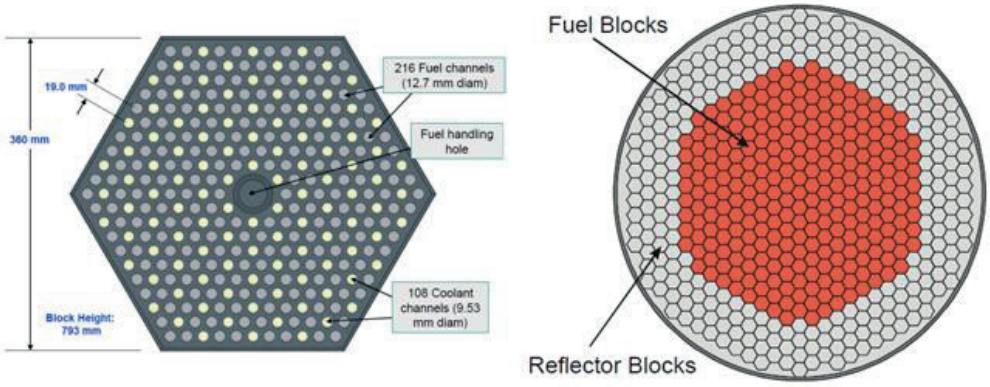

Figure 2: LS-VHTR hexagonal fuel assembly block [5] and reactor core layout [6]

2.2 Salt choice

There are several salts under consideration for use in the LS-VHTR such as: LiF-BeF_2 (FLiBe), $NaFBeF_2$, LiF-NaF-KF (FLiNaK), or NaF-ZrF_4 [4]. Salts are used for heat transport in this reactor. They are characterized by high boiling point, good heat transfer capabilities, and they enable the reactor to be operated at high temperatures. These characteristics lead to higher power efficiencies. Based on attractive neutronics as well as other properties including heat transfer characteristics, material compatibility, freezing temperature, cost and other criteria, FLiBe is usually preferred to other candidates to be the primary salt [6]. FLiNaK is considered as a good candidate for the intermediate loop [4], and was chosen as the intermediate salt in this study.

FLiBe is a compound of LiF (66%) and BeF2 (34%). It has a relatively low neutron absorption cross section. FLiBe salt shows great performance under activation; it does not generate gamma activity for more than one minute past being activated. Finally, the melting temperature of FLiBe is 459°C, and its boiling temperature is 1430°C [7].

FLiNaK is a compound of LiF (46.5%), NaF (11.5%) and KF (42%). It has a similar freezing point as FLiBe, but a lower heat capacity, lower thermal conductivity, and higher neutron absorption cross section. The melting and boiling temperature of FLiNaK are 454°C and 1570°C respectively [8]. FLiNaK is also cheaper than FLiBe [9].

3 METHODOLOGY

To evaluate the start-up of the LS-VHTR with natural circulation of the coolant, the neutronics and thermal-hydraulic aspects of the reactor have been studied. The CSAS6 [10] package of SCALE6.0 [11] was used to perform neutronic calculations. The thermal-hydraulics and kinetics calculations and simulations were done by employing the RELAP5-3D [12] code. The methodology developed to simulate the start-up of the reactor was as follows.

A 3-dimensional model of one fuel assembly of the LS-VHTR core was developed in SCALE6.0. Several simulations were run with different fuel temperatures to calculate the temperature reactivity feedback of the fuel assembly. The density of the coolant was then varied from 1.80 g/cm^3 to 2.05 g/cm^3 to get the coolant density reactivity dependency of the fuel assembly. Given that the fuel temperature feedback and the coolant density feedback of the entire core of the reactor are expected to be similar, it was decided to make the simulations on the fuel assembly only, with proper boundary conditions.

In this study, we are essentially interested in understanding how the temperature, pressure and flow in the primary loop and power profiles in the core would change during the start-up. Thus, only the primary loop and the intermediate loop of the nuclear power plant layout (see Figure 1) were modeled with the RELAP5 code. The primary loop, with FLiBe flowing through, was modeled as a closed loop in order to get as realistic results as possible. Only the heat exchanger of the intermediate loop was accurately modeled, the inlet and the outlet of the heat exchanger were treated as boundary conditions. Fuel temperature and coolant density feedback from the neutronic calculations were entered in the RELAP5 model as an input. RELAP5 was used to simulate three phases: normal operation, shutdown, and start-up. The reactor operation under steady-state conditions was first simulated. The shutdown of the reactor was then simulated using initial conditions from the previous simulation. Finally, using the reactivity feedbacks from the neutronics code, the thermal-hydraulic initial conditions from the shutdown simulation, and specifying a set of reactivity insertion steps the start-up of the LS-VHTR plant was simulated. This paper focuses on the results of the start-up simulation.

4 CORE PHYSICS

4.1 SCALE6.0 model

The effort to analyze the reactivity changes with respect to fuel temperature and coolant density is performed by modeling the reactor fuel assembly in the Standardized Computer Analyses for Licensing Evaluation Modular Code System (SCALE6.0). The SCALE system was developed by ORNL and is capable of performing criticality, shielding, spent fuel depletion or decay, and reactor physics calculations [13]. All calculations were done using the Criticality Safety Analysis Sequence (CSAS6) with KENO-VI [14] package of the SCALE6.0 code. It was decided to use fresh fuel everywhere in the fuel assembly for simplicity. Also, all of the calculations were made at the beginning of life of the fuel, which is 10% enriched in U^{235}. Future work should reexamine these coefficients for different fuel enrichment and burnups.

The three main materials encountered in the LS-VHTR core and modeled in SCALE6.0 are the fuel, the coolant, and the graphite used in the upper, lower and radial reflectors, and in the graphite blocks.

The TRISO fuel particles were modeled with the double-heterogeneity option of SCALE. The fuel kernel, graphite, and SiC layers composition were defined according to the specifications provided by ORNL. Silicon carbide is defined as a special mixture with the natural isotopic abundance of Silicon (^{28}Si = 92.23%, ^{29}Si = 4.67%, and ^{30}Si = 3.1%). The TRISO particle volume fraction was set to 0.30 based on the range of values considered in literature.

The primary coolant composition, FLiBe (66% LiF, 34% BeF_2), was also described as a weight percent mixture of its isotopic components. The lithium in FLiBe was assumed to be

enriched to 99.99% in ^{7}Li, given that it is difficult to produce Lithium with less than 0.01% of ^{6}Li [5].

Instead of modeling the actual reactivity control system, it was decided to mix boron with the graphite of the fuel assembly blocks and reflectors in order to get a multiplication factor around 1. Thus, a weight percent mixture of graphite and ^{10}B (99.9985% and 0.0015%) with a density of 1.74 g/cm^3 was defined for the material of the fuel assembly blocks and of the reflectors.

To accurately model the triangular pitch of the fuel assembly design, hexagonal lattice geometry was used to describe the fuel, coolant and graphite blocks. The fuel and coolant units are defined as a cylindrical form filled with fuel or FLiBe inserted in a hexagonal graphite block. These units were placed in an array to reproduce the pattern shown in Figure 2.

Mirror boundary conditions were set on the outer limit of the hexagon modeling the fuel assembly block, simulating the effect of the large core. This enabled us to make the calculations on the fuel assembly level and to assume that the results are similar to that we would obtain by simulating the whole core.

4.2 Results

To get enough statistical precision on the multiplication factor, KENO-VI simulations were preformed using 1,000 generations with 10,000 neutrons per generation. This resulted in a 1σ statistical uncertainty ranging from $1.4*10^{-4}$ to $1.9*10^{-4}$.

For the Doppler coefficient calculation, simulations were run with a coolant temperature of 1143 K, which is the temperature of the coolant right before the reactor is started-up. Seven simulations were run with fuel temperatures ranging from 873 K to 1473 K. The reactivity value (ρ) was calculated from the neutron multiplication factor value. The RELAP5 code requires that the reactivity be entered in dollars ($) in the kinetics input. Thus, the value of the reactivity in dk/k unit was divided by the effective delayed neutron fraction (β = 0.0065) to convert it into $ units. The results were arranged in a table and plotted. The equation of the relation between reactivity and fuel temperature (ρ = func(TF) were func is a function of the fuel temperature, TF) was extracted from this plot. The value of the derivative of this relation with respect to fuel temperature was finally calculated at different fuel temperatures to get the Doppler temperature coefficient of reactivity. The results of the CSAS6 simulations are presented in Figure 3.

The calculated Doppler fuel temperature coefficient of the core is – $0.0074 /K. This value is in acceptable agreement with the temperature coefficient estimated by ORNL for the AHTR: – $0.01 /K [5].

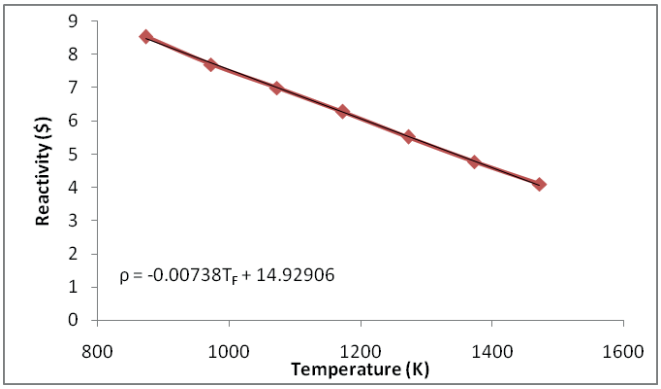

Figure 3: Calculated reactivity for 7 different fuel temperatures

For the coolant density reactivity coefficient calculation, the fuel temperature was set to 1150 K for all the simulations and the coolant temperature to 1140 K. These temperatures correspond to the average temperature in the fuel and coolant before the reactor is started-up.

Simulations were run for six different FLiBe densities, ranging from 1.60 g/cm^3 to 2.15 g/cm^3. Results and plots of the simulations are given in Figure 4.

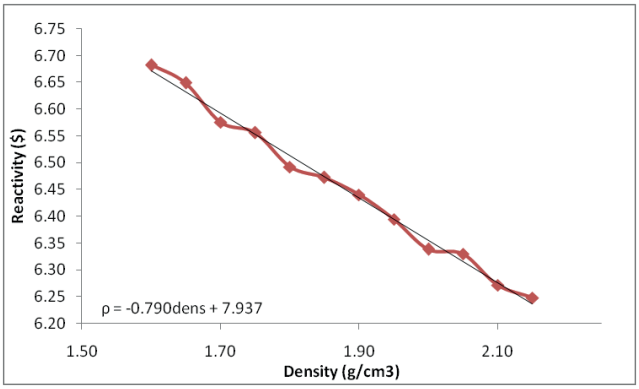

Figure 4: Calculated reactivity for 12 different coolant densities

The reactivity of the system decreases with increasing coolant densities. Given that an increase in coolant temperature results in a decrease of the coolant density, an increase in FLiBe temperature would lead to an increase of the reactivity of the system. This could lead to instabilities; however, for a coolant density change of 0.25 g/cm^3, the reactivity decreases from \$6.68 to \$6.47, i.e., only ~\$0.2. The following correlation, Eq. (1), was used for the FLiBe density with respect to temperature [15]:

$$\rho_{FLiBe} = A_D (T_{FLiBe} - 273.15) + B_D \quad (1)$$

With A_D = -0.4884 kg/m^3/K, and B_D = 2279.7 kg/m^3, it was calculated that densities ranging from 1.80 g/cm^3 to 2.05 g/cm^{3}correspond to temperatures ranging from 1250 K to 750 K. Thus, a coolant density decrease of 0.25 g/cm^3, corresponding to a coolant temperature increase of 500 K, would lead to about \$0.2 reactivity insertion. This effect is small, considering that during the start-up of the reactor, the temperature increase rate is usually on the order of magnitude of 50 K/hr. In addition, an increase in temperature also leads to a negative fuel temperature feedback that is much larger than the density feedback.

4.3 Radial and axial power distribution

The radial power distribution profile was established based on ORNL's calculations, done with MCNP and a 10-ring core model [6]. These 10 rings were grouped to form three radial regions across the core, as illustrated in Figure 4.

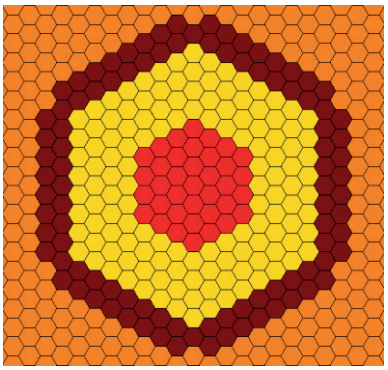

Figure 5: Inner, middle, and outer region of the LS-VHTR core

The inner region groups the rings 1, 2, 3 and 4. The rings 5, 6, 7 and 8 constitute the middle region. The outer region is composed of the two outer rows of fuel assemblies; rings 9 and 10. A

summary of the characteristics of the groups is given in Table 1. One can observe that the inner group produces more power per fuel assembly than the outer group.

	Group 1 (inner)	Group 2 (middle)	Group 3 (outer)
Number of assemblies in the region	37	132	96
Fraction of total number of assemblies	14%	50%	36%
Power generated by the region	446.04 MW	1278.34 MW	673.80 MW
Fraction of total power	18.60%	53.30%	28.10%
Peak to average factor	1.33	1.07	0.78

Table 1: Description of the model core regions

The axial power distribution profile is used by RELAP to calculate the heat transferred to the coolant channels in each axial segment modeling the core. An internal source multiplier value was specified for each axial segment of the three heat structures modeling the fuel channels of the three rings of the core. These values are multiplied by the total power (specified manually or calculated with the point reactor kinetics equations) to obtain the power generated in the heat structure [16]. The axial power profile chosen is based on a profile used by ORNL to model the LS-VHTR [6]. This axial distribution was also used for gas-cooled VHTR modeling [17]. The power profile that was chosen is shown in Figure 6. To get the power profile in each region of the core, the distribution of Figure 6 was multiplied by the power generated in every region, as specified in Table 1. The axial power distribution obtained for each group of fuel assemblies is shown in Figure 7.

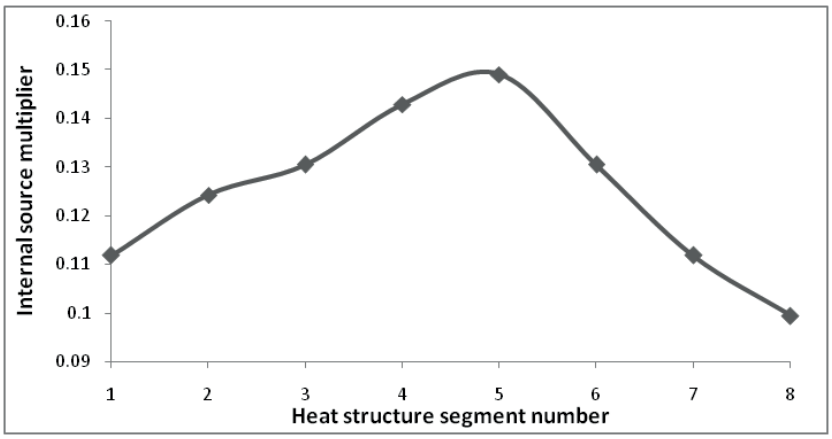

Figure 6: Representative axial power distribution profile

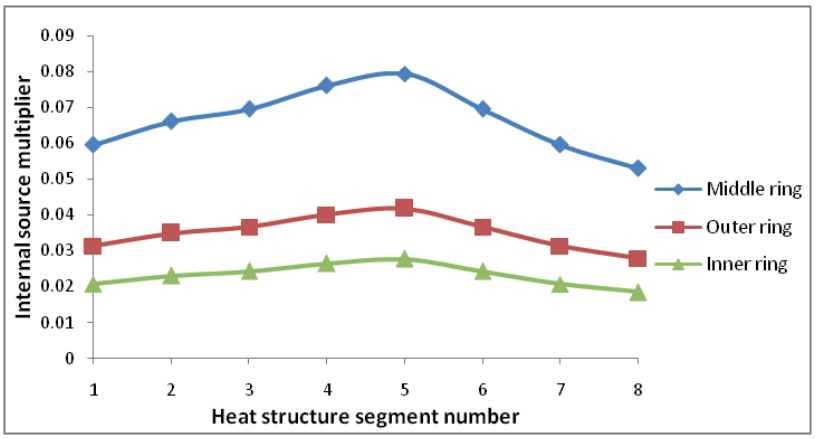

Figure 7: Axial power distribution profile in the core regions

E. Gros, B. Petrovic, D. Grgic, Liquid–salt–cooled Reactor Start–up with Natural Circulation, Journal of Energy, vol. 62 Number 1–4 (2013) Special Issue, p. 113–130

5 RELAP5 NODALIZATION/MODEL

Thermal-hydraulics analyses were performed using the Reactor Excursion and Leak Analysis Program (RELAP), developed at the Idaho National Laboratory (INL), which offers the capability to calculate the behavior of a reactor coolant system and the reactor kinetics during a transient. The RELAP5 code has been originally developed to model Light Water Reactors (LWRs). Though, the properties of several molten salts including FLiBe and FLiNaK have been subsequently incorporated [15], making the modeling of the LS-VHTR possible. The heat transfer coefficients used by RELAP5 for reactors with a salt coolant are the same as that used in the code to model LWRs, however, it was shown experimentally that this was an acceptable approximation.

5.1 Nodalization, hydrodynamic components and main parameters

The model encompasses the core, the primary coolant (FLiBe) loop, two IHXs, and part of the intermediate coolant loop. The primary salt flows upwards through the core and downwards through the shell side of the IHX. The secondary coolant (FLiNaK) flows upwards through the tube side of the IHX. A schematic of the RELAP5 model is given in Figure 8. The components 10, 20 and 30 represent the coolant channels, corresponding to three core regions (inner, middle, outer). The core has been divided radially in three groups of fuel assemblies to increase the fidelity of the model. The core is divided into 8 segments axially. For example, for the component 10, segments 1 through 8 model the same fuel assemblies at different elevations.

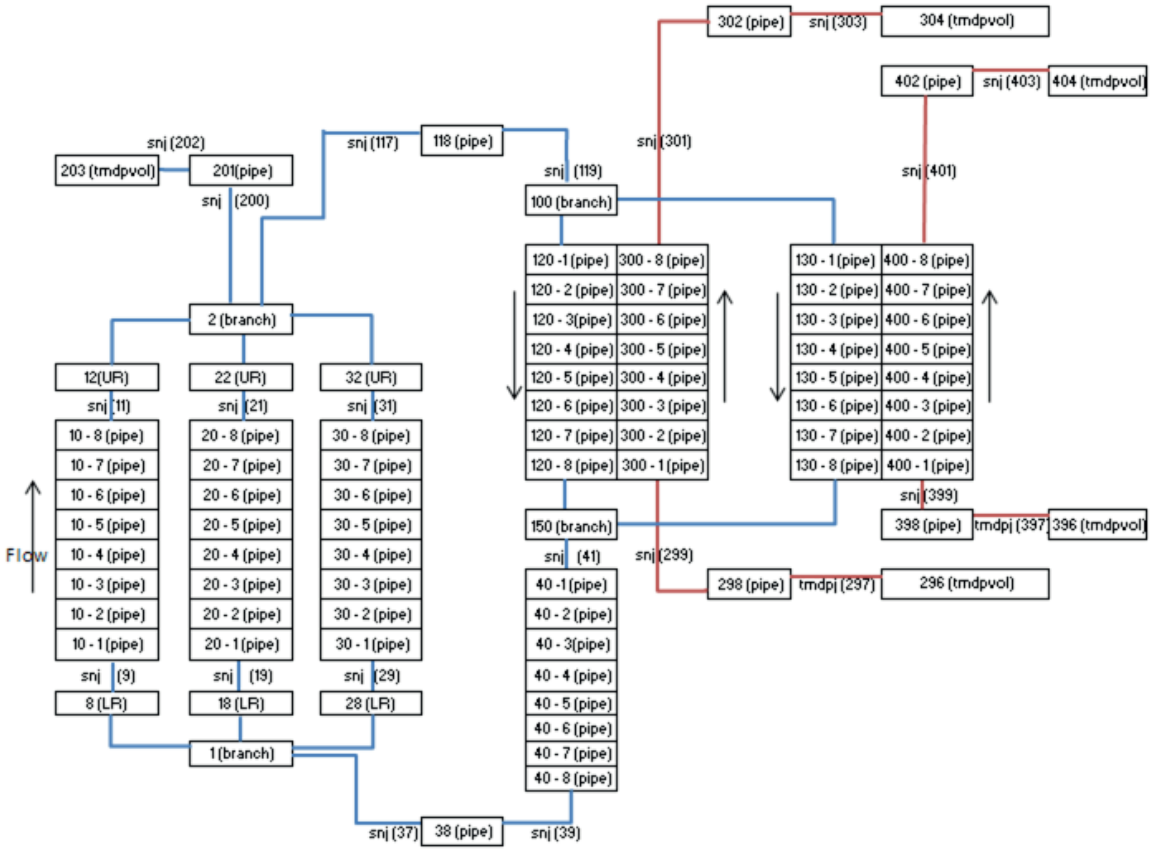

Figure 8: RELAP5 model of a LS-VHTR

The lower and upper reflectors are represented by the components 8, 18, 28 and 12, 22, 32 respectively. Given that the bypass flow in radial reflectors is assumed negligible (less than 5%), the radial reflectors were not modeled. Components 1 and 2 represent the lower and upper plenum

respectively. The pipe 201 and the time dependent volume 203 model the pressure maintenance system above the upper plenum. The pipes 118 and 38 make the connection between the upper plenum and the upper header of the IHXs (component 100) at the top, and between the downcomer (component 40) and the lower plenum at the bottom. Components 100 and 150 represent the upper head and lower head of the IHXs. Components 120 and 130 represent the shell side of the IHXs, while components 300 and 400 represent the tube side of the IHXs. Components 296, 298, 302 and 304, 396, 398, 402 and 404 represent the secondary loop. Boundary conditions were specified in the junctions 297 and 397, in order to force the flow of the secondary loop.

The basic core design values are as follows in the RELAP5 model:

- Graphite block: 36 cm flat-to-flat, 8 m height
- Fuel cylinder modeling the fuel kernels of the TRISO particles: 0.6762 cm diameter
- Coolant channel: 0.953 cm diameter
- Core: 265 fuel assemblies
- Primary coolant: FLiBe ($2LiF\text{-}BeF_2$)
- Primary coolant expected steady-state temperatures: 1173 K inlet, 1273 K outlet
- Thermal power: 2400 MW
- Core flow: 10,000 kg/s

The dimensions and main parameters assumed for the other components are listed below:

- Top and bottom reflectors: 1 m thick, same flow area as coolant channels
- Upper and lower plenums: 2 m and 1 m height respectively, same flow area as the core
- Heat exchanger: shell and tube heat exchanger
- Intermediate loop flow: 16,400 kg/s
- Intermediate loop steady state temperatures: 1140 K inlet, 1200 K outlet

The flow areas and length of the primary loop components were defined as follows:

- Plenum flow area: 2.032 m^2
- Inner assembly ring flow area and height: 0.284 m^2, 8 m
- Middle assembly ring flow area and height: 1.01 m^2, 8 m
- Outer assembly ring flow area and height: 0.736 m^2, 8 m
- Transport pipe flow area and length: 0.5 m^2 , 2 m
- Downcomer flow area and length: 0.5 m^2 , 3.2 m

The material properties (specific volumetric heat capacity and thermal conductivity) used in the analyses are as follows:

- Fuel: cp = 2.76e6 J/m^3K, k = 10.0 W/mK [4]
- Graphite blocks: cp = 3.276e6 J/m^3K, k = 30.0 W/mK [4]
- Coolant salt, FLiBe: cp= 4.39e6 J/m^3K, k = 1.1 W/mK [4]
- Hastelloy N alloy: cp = 5.12e6 J/m^3K, k= 23.6 W/mK [18]

5.2 Heat structures

Several heat structures have been defined in the model, attached to the coolant channels, the upper and lower reflectors, and the heat exchanger.

One heat structure has been implemented for each ring of the core (10, 20 and 30) to model the heat transferred to the coolant channels via the power generated by the fuel. The fuel heat structures are cylindrical, and their outer boundary is attached to the corresponding coolant channel hydrodynamic component. The RELAP5 code offers the capability to model a simple fuel configuration only. For instance, the following type of fuel structure can be modeled in RELAP5: a cylindrical fuel rod surrounded by a cladding layer and an external layer of another material. The coolant channel is connected to the heat structure as a boundary condition. The fuel used in the LS-VHTR is a fuel compact, made of TRISO fuel particles assembled together in a graphite moderating matrix. Finding a model that would exactly reproduce the TRISO fuel performance was intricate.

Thus, assumptions were made to approximate heat transfer as much as possible. The fuel heat structure model is as follows:

- One cylindrical rod was defined to model the fuel
- A layer of graphite was set around the fuel to model the TRISO particle outer carbide layers, the graphite moderating matrix of the compact, and the graphite of the fuel assembly blocks

The radius of the rod modeling the fuel was calculated using the proportion of fuel in the TRISO particles (fuel kernel size) and the proportion of TRISO particles in the fuel compact (packing fraction). The calculated radius of the fuel rod is: $3.3771*10^{-3}$ cm. One should note that this may not be the most accurate way to model the performance of the TRISO particles with the RELAP5 code. Though, since this study aims at providing a model to evaluate the stability and feasibility of a start-up procedure with natural circulation, it was decided that this modeling of the fuel was the only practical option and adequate for the objectives. Further work is needed to provide a more realistic model of the TRISO fuel, but this was out of the scope of this work.

Six heat structures have been defined to model the lower and upper reflectors. These heat structures are similar to the fuel heat structure, except that the material is graphite.

Each heat exchanger has an associated heat structure. The latter consists of a cylindrical layer of Hastelloy N alloy, with the secondary loop as the inner boundary (tube side of the IHX) and the primary loop as the outer boundary (shell side of the IHX). For simplicity, it was decided not to model the baffles. The heat structure as presented models a simple straight-tube shell-and-tube type heat exchanger.

The heat losses in the plenums are assumed negligible. Thus, no additional heat structure has been defined.

5.3 Form loss coefficients

Given that the start-up of the LS-VHTR under natural circulation was studied, it was essential to take the flow resistance in the loop into account. To do so, form loss coefficients were specified to model the friction losses due to the abrupt area changes at the entrance of the lower axial reflectors and at the exit of the upper axial reflectors. Form loss coefficients were also specified at the entrance and the exit of the heat exchanger. Each loss coefficient was assumed to be 0.25, based on the typical loss coefficient used in LS-VHTR RELAP5 model [6]. In this study, the pump was not modeled with the RELAP5 component “pump”. Instead, a time-dependant junction was used (junction 117 in Figure 8) to force the flow during steady-state conditions operation, and a simple junction was used to let RELAP5 calculate the flow during operation with natural circulation of the salt in the primary loop. A form loss coefficient of 1.0 was entered in the junction modeling the pump (in active or passive mode) to account for the pressure drop induced. This form loss coefficient was assumed; thus, the behavior of the pump as modeled might differ from the behavior of the actual pump in the LS-VHTR design. This assumption impacts the value of the natural circulation mass flow rates predicted by the RELAP5 code and should be taken into account when observing the results of the different simulations that will be presented later in this paper.

6 SIMULATIONS AND RESULTS

To model the start-up of the reactor under natural circulation of the coolant, the kinetics mode of RELAP5 was used to calculate the power and reactivity changes of the core during the transient. The flow in the different rings of the core was also calculated by the program. The initial temperature, pressure and flow conditions are set to the final values obtained at the end of a shutdown simulation, which is not presented in this paper. The initial power consists of only decay power, and is set to about 21.5 MW by specifying a power history table in the input file.

6.1 $0.15 step reactivity insertion simulation

In this simulation, $0.15 of reactivity is inserted at t = 100 s. The initial 100 s before inserting the reactivity rather than doing it at time t = 0 s is intended to allow the code to reach a steady state with the kinetics mode activated. Figure 9 shows the changes in reactivity, total power, decay, and fission power respectively during the transient that follows the insertion of reactivity in the core.

The positive reactivity is inserted at t = 100 s, while the power swing occurs only after 1500 s. This can be explained by the prompt jump approximation [19]. In this approximation, the fission power is initially increased by the factor: $\beta / (\beta-\rho)$, where ρ is the reactivity inserted. Then, the fission power increases exponentially by the factor e in magnitude every reactor period. Given that the initial fission power equals $2.15*10^{-5}$ W, it takes a certain time for the fission power to increase to significant values even if the increase is exponential. That initial value of the fission power was calculated by RELAP5, based on the power history table that was entered, and thus may differ from the actual value of fission power in the LS-VHTR eight hours after a shutdown from full power condition. The total core reactivity goes to $0.15 after the insertion and remains at this value for about 1500 s. After this time, due to the feedback, the total core reactivity oscillates to stabilize again at its initial $0 value at t = 3000 s. Thus, it takes less than an hour for the core to stabilize after a $0.15 positive reactivity insertion. The decay power slowly decreases until 1500 s, since no significant new fission occurs, and then increases because of the new fissions happening in the core. The results plotted show that the power level is increased from 21.5 MW to 98.5 MW. The core inlet, outlet, and fuel centerline peak temperature are at the time t = 4500 s: 1133.6, 1186.1 and 1191.8 K. The mass flow driven by natural convection is increased from 474.2 kg/s initially to 785.7 kg/s at the end of the simulation.

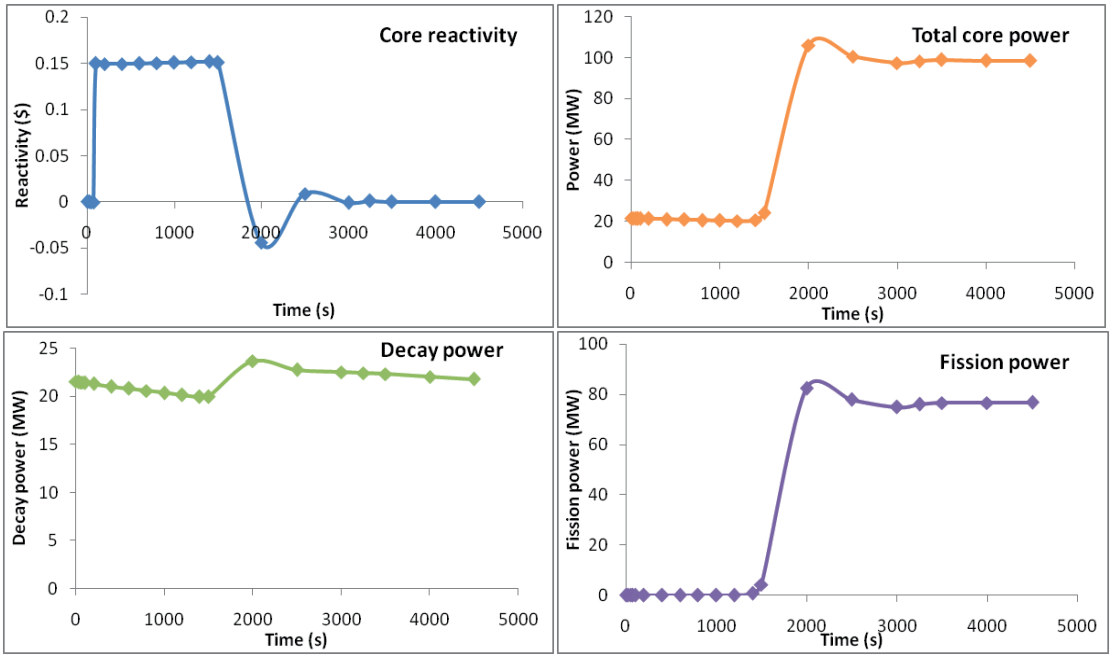

Figure 9: Changes in reactivity, total power, decay power, and fission power over time

In order to provide a thorough understanding of the phenomena happening during the transient following the control rods removal, other thermal-hydraulic parameter values were plotted in Figure 10.

The effect of the reactivity insertion on the flow and temperatures in the inner, middle and outer rings of the core can be seen after 1500 s. Due to the significant power increase, the outlet and inlet temperatures are increased. The outlet temperature increase equals about 38 K in the three core regions. Though, the temperature increase in the first axial segment of the inner region is twice as high as the increase in the inner or middle assemblies. This leads to a lower temperature differential

in the outer region of the core than in the inner and middle region. As a consequence of the varying temperature increases, the coolant behaves differently in each region of the core. Figure 5.27 shows that from t = 1200 s to t = 1800 s the mass flow in the outer fuel assembly ring decreases. This decrease is due to the natural circulation of the coolant, and should be kept limited to avoid counter-flow.

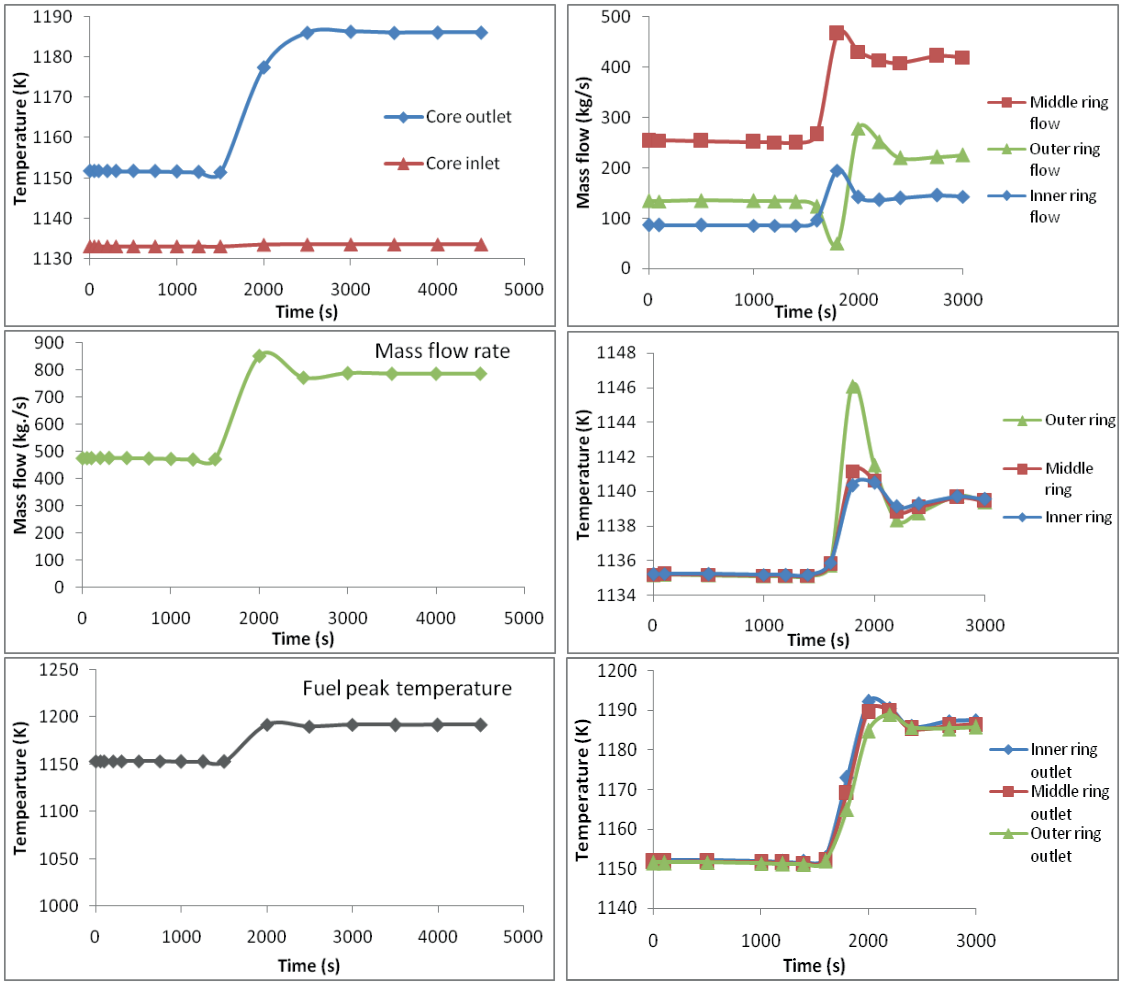

Figure 10: Changes in core outlet and inlet temperature, mass flow rate, fuel peak temperature, core mass flow rates, bottom of core temperature, and core outlet temperature

6.2 Summary of single step reactivity insertion simulations

Analysis for eight different single step reactivity insertions was performed, analogous to the \$0.15 insertion. The results of are summarized and presented in Table 2.

Reactivity inserted (\$)	Final Power (MW)	Fraction of total power achieved	Peak fuel temperature (K)	Negative flow during transient
0.00	21.5	0.90	1153.2	No
0.10	70.0	2.92	1179.0	No
0.15	98.6	4.11	1191.8	No
0.20	138.2	5.76	1204.4	Yes
0.50	369.2	15.38	1282.7	Yes
1.00	897.3	37.39	1418.0	Yes
1.25	1200.0	50.00	1486.0	Yes
1.50	1521.7	63.40	1554.0	Yes
1.55	1588.0	66.17	1567.7	Yes

Table 2: Summary of single step reactivity insertions

The results presented in Table 2 were analyzed to establish limits on the amount of reactivity that could be added by a single step insertion without jeopardizing the stability of the system. Also, the total amount of reactivity that could be inserted by making successive single step reactivity insertions without risk was evaluated.

As shown in section 6.1, the step insertion of reactivity may induce a reverse flow ("negative flow") in the outer fuel assemblies of the core. In order to proceed to a safe restart of the LS-VHTR, no such phenomenon should be observed. Several simulations were run to determine a limit on the inserted reactivity in order to avoid negative flows. It was found that reactivity insertion less or equal to \$0.18 would not induce reverse flow. Thus, no more than \$0.18 reactivity in one step should be added in order to avoid counter-flow.

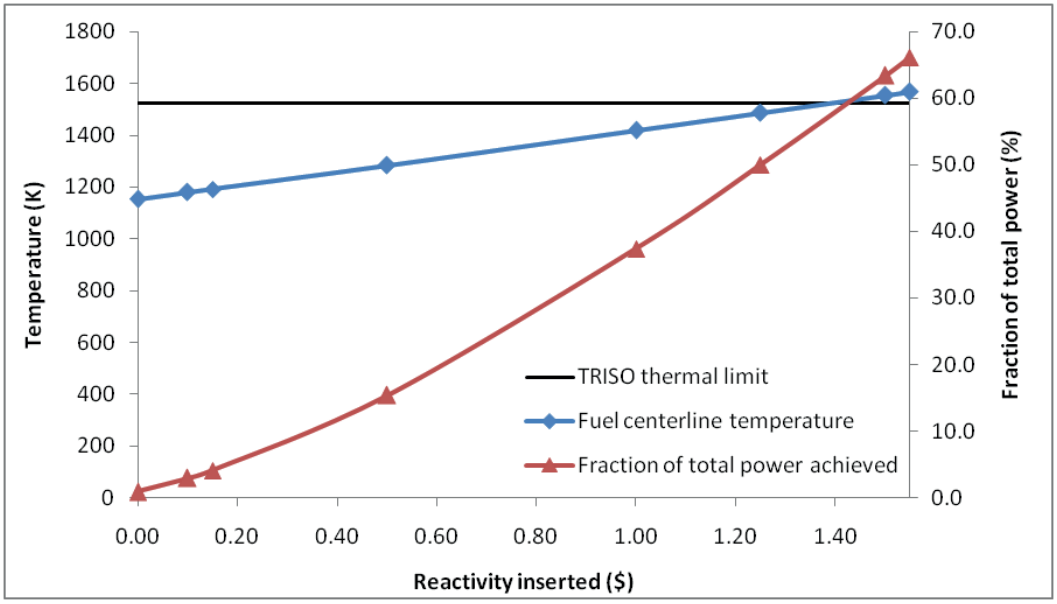

Figure 11: Peak fuel centerline temperature and fraction of total power achieved for 7 different step reactivity insertions

The limit on the fuel temperature was also examined. Current coated TRISO fuel particles offer the capability to operate for long periods at temperatures up to 1523 K (1250°C) [5]. Thus, the total amount of reactivity added to the core by successive step reactivity insertion should not make fuel centerline temperatures hotter than 1523 K. Among the simulations presented in Table 2, the fuel centerline temperature goes past this limit in the \$1.5 insertion case. Additional simulations with different amounts of reactivity inserted in the core were run, in order to study the impact of reactivity insertion on the fuel peak temperature. The maximum fuel temperature and the fraction of total power reached at the end of the transient after adding 7 different amounts of reactivity are shown in Figure 11.

The maximum fuel temperature is below the TRISO thermal limit for a \$1.25 insertion and above the limit for a \$1.5 insertion. The fuel centerline temperature curve intersects the TRISO thermal limit line for inserted reactivity around \$1.40. Thus, the amount of a single step reactivity insertion should remain below this value (plus some safety margin) to preserve the integrity of the TRISO fuel particles.

6.3 Potential start-up procedure and simulation

Given the results presented in sections 6.1, 6.2, and the experience of natural circulation power plant start-up from Dodewaard and the ESBWR, a potential start-up procedure for the LS-VHTR with natural circulation of the salt coolant was devised.

It was decided to define a similar kind of start-up, with successive positive step reactivity insertions. Based on the discussion made in the previous section, and in order to prevent any type of instability, it was decided to maintain the insertion of positive reactivity below or at \$0.15. As mentioned in section 6.2, the fuel temperature should not go past 1523 K in order to preserve the integrity of the TRISO fuel. As a consequence, the amount of successive step insertion was chosen so that the maximum fuel temperature in the core does not exceed that value. The initial reactivity inserted was done at time t = 100 s after the beginning of the simulation. The next insertion was done at time t = 2000 s, and the following insertions were made every 1000 s after this second insertion as shown in Figure 12. The total reactivity inserted with this set of eight \$0.15 reactivity additions was \$1.2.

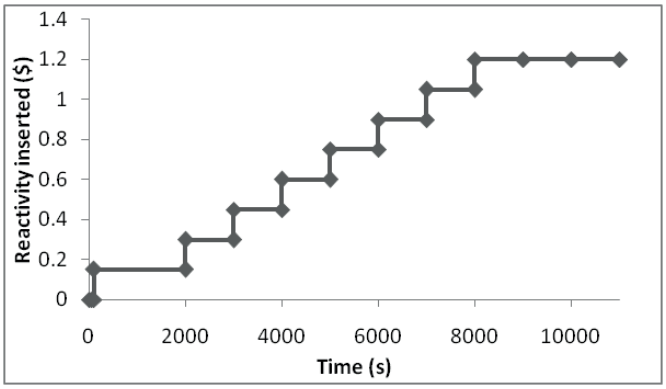

Figure 12: Reactivity insertion curve for the start-up simulation

Figure 13 shows the behavior of the total core reactivity, core power level, decay and fission power, temperature and flow with respect to time during the simulated start-up of the LS-VHTR. It can be observed that during the start-up, the reactivity oscillates between 0 and some positive values. This is due to the fact that a step of positive reactivity is inserted in the core every time that the total reactivity of the core decreases due to the feedback. No negative flow was observed in the outer ring of assemblies during the simulation. The total core mass flow reaches 1713.2 kg/s at the end of the start-up. This flow corresponds to 17.3% of the core mass flow under full power conditions. The core power level goes from 21.5 MW initially to 1138 MW after 18000 s. Thus, with this set of successive reactivity insertions, it takes 2.5 hours to bring the reactor to 47.5% of the total reactor power level.

The core inlet temperature was increased by 10 K while the core outlet temperature increase is 269.7 K. The maximum fuel temperature during the start-up is achieved at the end of the process, with 1472.5 K. This value is 50 K below the limit for preserving the integrity of the coated particles, maintaining this start-up procedure safe regarding fuel temperature.

The results of the start-up simulation showed that no more than 47.5% of the total reactor power level may be reached using natural circulation of the coolant. During the start-up and power increase, it is of course necessary to provide an ultimate heat sink. In order to achieve full power conditions, it is necessary to start generating electricity using the turbines and to restart the circulating pumps at some time during the start-up.

The pumping power required to run the pumps may be calculated using the following equation [20], Eq. (2):

$$P_{pump} = \frac{\Delta P \times \dot{V}}{0.9} \quad (2)$$

Where P_{pump} is the pumping power needed in W, ΔP is the pressure drop in Pa, and V is the volumetric flow rate in m^3/s. The denominator 0.9 is used to account for the pump efficiency. The pumping power needed will increase with time since it is proportional to the mass flow. Though, since the rate of the core power increase is greater than the rate of salt flow increase, at some time after the beginning of the start-up the amount of power generated will be sufficient to provide enough electricity to run the pumps. To estimate this time, one should take into account the power conversion efficiency, calculate the electrical power production capability of the reactor at any time during the start-up, and compare that value to the pumping power needed.

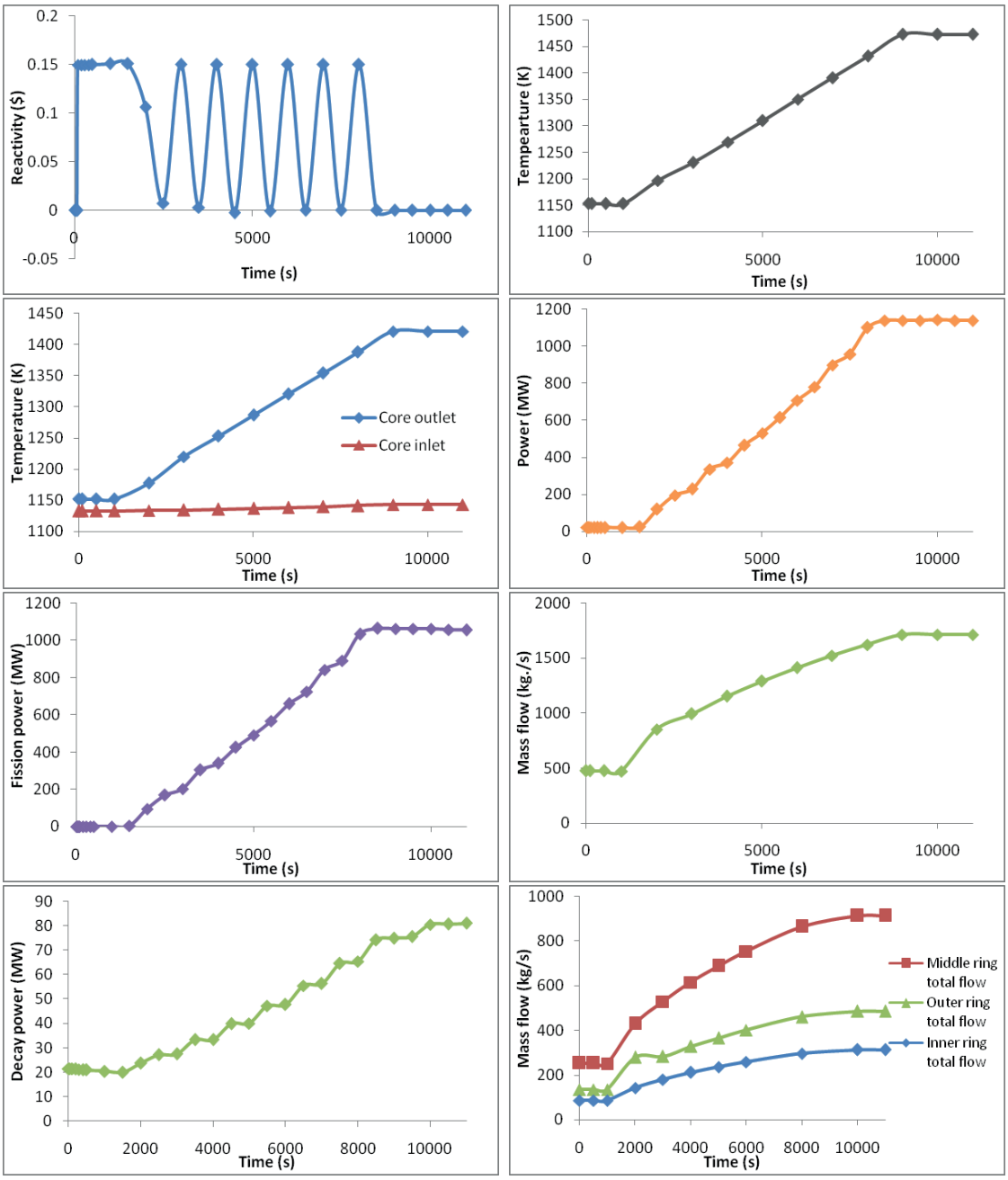

Figure 13: Core reactivity, total power, decay power, fission power, fuel peak temperature, core outlet and inlet temperatures, mass flow rate, and flow in the different rings over time

At the end of the start-up simulation presented previously, the thermal power is 1472.5 MW, the core mass flow is 0.95 m^3/s (FLiBe density is assumed to be 1800 kg/m^3), and the pressure drop is 0.2 MPa. Therefore, the calculated pumping power is 233.3 kWe. Using a thermal efficiency of 0.54, the electrical power generated at the end of the simulation would be 795.15 MWe which is many times more. Thus, the restart of the pumps using the electricity provided by the turbines is not limited by the electricity generation capability.

In real life, power production followed by synchronization to grid would be initiated at much lower power, perhaps 3-5% full power, and the electricity produced would need to provide not only pumping power, but the whole power plant electric needs. However, this was beyond the scope of this study and is left for future research.

7 CONCLUSIONS

Neutronic and thermal-hydraulic performance of a LS-VHTR were examined. The purpose of this study was to develop and analyze a start-up procedure for this reactor with natural circulation of the coolant, in order to evaluate its feasibility and stability. A model of the LS-VHTR core was developed using the CSAS6 sequence of the SCALE6.0 package to quantify the reactivity feedback due to changes in the fuel temperature or coolant density. A model of the reactor using ORNL baseline design specifications using the RELAP5 software was also developed to simulate the thermal-hydraulic behavior of the reactor during full power operation, shutdown and start-up, and to determine the core reactivity and power changes during a plant start-up. Simulations were performed to determine a potential start-up procedure for the LS-VHTR with natural convection of the coolant, and then to analyze and evaluate this process.

The neutronic calculations evaluated the negative Doppler coefficient for the reactor under study. It was also shown that a decrease in FLiBe density would lead to a positive reactivity feedback. However, it is essential to point out that the change in reactivity induced by the coolant density feedback is negligible compared to the effect of the fuel temperature feedback, thus making the overall reactivity feedback negative and the LS-VHTR passively safe.

Different step reactivity insertion cases were studied, and showed that inserting more than \$0.15 of reactivity in the LS-VHTR core eight hours after its shutdown from full operating conditions could lead to flow instability in the core. In addition, it was shown that inserting more than \$1.2 in the core would make fuel temperatures exceed the thermal capability of the TRISO particles. A potential start-up trajectory was then devised and simulated. The results obtained showed that the reactor power level can be brought to 47.5% of full power without exceeding the fuel thermal limits, and using natural convection of the primary coolant to transfer the heat generated to the intermediate loop.

It should be taken into account that assumptions were made, and the findings presented in this paper should be observed with an appropriate distance. The RELAP5 code was initially developed to simulate the behavior of systems with water as the coolant and was never validated for LS-VHTR, even if the properties of FLiBe and FLiNaK were subsequently added. Thus, this study only provides an indication about the stability and feasibility of a start-up procedure for the LS-VHTR with natural convection of the salt coolant.

Under the assumptions used in this work, it was shown that a stable procedure could be developed, as the one presented in section 6.3, and that a significant core power could be achieved by inserting reactivity stepwise eight hours after the shutdown of the reactor. Thus, this study demonstrated the potential for a passive start-up of the LS-VHTR. However, additional work is needed in order to get a thorough evaluation of the feasibility of a start-up procedure that would not require any offsite power.

In this study, the thermal-hydraulics modeling focused on the primary loop components. The flow and temperatures in the secondary loop were assumed and entered in the RELAP5 code as boundary conditions. Moreover, the power production loop was not modeled in this study, the

power conversion efficiency was assumed based on ORNL expectations for their LS-VHTR conceptual design, and the power needed for the instrumentation of the plant, for the circulating pumps of the intermediate and power production loop, and for the turbines was not taken into account. To get more realistic results, the modeling of the intermediate loop and of the power production loop should be included in future studies.

REFERENCES

[1] U.S. DOE Nuclear Energy Research Advisory Committee. "A Technology Roadmap for Generation IV Nuclear Energy Systems Executive Summary", March 2003.

[2] World Nuclear Association. "Nuclear Power in the Netherlands", http://www.world-nuclear.org/info/inf107.html.

[3] U.S. Nuclear Regulatory Commission. "Design certification application reviews - EBWR", http://www.nrc.gov/reactors/new-reactors/design-cert/esbwr/review- schedule.html.

[4] D. T. Ingersoll, C. W. Forsberg, P. E. MacDonald. "Trade Studies for the Liquid-Salt- Cooled Very High Temperature Reactor: Fiscal Year 2006 Progress Report", Oak Ridge National Laboratory, ORNL/TM-2006/140, February 2007.

[5] D. T. Ingersoll, C. W. Forsberg, L. J. Ott, D. F. Williams, J. P. Renier, D. F. Wilson, S. J. Ball, L. Reid, W. R. Corwin, G. D. Del Cul, P. F. Peterson, H. Zhao, P. S. Pickard, E. J. Parma, M. Vernon. "Status of Preconceptual Design of the Advanced High-Temperature Reactor (AHTR)", Oak Ridge National Laboratory, ORNL/TM-2004/104, May2004.

[6] D. T. Ingersoll. "Status of Physics and Safety Analyses for the Liquid-Salt-Cooled Very High-Temperature Reactor (LS-VHTR)", Oak Ridge National Laboratory, ORNL/TM-2005/218, December 2005.

[7] D. E. Holcomb. "Fluoride Salt Cooled High-Temperature Reactors (FHRs), Successor to the LWR?", Presentation for Georgia Tech Graduate Seminar, Oak Ridge National Laboratory, January 2011.

[8] L. C. Olson. "Materials Corrosion in Molten LiF-NaF-KF Eutectic Salt", University of Wisconsin-Madison, 2009.

[9] D. F. Williams, L. M. Toth, K. T. Clarno. "Assessment of Candidate Molten Salt for the Advanced High-Temperature Reactor (AHTR)", Oak Ridge National Laboratory, ORNL/TM-2006/12, March 2006.

[10] S. Goluoglu, D. F. Hollenbach, L. M. Petrie. "CSAS6: control module for enhanced criticality safety analysis with KENO-VI", Oak Ridge National Laboratory, January 2009.

[11] D. F. Hollenbach, J. A. Bucholz. "Theoretical background for calculational methods in SCALE", Oak Ridge National Laboratory, ORNL/TM-2005/39, January 2009.

[12] The RELAP5-3D Code Development Team. "RELAP5-3D© Code manual volume I: code structure, system models, and solution methods", Idaho National Laboratory, INEEL-EXT-98-00834, June 2005.

[13] RSICC. “SCALE code package”, http://www-rsicc.ornl.gov/codes/ccc/ccc7/ccc-750.html.

[14] D. F. Hollenbach, L. M. Petrie, S. Goluoglu, N. F. Landers, M. E. Dunn. “KENO-VI: a general quadratic version of the KENO program”, Oak Ridge National Laboratory, ORNL/TM-2005/39, January 2009.

[15] C. B. Davis. “Implementation of Molten Salt Properties into RELAP5-3D/ATHENA”, Idaho National Laboratory, September 2005.

[16] The RELAP5-3D© Code Development Team. “RELAP5-3D© Code Manual Volume II: User’s Guide and Input Requirements / Appendix A RELAP5-3D© Input Data Requirements”, Idaho National Laboratory, INEEL-EXT-98-00834-V2, 2005.

[17] P. E. MacDonald. “NGNP Preliminary Point Design - Results of Initial Neutronics and Thermal-Hydraulic Assessment During FY-03”, Idaho National Engineering and Environmental Laboratory, INEEL/EXT-03-00870, 2003.

[18] Haynes International Inc. “HASTELLOY® N alloy”, 2002.

[19] J. J. Duderstadt, L. J. Hamilton. “Nuclear Reactor Analysis”, WILEY Interscience, 1976.

[20] D. E. Holcomb, D. Ilas, V. K. Varma, A. T. Cisneros, R. P. Kelly, J. C. Gehin. “Core and refueling design studies for the advanced high temperature reactor”, Oak Ridge National Laboratory, ORNL/TM-2011/365, September 2011.

Journal of Energy
VOLUME 62 Number 1–4 | 2013 Special Issue
journal homepage: http://journalofenergy.com/

On the Estimation and Reduction of the Frequency of the Loss of Offsite Power Event

Hrvoje Grganić
Nuclear Power Plant Krško
Vrbina 12, 8270 Krško, Slovenia
hrvoje.grganic@nek.si

Zdenko Šimić
Faculty of Electrical Engineering at University of Zagreb, Department of Energy and Power Systems
Unska 3, 10000 Zagreb, Croatia
zdenko.simic@fer.hr

ABSTRACT

Loss of offsite power (LOOP) contributes significantly to the estimated core damage frequency (CDF) for the majority of nuclear power plants (NPPs). Based on experience from some near-miss events around the world and especially in Japan from Fukushima Daiichi accident and several other NPPs it was proven the how important power supply is for nuclear safety. Therefore comprehensive description of the LOOP initiating event is given in this paper. Specific experience of the NPP Krško (NEK) related operation is also presented with comparison to the U.S. NPPs' approaches and experience. Statistical data are given to explain main characteristics (frequency and duration) of the LOOP event. Important historical trends are also identified.

LOOP event frequency is often calculated using generic data because of statistical data base. Thereat, many important factors that influence LOOP are neglected, such as the specific power network configuration, load profiles, climate conditions, and ageing of the equipment. Several different approaches that take these factors into consideration are therefore presented and discussed. Familiarity with the actual state of the NPP, power network and weather conditions helps in the proper planning process of the test and maintenance (T&M) activities and reducing of the risk. This is significant for better online risk estimate.

Due to the Fukushima accident, it is necessary to review the safety of the NPPs from new different angles. This paper also shortly reviews planned modifications in NEK that will increase the electric power supply availability (i.e., reduce LOOP event frequency. Other, worldwide solutions that can help to avoid or mitigate LOOP effects are briefly presented.

1 INTRODUCTION

Not very different from the other, nuclear industry strives to minimize the probability of the accidents, and to limit the consequences if they happen. In the other words, the goal is to increase safety, i.e. to reduce the risk:

$$risk = probability \times consequence \tag{1}$$

NPPs are generating electricity most of the time. When not, NPPs need electricity from the grid for different reasons, such as operation of various equipment, maintenance work and most importantly, to power safety systems. Once the chain reaction in the reactor is stopped, decay heat is still generated. Hence, the reactor cooling has to be provided to avoid the meltdown. That cannot be achieved without the electricity provided to the reactor cooling system and the heat sink.

H. Grganić, Z. Šimić, On the Estimation and Reduction of the Frequency of the Loss of Offsite Power Event, Journal of Energy, vol. 62 Number 1–4 (2013) Special Issue, p. 131–141

It is important for all NPPs to have permanent and reliable electrical power sources. That raises the level of safety in the power plant during different modes of operation. Electrical power systems can be either offsite or onsite. Offsite power sources are used if available. If not, onsite power sources are used instead. It is necessary to consider the possibility that offsite power sources can be lost. That event is well known in literature as the Loss of offsite power.

LOOP as the initiating event contributes significantly to core damage frequency (CDF). This is shown in figure below [1].

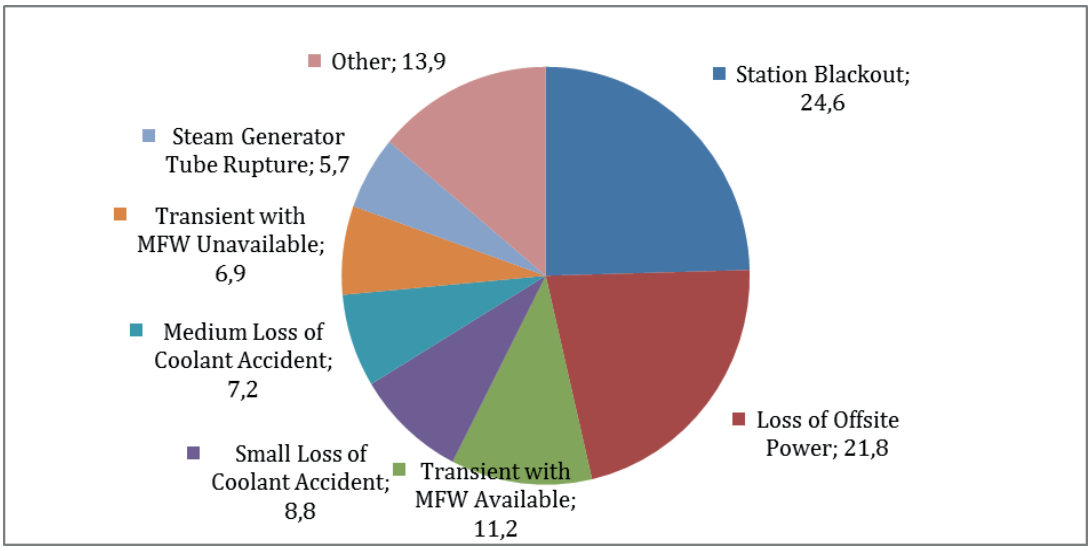

Figure 1: The main contributors to CDF

Hence, it is important to understand the LOOP event, its causes, possible consequences and methods to reduce the risk.

2 NEK ELECTRICAL SYSTEM

2.1 Design basis

It is important already in the design phase to choose appropriate location for the NPP. That means, among the other things, to consider the electric grid to which the NPP will connect. Some of the key parameters are [2]:

- Off-peak electricity has to be high enough so that NPP can work in the baseload mode. That can be assured by locating the NPP near the centers of the electricity demand,
- reserve generating capacity has to be large enough to ensure grid stability during the planned outages, and
- sudden disconnect of the NPP should not cause the instability of the power network. The larger the power network, the more stable it is. The UCTE is an example of such a network.

Nuclear site which is in the accordance with those three requests reduces the LOOP risk.

2.2 NEK electrical system description

The main generator is connected to the 400 kV bus via generator load breaker (BBC), two main step-up transformers GT1 and GT2 and substation breaker. NEK is connected to the offsite power sources via:

- Double 400 kV transmission line towards Zagreb
- Single 400 kV transmission line towards Maribor
- Single 110 kV transmission line towards Brestanica

H. Grganić, Z. Šimić, On the Estimation and Reduction of the Frequency of the Loss of Offsite Power Event, Journal of Energy, vol. 62 Number 1–4 (2013) Special Issue, p. 131–141

During the normal operation, main generator supplies electrical network over main transformers GT1 and GT2. It also supplies onsite power supply over unit the transformers T1 and T2 to two Class 1E (MD1 and MD2) 6,3 kV busses and two Non 1E (M1 and M2) 6,3 kV busses. Class 1E busses are also powered from their respective 3,5 MW diesel generators. The maximum operation duration of the DGs is 7 days.

Alternatively, if that power supply is not available, all four busses that provide onsite power supply can be energized from station auxiliary transformer T3, which is connected to the 110 kV RTP Krško (underground cable) and directly to combined gas-steam power plant Brestanica. Direct connection can be established over the Q92 switch which bypasses the 110 kV switchyard RTP Krško. Brestanica is equipped with three gas powered units of 23 MVA (23 MW) capable of the blackstart in the event of a breakdown of the 110 kV system and to provide electrical power to NEK station auxiliary transformer in 20 minutes. It is an obligation of the system operator to establish electrical power to NEK.

All self-supply safety systems are Class 1E. Safety systems are connected to the one of the following voltage levels:

- 6,3 kV AC, busses MD1 and MD2
- 400 V AC distribution system, 4 busses (LD11, LD12, LD21, LD22) and 17 Motor Control Centers (MCCD) connected to them
- 125 and 220 V DC distribution systems
- 118 V AC distribution system

NEK simplified electrical network scheme is shown on the Figure 2. Newly added diesel generator DG3 enhances Krško Emergency Power Supply. It can be used as an alternate AC source and as the source to MD1 and MD2, i.e. as the replacement for DG1 and DG2.

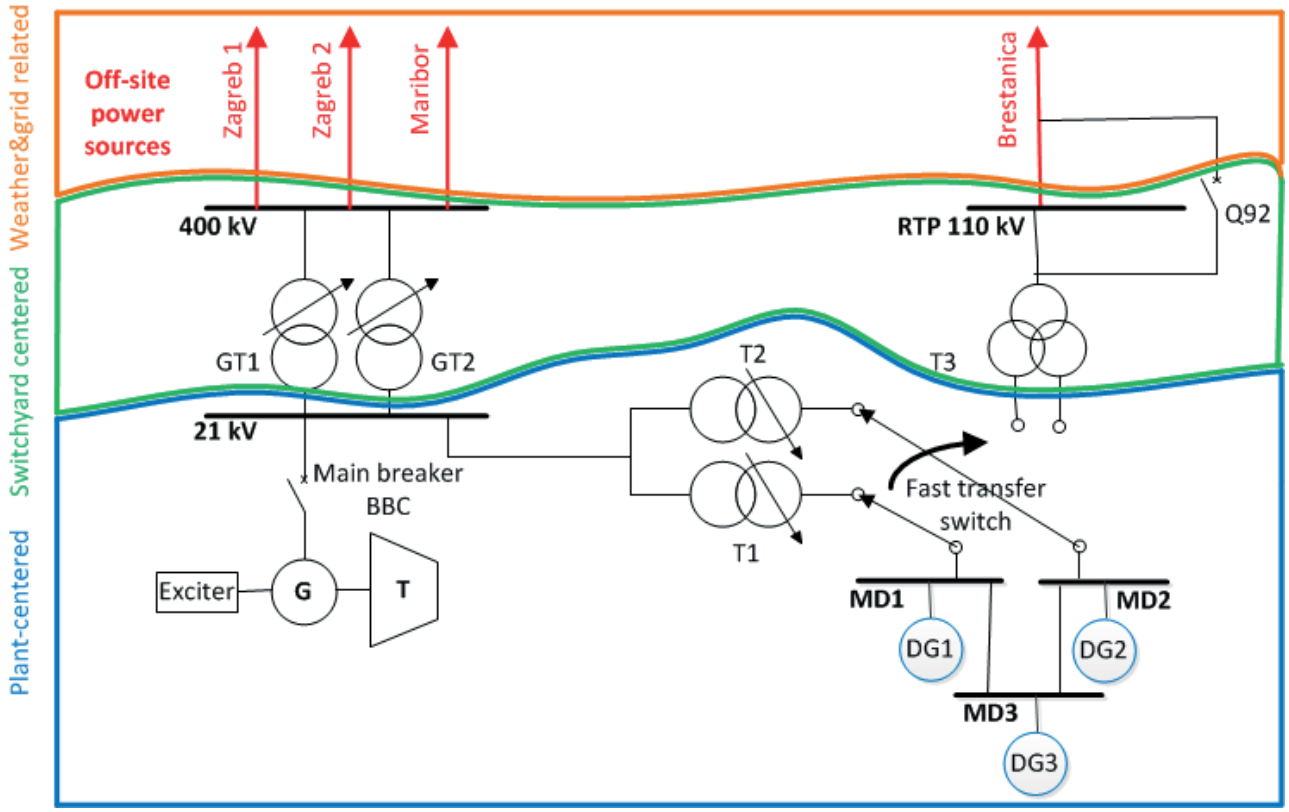

Figure 2 NEK simplified electrical power scheme

Loss of AC power includes loss of both offsite and onsite AC power. Offsite power can be lost because of the failure of either connection to the grid or grid itself [3]. The first possibility refers to the switchyard related events, as comprehensively studied in the next chapter. Onsite AC power, i.e. DGs can be lost either due to T&M activities or their fail.

H. Grganić, Z. Šimić, On the Estimation and Reduction of the Frequency of the Loss of Offsite Power Event, Journal of Energy, vol. 62 Number 1–4 (2013) Special Issue, p. 131–141

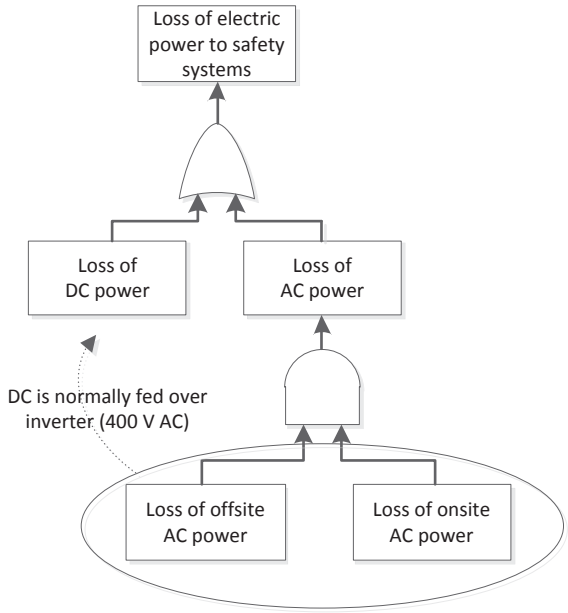

Figure 3 Simplified fault tree on electric power

3 LOOP ANALYSIS

LOOP events can be caused by different events. It is easier to understood and analyze it if those events are grouped in categories.

LOOP causes are commonly divided into four categories [4]:

- Plant centered
- Switchyard centered
- Grid related
- Weather related

Classification of the LOOP causes is not unique. Depending on the NPP characteristics, different classification can be made.

Before the deeper analysis, it is necessary to describe all four categories [4]. Plant centered events are typically caused by human errors, hardware failures, design deficiencies and localized weather-induced faults. They occur inside the power plant, up to main and station power transformer high voltage terminals (GT1&2 and T3 for NEK). From that point, up to the output bus bar in the switchyard is the zone where switchyard centered events occur. The most common causes are failures in the equipment, possibly human induced. These two types of LOOP are under the NPP personnel control. Grid related LOOP events are those whose initial failure occurs outside the power plant, in the transmission power grid. They are mainly the responsibility of the transmission grid personnel. Weather related events are caused by severe weather, in which the weather was widespread. That condition excludes the lightning strikes from this category. A separate category of the extreme weather can be also found in some literature. In this paper both severe and extreme weather are merged to one category.

The latest available study, NUREG/CR-6890 [4], that covers time period 1986 - 2004 and 103 NPP across the USA has distinguished two characteristic LOOP parameters:

- LOOP frequency
- LOOP duration

The CDF risk is larger for the larger values of the LOOP frequency. Longer LOOP duration also increases the CDF risk. In the example of NEK, if one offsite power source is unavailable, it has to be restored within 72 hours. Otherwise, power plant has to be taken to Hot stand-by and afterwards to Cold shutdown mode.

The NUREG/CR-6890 study results are presented below. Plant centered causes are analyzed together with the switchyard centered.

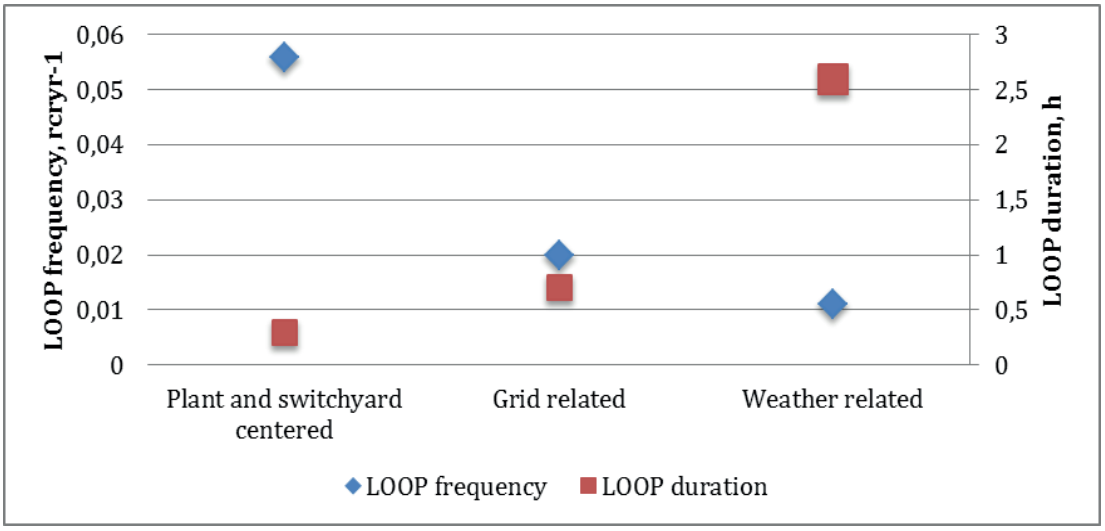

Figure 4: LOOP frequency and duration according to NUREG/CR-6890 [4]

It can be seen that plant centered causes are the most common, but with the shortest duration. Vice versa, weather related causes are the most infrequent, but with the longest duration. Due to severe weather, the power network can be seriously damaged, and hence the long time for its restoration is needed. This result does not reveal another important difference. Basically, LOOP can happen in two different NPP states:

- LOOP during the operation (reactor is critical)
- LOOP during the shutdown

More likely event is LOOP during shutdown, with mean frequency $1{,}96 \times 10^{-1}$, i.e. once per 5 years, compared to mean frequency during critical operation of $3{,}59 \times 10^{-2}$, i.e. once per 28 years. That result is not surprising. During the shutdown, typically outage, numerous maintenance work takes place, and not all of the equipment is operable. Below shown results point out that grid related LOOP events dominate during the critical operation, and switchyard related events dominate during the shutdown. This difference between the critical operation and the shutdown state roughly indicates main risks to which attention should be paid.

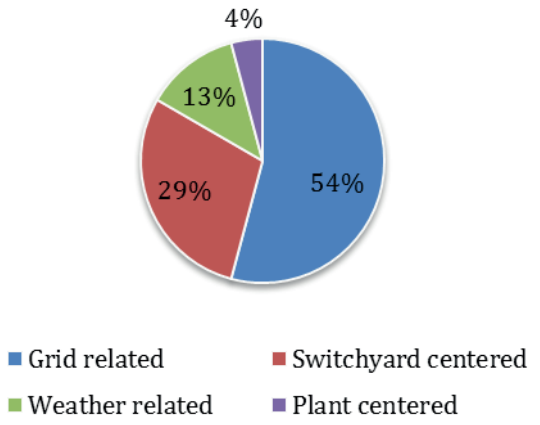

Figure 5: LOOP causes according to NUREG/CR-6890 during critical operation

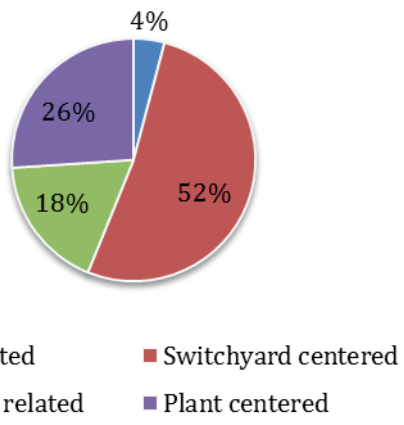

Figure 6: LOOP causes according to NUREG/CR-6890 during shutdown

The most common duration of the offsite power sources unavailability, either 110 or 400 kV, was less than 1 hour. The complete data is shown on the histogram below.

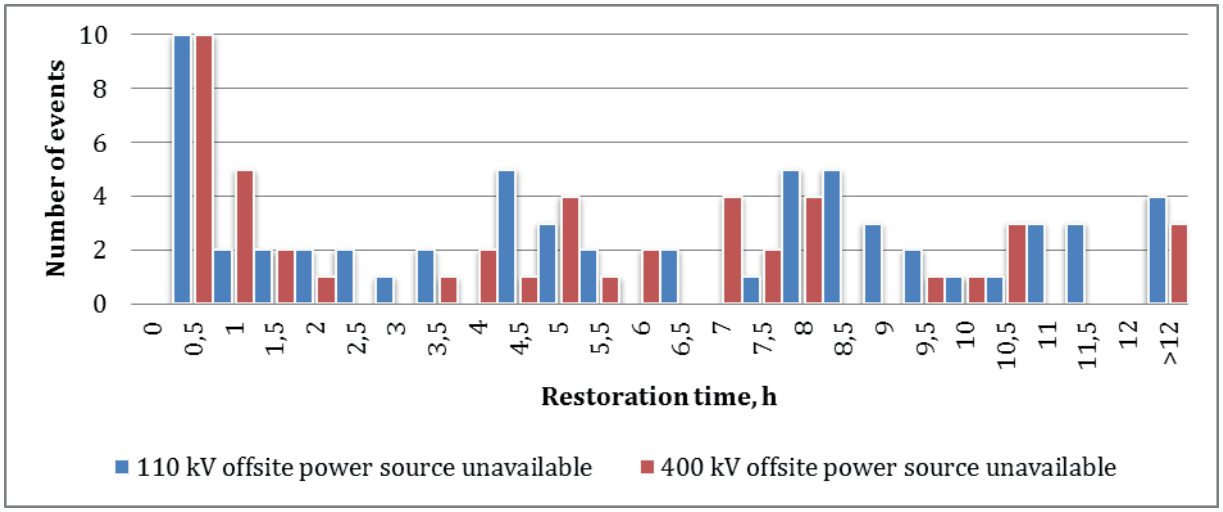

Figure 7: Duration of loss of one offsite power source events histogram for NEK

3.1 Mathematical background

In order to calculate the LOOP frequency, it is necessary to know the distribution of the events. All four types of LOOP events have Poisson distribution. But, it is not needed to know frequency for every of the four types of LOOP events to calculate the overall frequency, because the sum of the Poisson independent variables is again a Poisson variable. It is enough to know the overall frequency. Proof is given in [5]. Hence, the only needed information is frequency of all LOOP events, regardless their type. This simplifies the LOOP frequency analysis. Under stable conditions and given a failure rate λ, the number of LOOP incidents during a time period t, denoted by X, can be reasonably assumed to have a Poisson distribution:

$$P(x\_incidents\_in\_time\_t \mid given\_\lambda) = \frac{e^{-\lambda t}(\lambda t)^x}{x!} \quad (2)$$

H. Grganić, Z. Šimić, On the Estimation and Reduction of the Frequency of the Loss of Offsite Power Event, Journal of Energy, vol. 62 Number 1–4 (2013) Special Issue, p. 131–141

Assumption of a Poisson distribution is reasonable. That is confirmed in the NUREG/CR-6890 for the time period 1997 - 2004 [4]. Also, it predicted one LOOP for NEK in the 30 years with the highest probability of 0,328. The only LOOP event in NEK occured in 1986.

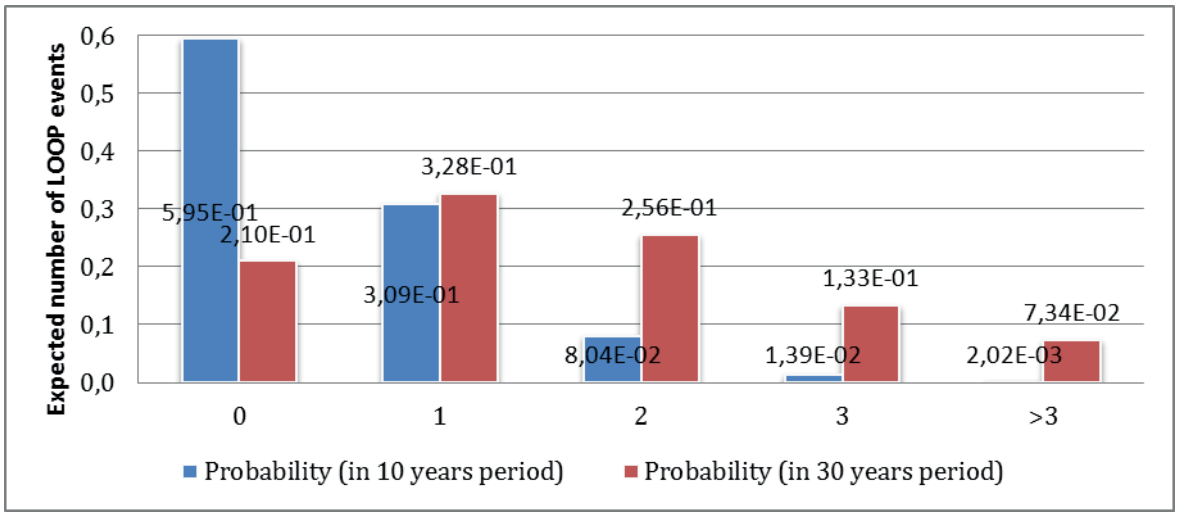

Figure 8: Probabilities of *N* LOOP events for NEK

4 NEK LOOP FREQUENCY CALCULATION

The last calculation of the LOOP frequency for NEK was made in year 2000, based on plant experience up to the end of 1999. The downside of this calculation is that NEK On-Line Maintenance (OLM) program was initiated at the end of the 1997. Hence, only a short period of time is observed. More accurate results are expected within the new Technical Report. The value of LOOP frequency is currently estimated as:

$$IEV - LSP = \frac{(T - T_{110kV})\lambda_{LSP} + T_{110kV}\lambda_{110kV}}{T} \quad (3)$$

T total number of plant operating hours

T_{110kV} total number of operating hours while 110 kV power source is unavailable

λ_{LSP} baseline LOOP frequency, i.e. when it is known that 110 kV power source is not unavailable due to OLM. This is the value, which was used as an estimator of "IEV-LSP" before the NEK OLM was introduced. Here presumed value is 0,05 $rcryr^{-1}$ [1].

λ_{110kV} estimation of conditional LOOP frequency while the 110 kV power source is unavailable due to preventive OLM. Presumed value is 0,25 $rcryr^{-1}$ [1].

This equation is a rough approximation. Baseline Loss of offsite frequency λ_{LSP} is taken from the NUREG-1784 [6]. In that report value of 0,05 LOOPs/rcryr is stated as the value that was valid before the deregulation (1985 – 1986). After the deregulation the LOOP frequency is estimated to be 0,014, i.e. much smaller.

One of the fundamental steps in carrying out a probabilistic analysis is choosing the failure rates of components. In principle, specific plant data should be used, that is obtained by the operating experience of the plant itself [7]. Whenever plant specific data are not available generic data from different generic databases are used.

The 110 kV unavailability represents unavailability of 110 kV power source, or unavailability of station auxiliary transformer T3.

Data about unavailability of the 110 kV power source be found in NEK OLM Risk Evaluation Weekly Reports, while OLM activities are performed at NEK on weekly base [8].

Table 1 Input data for IEV-LSP calculation

Year	NEK total operating time, h	NEK operating time (110 kV source unavailable), h
1998	7913	70,3
1999	7479	89,3
Total	15392	159,6

Taking into the account data from above, NEK LOOP frequency is IEV-LSP=0,052 rcryr^{-1}.

Comparison with the other known results is given below. If the results are expressed in the other way, for NEK it is expected to have one LOOP every 19 years, Surry NPP every 13 years, while NUREG results is one LOOP per approximate 28 years.

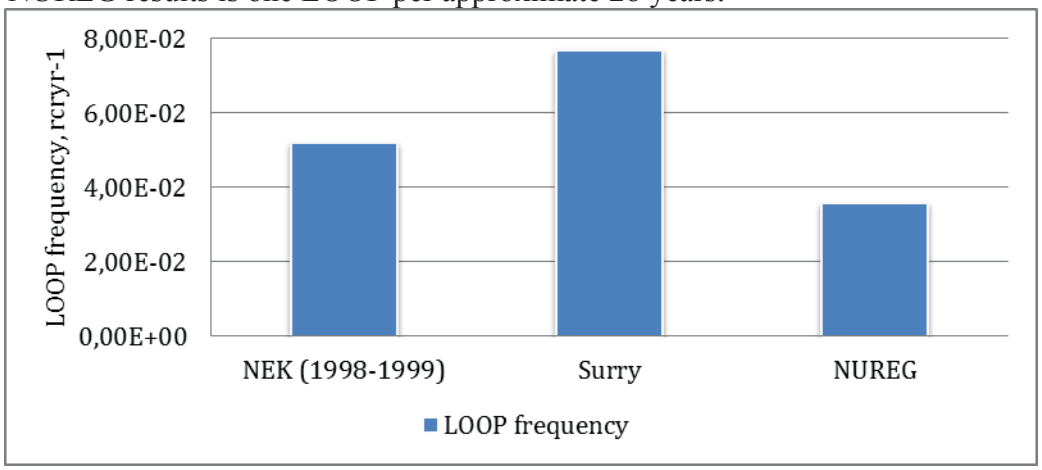

Figure 9: Comparison of LOOP frequencies

LOOP frequency calculation can be improved. Instead of using the generic data, it is recommended to find power plants with the similar offsite power configuration and to study their experience. Furthermore, known data for NEK should be used. Weather data for the Krško area is available and extensive. Also, grid reliability evaluations should be performed.

Some literature as NUMARC 87-00 [9] proposes empirical formulas for calculating LOOP frequencies. Mentioned source gives estimated LOOP frequency due to severe weather. The inputs for their equation are the annual expectations of snowfall, tornadoes above given severity, storms with the wind velocities between 75 and 124 mph, and storms with significant salt spray.

DGs in NEK are even more reliable than the offsite grid. The probability that one diesel generator will fail is 3,3%, and probability for the failure of both is 0,21%, compared to the LOOP frequency of 5,21%.

5 INFLUENCE OF THE POWER NETWORK ON LOOP FREQUENCY

As already mentioned in the Chapter 5, LOOP events can be plant centered, switchyard centered, grid related and weather related. This chapter provides a deeper analysis of the grid and weather related LOOP events.

Electric power grid reliability strongly influences the operation of a NPP, and vice versa. Typical grid problems that impact NPP are [10]:

- load rejection, loss of external load
- degraded voltage frequency
- NPP trip causing grid collapse and hence the LOOP to NPP
- LOOP due to external grid disturbance

Reliability of the power system includes its redundancy, diversity and lack of the choke points. Most of the disturbances are related to the environment, e.g. lightning, wind or birds. Other possible causes are the faults of the technical equipment, human errors and other, less important. The most common technical faults are related to overhead lines. Significantly less frequently are

faults of the transformers, breaker and disconnector faults, cable, protection, control equipment faults and other [11]. Power system component failures are affected by maintenance practice, design useful life and operation environment and conditions. The Croatian power system is already aged (220 and 400 kV network are approx. 50 and 35 years old, respectively). It is reasonable to assume that aging failures of the components will become a dominant factor of system unreliability [12].

Weather conditions affect both frequency and duration of the faults in the power network. Prediction of the duration helps in the planning of the recovery efforts. Paper [13] compares statistical methods for modeling power outage durations during hurricanes. It is interesting because it ranks influences of the different factors on the power restoration time.

Generally, in heavily loaded power networks happens more faults and they are less reliable. Important information is power flow through the particular power lines. The reinforcement of the existing grid would contribute to the decreased LOOP frequency. With a new 400 kV power line between Krško and Beričevo LOOP frequency is expected to be reduced for approximately 50%. Number of lines (single or double) does not change the result significantly. This transmission line is already under construction. It is expected to be finished in the late 2013.

Proper communication protocols between TSO and NPP operators keep NPP personnel better informed about the possible threats. Also, it gives them more time to react. This is especially desirable during times of high grid load and stress, which is usually easy to predict [14].

Calculation of the LOOP frequency for NEK assuming the different grid layouts is described in the paper [15].

6 FUKUSHIMA EVENT CONSEQUENCES AND LESSONS

A short overview of the Fukushima Daiichi event, mostly from the perspective of the Unit 1, and with the accent on electrical power supply is given below.

On March 11, 2011, three out of six units at the Fukushima Daiichi site automatically shut down due to the earthquake which caused LOOP. The cause of that LOOP was the damaged transformer station about 10 kilometers from the plant. Design basis acceleration in the horizontal direction, measured at the Fukushima Daiichi site, was exceeded. The probability for that was in the range 10^{-4} to 10^{-6} rcryr^{-1} [16]. The emergency DGs started as expected. Exceptionally, DG in Unit 4 was out of service due to maintenance.

The earthquake caused seven tsunamis, which have hit the site more than 24 hours after. Flooding of the electrical switchgear and some of the diesel rooms caused the Loss of all AC power for units 1 - 5. After that, portable electric generators have been delivered to the site, despite the problems with the transportation and installation. The explosion caused by the buildup of hydrogen damaged the mobile generator that had been installed to power the standby liquid control pumps. All DC power on Units 1 and 2 was lost. Although installed batteries have the capacity to power the system for 8 hours, they were flooded, and DC distribution system was damaged. Without the AC power and the ultimate heat sink, core cooling was not possible. Offsite power to the Units 1 and 2 was restored 9 days after the earthquake.

That scenario could have been avoided with simple measures. Here are mentioned those related to the electrical power supply. The first one is sufficiently high location of DG. That is a standard in neighboring countries as South Korea. Secondly, portable electric generators were not immediately available. Also, secure, and earthquake resistant cable that connects NPP with the offsite source would have to mitigate the consequences. That solution is applied on the similar NPP in Taiwan. Finally, at Fukushima Daini Nuclear Power Station, units 1 - 4 are connected by two 550kV transmission lines and two 66 kV transmission lines; in addition, power can be shared among units [17].

Due to the Fukushima accident, comprehensive review of the safety in NPPs is requested (so-called Stress tests). Slovenian Nuclear Safety Administration (SNSA) requested from NEK to

perform Special Safety Review, which is completely in line with the specifications of European Stress Tests. NEK has sent full scope Stress Test Final Report to SNSA in the December 2011 [18].

Several natural phenomena can cause LOOP. Earthquakes affect the ceramic insulators in the switchyard. Flooding can affect either the switchyard or the wider grid. Strong winds usually cause damage to the wider grid. Extremely low temperatures lead to the icing of the cables and thus to the grid failure. Some of these phenomena are not applicable to the NEK. Despite that, it is important to carry out a high quality and detailed PSA and to study the possible influence.

The CDF for events initiated by LOOP is reduced by installation of the third emergency DG. This modification is finished in 2012 outage. The third emergency DG is located in a separate building. It is connected to the separate safety bus (MD3) which can be connected to the one of the existing busses, either MD1 or MD2. Both DG and MD3 are seismic qualified. Also it is possible to connect smaller, mobile DG to the MD3. The similar safety measure can be found in the other countries' Stress test reports also. Besides the new diesel generator, other improvements in NEK are also proposed, such as already mentioned power line Krško - Beričevo.

7 CONCLUSION

The principle requirement for the NPP operation is ensuring safety.

It is important to understand the LOOP event, its causes, possible consequences and methods to reduce the risk, since it is one of the main contributors to the CDF. LOOP risk can be significantly decreased already during the site location selection.

Proper planning of the DG T&M contributes to the increased safety. Fine weather conditions decrease the LOOP frequency. It is desirable to postpone the T&M otherwise. Same as for weather, power grid also influences LOOP frequency. TSO's online monitoring and the proper communication between NPP and TSO have the potential to reduce the LOOP risk. The latest grid state and weather data are prerequisite needed to prevent LOOP events.

Fukushima event already caused instantaneous improvements in the safety of the NPPs. Stress tests identify the possible weak points by observing the plant response in the extreme situations.

Comprehensive operational experience of the U.S. NPPs and well documented event history are applicable to NEK. It is useful to compare NEK to similar U.S. NPPs as the starting point in the LOOP analysis.

Sensitivity studies indicated that emergency diesel reliability strongly reduces Station Blackout CDF [4]. The risk for NEK is significantly reduced by the installation of the third DG which is installed in the outage '12 and new power line that will connect Krško and Beričevo.

REFERENCES

[1] M. Kaštelan, I. Vrbanić, I. Košutić, “Post-modernization NEK PSA Baseline Model Update and IAEA IPSART Mission Comments Implementation”, NEK ESD-TR-20/00, 2000

[2] International Atomic Energy Agency, “Interfacing Nuclear Power Plants with the Electric Grid: the Need for Reliability and Complexity”, 2009

[3] Z. Šimić, V. Mikuličić, I. Vuković, “Use of Probabilistic Safety Assessment for Infrastructure Risk Modeling”, 2007

[4] Nuclear Regulatory Commission, “Reevaluation of Station Blackout Risk at NPPs, Analysis of LOOP Events: 1986-2004”, NUREG/CR-6890, 2005

[5] R. Johnson, “Probability and Statistics for Engineers, Sums of Independent Random Variables”, 2007

[6] Nuclear Regulatory Commission, “Operating Experience Assessment - Effects of Grid Events on Nuclear Power Plant Performance”, NUREG/CR-1784, 2003

[7] G. Petrangeli, “Nuclear Safety”, Elsevier, 2006

[8] I. Vrbanić, I. Košutić, “NEK PSA Parameters Update”, NEK ESD-TR-20/99, 1999

[9] Nuclear Management and Resources Council, Inc, “Guidelines and Technical Bases for NUMARC Initiatives Addressing Station Blackout at Light Water Reactors”, NUMARC 87-00, 2001

[10] J. H. Bickel, “Grid Stability and Safety Issues Associated With Nuclear Power Plants”, 2001

[11] G. H. Kjølle, “What do fault statistics tell us regarding causes resulting in power outages”, 2011

[12] X. Kaigui, L. Wenyuan, “Analytical model for unavailability due to aging failures in power systems”, 2008

[13] R. Nateghi, S. D. Guikema, S. M. Quirking, “Comparison and Validation of Statistical Methods for Predicting Power Outage Durations in the Event of Hurricanes”, 2011

[14] Nuclear Regulatory Commission, “Operational Readiness Of Offsite Power And Impact On Plant Risk”, TI 2515/165, 2006

[15] A. Volkanovski, “Impact of offsite power system reliability on nuclear power plant safety”, 2008

[16] Institute of Nuclear Power Operations, “Special Report on the Nuclear Accident at the Fukushima Daiichi Nuclear Power Station”, INPO 11-005, 2011

[17] Tokyo Electric Power Company, “Security of offsite power supply of Fukushima Daini Nuclear Power Station”, 2011

[18] Slovenian Nuclear Safety Administration, “Slovenian National Report on Nuclear Stress Tests, Final Report”, 2011

Journal of Energy
VOLUME 62 Number 1–4 | 2013 Special Issue
journal homepage: http://journalofenergy.com/

Validation of EOPs/FRGs Procedures Using LOHS Scenario

Damir Konjarek, Josip Vuković, Tomislav Bajs
Enconet d.o.o.
Miramarska 20, 10000 Zagreb, Croatia
damir.konjarek@enconet.hr, josip.vukovic@enconet.hr, tomislav.bajs@enconet.hr

ABSTRACT

Validation of EOPs (Emergency Operating Procedures) and FRGs (Function Restoration Guidelines) can be achieved either through plant full scope simulator or on desk top exercises. The desk top exercise is conducted when for the given scenario plant full scope simulator is not suitable. In either verification cases predefined scenario should be evaluated and possible branching foreseen. The scenario presented is LOHS, with bleed and feed procedure initiated. Best estimate light water reactor transient analysis code RELAP5/mod3.3 was used in calculation. Standardized detailed plant model was used. Operator actions were modelled from beginning of the scenario to its termination.

1 INTRODUCTION

The Emergency Operating Procedures validation objective is to ensure that operators can manage emergency conditions using the EOPs. The methods of validation:

(a) The simulator method is a validation method by which control room operators perform control functions on simulator equipment according to a scenario and for an observer/reviewer.

(b) The table top validation is method by which personnel explain and/or discuss procedure action steps in response to a scenario and for an observer/reviewer.

The validation method that will provide the most meaningful and thorough scrutiny for the EOP set is the simulator method. However, the table top methods will have to be used when there is no simulator or if the simulator modelling is incapable of producing a situation that a specific procedure addresses. That alternate validation method must also be performed when actions occur outside the control room. Modelling limitations of the full scope simulator could typically be experienced in a complex thermalhydraulic accident. The EOP developers could validate the accidents that are not covered by the simulator models in table top validation. In all cases the validation should be carried out under conditions that, to the greatest extent possible, simulate conditions during an emergency and include workload and instrument response. Correct application of EOP validation will ensure that the EOPs are usable and correct. Usability encompasses two concepts, level of detail and ease of understanding. The level of detail must be sufficient but not excessive. There should be a balance between providing all possible information and the minimum information needed. The plant specific writer's guide should address the desired level of detail. During validation, the user and observer judge whether the level of detail is sufficient.

When developing validation scenarios the goal is to exercise as many procedures and transitions as possible. It is not expected that every conceivable scenario will be covered.

D. Konjarek, J. Vuković, T. Bajs, Validation of EOPs/FRGs Procedures Using LOHS Scenario, Journal of Energy, vol. 62 Number 1–4 (2013) Special Issue,
p. 142–158

2 EMERGENCY OPERATING PROCEDURE - CONCEPT [1], [2], [3]

The Emergency Operating Procedures (EOP) provide a network of predefined and prioritized symptom based response strategies that guide the operator in management of emergency transients. Event related recovery and function related restoration strategies are combined to guide diagnosis and plant recovery to the optimal end state while ensuring explicit diagnosis and restoration of the plant safety state independent of event sequence.

The approach to the development of the Emergency Operating Procedures (EOPs) depends on the plant design configuration from a standpoint of the plant response to emergency transients. For example, the maximum shutoff pressure of the safety injection system strongly influences plant response to the postulated accident conditions. Based on this fact, the plant can be considered as low pressure (LP) or high pressure (HP) type. The HP type approach is applicable to the plants that are designed with a safety injection system shutoff pressure greater than the reactor coolant system pressurizer power operated relief valve (PORV) pressure setpoint. High pressure plants utilize the charging pumps as safety injection pumps. The LP version is applicable to plants that are designed with a safety injection system shutoff pressure less than the reactor coolant system pressurizer power operated relief valve (PORV) pressure setpoint. Low pressure plants do not utilize the charging pumps as safety injection pumps. Transient presented in the paper will show response of HP plant.

In general, two types of EOPs are known: Optimal Recovery (Event Oriented) and Critical Safety Function Restoration Concept (Symptom Oriented).

The concept of Optimal Recovery is based on the premise that radiation release and equipment damage can both be minimized through associating the symptoms of an emergency transient with a predefined plant condition and implementing an associated predefined event related recovery strategy to achieve an optimal plant end state. Recovery implies changing the plant state to the optimal end state.

The concept of Critical Safety Function Restoration (symptom related recovery strategies) is based on the premise that radiation release to the environment can be minimized if the barriers to radiation release are protected. Restoration implies returning the plant state to a safe state in which the Critical Safety Functions are satisfied. Hence, a fundamental goal of nuclear safety is the prevention of uncontrolled releases of radioactive materials from nuclear power plants. In order to accomplish this goal the concept of "defence in depth" [4], which translates into providing multiple barriers to the release of the radioactive material, was adopted at the start of the commercial development of nuclear energy as a cornerstone of nuclear safety. As long as the fuel matrix/cladding, reactor coolant system pressure boundary and containment barriers are intact in a nuclear power plant, that plant poses no threat to the health and safety of the general public.

The whole EOPs should provide emergency response strategies that utilize both emergency operations concepts. The Optimal Recovery concept is utilized as the primary emergency operations concept. The associated symptom based recovery strategies are structured to implicitly maintain the Critical Safety Functions. In this way the event related recovery strategies provide guidance to obtain the optimal plant end state while maintaining the Critical Safety Functions.

3 LOSS OF HEAT SINK [5]

A loss of secondary heat sink can occur as a result of several different initiating events. Possibilities are a loss of main feedwater during power operation, a loss of offsite power, or any other scenario for which main feedwater is isolated or lost when the steam generators provide the main heat removal path. For these initiating transients a failure of the auxiliary feedwater (AFW) system to inject or a loss of AFW early in the cooldown, before RHR (Residual Heat Removal) System operation can be established, could lead to a loss of secondary heat sink.

A loss of all feedwater transient is characterized by a depletion of secondary inventory and eventual degradation of secondary heat transfer capability. As secondary heat transfer capability

D. Konjarek, J. Vuković, T. Bajs, Validation of EOPs/FRGs Procedures Using LOHS Scenario, Journal of Energy, vol. 62 Number 1–4 (2013) Special Issue,
p. 142–158

degrades, a loss of secondary heat sink results and core decay heat generation will increase RCS (Reactor Coolant System) temperature and pressure until the pressurizer PORVs or safety valves (SVs) open to relieve the increasing RCS pressure. At this point the opening and closing of the PORVs or safety valves will result in a loss of RCS inventory similar in nature to a Small Break Loss of Coolant Accident (SBLOCA). If operator action is not taken, the pressurizer PORVs or SVs will continue to cycle open and closed at the valve setpoint pressure removing RCS inventory and a limited amount of core decay heat until eventually enough inventory will be lost to result in core uncovery.

3.1 "Bleed and feed" vs. "feed and bleed" technique [6], [7]

Bleed and feed is the process of manually initiating high pressure safety injection and manually opening the pressurizer PORVs to depressurize the RCS to allow the injection of sufficient water which will provide decay heat removal and core cooling. Feed and bleed is the process of manually initiating HPSI (High Pressure Safety Injection - SI charging) and permitting the automatic cycling of the PORVs at their set pressure to vent RCS inventory and provide decay heat removal and core cooling. This process then takes place at RCS pressures at and above the PORV setpoint pressure. The Feed and bleed process is only possible in HP type plants.

Bleed and feed is established by first starting all HPSI and/or HHSI (High Head Safety Injection) pumps and verifying their delivery and, then, manually opening and holding open all PORVs. Feed and bleed is established by starting all HPSI. The injection from the HPSI pumps and the RCS heatup will force an intermittent release of RCS inventory by the pressurizer PORVs. Thus, during the feed and bleed process the pressurizer PORVs are forced to open (automatically) and close repeatedly, relieving excess RCS inventory as a result of HPSI and RCS heatup.

The recommended alternate heat removal method is bleed and feed. Adequate PORV reliability is required to be demonstrated to support the use of feed and bleed since the PORV will open and close continuously over a long period of time. If feed and bleed were initiated when the symptoms of loss of heat sink were observed, the option to later revert to bleed and feed would be lost, since in feed and bleed the SI flow rate is low enough such that the system would begin to boil after a short period of time. Once boiling began, depressurization of the RCS using PORVs without having core uncovery would be highly unlikely. Core uncovery would be necessary to reduce the steam generation rate to a rate that permitted RCS depressurization using pressurizer PORVs. Thus, the use of feed and bleed precludes the use of bleed and feed without core uncovery and possible core damage. Therefore, based on the above arguments, feed and bleed is not recommended to provide an alternative heat removal method during a loss of secondary heat sink condition.

4 DESCRIPTION OF MODEL [8]

Model has been developed to a high level of detail and includes detailed discretization of all important components of the plant primary and secondary side (Reactor Pressure Vessel – RPV and Stem Generators - SG) and the models of the Emergency Core Cooling System - ECCS, Main Feedwater - MFW and Auxiliary Feedwater - AFW and simplified model of charging and letdown system. The ECCS consist of HPSI (High Pressure Safety Injection - SI charging), HHSI (High Head Safety Injection), ACC (Accumulators) and LPSI (Low Pressure Safety Injection - RHR system). Protection and control system has been developed according to the plant available documentation. The model has been developed with necessary fidelity of geometrical and operating parameters. Verified and recommended RELAP5 modelling techniques are used in preparation of RELAP5 input deck.[9] Steady state calculation was verified against real plant data and was found satisfactory. [8] Nodalization has been qualified on steady state and transient level. [10], [11] The overview of SI system is presented in Table 1.

Table 1 Overview of the Plant SI injection system

System	Shut off Pressure [MPa]	Maximum Delivery Capacity Pressure [MPa]
HPSI	20.00	8.24
HHSI	10.50	5.00
ACC	5.00	-
LPSI	1.39	1.05

5 TRANSIENT DESCRIPTION

The plant presented is high pressure (employees charging pumps as safety injection pumps), two loop PWR. Power to primary volume ratio is approximately two times smaller than what is usual. This results in smaller amount decay heat needed to be transferred to SGs, and longer time for SGs to lose their function as a heat sink. Because of that the operator have longer available time before initiating bleed and feed process.

5.1 Main Transient Conditions

From the beginning of transient there is following equipment status:

- MFW (Main Feed Water) and AFW (Auxiliary Feed Water)
- Steam Dump is not Available
- SGs' PORVs and SVs are available
- MSL (Main Steam Line) isolation occurs on the start of transient
- 1/2 ECCS operational - (one HPSI, two HHSI and one LPSI pump)

5.2 Results

Transient starts from full power operation (1000 MWt) and loss of MFW. At the same time both steam lines (SL) are isolated on spurious signal. Overview of sequence of events is given in Table 2.

Table 2 Time Sequence of Events

Event	Time
MFW isolation	0.05 s (on start of LOHS)
SL isolation	0.05 s (on start of LOHS)
Reactor trip (RX)	17.96s (lo-1 SG2 level (SG2 NR (Narrow Range) <setpoint) and steam/FW2 mismatch SG2 setpoint)
Turbine trip	18.46s (on RX trip)
Reactor Coolant Pump (RCP) trip	900s (manual operator trip at Step 4 of FR-H.1)
SI signal	3315.40s (manual - FR-H.1 procedure Caution 1 Step 3 SG2 WR (Wide Range) < setpoint)
Letdown isolated	3315.40s (automatic on SI actuation)
Containment isolation	3315.40s (automatic on SI actuation)
Pressurizer (PRZ) PORVs open	3700s (manual operator opening at Step 16 of FR-H.1)
AFW started	7300s (restoration - minimal to both SG)

Main events and operator actions are shown at Figure 1. The operators actions are based on parameters presented from Figure 2 to Figure 19. The containment response is not modelled. Until implementation of bleed and feed technique it is unlikely that there are conditions for adverse containment setpoints. Afterwards it is possible that the containment parameters will dictate change to adverse containment setpoints. This does not change the overall behaviour of the transient, only time window to achieve required setpoints. Because of that, through transient normal containment setpoints will be used.

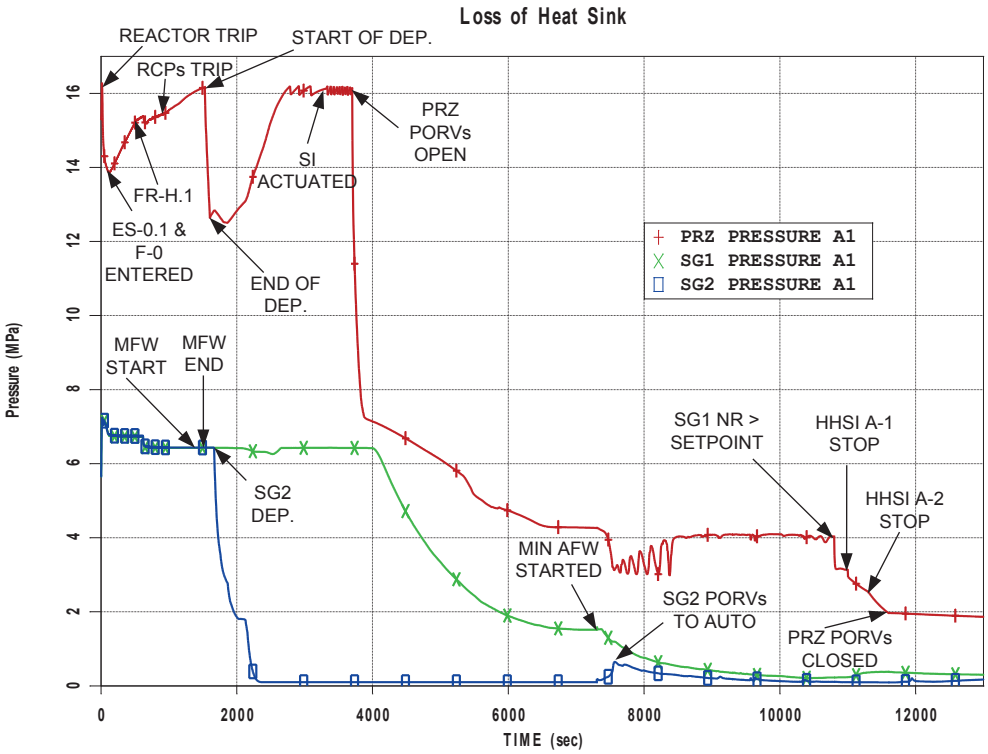

Figure 1: RCS and SGs Pressure

The transient progression is as follows. Procedure E-0 (Reactor Trip or Safety Injection) is entered as response to RX trip (Figure 2). The SGs' NR level is lost at t=80s (Figure 4), but operator missed it. Transition from E-0 to ES-0.1 is made as SI was not actuated and according to readings is not needed at t=100s (Figure 1 and Figure 3). According to rules of usage, F-0 procedure (Critical Safety Function Status Tree - CSFT) is implemented. From F-0 procedure normal containment setpoints are used. From Figure 6 to Figure 8 operator verifies steps at ES-0.1 and F-0 CSFT priorities. At t=500s RED path in F-0 on Heat Sink status tree is recognised (Figure 4 and Figure 9).

This tree represents the third highest priority Critical Safety Function, and as such, is always entered directly after the Subcriticality and Core Cooling tree. The most serious challenge to the Heat Sink Critical Safety Function is an indication of loss of secondary heat sink. A loss of secondary heat sink occurs if decay heat removal is needed through the SGs and all feed flow capability is lost. Feed flow must be re-established or an alternative heat removal mode (e.g., bleed and feed) must be established to prevent core uncovery and eventually an inadequate core cooling condition. Since this is an extreme challenge to the fuel clad/matrix barrier to radioactivity release, immediate operator action is required and a RED priority is warranted. The loss of secondary heat sink condition is the only RED priority included on Heat Sink status tree.

D. Konjarek, J. Vuković, T. Bajs, Validation of EOPs/FRGs Procedures Using LOHS Scenario, Journal of Energy, vol. 62 Number 1–4 (2013) Special Issue,
p. 142–158

Transfer from ES-0.1 to FR-H.1 Response to Loss of Secondary Heat Sink is made at t=500s (Figure 4 and Figure 9). The guideline FR-H.1 provides guidance to address an extreme challenge (i.e., RED priority) to the Heat Sink Critical Safety Function that results if total feed flow is below a minimum value and level is below the narrow range in all SGs at any time. An early indication that secondary heat transfer capability may be challenged is that AFW flow is not available to any steam generator. Following a RX trip and/or SI, main feedwater isolation is automatically initiated. In this transient MFW is not available and is the initiator of the transient. Auxiliary feedwater flow to the steam generators must be automatically or manually initiated in order to maintain adequate secondary inventory for decay heat removal. Consequently, a failure of the AFW system results in a challenge to the Heat Sink Critical Safety Function. The operator is directed to implement guideline FR-H.1. The objective is to maintain RCS heat removal capability by establishing feed flow to an SG or through establishing RCS bleed and feed heat removal. It is entered at the first indication that secondary heat removal capability may be challenged. This permits maximum time for operator action to restore feedwater flow to at least one steam generator before secondary inventory is depleted and secondary heat removal capability is lost. Once secondary heat removal capability is lost, RCS bleed and feed must be established to minimize core uncovery and prevent an inadequate core cooling condition.

After failure to establish AFW flow to SGs from control room, local operator is dispatched to restore it. The operator then manually trips RCPs (t=900s, Figure 6). Operation of reactor coolant pumps will affect the dryout time of the steam generators due to RCPs heat addition and, therefore, will affect the time at which operator action to initiate bleed and feed must occur. By tripping the RCPs, the effectiveness of the remaining water inventory in the SGs is extended, which extends the time at which the operator action to initiate bleed and feed must occur. This extension of time is additional time for the operator to restore feedwater flow to the SGs.

The next step is for operator to try to start MFW pumps. The MFW is the next source of high pressure water readily available to the operator to re-establish the secondary heat sink. Prior to restoring MFW flow to the SGs, the operator verifies condensate system operation to ensure a source of water to the MFW pumps. Then the MFW isolation valve status is checked. If feedwater isolation has occurred, various actions may be required, depending upon the plant specific logic for FW isolation, to reset SI and FW isolation signals and reopen the FW isolation valves. If either the condensate system cannot be placed in service or no FW isolation valves can be opened, the operator is directed to check the status of the secondary heat sink. If the condensate system is operational and FW isolation valves are open, then MFW is established by the operator. If MFW cannot be established, the operator is directed to attempt to establish condensate flow. In transient reinitiation of MFW is partly successful as the MFW delivers some flow to SG1 for two minutes (from t=1380-1500s, Figure 9). This has no visible effect as seen on Figure 5.

As MFW injection was not successful operator is trying to establish feed flow from the condensate system. For injection from the condensate system to be successful it is required to depressurize SG (low pump head of system). This in turn requires primary depressurization (t=1530s using PRZ PORV) to less than P.06 (so that SI signal can be blocked at t=1660s, Figure 1 and Figure 10). This action is done because of SG depressurization which can lead to fast primary depressurization and automatic SI signal could be reached on either primary or secondary low pressure. In this way SI actuation is prevented and can not hamper or delay recovery. For secondary depressurization SG2 is chosen as some flow from MFW reached SG1. The SG2 is depressurized to below setpoint of condensate booster pump head pressure using SG2 PORV (t=1670-2200s, Figure 1, Figure 10 and Figure 14). Further SG2 depressurization is continued to achieve maximum condensate system flow (SG PORV is left in open position). Time of 15 minutes is left for operator to try to establish flow from the condensate system. The condensate flow was not established, and the operator checks for SGs NR level at t=3100s which is below range. Afterwards operator is checking SGs WR for setpoint which determines actuation of bleed and feed (Figure 5). At that time the setpoint is not reached in both SGs, and operator is instructed to go to first step of FR-H.1 (t=3160s).

At t=3315s setpoint for bleed and feed is reached (Figure 5), and transition to initiating step is made. This step initiates manual SI actuation (Figure 11 and Figure 12). After SI delivery verification of both PRZ PORVs opening is made at t=3700s (Figure 10 and Figure 13). Verification of bleed path is performed (Figure 11 and Figure 12). While proceeding with FR-H.1 the operator is instructed to perform steps in E-0. These steps are performed because it is possible to make a transition to FR-H.1 without having performed the verification of automatic SI actions in E-0. This step specifically instructs the operator to perform that verification. Performing steps in E-0 does not initiate any additional operator action in this transient except verifying plant status. Through bleed and feed implementation RWST level is monitored for need to switch to containment sump (Figure 18).

The operator reach step loop in FR-H.1 where he is trying to establish secondary heat sink and checking for SG WR indication. This loop is maintained, and at t=7300s the minimum AFW for heat removal becomes available (Figure 9). Five minutes after, SG2 PORV is closed (Figure 1, Figure 10 and Figure 14). The operator remains in the step loop monitoring secondary heat sink. The SG1 NR criteria for end of LOHS is reached at t=10 480s (Figure 4).

Following restoration of secondary heat sink in SG1 (later SG2), the operator is instructed to verify core cooling and reduce SI flow. After SI reduction (only HPSI remains - SI charging, Figure 15, Figure 16, Figure 17, Figure 1, Figure 11 and Figure 19) operator is instructed to close PRZ PORVs one by one and to place them in auto position (Figure 1 and Figure 10). During this process primary pressure is closely monitored as PRZ is water solid (Figure 13) and any sharp change in primary pressure could have devastating effects on RCS. In this transient it is assumed that PRZ PORVs will close even after long water discharge. If this would not be the case, the transient would propagate in SBLOCA. The verification of bleed and feed termination is done (Figure 12). Operator establishes normal letdown and charging (Figure 11). The charging and letdown flow is tuned to drain PRZ in normal operating range. The transient ends at t~12000s.

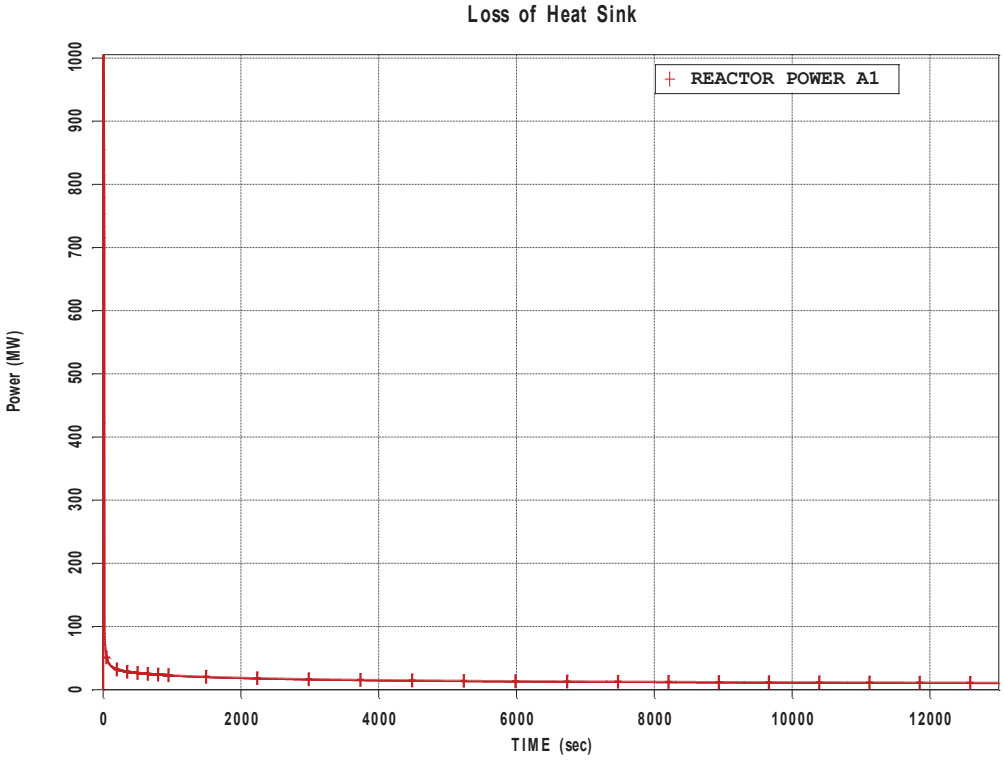

Figure 2: Reactor Power

D. Konjarek, J. Vuković, T. Bajs, Validation of EOPs/FRGs Procedures Using LOHS Scenario, Journal of Energy, vol. 62 Number 1–4 (2013) Special Issue,
p. 142–158

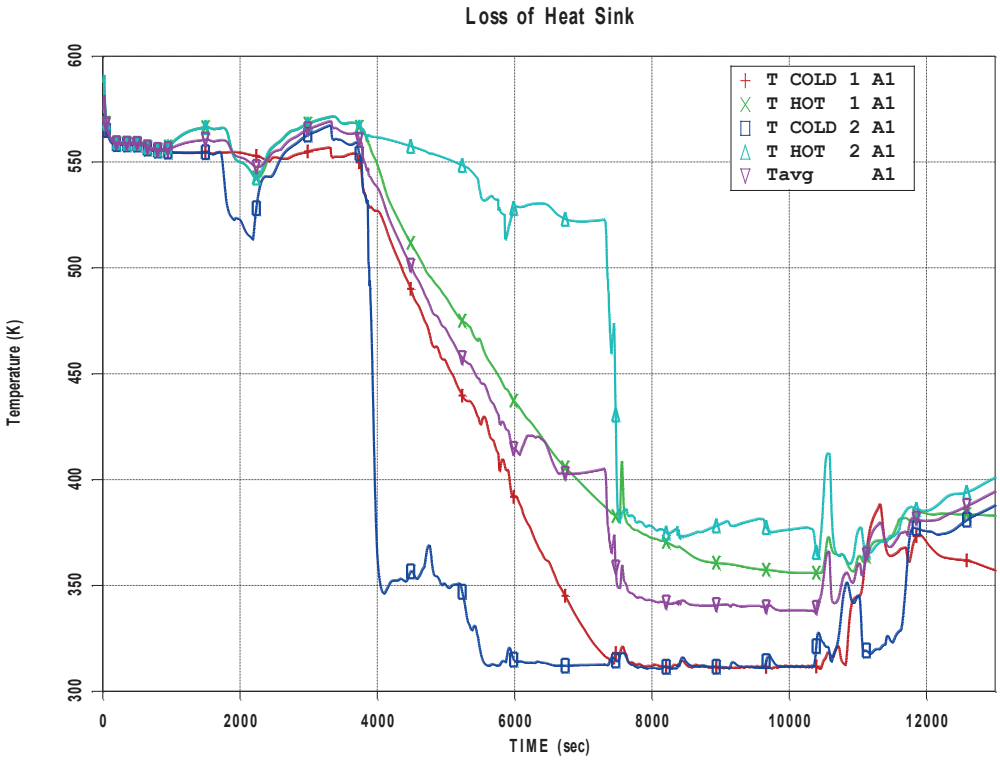

Figure 3: Temperatures Cold Leg, Hot Leg, Tavg

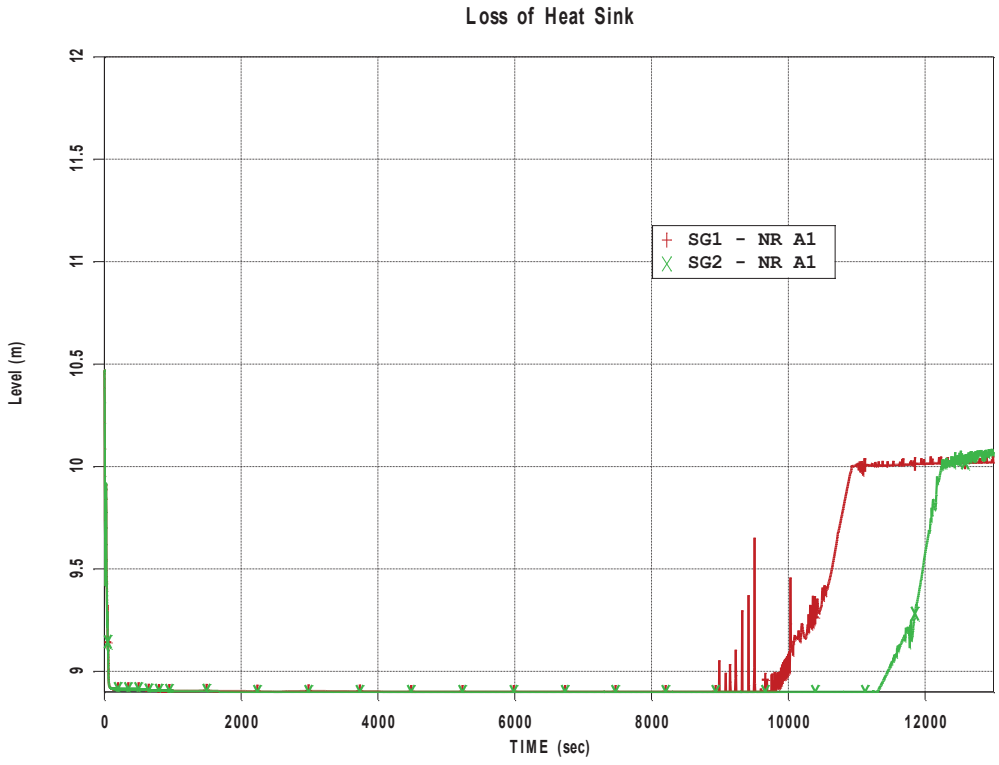

Figure 4: SGs Level - Narrow Range

D. Konjarek, J. Vuković, T. Bajs, Validation of EOPs/FRGs Procedures Using LOHS Scenario, Journal of Energy, vol. 62 Number 1–4 (2013) Special Issue,
p. 142–158

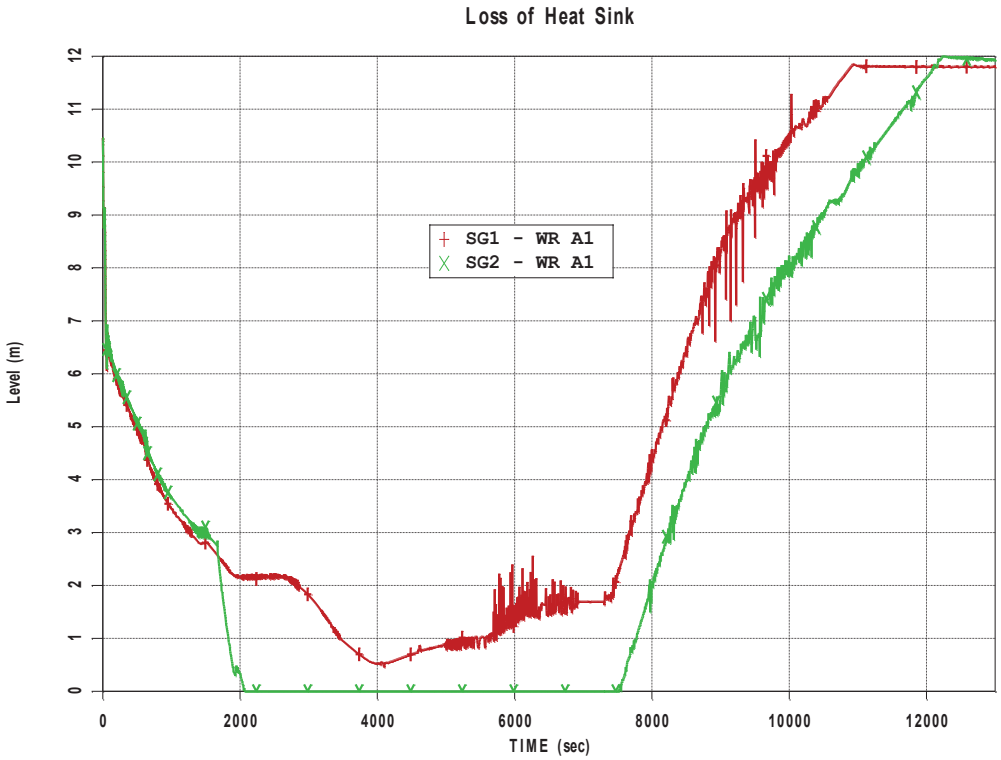

Figure 5: SGs Level - Wide Range

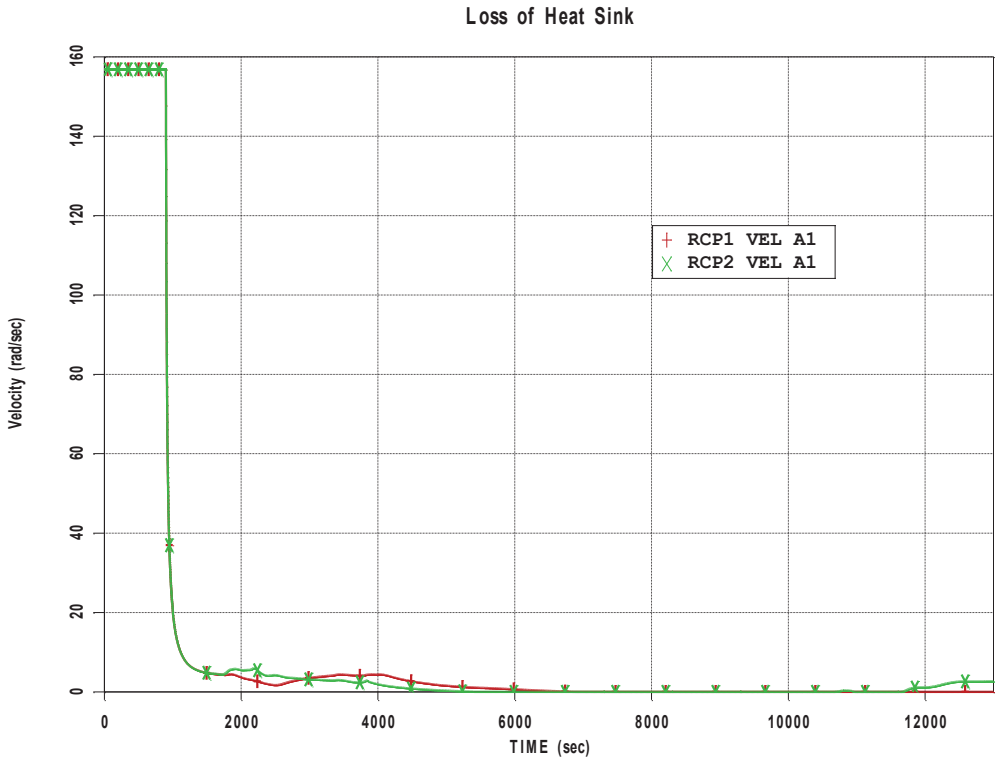

Figure 6: RCPs Velocity

D. Konjarek, J. Vuković, T. Bajs, Validation of EOPs/FRGs Procedures Using LOHS Scenario, Journal of Energy, vol. 62 Number 1–4 (2013) Special Issue,
p. 142–158

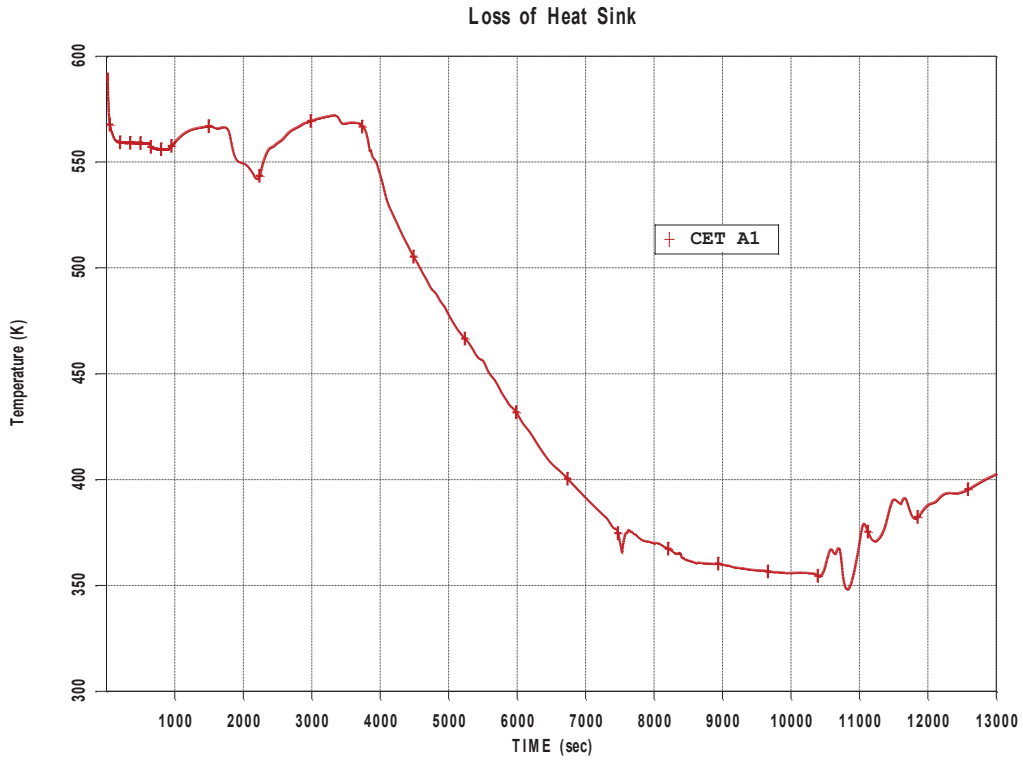

Figure 7: Core Exit Thermocouples (CET) Temperature

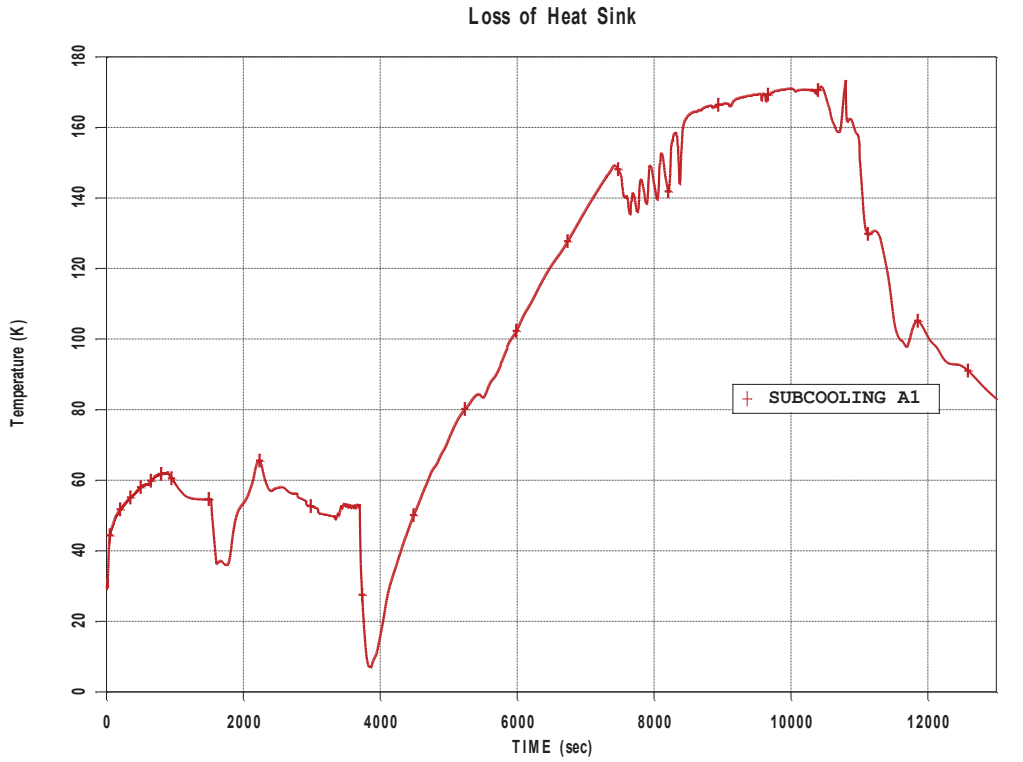

Figure 8: Subcooling

D. Konjarek, J. Vuković, T. Bajs, Validation of EOPs/FRGs Procedures Using LOHS Scenario, Journal of Energy, vol. 62 Number 1–4 (2013) Special Issue,
p. 142–158

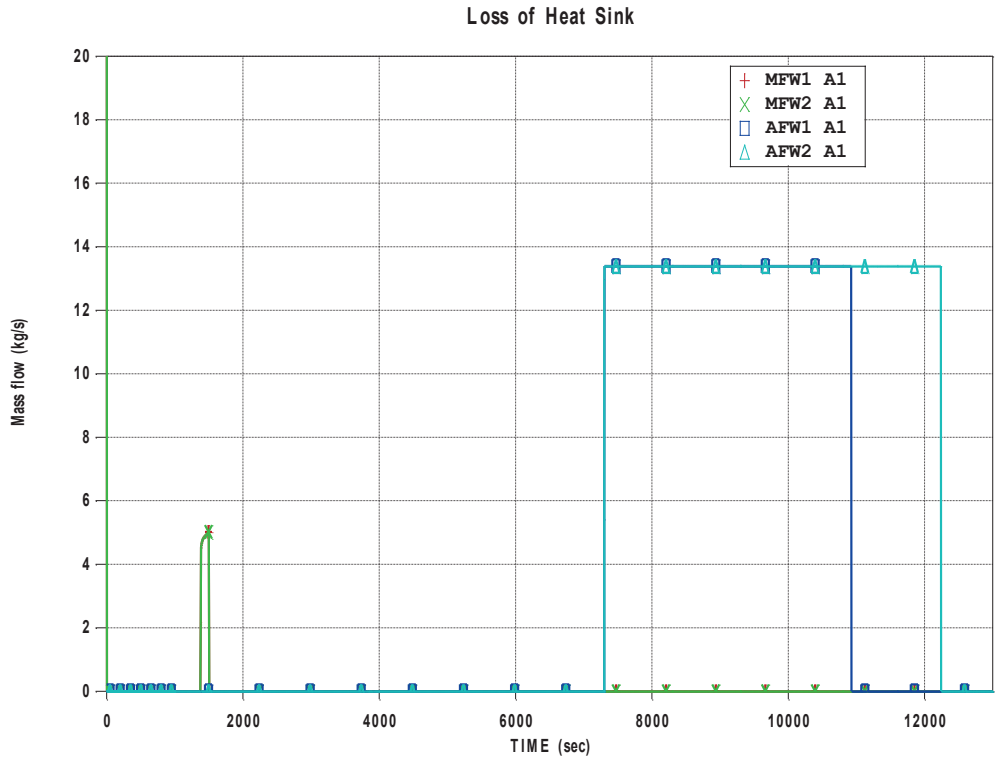

Figure 9: MFW and AFW Flow

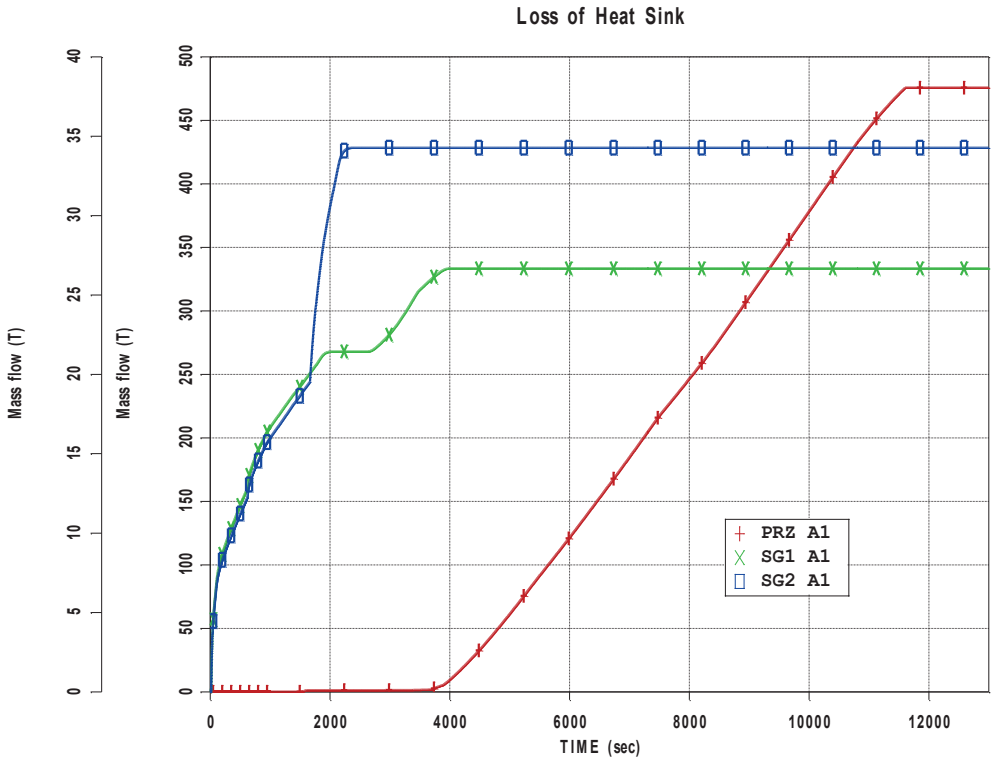

Figure 10: PRZ and SGs Valves Integral

D. Konjarek, J. Vuković, T. Bajs, Validation of EOPs/FRGs Procedures Using LOHS Scenario, Journal of Energy, vol. 62 Number 1–4 (2013) Special Issue,
p. 142–158

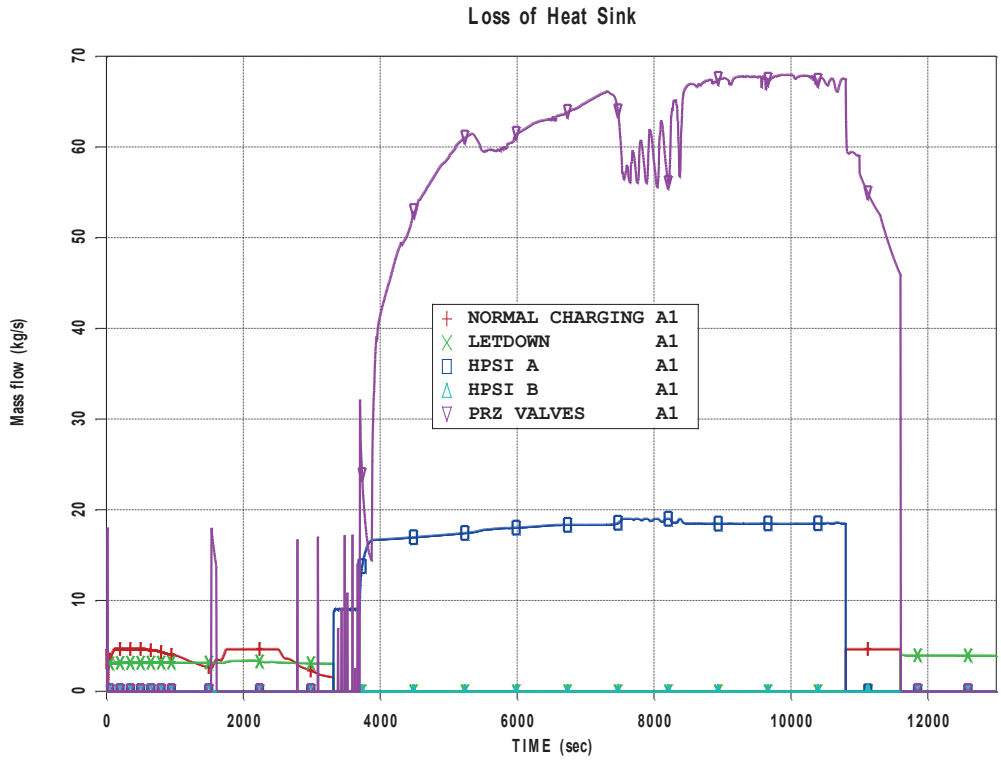

Figure 11: PRZ PORVs, Charging, Letdown and HPSI Mass Flow

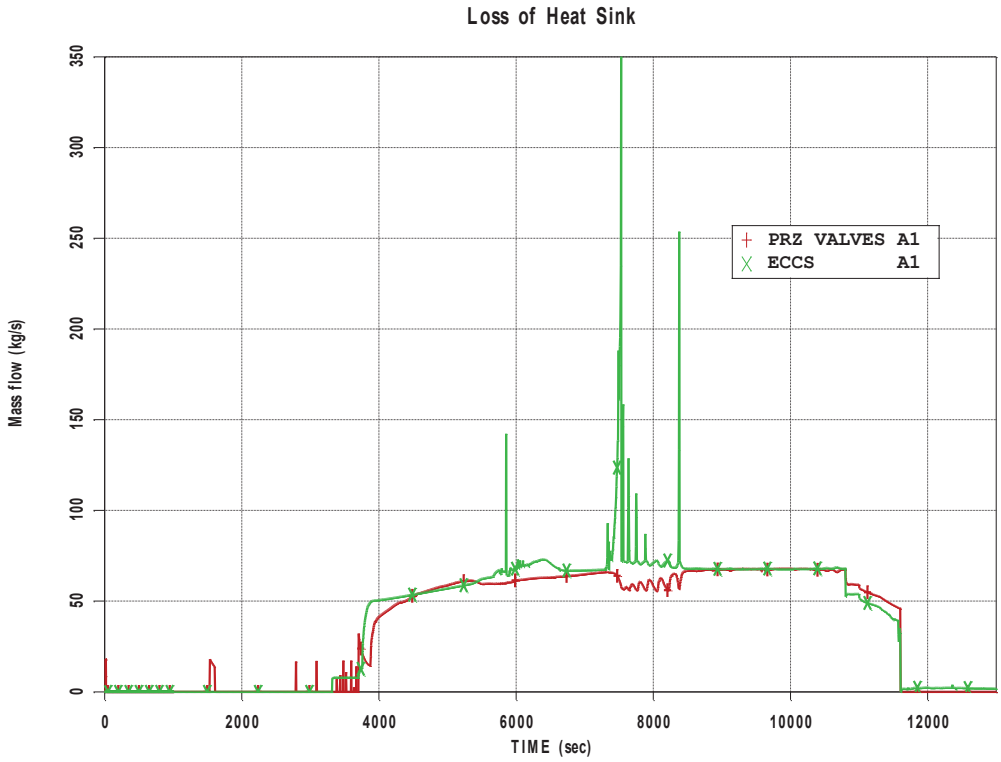

Figure 12: PRZ PORVs and ECCS Flow

D. Konjarek, J. Vuković, T. Bajs, Validation of EOPs/FRGs Procedures Using LOHS Scenario, Journal of Energy, vol. 62 Number 1–4 (2013) Special Issue,
p. 142–158

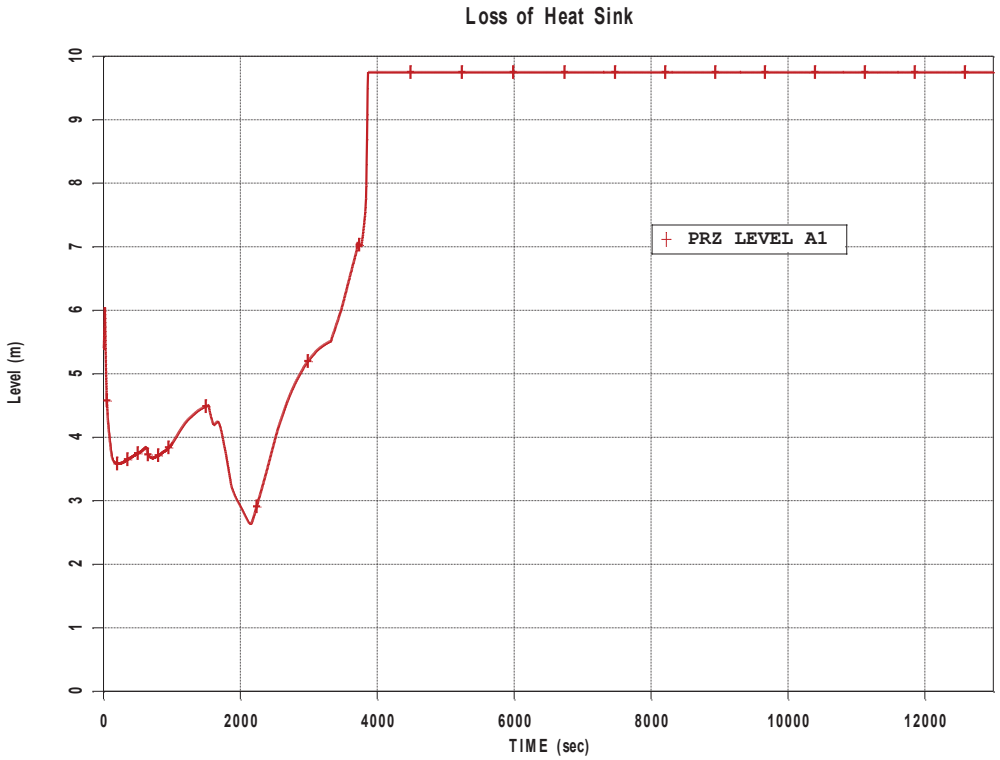

Figure 13: Pressurizer Level

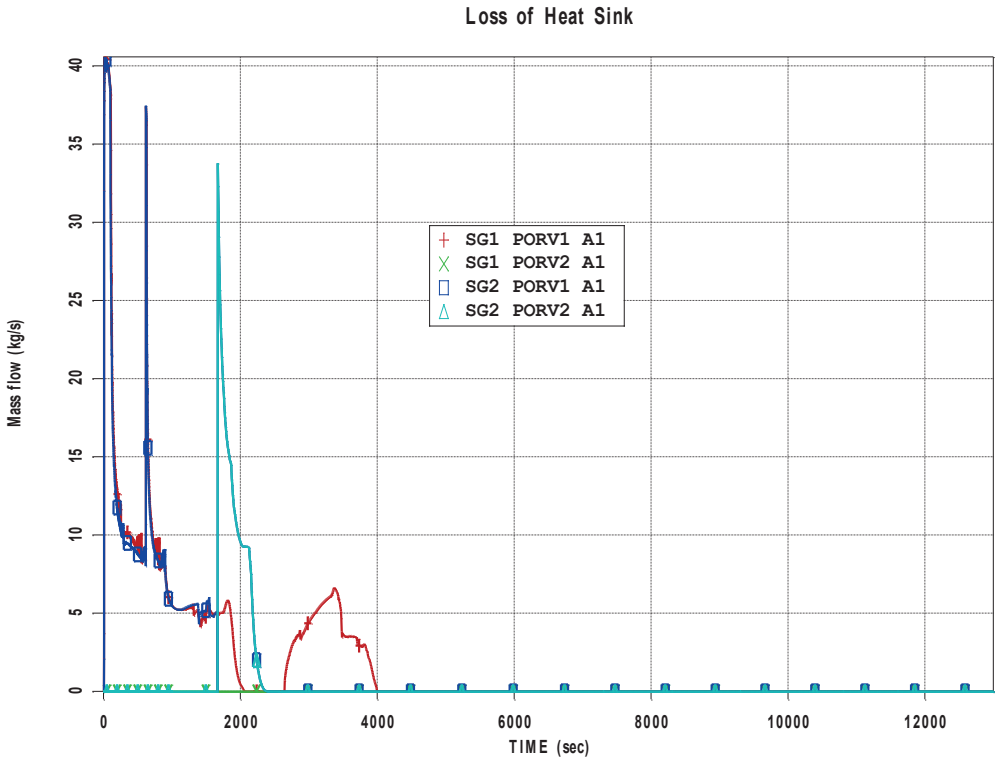

Figure 14: SGs PORVs Mass Flow

D. Konjarek, J. Vuković, T. Bajs, Validation of EOPs/FRGs Procedures Using LOHS Scenario, Journal of Energy, vol. 62 Number 1–4 (2013) Special Issue,
p. 142–158

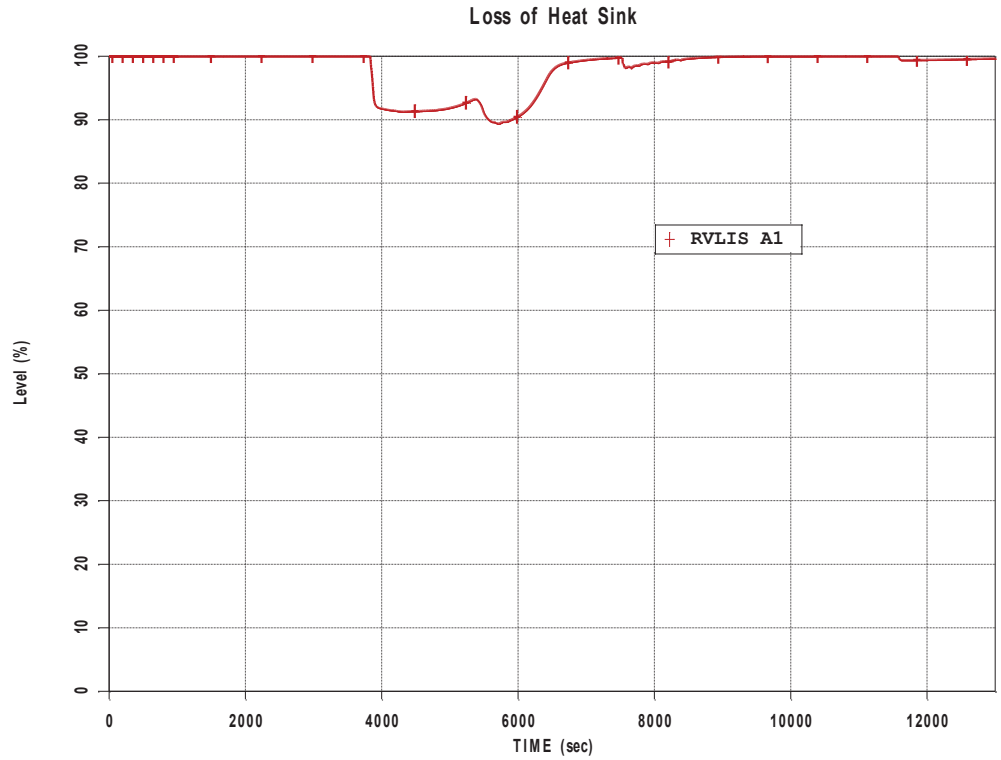

Figure 15: RVLIS Level

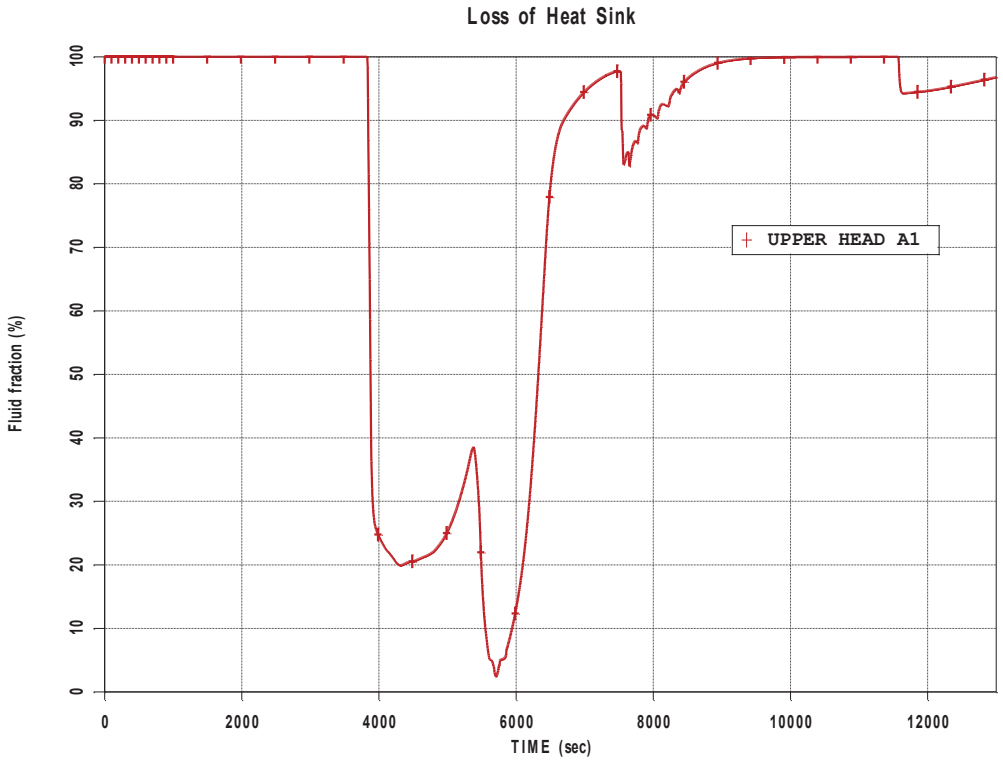

Figure 16: Upper Head Liquid Fraction

D. Konjarek, J. Vuković, T. Bajs, Validation of EOPs/FRGs Procedures Using LOHS Scenario, Journal of Energy, vol. 62 Number 1–4 (2013) Special Issue,
p. 142–158

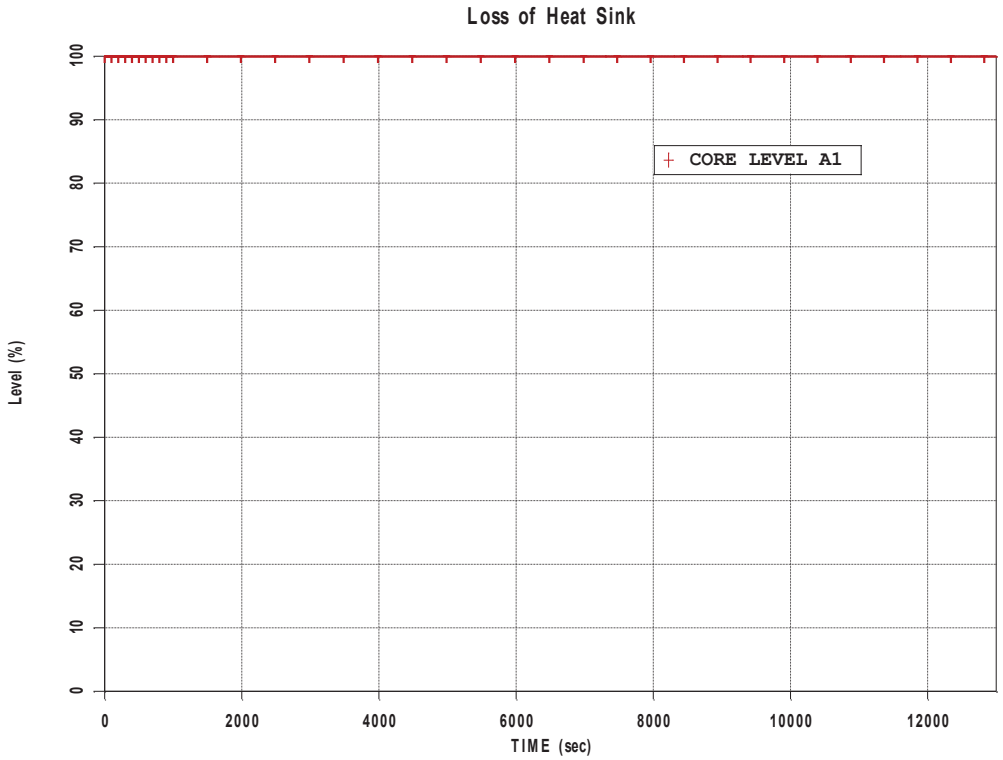

Figure 17: Core Level

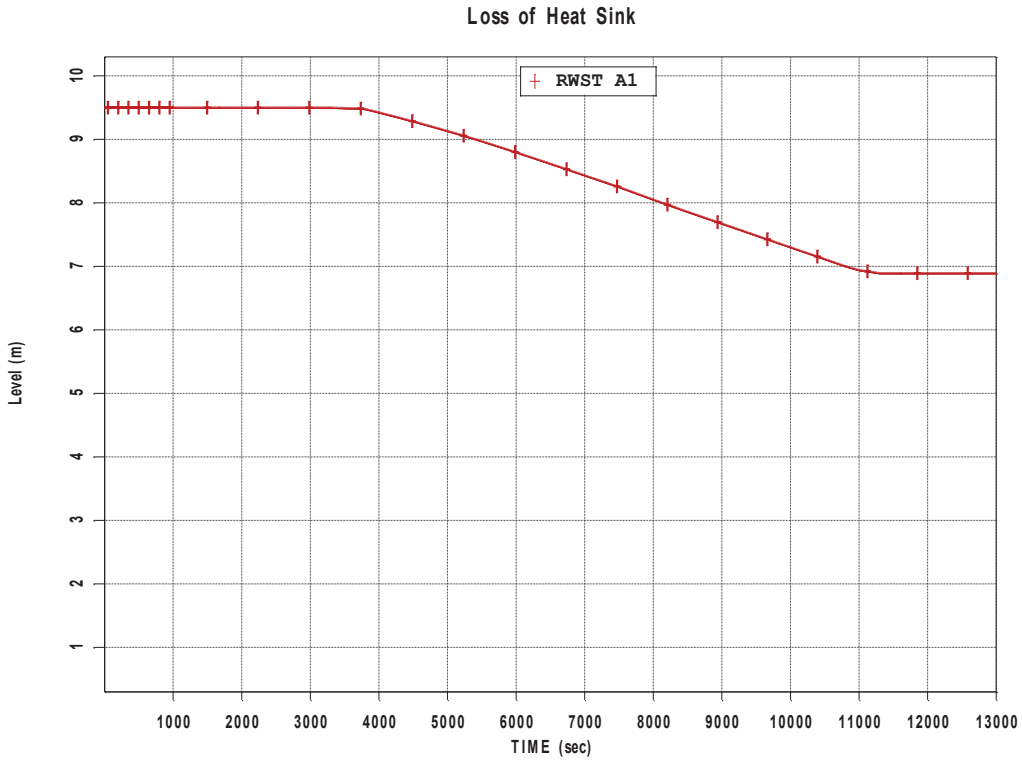

Figure 18: RWST Level

D. Konjarek, J. Vuković, T. Bajs, Validation of EOPs/FRGs Procedures Using LOHS Scenario, Journal of Energy, vol. 62 Number 1–4 (2013) Special Issue,
p. 142–158

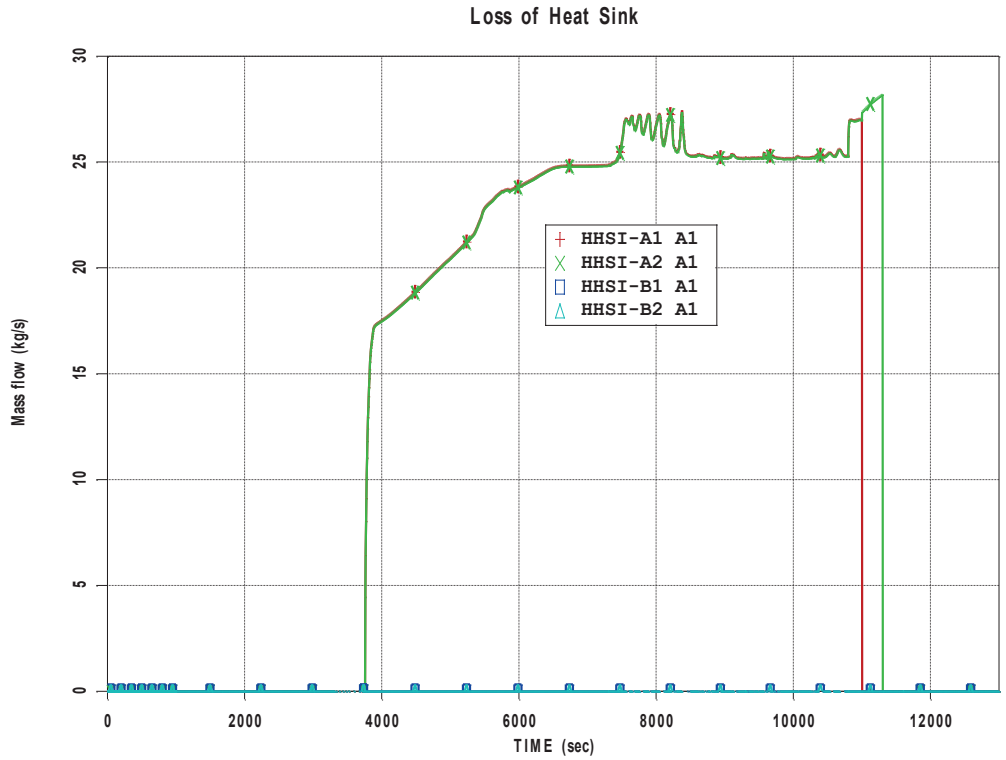

Figure 19: HHSI Pumps Mass Flow

6 CONCLUSION

The paper presents alternative possibility of EOPs and FRGs validation through desk top exercise. The desk top evaluation is conducted when plant full scope simulator is not suitable for given transient or does not have sufficient capabilities to realistically model plant response.

Validation scenario presented was LOHS, with bleed and feed technique initiated. Transient was computed using RELAP5 model which was suitable for the purpose. As presented, modelling of operator actions were done from the start of transient to its termination.

Procedures that were mostly covered are E-0, F-0 and FR-H.1, while ES-0.1 was just barely verified. While performing validation it cannot be expected to pass through every possible scenario and step of procedures. The aim is to focus on procedures intention, its background and the reasoning for operator actions as well as to cover as many steps as possible.

D. Konjarek, J. Vuković, T. Bajs, Validation of EOPs/FRGs Procedures Using LOHS Scenario, Journal of Energy, vol. 62 Number 1–4 (2013) Special Issue,
p. 142–158

REFERENCES

[1] International Atomic Energy Agency, “Development and Review of Plant Specific Emergency Operating Procedures”, IAEA-SAFETY REPORT SERIES-48, Vienna, 2006

[2] U.S. Nuclear Regulatory Commission, “Guidelines for the Preparation of Emergency Operating Procedures”, NUREG-0899, August 1982

[3] U.S. Nuclear Regulatory Commission, “Lessons Learned From the Special Inspection Program for Emergency Operating Procedures”, NUREG-1358, April 1989

[4] International Atomic Energy Agency, “Defence in Depth in Nuclear Safety”, IAEA-INSAG-10, Vienna, 1996

[5] N. S. DeMuth, D. Dobranich, and R. J. Henninger, “Loss-of-Feedwater Transients for the Zion-1 Pressurized Water Reactor”, Los Alamos National Laboratory report LA-9296-MS, NUREG/CR-2656, May 1982

[6] G.G. Loomis, J.M. Cozzuol, “Decay Heat Removal Using Feed-and-Bleed for U.S. Pressurized Water Reactors”, NUREG/CR-5072, EGG-2526, EG&G Idaho, Inc., Idaho Falls, ID, 1988

[7] D.J. Shimeck, et al., “Analysis of Primary Feed-and-Bleed Cooling in PWR Systems”, EGG-SEMI-6022, 1982

[8] T. Bajs, D. Konjarek, I. Iveković, “Application of the UMAE Methodology for the Uncertainty Evaluation in Support to the EOP Background Analysis”, ASME 2010 3rd Joint US-European Fluids Engineering Summer Meeting collocated with 8th International Conference on Nanochannels, Microchannels, and Minichannels (FEDSM2010), Montreal, Quebec, Canada, August 2010

[9] RELAP5/mod3.3 Code Manual Volume II: User's Guide and Input Requirements, NUREG/CR 5535/Rev 1-Vol II, ISL, Inc., Rockville, Maryland, December 2001

[10] T. Bajs, N. Debrecin, B. Krajnc: “Development of the Qualified Plant Nodalization for Safety and Operational Transient Analysis”, International Conference of Croatian Nuclear Society: Nuclear Option in Countries with Small and Medium Electricity Grid, Dubrovnik, June 1998

[11] T. Bajs, M. Bonuccelli, F. D'Auria, N. Debrecin, G.M. Galassi: “On Transient Qualification of Lobi/Mod2, Spes, Lstf, Bethsy and Krsko Plant Nodalizations for Relap5/Mod2 Code”, University of Pisa Report, DCMN-NT 185 (91), Pisa (I), December 1991

Journal of Energy
VOLUME 62 Number 1–4 | 2013 Special Issue
journal homepage: http://journalofenergy.com/

Criticality Safety Analysis of Spent Fuel Storage Pool for NPP Mochovce using MCNP5 Code

Ján Haščík[1], Gabriel Farkas[1], Jakub Lüley[1], Branislav Vrban[1], Róbert Hinca[1],Martin Petriska[1], Vladimír Slugeň[1],Jozef Lipka[1],

[1] Slovak University of Technology, Faculty of Electrical Engineering and Information Technology, Institute of Nuclear and Physical Engineering, Ilkovicova 3, 812 19 Bratislava, Slovakia
jan.hascik@stuba.sk, gabriel.farkas@stuba.sk, jakub.luley@stuba.sk, branislav.vrban@stuba.sk, robert.hinca@stuba.sk, martin.petriska@stuba.sk, vladimir.slugen@stuba.sk, jozef.lipka@stuba.sk.

Peter Urban[2]
[2] SE a.s., NPP Mochovce, Slovakia
peter.urban@enel.com.

ABSTRACT

The paper presents results of nuclear criticality safety analysis of spent fuel storage and handling for the 1st and 2nd unit of NPP Mochovce. Spent fuel storage pool (compact and reserve grid) and T-12 transport cask were modeled using the Monte Carlo code MCNP5. Conservative approach was applied and calculation of k_{eff}^{max} values was performed for normal and various postulated emergency conditions in order to evaluate the final maximal k_{eff}^{max} values. The requirement of current safety regulations to ensure 5% subcriticality was met except some especially conservative cases.

Keywords: sub criticality, spent fuel storage, safety regulation

1 INTRODUCTION

Criticality safety associated with the packaging of spent nuclear fuel is a challenging issue for the scientific and legislative communities involved in efforts to prevent criticality accidents [3]. Safety issues associated with criticality accidents are assessed through appropriate nuclear criticality calculations which are usually performed on the assumption that the spent nuclear fuel is represented by its fresh composition. This is a simple approach, doing unnecessary any knowledge of the fuel irradiation history. However, it overlooks any possible decrease in the fuel reactivity due to the changes in fuel nuclide composition. Some of these nuclides are responsible for the decrease in the reactivity of the spent fuel. Therefore, the inclusion of these nuclides may result in a considerable improvement regarding criticality safety [6]. In this work criticality safety analysis of the spent fuel storage pool (both compact and reserve grid) was performed. Two basic loading scenarios were considered for the analysis - full loading with fresh Gd-II fuel assemblies (enrichment of 4.87 %) and partial loading with fresh and highly burned (45 and 50 MWd/kg) fuel assemblies.

2 ANALYSIS CODE AND VALIDATION

The criticality safety analysis was based on the determination of the effective neutron multiplication factor (k_{eff}) which is a key parameter for criticality safety. The continuous-energy

Monte Carlo Code MCNP5, version 1.40 and continuous-energy neutron cross section data ENDF/B-VII.0 were used [7]. Additionally, S(α,β) thermal scattering data for hydrogen in light water was applied to water and concrete. Code validation was conducted analyzing the BaW XI (2) case of the Criticality Safety Validation Suite [4, 5]. Based on this validation, bias and its uncertainty to be taken into consideration for criticality safety analysis are 0.0001 and 0.00142 respectively. The MCNP5 validation calculation was run with 200 active cycles. This number of active cycles was sufficient to rend the computation uncertainty from the MCNP5 calculation essentially negligible relative to the given benchmark uncertainty.

Table 1: MCNP5 result for BaW XI (2) case of the Criticality Safety Validation Set.

Case	Benchmark k_{eff}	Calculated k_{eff} ENDF/B-VII.0
BaW XI (2)	1.0007 ± 0.0012	1.0006 ± 0.00076

The bias and its uncertainty were calculated according formulas:

$$\Delta_{bias} = k_{eff}^{bench} - k_{eff}^{calcul} \tag{1}$$

$$\sigma_{bias} = \sqrt{\sigma_{bench}^2 - \sigma_{calcul}^2} \tag{2}$$

where:

Δ_{bias}	is	the bias,
σ_{bias}	is	the bias uncertainty derived from the code validation,
k_{eff}^{bench}	-	the benchmark (experimental) k_{eff},
k_{eff}^{calcul}	-	the calculated k_{eff},
σ_{bench}	-	uncertainty of the benchmark k_{eff} value,
σ_{calcul}	-	uncertainty of the calculated k_{eff} value.

3 EVALUATION METHOD

Conservative approach was applied and calculation of k_{eff} values was performed for normal and various postulated emergency conditions in order to evaluate the final maximal k_{eff} values. All conditions improving neutron multiplication in the storage pool were taken into account. Selected conservative parameters are listed in Table 2.

Table 2: Selected conservative parameters

No	Parameter	Nominal value	Tolerance	Conservative value
1	Lattice pitch of fuel pins	12.3 mm	± 0.12 mm	12.42 mm
2	Lattice pitch of absorption tubes of the compact grid	162 mm	± 0.842 mm	161.158 mm
3	Lattice pitch of the reserve grid	225 mm	± 0.842 mm	224.158 mm
4	Lattice pitch of hermetic tubes of the compact grid	230 mm		230 mm
5	Average fuel enrichment of fresh Gd-II fuel assembly	4.87 w%	± 0.05 w%	4.92 w%
6	Gd_2O_3 ratio in the fuel	3.35 w%	± 0.15 w%	3.2 w%
7	Uranium mass in the FA	126.3 kg	± 1.9 kg	128.2 kg
8	Boron content of NEUTRONIT steel of	1.05 – 1.2 %		1.05 %

	the compact grid			
9	Coolant temperature in the compact grid of the storage pool	50 °C		4 °C
10	Coolant temperature in the reserve grid of the storage pool	50 °C		100 °C

The maximal effective multiplication factor $k_{eff}^{\max}$ was evaluated as a sum of the calculated conservative k_{eff}, the systematic error Δ_{bias}, and the combined uncertainty multiplied by 1.645 which is the one-sided tolerance limit factor for a normal distribution at 95% probability.

$$k_{eff}^{\max} = k_{eff}^{conser} + \Delta_{bias} + 1.645\sqrt{\sigma_{bench}^2 + \sigma_{calcul}^2 + \sigma_{conser}^2} \qquad (3)$$

where:

k_{eff}^{conser} is the calculated conservative k_{eff},

σ_{conser} - uncertainty of the calculated conservative k_{eff}.

4 CALCULATION MODEL

The following detailed models were developed in the MCNP5 for criticality safety analysis:

- model of compact grid of the spent nuclear fuel storage pool, Figure 1 – 5,
- model of reserve grid of the spent nuclear fuel storage pool, Figure 6.

MCNP model of the compact grid consists of 603 hexagonal absorption tubes filled with profiled Gd-II fuel assemblies with the enrichment of 4.87 %, 54 hermetic tubes, supporting plate, and concrete well. Nominal lattice pitch of the absorption tubes represents 162 mm and 230 mm for the hermetic tubes. The reserve grid model consists of 296 fuel assemblies, 54 hermetic tubes, supporting plate, and concrete well.

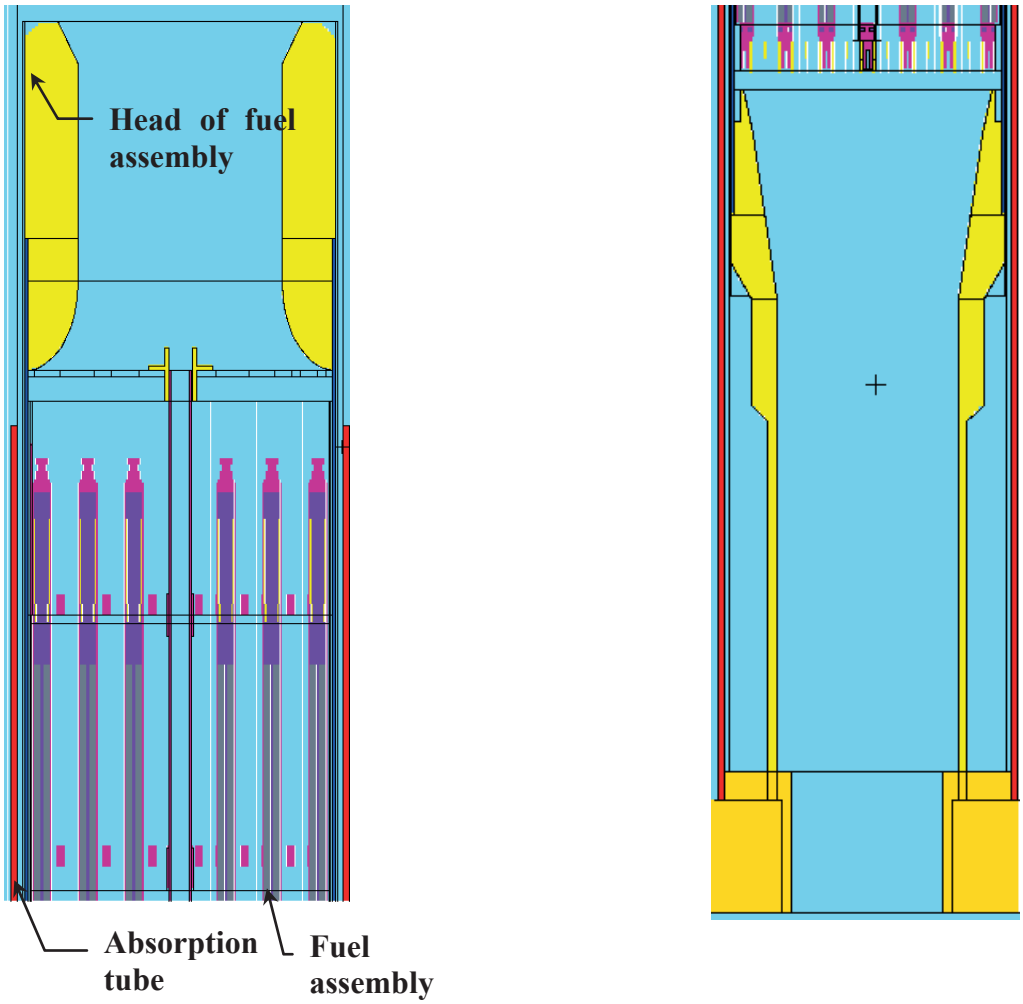

Figure 1: MCNP model of the hexagonal absorption tube filled with FA – vertical cross section.

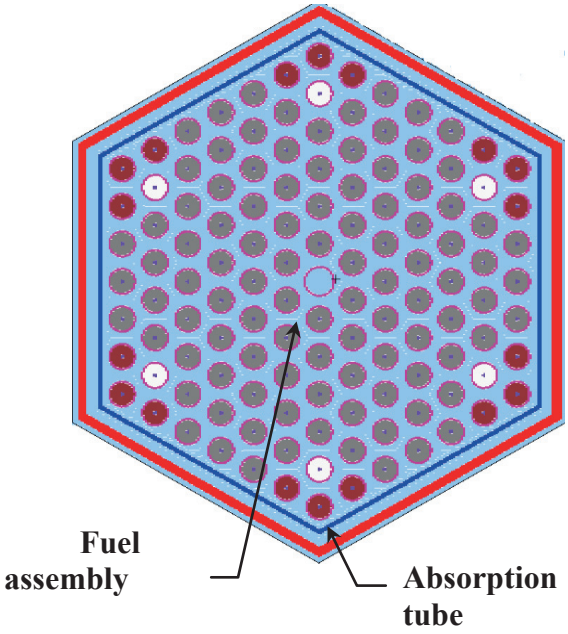

Figure 2: MCNP model of the hexagonal absorption tube filled with FA – horizontal cross section.

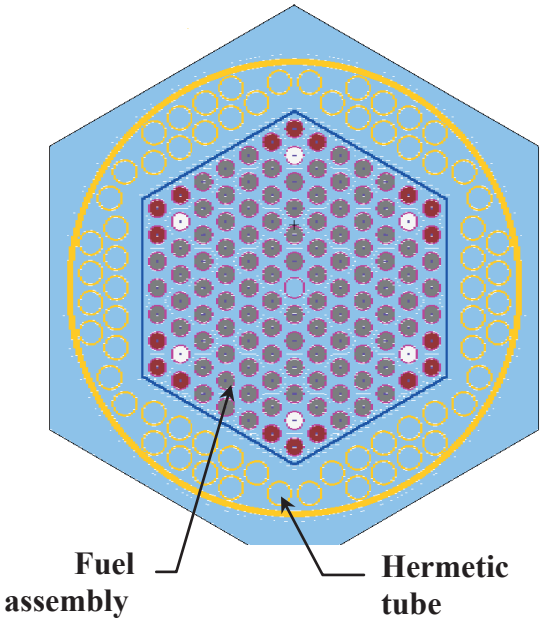

Figure 3: MCNP model of the hermetic tube filled with FA - horizontal cross section.

J. Haščík, G. Farkas, J. Lüley, B. Vrban, R. Hinca, M. Petriska, V. Slugeň, J. Lipka, P. Urban, Criticality Safety Analysis of Spent Fuel Storage Pool for NPP Mochovce using MCNP5 Code, Journal of Energy, vol. 62 Number 1–4 (2013) Special Issue, p. 159–170

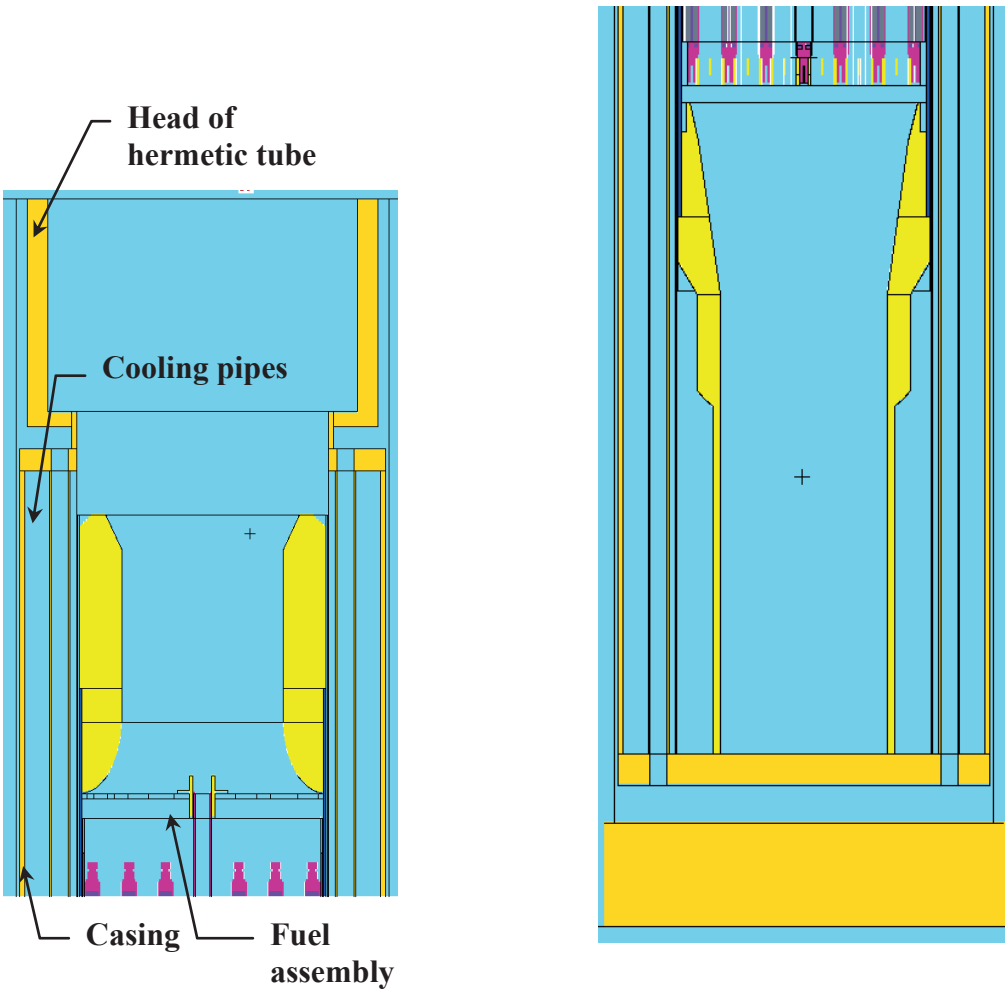

Figure 4: MCNP model of the hermetic tube with FA – vertical cross section.

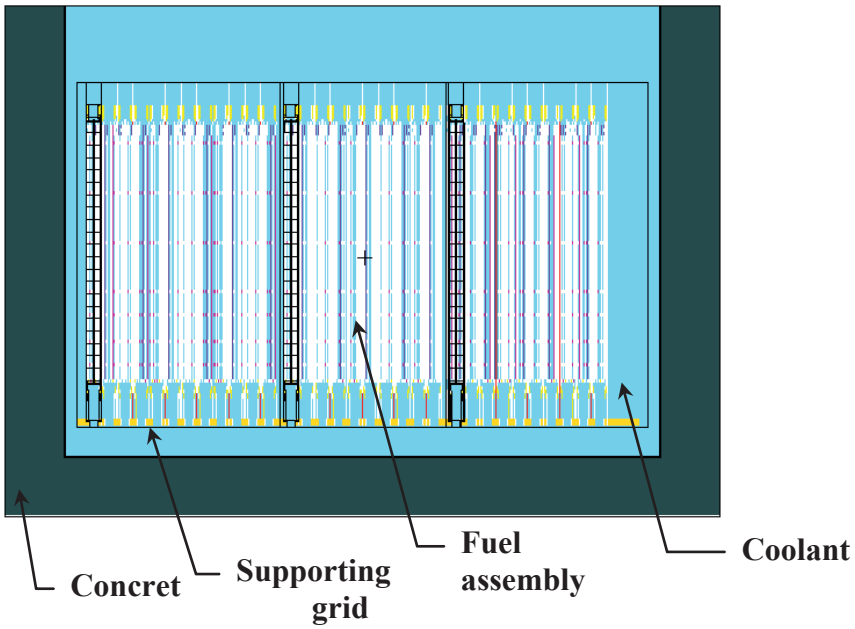

Figure 5: MCNP model of compact grid of the spent fuel storage pool – vertical cross section.

J. Haščík, G. Farkas, J. Lüley, B. Vrban, R. Hinca, M. Petriska, V. Slugeň, J. Lipka, P. Urban, Criticality Safety Analysis of Spent Fuel Storage Pool for NPP Mochovce using MCNP5 Code, Journal of Energy, vol. 62 Number 1–4 (2013) Special Issue, p. 159–170

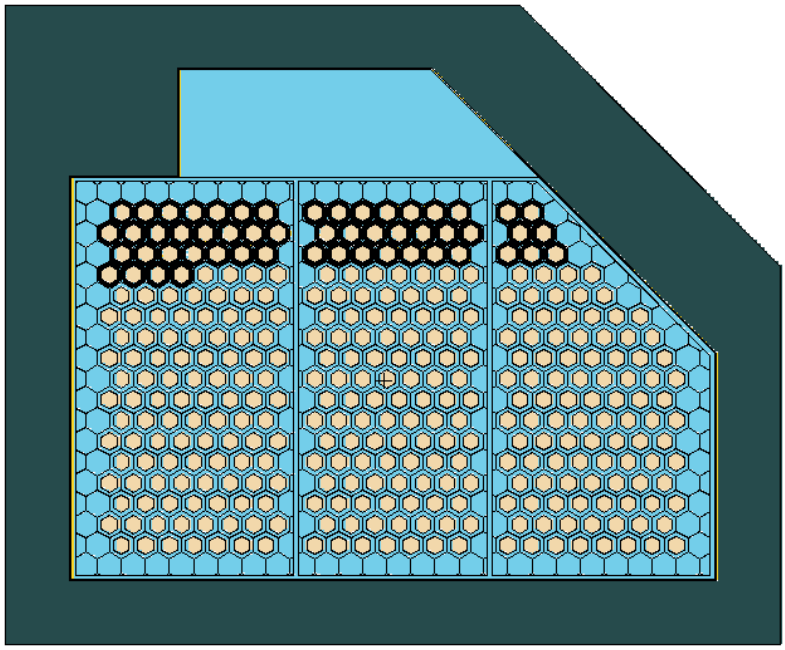

Figure 6: MCNP model of reserve grid of the spent fuel storage pool – horizontal cross section.

(Variant R1– full loading with 4.87 % enriched FAs, variant R2 – full loading with 45 MWd/kg burned FAs).

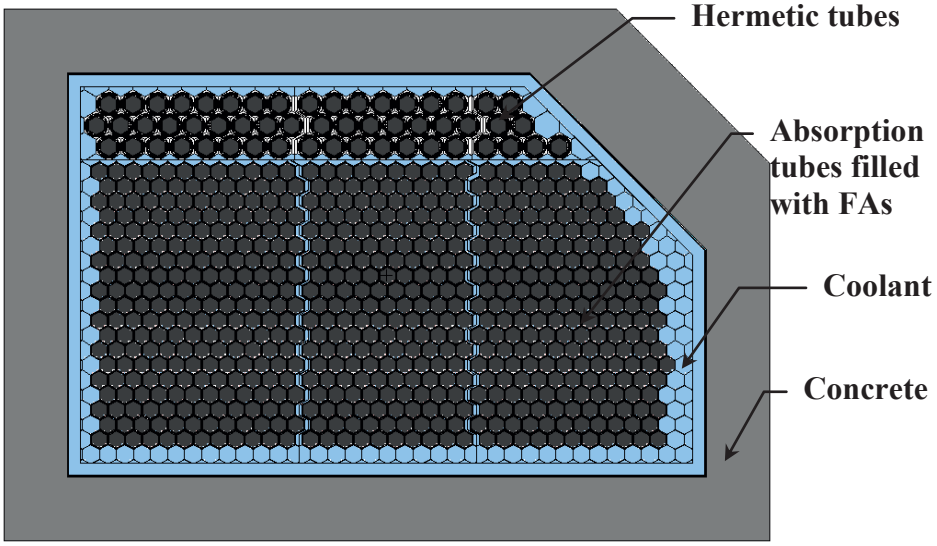

Figure 7: MCNP model of compact grid of the spent fuel storage pool – horizontal cross section.

(Variant A – all positions loaded with 4.87 % enriched fresh FAs.)

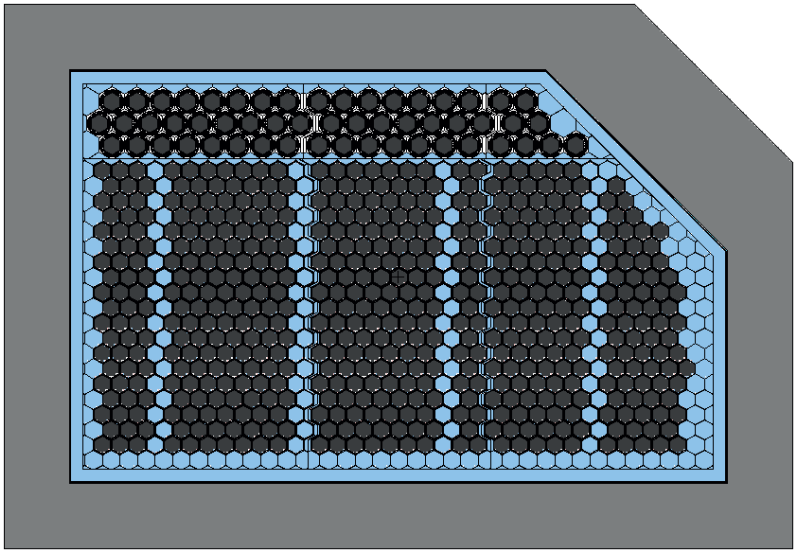

Figure 8: MCNP model of compact grid of the spent fuel storage pool – horizontal cross section.

(Variant B – loading with 4.87 % enriched fresh FAs and four empty rows.)

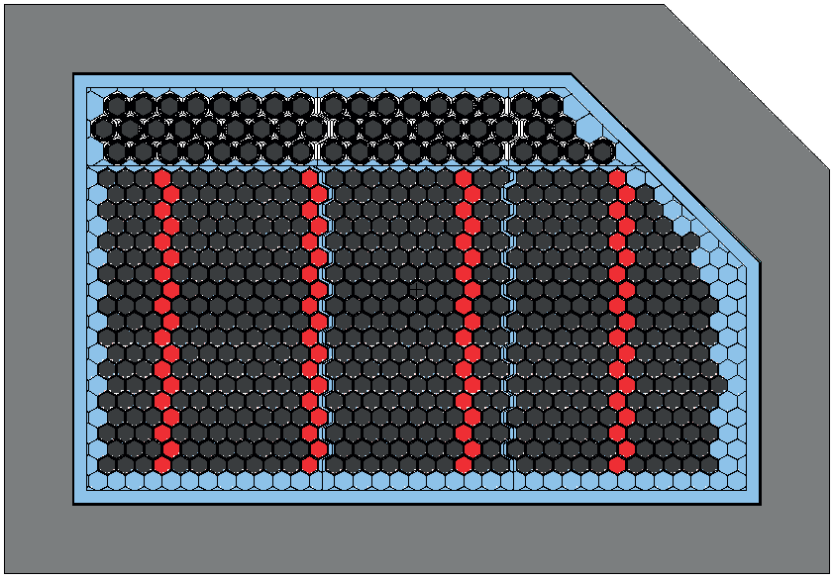

Figure 9: MCNP model of compact grid of the spent fuel storage pool – horizontal cross section.

(Variant C1 (D1) – loading with 4.87 % enriched FAs and four rows of 45 MWd/kg (50 MWd/kg) burned FAs.)

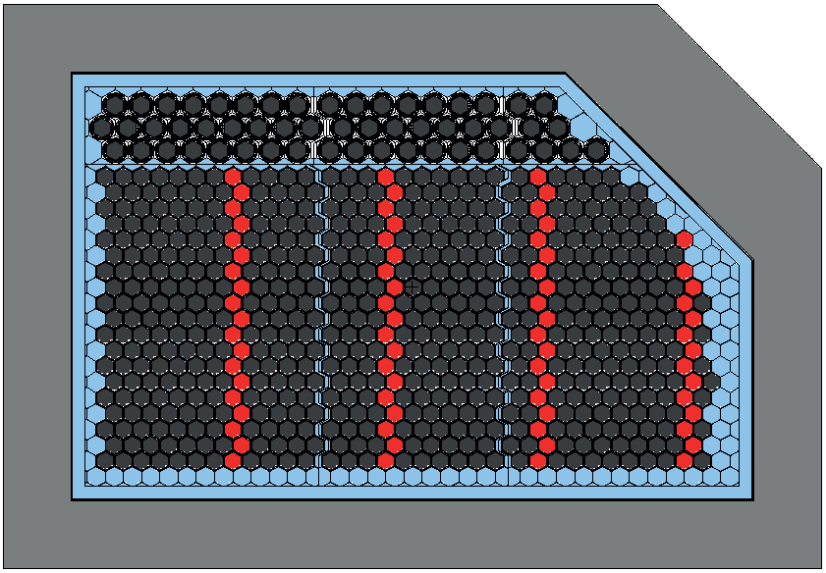

Figure 10: MCNP model of compact grid of the spent fuel storage pool – horizontal cross section. (Variant C2 (D2) – loading with 4.87 % enriched FAs and four rows of 45 MWd/kg (50 MWd/kg) burned FAs.)

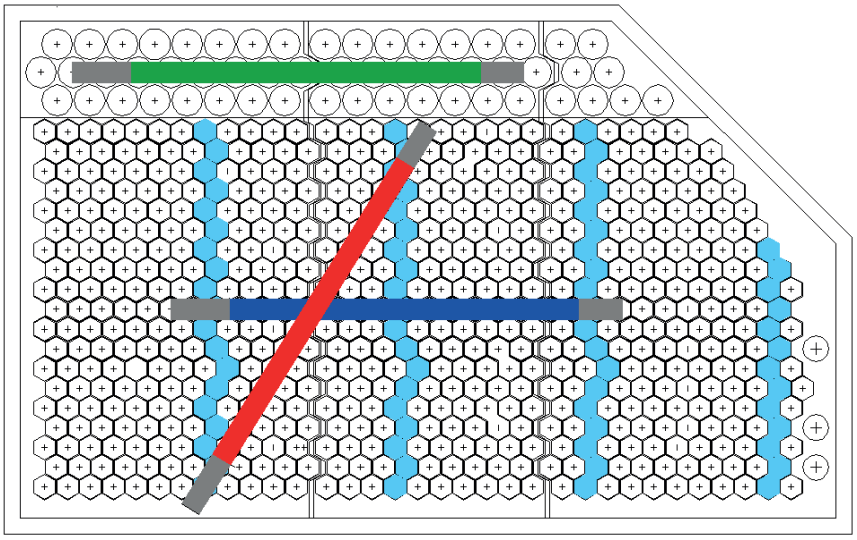

Figure 11: Compact grid with positions of fallen fuel assembly.

(red – diagonal downfall, blue – longitudinal downfall, grenn – downfall on the hermetic tubes)

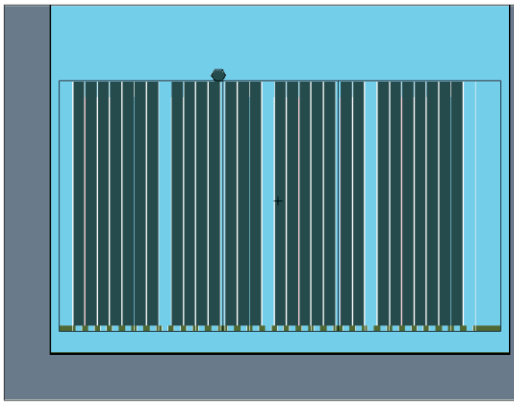

Figure 12: MCNP model of fully loaded compact grid with fresh FAs, four empty rows, and diagonally fallen fresh fuel assembly–variant E11.

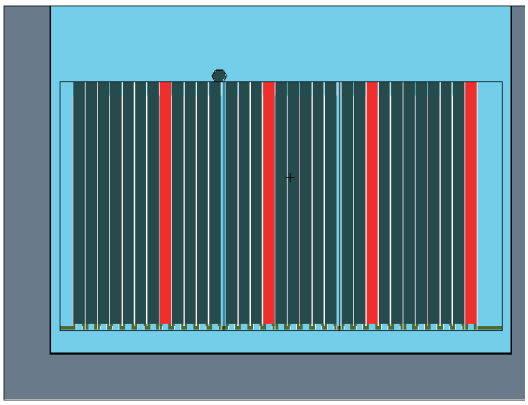

Figure 13: MCNP model of fully loaded compact grid with fresh FAs, four rows of 45 MWd/kg burned FAs, and diagonally fallen fresh fuel assembly – variant E12.

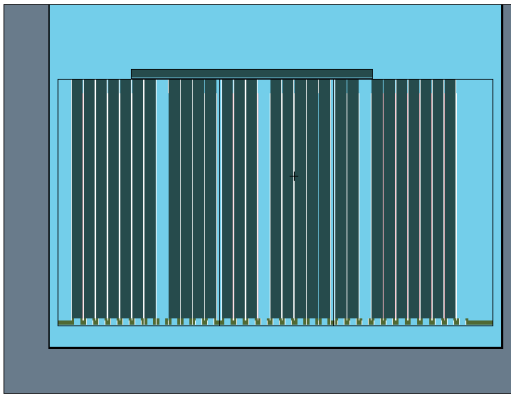

Figure 14: MCNP model of fully loaded compact grid with fresh FAs, four empty rows, and longitudinally fallen fresh fuel assembly

– variant E21.

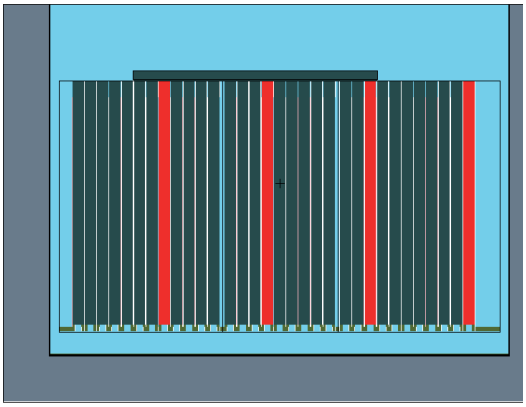

Figure 15: MCNP model of fully loaded compact grid with fresh FAs, four rows of 45 MWd/kg burned FAs, and longitudinally fallen fresh fuel assembly – variant E22.

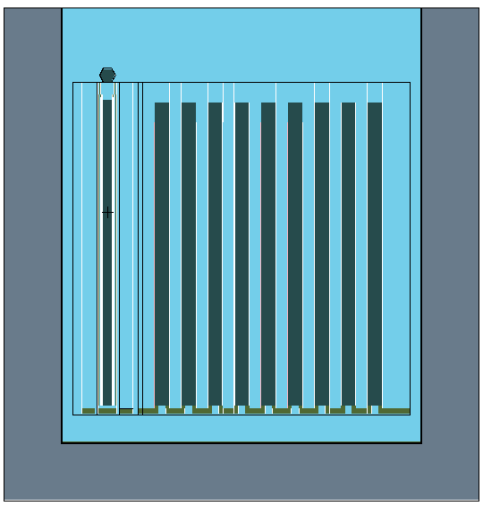

Figure 16: MCNP model of the compact grid, and longitudinally fallen fresh fuel assembly on the hermetic tubes –

variant E31 and E32.

5 RESULTS

Concerning criticality safety analysis of the compact grid, the following basic variants of storage pool loading were investigated:

variant A all positions loaded with 4.87 % enriched fresh FAs (Figure 7),
variant B loading with 4.87 % enriched fresh FAs and four empty rows (Figure 8),
variant C1 loading with 4.87 % enriched FAs and four rows of 45 MWd/kg burned FAs (Figure 9),
variant C2 loading with 4.87 % enriched FAs and four rows of 45 MWd/kg burned FAs (Figure 10),
variant D1 loading with 4.87 % enriched FAs and four rows of 50 MWd/kg burned FAs (Figure 9).
variant D2 loading with 4.87 % enriched FAs and four rows of 50 MWd/kg burned FAs (Figure 10).

Table 3: Results of the criticality safety analysis for compact grid (basic variants).

Variant	k_{eff}^{conser}	σ_{conser}	$k_{eff}^{\max}$
A	0.95136	0.00004	**0.95520**
B	0.93672	0.00004	**0.94056**
C1	0.94152	0.00007	**0.94397**
C2	0.94064	0.00007	**0.94309**
D1	0.94042	0.00007	**0.94287**
D2	0.93949	0.00007	**0.94194**

variant R1 all positions loaded with 4.87 % enriched fresh FAs (Figure 6),
variant R2 all positions loaded with 45 MWd/kg burned FAs (Figure 6).

Table 4: Results of the criticality safety analysis for reserve grid.

Variant	k_{eff}^{conser}	σ_{conser}	$k_{eff}^{\max}$
R1	0.90877	0.00003	**0.91261**
R2	0.73597	0.00005	**0.73842**

In order to evaluate the influence of fallen fresh FA into the compact grid on $k_{eff}^{\max}$ value, the following six emergency conditions were investigated:

variant E11 loading with 4.87 % enriched FAs, four empty rows, and diagonally fallen fresh FA (Figure 12),
variant E12 loading with 4.87 % enriched FAs, four rows of 45 MWd/kg burned FAs, and diagonally fallen fresh FA (Figure 13),
variant E21 loading with 4.87 % enriched FAs, four empty rows, and longitudinally fallen fresh FA (Figure 14),
variant E22 loading with 4.87 % enriched FAs, four rows of 45 MWd/kg burned FAs, and longitudinally fallen fresh FA (Figure 15),
variant E31 loading with 4.87 % enriched FAs, four empty rows, and longitudinally fallen fresh FA on the hermetic tubes (Figure 16),
variant E32 loading with 4.87 % enriched FAs, four rows of 45 MWd/kg burned FAs, and longitudinally fallen fresh FA on the hermetic tubes (Figure 16).

Table 5: Results of the criticality safety analysis for compact grid (emergency variants).

Variant	k_{eff}^{conser}	σ_{conser}	$k_{eff}^{\max}$
E11	0.93640	0.00007	**0.93885**
E12	0.94069	0.00007	**0.94314**
E21	0.93631	0.00010	**0.93877**
E22	0.94057	0.00010	**0.94303**
E31	0.93645	0.00007	**0.93890**
E32	0.94046	0.00007	**0.94291**

6 CONCLUSION

Criticality issues associated with compact and reserve grid of the spent fuel storage pool, located in the NPP Mochovce 1 and 2, were investigated using MCNP5. The criticality safety analysis focused on the evaluation of maximal neutron multiplication factor values at normal and some emergency conditions applying conservative approach. The outcomes of the investigations showed that the requirement of current safety regulations to ensure 5 % subcriticality was met (including postulated emergency conditions), except one especially conservative case of the fully loaded compact grid with fresh 4.87 % enriched Gd-II FAs. Only in this case, the calculated $k_{eff}^{\max}$ value exceeded the required subcriticality limit of 0.95 by 0.55 %. Except this one scenario the analyses showed that nuclear criticality safety criteria in terms of the spent fuel storage pool are satisfied.

LIST OF NOMENCLATURE

EN Evaluated Nuclear Data File
DF
FA Fuel Assembly
MC Monte Carlo N-Particle Transport Code
NP
NPP Nuclear Power Plant

7 REFERENCES

[1] F. B. Brown, “Theory & Practice of Criticality Calculation with MCNP5”, LA-UR-08-0849, Los Alamos National Laboratory (2008)

[2] F. B. Brown, B. Nease, & J. Cheatham, “Convergence Testing for MCNP5 Monte Carlo Eigenvalue Calculations”, M&C+SNA-2007, ANS Mathematics & Computation Topical Meeting Monterey, CA, 15-19 April 2007, LA-UR-07-1123 (2007)

[3] Implementation of Burnup Credit in Spent Fuel Management Systems. International Atomic Energy Agency, IAEA-TECDOC-1241, Vienna (2000)

[4] International Handbook of Evaluated Criticality Safety Benchmark Experiments, NEA/NSC/DOC(95)3, OECD Nuclear Energy Agency, ISBN 978-92-64-99140-8 (2006)

[5] R. D. Mosteller, “ENDF/B-VII.0, ENDF/B-VI, JEFF-3.1, and JENDL-3.3 Results for the MCNP Criticality Validation Suite and Other Criticality Benchmarks”, LA-UR-07-6284, Los Alamos National Laboratory (2007)

[6] G. Nicolaou, N. Tsagas, “Criticality Safety of Spent Nuclear Fuel Assemblies from the Transmutation of Minor Actinides in Fast Reactors”, Annals of Nuclear Energy, 33 (2006), pp. 305 – 309

[7] X-5 Monte Carlo Team, "MCNP – A general N-Particle Transport Code, Version 5 – Volume I: Overview and Theory", LA-UR-03-1987, Los Alamos National Laboratory (April 2003)

Journal of Energy
VOLUME 62 Number 1–4 | 2013 Special Issue
journal homepage: http://journalofenergy.com/

Monte Carlo Codes for Neutron Buildup Factors

Krešimir Trontl, Dubravko Pevec, Mario Matijević
University of Zagreb, Faculty of Electrical Engineering and Computing
Unska 3, 10000 Zagreb, Croatia
kresimir.trontl@fer.hr, dubravko.pevec@fer.hr, mario.matijevic@fer.hr

ABSTRACT

The point-kernel method is a widely used practical tool for gamma-ray shielding calculations. However, application of that method for neutron transport simulations is very limited. The accuracy of the method strongly depends on the accuracy of buildup factors used in the calculations. Buildup factors are usually obtained using appropriate computer codes, either based on discrete ordinates transport method or Monte Carlo approach. Since these codes put strong demands on computer resources, they are applied on a limited number of shielding configurations and an attempt is made to use these results and formulate an empirical expression for buildup factors estimation. Due to high physical complexity of neutron transport through shielding material it is very hard to perform parameterisation in order to establish adequate empirical formula. Existing formulas are very limited and are usually applicable to a narrow neutron energy range for few commonly used shielding materials, mostly in monolayer configuration.

Recently, a new approach has been proposed for determination of gamma ray buildup factors for mono-layer, as well as multi-layer shielding configurations covering a wide gamma ray energy range. The new regression model is based on support vector machines learning technique, which has theoretical background in statistical learning theory. Development of named regression model required a large number of experimental data obtained by Monte Carlo computer code. More than 7000 Monte Carlo runs were required. Due to physical complexity neutron transport is likely to require even more experimental data in order to generate a model of reasonable accuracy. Therefore, the choice of appropriate Monte Carlo code is a very important question. One has to take into account the accuracy as well as the time required for input preparation and running the code. What also has to be considered is the possibility of the code to be incorporated in an algorithm for automated generation of experimental data.

In this paper three Monte Carlo codes are analysed, namely SCALE4.4 code package (SAS3 sequence), SCALE6.0 code package (MAVRIC sequence), and MCNP5. Two simple experimental setups based on a point isotropic source in spherical and slab-like shield are modelled, and the codes are examined on previously mentioned issues.

The comparison results show that each one of the examined codes has potential to be used for neutron buildup factor model generation. However, some aspects of their utilization require further analysis prior to final selection.

1 INTRODUCTION

The point-kernel method is a widely used practical tool for gamma-ray shielding calculations in shielding design and radiation safety analysis. However, application of that method for neutron transport simulations is very limited. In general, point-kernel method is primarily used for preliminary engineering calculations, where ease and speed are more appreciated than the accuracy obtained by more demanding codes employing transport or Monte Carlo methods, which usually

require more expertise and training to use and are often much slower in reaching the final solution. In the point-kernel approach, the desired quantity (flux, fluence, or dose equivalent) is obtained by multiplying the portion of the quantity resulting from uncollided flux with the parameter called buildup factor, which accounts for the scattered radiation in the medium. It is therefore clear, that the accuracy of the final result is highly dependent on the accuracy of buildup factor used in the calculations.

Buildup factors are usually obtained using appropriate computer codes, either based on discrete ordinates transport method or Monte Carlo approach. Since these codes put strong demands on computer resources, they are applied on a limited number of shielding configurations and an attempt is made to use obtained results and formulate an empirical expression for buildup factors estimation. Due to high physical complexity of neutron transport through shielding material it is very hard to perform parameterisation in order to establish adequate empirical formula. Buildup of scattered neutrons depends strongly on the material composition, incident neutron energy spectrum, and the geometry of the problem [1]. Since the fast neutron scattering cross section is greater than the absorption cross section for most materials, the buildup of scattered neutrons can assume large values. Also the size and shape of the shield medium as well as the energy dependence of the materials cross sections greatly affect the neutron flux density. Therefore, existing neutron buildup factor formulas are very limited and are usually applicable to a very limited neutron energy range for few commonly used shielding materials, mostly in monolayer configuration. For example, Dunn et al. [2] investigated neutron dose-equivalent buildup factors for infinite slabs. Computer experiments were carried out on 6 materials in combination with 7 source neutron energies ranging from 10^{-7} MeV up to 14 MeV, and a simple two-parameter model has been proposed. Values for both parameters differ not only for every material, but also for all energies. Tested 42 material-energy combinations resulted in 42 pairs of different parameters values. Shin et al [3] investigated point isotropic buildup factors for concrete, iron, and a double-layer iron-concrete shield for 7 neutron energies ranging from 400 MeV down to 10 MeV. The proposed empirical formula is based on three parameters for single-layer shield, while the formula for double-layer configurations uses single-layer buildup factors of both materials and a fourth parameter. The parameterisation process resulted in different parameters values for all energies and materials, all together 14 different parameter triples for single-layer shield configurations. The fourth parameter, reguired to calculate double-layer shield configuration, is also energy dependent.

Recently, a new approach has been proposed for determination of gamma ray buildup factors for mono-layer, as well as multi-layer shielding configurations covering a wide gamma ray energy range [4]. The new regression model is based on support vector machines learning technique, which has theoretical background in statistical learning theory [5]. Development of named regression model required a large number of experimental data obtained by Monte Carlo computer code. More than 7000 Monte Carlo runs were required. Since neutron transport, due to high physical complexity, is likely to require even more experimental data in order to generate a model of reasonable accuracy, the choice of appropriate Monte Carlo code is a very important question. One has to take into account the accuracy as well as the time required for input preparation and running the code. What also has to be considered is the possibility of the code to be incorporated in an algorithm for automated generation of experimental data.

Therefore, in this paper three Monte Carlo codes are analysed, namely SCALE4.4 code package (SAS3 sequence), SCALE6.0 code package (MAVRIC sequence), and MCNP5. Two simple experimental setups based on a point isotropic source in spherical and slab-like shield are modelled, and the codes are examined on previously mentioned issues. To validate the accuracy, the results are compared to available references.

Short description of used Monte Carlo codes is given in Section 2. Methodology applied for the analyses of the Monte Carlo codes is presented in Section 3, while the results are given in Section 4. In Section 5 we draw conclusions based on this work. Used references are listed at the end of the manuscript.

2 MONTE CARLO CODES

Based on our previous experience, as well as on available computer codes, we decided to test SCALE code package and MCNP code. Shielding Analyses Sequnce No.3 (SAS3) available in SCALE4.4 [6] code package was used for gamma-ray buildup factors research and proved to be reliable and easy to handle. Therefore, it was also selected for this particular analysis. New version of the SCALE code package, namely SCALE6 [7], does not include SAS3 sequence. Monte Carlo shielding analysis is conducted through MAVRIC sequence. It was therefore reasonable to investigate the applicability of that particular sequence. MCNP code [9] is a widely used tool for neutron transport analyses which triggered our interest in the code and its possibilities in view of neutron buildup factor investigation.

2.1 SCALE code package

The SCALE (Standardized Computer Analyses for Licensing Evaluation) code system was developed at Oak Ridge National Laboratory for the U.S. Nuclear Regulatory Commission to satisfy a need for a standardized method of analysis for the evaluation of nuclear facilities and package designs.

SAS3 sequence is a part of an older version of SCALE code package, namely SCALE4.4 version [6]. It has an automated procedure for coupling cross section processing with Monte Carlo shielding calculations performed by MORSE-SGC, a SCALE version of the MORSE family of Monte Carlo programs. Eight cross-section libraries are automatically available in SCALE4.4 system. We used 27N-18COUPLE library, based on ENDF/B-IV data, which is a 27-neutron-group and 18-gamma-group library widely used and validated in LWR spent fuel shielding calculations. Corresponding neutron energy group structure is given in Table 1.

Table 1 Neutron energy groups of 27N-18COUPLE library (SCALE6)

Group	Upper boundary [eV]	Lower boundary [eV]	Mean [MeV]	Group	Upper boundary [eV]	Lower boundary [eV]	Mean [eV]
1	2.00E+07	6.43E+06	1.32E+07	15	3.05E+00	1.77E+00	2.41E+00
2	6.43E+06	3.00E+06	4.72E+06	16	1.77E+00	1.30E+00	1.54E+00
3	3.00E+06	1.85E+06	2.43E+06	17	1.30E+00	1.13E+00	1.22E+00
4	1.85E+06	1.40E+06	1.63E+06	18	1.13E+00	1.00E+00	1.07E+00
5	1.40E+06	9.00E+05	1.15E+06	19	1.00E+00	8.00E-01	9.00E-01
6	9.00E+05	4.00E+05	6.50E+05	20	8.00E-01	4.00E-01	6.00E-01
7	4.00E+05	1.00E+05	2.50E+05	21	4.00E-01	3.25E-01	3.63E-01
8	1.00E+05	1.70E+04	5.85E+04	22	3.25E-01	2.25E-01	2.75E-01
9	1.70E+04	3.00E+03	1.00E+04	23	2.25E-01	1.00E-01	1.63E-01
10	3.00E+03	5.50E+02	1.78E+03	24	1.00E-01	5.00E-02	7.50E-02
11	5.50E+02	1.00E+02	3.25E+02	25	5.00E-02	3.00E-02	4.00E-02
12	1.00E+02	3.00E+01	6.50E+01	26	3.00E-02	1.00E-02	2.00E-02
13	3.00E+01	1.00E+01	2.00E+01	27	1.00E-02	1.00E-05	5.01E-03
14	1.00E+01	3.05E+00	6.53E+00				

MAVRIC (Monaco with Automated Variance Reduction using Importance Calculations) shielding sequence is a part of a new SCALE6 code package [7]. 3-D Monte Carlo calculations are performed through MONACO functional module, which is a MORSE successor. This time, V7-27N19G library has been selected as a cross section library. It has same group structure as 27N-18COUPLE library, but is is based on ENDF/B-VII data [8]. Although fine-group neutron-gamma libraries are available for radiation transport calculations with SCALE shielding modules, we decided to use broad-group library to enable easier comparison of the result.

2.2 MCNP code

MCNP is a general-purpose Monte Carlo N-Particle code that can be used for neutron, photon, electron, or coupled neutron/photon/electron transport. Pointwise cross-section data are typically used, although group-wise data also are available. For neutrons, all reactions given in a particular cross-section evaluation (such as ENDF/B-VII) are accounted for. We used MCNP5 [9] with pointwise cross-section data based on ENDF/B-VII.

3 METHODOLOGY

The methodological approach is primarily guided by the main goal of this particular research stage, which is to identify the most suitable Monte Carlo code to be used in proceeding analyses of neutron buildup factor determination. To recall, suitability in the context of this research is defined through:

- accuracy of the obtained results compared to reference data,
- time requirements including time needed for input preparation and subsequent input modifications, as well as running time,
- incorporation possibilities implying ease of coupling selected Monte Carlo code with appropriate algorithm for automated neutron buildup factor model generation.

Accuracy and running time are two categories that have to be jointly analyzed. The accuracy of the obtained result represents discrepancy of the result compared to the reference results. But what also has to be taken into account is the Monte Carlo precision, usually expressed as Monte Carlo error on one sigma level defined as one sigma divided by the average value. Running time is closely connected to the desired Monte Carlo error. In practice it means that Monte Carlo description of the specific problem and the number of neutron histories involved in the calculation strongly influence running time, as well as the precision. Depending on problem complexity, a particular Monte Carlo input may or may not lead to satisfactory result, including not only its accuracy but also its Monte Carlo error. In the latter case, modifications on the input are required, usually including changes of parameters controlling variance reduction and the number of analyzed neutron histories. Based on this short elaboration, we decided to predefine desired Monte Carlo error on one sigma level to 5%. Calculation starts with 10,000 histories and an initial set of Monte Carlo parameters controlling variance reduction. In the case that the obtained result breaks 5% error level, the calculation is repeated by increasing the number of neutron histories and modifications of variance reduction parameters. Selection of the initial set of Monte Carlo parameters and number of neutron histories "milestones" is based on our previous experience, as well as on observations made by Dunn et al. [2]

Reference data to which our results are compared to were taken from the research conducted by Dunn et al. [2], Shin et al. [3], and Shirani and Shahriari [10]. That choice also governed experimental setup preparation. Dunn et al. as well as Shirani and Shahriari used point isotropic source in slab-like shields, while Shin et al. used point isotropic source in spherical shields. More attention was put on Dunn et al. as well as Shirani and Shahriari researches, since their investigated energy range is based on neutronics of nuclear power plant operation. On the other hand Shin et al. investigated higher neutron energies corresponding to accelerator facilities. Dunn et al. used a combination of Boltzmann transport equation model for the calculation of uncollided flux and a Monte Carlo model for the calculation of collided flux, while Shirani and Shahriari used Monte Carlo model through MCNP4c code. Shin et al. used S_N code ANISN.

4 RESULTS AND REMARKS

Although three investigated codes have been tested on all variations of two experimental setups and the results have been thoroughly compared to reference material data, in this section only a brief overview of most interesting observations is presented.

4.1 Slab shield experimental setup

In a slab shield experimental setup point isotropic mono-energetic source is placed on one side of the slab shield. Point detector is located on the other side of the shield, opposite to point source. Therefore, the distance between source and detector is equal to the shield thickness. All together, six different materials have been analysed (Table 2). For every material eight different shield thicknesses, expressed by mean free path (mfp) have been modelled (0.5 mfp and 1 mfp up to 7 mfp with the increment of 1 mfp). The mean free path has been calculated as inverse value of the total neutron cross section (1 mfp = $1/\Sigma_t$).

Table 2 Materials analysed in slab shield experimental setup

Material	Density [g/cm^3]	Element	Z	Weight fraction
Aluminium	2.694	Aluminium	13	1.0
Iron	7.86	Iron	26	1.0
Lead	11.33	Lead	82	1.0
Water	1.0	Hydrogen	1	0.1119
		Oxygen	8	0.8881
Polyethylene	0.95	Hydrogen	1	0.1438
		Carbon	6	0.8562
Concrete	2.3	Hydrogen	1	0.00562
		Oxygen	8	0.50010
		Sodium	11	0.01716
		Aluminium	13	0.04577
		Silicon	14	0.31694
		Potassium	19	0.01927
		Calcium	20	0.08290
		Iron	26	0.01224

In this paper, detailed results for water shield with the thickness of 0.5 mfp, 4 mfp, and 7 mfp and lead shield with the thicknesses of 0.5 mfp and 4 mfp, as well as iron shield with the thickness of 4 mfp, are given. Results for water shield are depicted on Figures 1 – 3, and for lead shield on Figure 4 and Figure 5. Graphical representation of buildup factors for 4 mfp thick iron shield is given on Figure 6.

One of the crucial differences between SCALE code package and MCNP5 is the fact that explicit definition of the incident neutron energy is not possible in SCALE, but rather the definition of the "incident" energy group, as given in Table 1. On all figures, SCALE energy group interval is characterized by group mean energy (Table 1).

In the case of water shield, buildup factors obtained by SCALE4.4 (SAS3) are very similar to Shirani and Shahriari [10] on the entire examined neutron energy range. For neutron energies up to 0.01 MeV they are consistently higher than the ones obtained by Dunn et al. [2], with the exception of very thick shield (7 mfp) and low energy of 10^{-7} MeV. For higher energies, behaviour of the results cannot be uniquely characterized, especially for neutron energy of 0.1 MeV. Buildup factors obtained by MCNP5 code are consistently lower than all other buildup factors, except for the lowest energy of 10^{-7} MeV. Similar behaviour was observed for polyethylene and concrete shields.

All SCALE4.4 and MCNP5 results are based on 5% precision premise, and that precision was relatively easy to obtain for thin shields, while for thicker shields number of neutron histories had to be increased up to 1 million. On the average, SCALE4.4 running time can be expressed in seconds, while MCNP5 running time is expressed in tens of seconds.

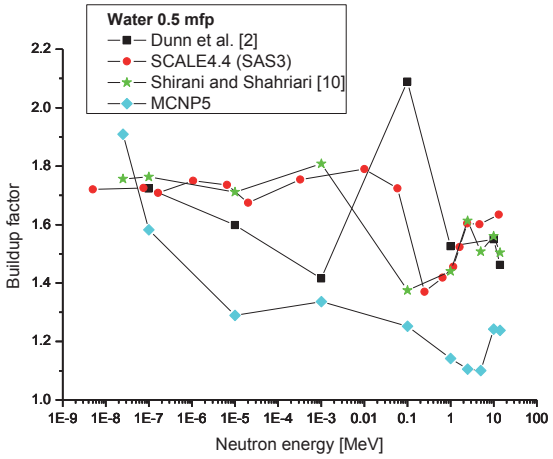

Figure 1: Comparison of buildup factors for 0.5 mfp thick water shield calculated by SCALE4.4 and MCNP5 with reference values extracted from Dunn et al. [2] and Shirani and Shahriari [10]

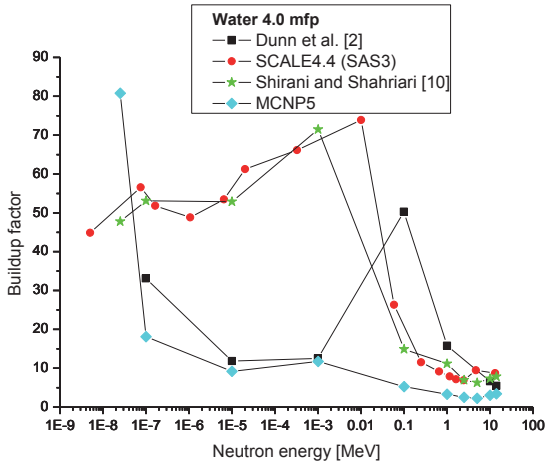

Figure 2: Comparison of buildup factors for 4 mfp thick water shield calculated by SCALE4.4 and MCNP5 with reference values extracted from Dunn et al. [2] and Shirani and Shahriari [10]

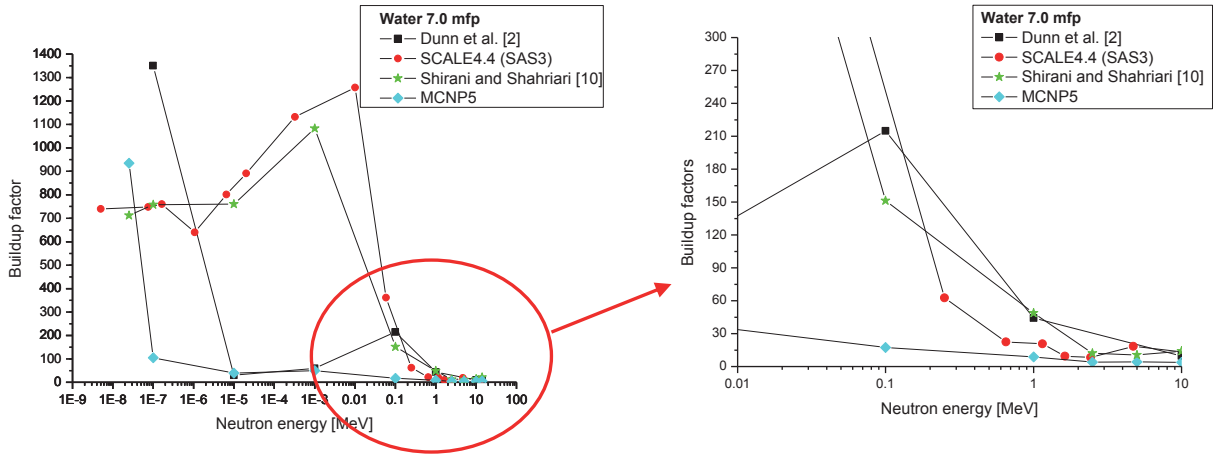

Figure 3: Comparison of buildup factors for 7 mfp thick water shield calculated by SCALE4.4 and MCNP5 with reference values extracted form Dunn et al. [2] and Shirani and Shahriari [10]

In the case of lead shield, buildup factors obtained by SCALE4.4 (SAS3) are very similar to Shirani and Shahriari [10], as well as Dunn et al. [2] for all shield thicknesses and neutron energies up to 1 MeV. For higher energies SCALE4.4 buildup factors have the same behaviour as Shirani and Shahriari, and are higher than Dunn et al. MCNP5 buildup factors are lower than others for neutron energies up to 1 MeV. For higher energies they show stronger dependence on shield thickness, but are generally higher than Dunn et al., and lower than SCALE4.4 and Shirani and Shahriari, except for the neutron energies of 2.5 MeV and 5 MeV. Precise analysis is limited by the fact that Dunn et al. did not analyse these particular energies.

Similar behaviour is observed for iron shields, except for transition towards lower energies. Therefore, the change of behaviour is noticed on neutron energy of 10^{-3} MeV.

4.2 Spherical shield experimental setup

In a spherical shield experimental setup point isotropic mono-energetic source is located in the origin of spherical shield configuration. Shin et al. [3] investigated single-layer (iron and

concrete) and double-layer shield configurations (iron + concrete). Focus of their research was on high neutron energies above 10 MeV. For our research the only interesting energy is 10 MeV. We analysed empirical formula for double-layer shield comprised of iron and concrete obtained by Shin et al. It has to be noted that the formula was developed from data obtained for relatively thick shields were the first (iron) layer is 50+ cm. Our interest was to test the applicability of the formula for thinner shields on neutron energy which represents the energy applicability boundary of the formula. The results for the combinations of 1 mfp of iron followed by 1 mfp, 3 mfp, and 5 mfp of concrete, as well as 3 mfp of iron followed by 1 mfp, 3 mfp, and 5 mfp of concrete are depicted on Figure 7 and Figure 8, respectively.

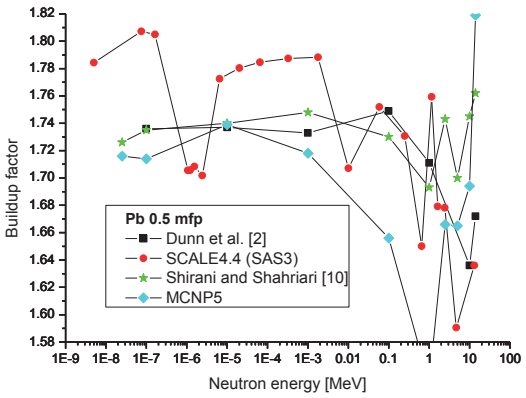

Figure 4: Comparison of buildup factors for 0.5 mfp thick lead shield calculated by SCALE4.4 and MCNP5 with reference values extracted from Dunn et al. [2] and Shirani and Shahriari [10]

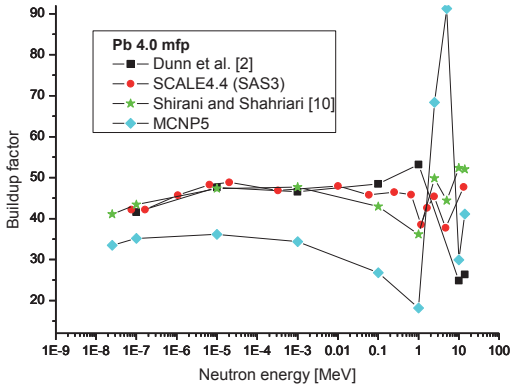

Figure 5: Comparison of buildup factors for 4 mfp thick lead shield calculated by SCALE4.4 and MCNP5 with reference values extracted from Dunn et al. [2] and Shirani and Shahriari [10]

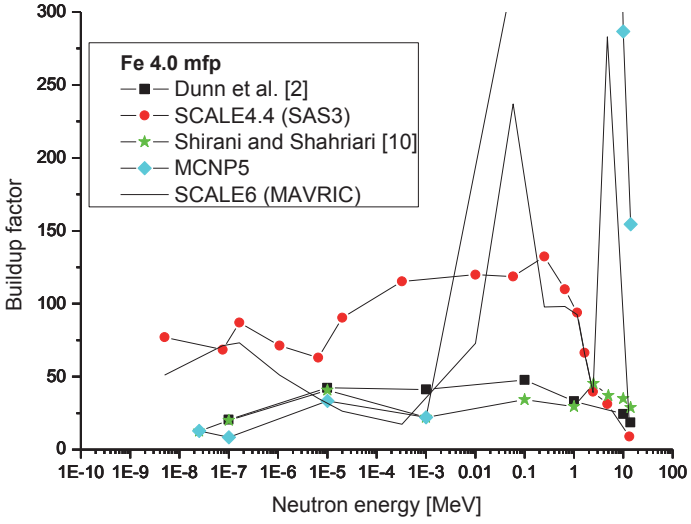

Figure 6: Comparison of buildup factors for 4 mfp thick iron shield calculated by SCALE4.4, SCALE6 and MCNP5 with reference values extracted from Dunn et al. [2] and Shirani and Shahriari [10]

In SCALE, two neutron energy groups (group 1 and group 2 as given in Table 2) were analysed. SCALE4.4, as well as SCALE6 buildup factors are higher than the ones obtained by Shin et al., but they show similar behaviour regardless of first-layer shield thickness (iron). MCNP5 buildup factor behaviour, and the values of buildup factors, show strong dependence on first-layer shield thickness which is obviously connected to MCNP5 treatment of iron in general and has to be analysed in conjunction with results depicted on Figure 6.

The precision of 5% was reached with approximately 1 million neutron histories in all cases. As far as the code's running time, the fastest is SCALE4.4, followed by SCALE6, and finally MCNP5.

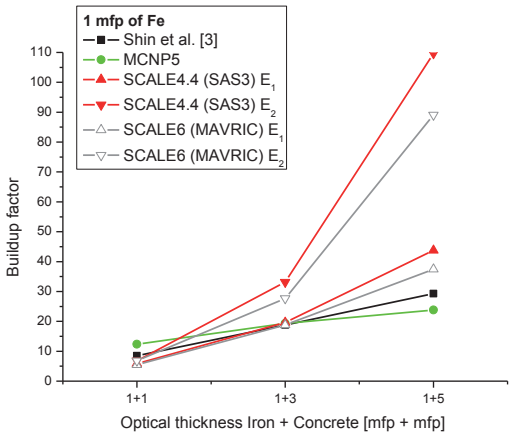

Figure 7: Comparison of buildup factors for double-layer shield comprised of 1 mfp of iron and concrete calculated by SCALE and MCNP5 with reference values extracted from Shin et al. [3]

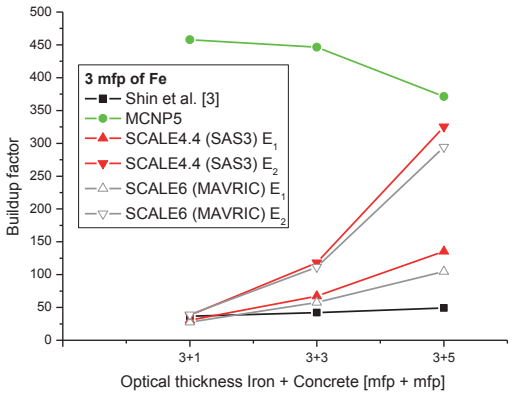

Figure 8: Comparison of buildup factors for double-layer shield comprised of 3 mfp of iron and concrete calculated by SCALE and MCNP5 with reference values extracted from Shin et al. [3]

5 CONCLUSION

In this paper three Monte Carlo codes, namely SCALE4.4 code package (SAS3 sequence), SCALE6.0 code package (MAVRIC sequence), and MCNP5, are analysed for possible application in neutron buildup factor general model development. Two simple experimental setups based on a point isotropic source in spherical and slab-like shield are modelled, and the codes are examined on accuracy, precision, running time, and ease of implementation issues.

Precision of 5% for all three codes can be obtained in reasonable running time measured in seconds or tens of seconds on Quad core 2.66 GHz personal computer. Once the input file is prepared, all three codes can be executed through batch files, and proceeding input file changes can be easily performed. Therefore, the choice of the code by which neutron buildup factor general model is to be developed is primarily based on accuracy and the vision of model applicability.

Although, MCNP5 has the possibility to explicitly define incident neutron energy, which is a desired quality for neutron buildup factor general model development, the behaviour of the code compared to behaviour of SCALE4.4, SCALE6, and reference data is rather unpredictive and requires further analysis.

On the other hand, implementation of SCALE code package for neutron buildup factor model development would imply that the model could be used only for neutron energy groups buildup factor calculations, rather than for particular neutron energy buildup factor calculation.

REFERENCES

[1] R.E. Faw, J.K. Shultis, "Radiological assessment: sources and doses", American Nuclear Society, Inc., La Grange Park, Illinois, USA, 1999

[2] W.L. Dunn, A.M. Yacout, F. O'Foghludha, "Gamma-Ray and Neutron Dose-Equivalent Buildup Factors for Infinite Slabs", Nuclear Science and Engineering, Vol. 110, 1992, pp. 134-156

[3] K. Shin, H. Kotegawa, Y. Sakamoto, Y. Nakane, H Nakashima, S. Tanaka, Y. Uwamino, S. Ban, H. Hirayama, S. Tanaka, "Point Isotropic Build-up Factors of Medium Energy Neutrons for Concrete, Iron and a Double Layer of Iron Followed by Concrete", Radiation Protection Dosimetry, Vol. 71, No. 4, 1997, pp. 269-278

[4] K. Trontl, T. Šmuc, D. Pevec, "Support vector regression model for the estimation of γ-ray buildup factors for multi-layer shields", Annals of Nuclear Energy, Vol. 34, 2007, pp. 939-952

[5] V.N. Vapnik, "Statistical learning theory", Wiley, New York, USA, 1998

[6] RSICC, "SCALE-4.4: Modular Code System for Performing Standardized Computer Analyses for Licensing Evaluation", NUREG/CR-0200, Radiation Safety Information Computational Center at Oak Ridge National Laboratory, 2009

[7] RSICC, "SCALE: A Modular Code System for Performing Standardized Computer Analyses for Licensing Evaluation", ORNL/TM-2005/39 Version 6, Radiation Safety Information Computational Center at Oak Ridge National Laboratory, 2009

[8] M.B. Chadwick, et al, „ENDF/B-VII.0: Next Generation Evaluated Nuclear Data Library for Nuclear Science and Technology", Nuclear Data Sheets, 107, 12, pp. 2931-3060, 2006.

[9] X-5 Monte Carlo Team, "MCNP — A General Monte Carlo N-Particle Transport Code, Version 5",LA-UR-03-1987, Los Alamos National Laboratory, 2008

[10] A. Shirani, E. Shahriari, "Determination of Neutron Dose-Equivalent Buildup Factors for Infinite Slabs Irradiated by Point Isotropic Neutron Sources Using the MCNP code", Journal of Sciences, Islamic Republic of Iran, Vol. 18, No. 2, 2007, pp. 177-180

Journal of Energy
VOLUME 62 Number 1–4 | 2013 Special Issue
journal homepage: http://journalofenergy.com/

24-Month Operating Cycle Containing Gadolinium Integral Burnable Absorbers for NPP Krško

Krešimir Trontl, Dubravko Pevec
University of Zagreb, Faculty of Electrical Engineering and Computing
Unska 3, 10000 Zagreb, Croatia
kresimir.trontl@fer.hr, dubravko.pevec@fer.hr

Tomislav Belavić
PRONERG d.o.o.
Lukoranska 2, 10000 Zagreb, Croatia
belavic@pronerg.hr

ABSTRACT

A few years ago Westinghouse innovations in PWR technology resulted in a proposal for a new type of integral fuel burnable absorbers containing Gadolinium. Preliminary designs of loading patterns for NPP Krško were made for 18 month fuel cycles with standard VANTAGE+ fuel type containing Integral Fuel Burnable Absorbers (IFBA) with enriched Boron, as well as newly proposed Gadolinium based absorbers. In this paper we investigate the possibility to design 24 month cycle for the NPP Krško with VANTAGE+ fuel type and Gadolinium based integral absorbers. The key fuel cycle parameters are compared to the one based on IFBAs. The analysis is performed by the latest version of FUMACS code package capable of simulating Gadolinium based integral fuel burnable absorbers.

1 INTRODUCTION

At the moment, the Nuclear Power Plant (NPP) Krško is running on 18-month cycle, although studies, like Bilić et al. [1], have been conducted almost fifteen years ago examining the possibility to implement 24-month cycle. Those studies, as well as current NPP Krško operational experience, are mostly based on standard Westinghouse fuel (Standard, Vantage5, Vantage+) and integral fuel burnable absorbers containing natural or enriched Boron (IFBA). The exceptions are a few cycles in which burnable poison rods (BPR) and KWU type of fuel have been used.

However, a few years ago Westinghouse innovations in PWR technology resulted in a proposal for a new type of integral fuel burnable absorbers containing Gadolinium. Preliminary designs of loading patterns for NPP Krško were made for 18 month fuel cycles with standard, VANTAGE+, fuel type containing IFBAs with enriched Boron, as well as newly proposed Gadolinium based absorbers [2].

In general, longer operating cycles should lead to reduction of total electricity generation costs by decrease of outage frequency and improvement of capacity factor. On the other hand, longer cycles require higher enrichment of fresh fuel containing large quantities of burnable absorbers, what leads to increase of fuel fabrication costs. Prior to analysing economic impacts of longer cycle, one has to analyse whether such a cycle would satisfy safety limits. Therefore, in this paper we investigate the possibility to design 24-month cycle for the NPP Krško with VANTAGE+ fuel type and Gadolinium based integral absorbers. The key 24-month fuel cycle parameters of the

K. Trontl, D. Pevec, T. Belavić, 24–Month Operating Cycle Containing Gadolinium Integral Burnable Absorbers for NPP Krško, Journal of Energy, vol. 62 Number 1–4 (2013) Special Issue, p. 180–188

proposed design are compared to the one based on VANTAGE+ fuel type containing IFBAs with enriched Boron. The design is performed by FUMACS-FEEC 2008 code package.

A short description of the FUMACS-FEEC 2008 code package is given in Section 2. Design of the Gadolinium based 24-month equilibrium cycle is conducted in Section 3, while the comparison of the 24-month cycles based on IFBAs containing enriched Boron and Gadolinium is performed in Section 4. Conclusion is given in Section 5, and used references are listed at the end of the manuscript.

2 FUMACS-FEEC 2008 CODE PACKAGE

The first version of the FUMACS code package was developed at "Ruđer Bošković" Institute in the year 1991 for in-core fuel management analysis of the NPP Krško core and it was designed as a stand-alone application for PC DOS environment [3]. It consisted of the PRELEO pre-processing code (preparation of ready-to-execute PSU-LEOPARD/RBI input data files), PSU-LEOPARD code (generation of a cross sections library for various fuel types, represented by polynomial coefficients depending on burnup and Boron concentration), and the MCRAC code (global analysis of PWR core using a library of cross sections generated by PSU-LEOPARD/RBI).

Throughout the years all of these codes were constantly improved and modified, with the addition of new options and calculational modules, to reflect improvements and innovations in PWR technologies. NPP Krško uprate and modernization process which took place in the year 2000, required major modifications of the code package, finally resulting in the new version of the FUMACS code package developed in the year 2001, marked as FUMACS/FEEC 2001, and built for Windows platforms [4]. In that version the first graphical user interface (GUI) was introduced in the code package and marked as FUMACS-G [5]. In the year 2005, FUMACS/FEEC 2005 version was developed with new fully automated calculational module that enabled core modeling with different integral fuel burnable absorber loadings containing enriched Boron [6]. With this new feature, long-term planning and depletion modeling of extended operating cycles has been enabled. To make the FUMACS-G, i.e., GUI, as user friendly as possible, the initial FUMACS/FEEC 2005 code package was improved with implementation of new GUI automated procedures, at the end resulting in simplification of different user actions. To reflect Westinghouse innovations, discussed in previous section, and to prepare the code package for possible implementation of NGF fuel type as well as Gadolinium based burnable absorbers in standard NPP Krško operation, the third major modification of FUMACS code package took place in the year 2008 resulting in FUMACS-FEEC 2008 code package version [7]. Upgraded version of the FUMACS code package has been verified and validated on 3 NPP Krško preliminary designed cycles using standard and NGF fuel assemblies containing enriched Boron and Gadolinium. The main goal has been to show the acceptance of the upgraded FUMACS code package in preliminary analysis for global core calculation in order to reach the predefined quality assurance requirements. Verification and validation procedure has shown satisfying deviations of the estimates of key technical and safety parameters [8].

3 24-MONTH EQUILIBRIUM CYCLE WITH GADOLINIUM

The design of the Gadolinium based 24-month equilibrium cycle started with NPP Krško preliminary designed cycle using standard fuel assemblies containing Gadolinium – Cycle 25 B [2]. All together, three transient cycles have been analysed prior to reaching desired 24-month equilibrium cycle: cycle 26 as an 18-month cycle, and cycles 27 and 28 as 24-month cycles.

Targeted length of Cycle 29 was set to 25000 MWd/tU, resulting from the assumptions of 0.9 capacity factor and a 30 days outage period.

In the Cycle 29 (Gadolinium based 24-month equilibrium cycle) 4 different fuel assembly regions are used (29A, 29B, 30A, and 30B). There are 72 fresh fuel assemblies (FA) in a split-feed

configuration from regions 30A and 30B with nominal fuel enrichment 4.750 w/o U-235 (region 30A) and 4.950 w/o U-235 (region 30B). In total 1312 Gadolinium rods, with different Gd contents are used. The details are provided in Table 1, where the type of absorber is represented by the number of rods containing Gadolinium and Gadolinium content.

Table 1 Types of Gadolinium burnable absorbers used in equilibrium cycle

Type	No. of FA from region 30 A (4.75 w/o U-235)	No. of FA from region 30 B (4.95 w/o U-235)
24 rods with 6% Gd	-	4
24 rods with 4% Gd	16	-
20 rods with 4% Gd	-	24
16 rods with 4% Gd	-	12
12 rods with 4% Gd	-	8
8 rods with 4% Gd	-	8
Total FA and Gd rods	16 / 384	56 / 928

The loading pattern for the equilibrium cycle and assemblywise power and burnup distribution for the end of the cycle (EOC) are given in Figure 1 and Figure 2, respectively.

Figure 1: Gadolinium based equilibrium cycle loading pattern

Gadolinium based equilibrium cycle stepwise power peaking factor ($F_{\Delta H}$) and critical Boron concentration are given in Table 2. Both, critical Boron concentration as well as power peaking factor, are within safety margins. Obtained cycle length was 24500 MWd/tU with capacity factor of 0.89, while the corresponding discharged burnup was 41158 MWd/tU.

Figure 2: Gadolinium based equilibrium cycle EOC assemblywise power and burnup distribution

Table 2 Stepwise power peaking factor ($F_{\Delta H}$) and critical Boron concentration for Gadolinium based equilibrium cycle

tep	B urnup	BC (ppm)	ΔH
	0	21	
	.	02.	.436
	1	15	
	50.	97.	.417
	1	15	
	000.	00.	.429
	2	16	
	000.	09.	.439
	4	17	
	000.	58.	.437
	6	18	
	000.	07.	.437
	8	17	
	000.	70.	.445
	1	16	
	0000.	63.	.450
	1	14	
	2000.	90.	.447
	1	10	
0	6000.	38.	.455
	2	53	

1	0000.	1.	.415
	2	-4.	
2	4500.		.358

4 COMPARISON OF GADOLINIUM AND BORON BASED CYCLES

In the previous section we have shown that Gadolinium based 24-month equilibrium cycle can be designed to satisfy safety requirements. In this section we compare Gadolinium and IFBA based 24-month equilibrium cycles.

For IFBA based equilibrium cycle we used identical fresh fuel split feed configuration as in Gadolinium case. Therefore, regions 30A and 30B with nominal fuel enrichment 4.750 w/o U-235 (region 30A) and 4.950 w/o U-235 (region 30B) were used. In total 7744 IFBAs containing enriched Boron were used (148 IFBA × 16 FA = 2368 IFBAs from region 30A; 48 IFBA × 8 FA + 64 IFBA × 8 FA + 92 IFBA × 12 FA + 116 IFBA × 24 FA + 148U IFBA × 4 FA = 5376 IFBAs from region 30B).

The loading pattern for the IFBA based equilibrium cycle and assemblywise power and burnup distribution for the end of the cycle are given in Figure 3 and Figure 4, respectively.

Figure 3: IFBA based equilibrium cycle loading pattern

IFBA based equilibrium cycle stepwise power peaking factor ($F_{\Delta H}$) and critical Boron concentration are given in Table 3. Both, critical Boron concentration, as well as power peaking factor, are within safety margins. Obtained cycle length was slightly over 24500 MWd/tU, with capacity factor of 0.89, while the corresponding discharged burnup was 41151 MWd/tU.

Loading pattern arrangement applicable for Gadolinium, as well as IFBA based equilibrium cycle is given in Figure 5.

Graphical representations of stepwise critical Boron concentration and power peaking factor for Gadolinium based equilibrium 24-month cycle compared to IFBA based equilibrium cycle are depicted on Figure 6 and Figure 7, respectively. There are slight differences between these two types of equilibrium cycles. Boron concentration for IFBA based cycle is slightly higher in the burnup interval ranging from 150 MWd/tU to 6000 MWd/tU, and slightly lower in the burnup interval ranging from 6000 MWd/tU to 20000 MWd/tU. Power peaking factor shows similar behaviour except that the intervals are moved towards higher values. These differences can be attributed to different characteristics of used burnable absorbers.

1 29B GC30 0.968 0.994 55218.	2 30A GD01 1.187 1.221 29650.	3 29B GC29 1.019 1.047 50882.	4 30A GD02 1.201 1.236 30943.	5 29B GC21 1.023 1.059 50753.	6 30B GD21 1.089 1.273 25090.	7 29A GC01 0.523 0.771 40001.
8 30A GD03 1.187 1.221 29650.	9 29B GC23 1.013 1.041 50622.	10 30A GD04 1.194 1.241 30901.	11 29B GC26 1.057 1.099 49317.	12 30B GD22 1.231 1.304 31319.	13 30B GD23 1.061 1.278 24743.	14 29A GC04 0.479 0.786 40190.
15 29B GC32 1.019 1.047 50885.	16 30A GD05 1.194 1.241 30902.	17 29B GC34 1.032 1.081 52109.	18 30B GD24 1.251 1.292 33244.	19 30B GD25 1.214 1.321 30431.	20 30B GD26 0.951 1.285 21424.	
21 30A GD06 1.201 1.236 30944.	22 29B GC33 1.056 1.099 49321.	23 30B GD27 1.251 1.292 33244.	24 30B GD28 1.243 1.322 31362.	25 30B GD29 1.058 1.360 24529.	26 29B GC25 0.546 0.912 41540.	
27 29B GC35 1.022 1.059 50761.	28 30B GD30 1.231 1.303 31318.	29 30B GD31 1.214 1.321 30430.	30 30B GD32 1.058 1.360 24528.	31 29B GC28 0.597 0.951 43622.		
32 30B GD33 1.089 1.272 25087.	33 30B GD34 1.061 1.278 24740.	34 30B GD35 0.951 1.285 21423.	35 29B GC31 0.546 0.911 41543.			
36 29A GC03 0.523 0.770 40000.	37 29A GC05 0.478 0.785 40246.					

Location Region	FA ID
Assembly Power	
Maximum Power	
Cumulated Burnup	

Figure 4: IFBA based equilibrium cycle EOC assemblywise power and burnup distribution

Table 3 Stepwise power peaking factor ($F_{\Delta H}$) and critical Boron concentration for IFBA based equilibrium cycle

tep	B urnup	BC (ppm)	ΔH
	0	20	
	.	63.	.431
	1	15	
	50.	92.	.414
	1	16	
	000.	97.	.433
	2	17	

K. Trontl, D. Pevec, T. Belavić, 24–Month Operating Cycle Containing Gadolinium Integral Burnable Absorbers for NPP Krško, Journal of Energy, vol. 62 Number 1–4 (2013) Special Issue, p. 180–188

	000.	91.	.438
	4	18	
	000.	75.	.448
	6	18	
	000.	48.	.457
	8	17	
	000.	40.	.459
	1	15	
	0000.	69.	.457
	1	13	
	2000.	66.	.446
	1	93	
0	6000.	1.	.412
	2	50	
1	0000.	5.	.385
	2	33.	
2	4500.		.360

The difference between discharge burnup for two types of cycles is negligible (41158 MWd/tU for Gadolinium based equilibrium cycle compared to 41151 MWd/tU for IFBA based equilibrium cycle).

IFBA based equilibrium 24-moth cycle can be slightly longer than Gadolinium based cycle. Although we compared discharge burnup for cycle length of 24500 MWd/tU it can be observed in Table 2 and Table 3 that EOC soluble Boron concentration (24500 MWd/tU) for Gadolinium based cycle is -4 ppm, while for the IFBA based cycle it is 33 ppm. That indicates that IFBA based cycle can be extended for a couple of hundreds of MWd/tU, which would also effect discharge burnup.

EOC position	BOC position
H-9	H-13
I-8	M-8
J-10	K-11
G-8	G-13
H-7	M-7
L-7	K-7
G-12	G-11
K-10	G-9
K-10	I-7
H-12	H-8
L-8	I-9
I-12	H-10
L-9	J-8
I-11	J-12
K-9	L-10
K-8	G-7

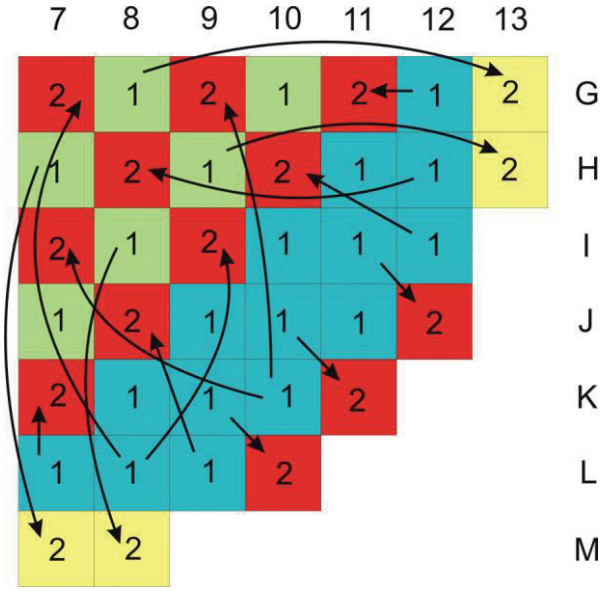

Figure 5: Equilibrium cycle loading pattern arrangement

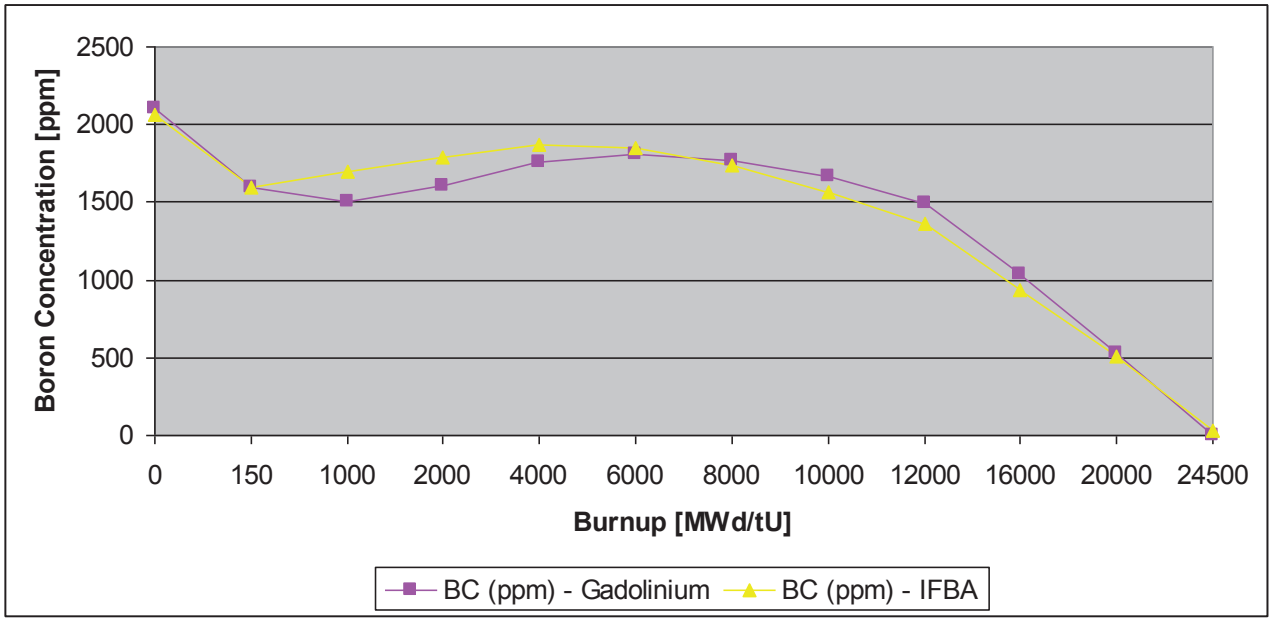

Figure 6: Stepwise critical Boron concentration for Gadolinium and IFBA based 24-month equilibrium cycles

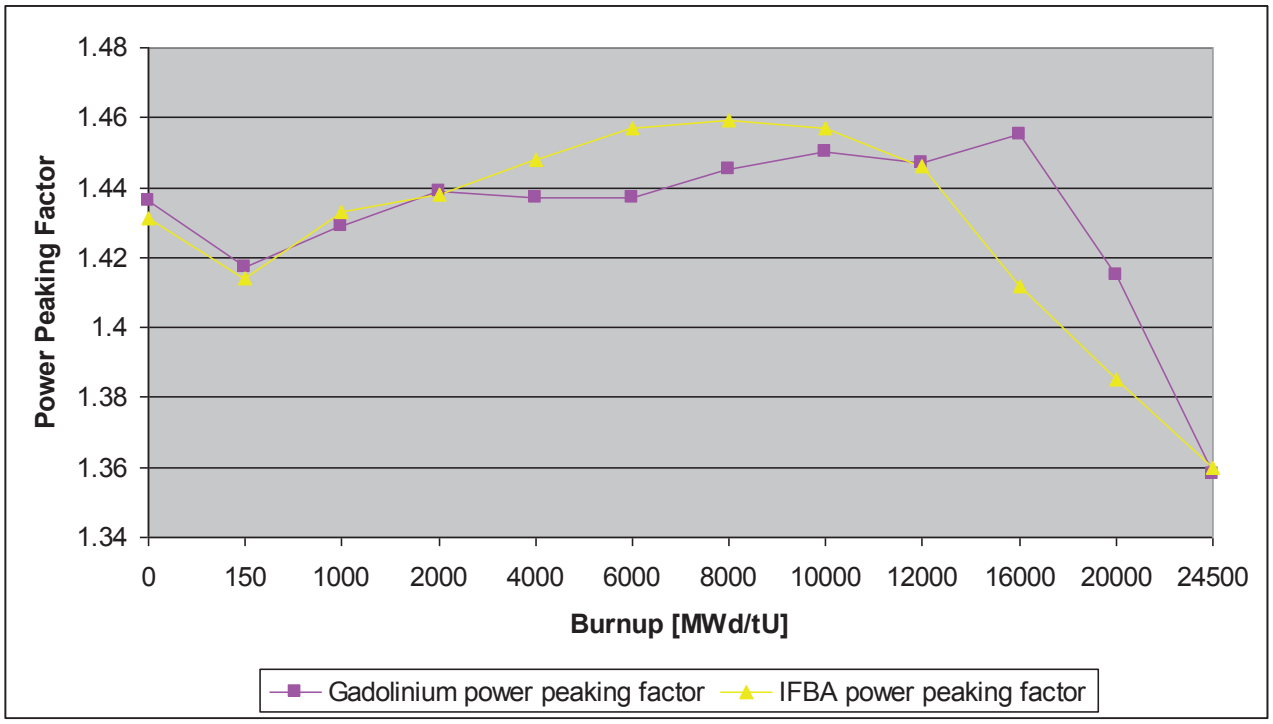

Figure 7: Stepwise power peaking factor for Gadolinium and IFBA based 24-month equilibrium cycles

5 CONCLUSION

In this paper we investigate the possibility to design 24-month equilibrium cycle for the NPP Krško with VANTAGE+ fuel type and Gadolinium based integral absorbers using FUMACS-FEEC 2008 code package. We showed that it is possible to design desired loading pattern and maintain safety parameters within prescribed limits. Obtained cycle length was 24500 MWd/tU with capacity factor of 0.89, while the corresponding discharged burnup was 41158 MWd/tU.

K. Trontl, D. Pevec, T. Belavić, 24–Month Operating Cycle Containing Gadolinium Integral Burnable Absorbers for NPP Krško, Journal of Energy, vol. 62 Number 1–4 (2013) Special Issue, p. 180–188

Designed Gadolinium based equilibrium cycle has been compared to 24-month equilibrium cycle based on VANTAGE+ fuel type containing IFBAs with enriched Boron. Obtained cycle length was slightly over 24500 MWd/tU, with capacity factor of 0.89, while the corresponding discharged burnup was 41151 MWd/tU. Comparison revealed slight differences in stepwise critical soluble Boron concentration and power peaking factor behaviour. These differences can be attributed to different characteristics of used burnable absorbers.

REFERENCES

[1] T. Bilić, D. Pevec, T. Šmuc: "Investigating a Possibility to Implement 24-month Cycle in NPP Krško", Proceedings of International Conference Nuclear Energy in Central Europe '98, p. 107-113, Čatež, Slovenia, (1998).

[2] J. Jensen-Tornehed: "Krško Fuel Management Report 2005", BTF 05-114, rev 1, NF-NEK-07-29, Westinghouse Electric Sweden AB, (2007).

[3] B. Petrović, D. Pevec, T. Šmuc: "FUMACS – Fuel Management Code System", Ruđer Bošković Institute, Zagreb, (1991).

[4] D. Pevec, D. Grgić, R. Ječmenica, K. Trontl, K. Gergeta, T. Šmuc: "Upgrade of the FUMACS Code Package", Proceedings of International Conference Nuclear Energy in Central Europe 2001, p. 113.1-113.8, Portorož, Slovenia, (2001).

[5] K. Trontl, K. Gergeta, T. Šmuc: "FUMACS-G, a Graphical User Interface for FUMACS Code Package", Proceedings of 4th International Conference Nuclear Option in Countries with Small and Medium Electricity Grids, p. 4.11.1-4.11.8, Dubrovnik, Croatia (2002).

[6] D. Pevec, T. Šmuc, K. Trontl, K. Gergeta, R. Ječmenica: "Upgrade of FUMACS Code Package for Modeling of Cycle 21 and Following Cycles, Final Report", FER-ZPF/SA/DA-TR02/05-0, Faculty of Electrical Engineering and Computing, (2005).

[7] D. Pevec, K. Trontl, R. Ječmenica, M. Matijević, D.Grgić, T. Belavić:"Upgrade of the FUMACS 2005 Code Package", Proceedings of the 8th International Conference on Nuclear Option in Countries with Small and Medium Electricity Grids, p. S7-65.1-S7-65.16, Dubrovnik, Croatia, (2010).

[8] D. Pevec, T. Šmuc, D. Grgić, K. Trontl, R. Ječmenica, K. Gergeta, M. Matijević: "Upgrade of FUMACS Code Package for Modeling of NGF and Gadolinium, Final Report", FER-ZPF/SA/DA-TR03/08-1, Faculty of Electrical Engineering and Computing, (2009).

Journal of Energy

VOLUME 62 Number 1–4 | 2013 Special Issue

journal homepage: http://journalofenergy.com/

Full Core Criticality Modeling of Gas-Cooled Fast Reactor using the SCALE6.0 and MCNP5 Code Packages

Mario Matijević, Dubravko Pevec, Krešimir Trontl, Radomir Ječmenica
University of Zagreb, Faculty of Electrical Engineering and Computing
Unska 3, 10000 Zagreb, Croatia
mario.matijevic@fer.hr, dubravko.pevec@fer.hr, kresimir.trontl@fer.hr, radomir.jecmenica@fer.hr

ABSTRACT

The Gas-Cooled Fast Reactor (GFR) is one of the reactor concepts selected by the Generation IV International Forum (GIF) for the next generation of innovative nuclear energy systems. It was selected among a group of more than 100 prototypes and his commercial availability is expected by 2030. GFR has common goals as the rest GIF advanced reactor types: economy, safety, proliferation resistance, availability and sustainability. Several GFR fuel design concepts such as plates, rod pins and pebbles are currently being investigated in order to meet the high temperature constraints characteristic for a GFR working environment. In the previous study we have compared the fuel depletion results for heterogeneous GFR fuel assembly (FA), obtained with TRITON6 sequence of SCALE6.0 with the results of the MCNPX-CINDER90 and TRIPOLI-4-D codes. Present work is a continuation of neutronic criticality analysis of heterogeneous FA and full core configurations of a GFR concept using 3-D Monte Carlo codes KENO-VI/SCALE6.0 and MCNP5. The FA is based on a hexagonal mesh of fuel rods (uranium and plutonium carbide fuel, silicon carbide clad, helium gas coolant) with axial reflector thickness being varied for the purpose of optimization. Three reflector materials were analyzed: zirconium carbide (ZrC), silicon carbide (SiC) and natural uranium. ZrC has been selected as a reflector material, having the best contribution to the neutron economy and to the reactivity of the core. The core safety parameters were also analysed: a negative temperature coefficient of reactivity was verified for the heavy metal fuel and coolant density loss. Criticality calculations of different FA active heights were performed and the reflector thickness was also adjusted. Finally, GFR full core criticality calculations using different active fuel rod heights and fixed ZrC reflector height were done to find the optimal height of the core. The Shannon entropy of the GFR core fission distribution was proved to be useful technique to monitor both fission source convergence (stationarity) and core eigenvalue convergence (k_{eff}) to fundamental eigenmode with MCNP5. All calculations were done with ENDF/B-VII.0 library. The obtained results showed high similarity with reference results.

1 INTRODUCTION

The Gas-cooled Fast Reactor is one of the reactor concepts selected by the Generation IV International Forum (GIF) for the next generation of innovative nuclear energy systems. Several GFR fuel design concepts (plates, rod pins and pebbles) are currently being investigated [1] in order to meet the high temperature constraints characteristic for a GFR working environment. GFR has common goals as the rest GIF advanced reactor types: economy, safety, proliferation resistance, availability and sustainability. Ceramic fuels have been proposed because these materials are based on compounds of carbides and nitrides, which have a good performance in the fast neutron energy spectrum. With helium used as a coolant and high operating temperatures, the GFR is expected to

have a thermodynamic efficiency of close to 50%. The GFR will use closed nuclear fuel cycle with the ability to use own depleted fuel or fuel from another reactor. This characteristic of actinides incinerator is making GFR very attractive as a sustainable technological alternative among other advanced reactors: it can be used as electric power plant, as a cogeneration plant for hydrogen production or heat production facility for any industry. Commercial availability of GFR is expected by 2030.

In this work we modeled the GFR heterogeneous core with KENO-VI/SCALE6 [2] and MCNP5 [3] Monte Carlo codes. The used codes together with nuclear data libraries are described in section 2. The GFR fuel assembly is described in section 3. Description of reactor core design is given in section 4, including: calculation of reactor core safety parameters, estimation of the axial reflector thickness, material reflector selection and estimation of the dimensions of the GFR core. Discussion of the results and effective multiplication factor (k_{eff}) of full-core criticality calculations for different active heights is given in section 5. Conclusions are given in section 6. Referenced literature is given at the end of the paper.

2 KENO-VI AND MCNP5 CODES

In this work we modeled the GFR heterogeneous core with KENO-VI/SCALE6 and MCNP5 Monte Carlo codes. Various criticality calculations for determination of reactor safety parameters were done for different heterogeneous FA models. Both codes are well established multi-functional 3D Monte Carlo codes with advanced criticality eigenvalue and shielding capabilities. KENO-VI is a functional module of CSAS6, the main analytical sequence for criticality calculations with SCALE6, while MCNP5 is a general-purpose Monte Carlo N-Particle code that can be used for neutron, photon, electron, or coupled neutron/photon/electron transport. Pointwise cross-section data [4] were used within MCNP5: auxiliary program MAKXSF prepares cross-section libraries with Doppler broadening. Multigroup neutron data in form of v7-238 were used with KENO-VI: cross-section processing was done with BONAMI (unresolved resonance energy range) and CENTRM/PMC (resolved resonance range). Both working libraries are based on the ENDF/B-VII.0 library. All the criticality calculations were performed with the following control parameters, unless told otherwise: neutron source size per cycle was 1000, initial guess for k_{eff} was 1.0, number of settling (i.e. skipped for statistics) cycles was 50 and the total cycles per run was 1000. Used CPU was QuadCore6600 with 8GB of RAM.

3 THE GFR FUEL ASSEMBLY

The geometry of GFR fuel assembly is based on a hexagonal mesh composed of 271 unit cells. The unit cell is comprised of four regions: cylindrical fuel rod in the centre (heavy metal fuel), annular cylindrical region that surrounds the fuel rod (helium gas), annular cylindrical region of cladding (silicon carbide), hexagonal outer surface that surrounds the cylindrical rod (helium gas). The fuel is composed of heavy metal uranium-plutonium carbide (80 w/o U+Pu, 20 w/o C) while mixture of silicon carbide SiC (50 w/o Si, 50 w/o C) is used for the cladding. This type of material withstands very high temperatures (> 2000 K) within high irradiation environments. Also, since SiC material is used in several reactors, a wide nuclear data-base is known based on its operating experience [5]. Helium gas is used as a coolant. All mixtures are assumed to have working temperature at T = 1200 K. Main characteristics of the unit cell and fuel assembly are taken from reference [6]. KENO-VI and MCNP5 model of heterogeneous GFR fuel assembly is depicted in Figure 1.

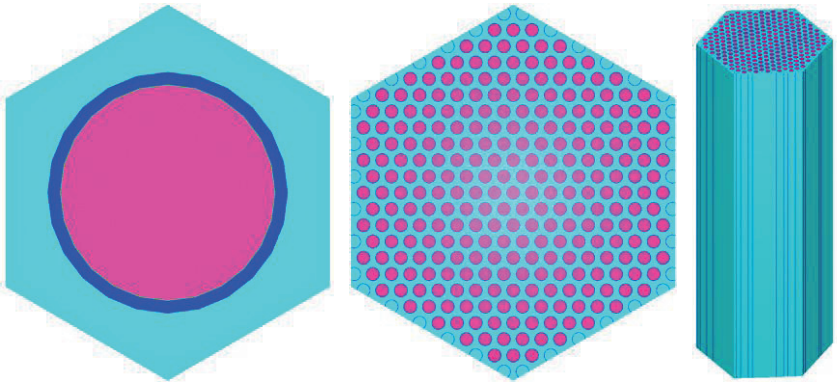

Figure 1: Elements of GFR fuel assembly (unit cell, cross sectional view, stereometric view)

4 THE GFR CORE DESIGN

In this section a calculational model of FA design is given, which includes: calculation of reactor safety parameters, estimation of the axial reflector thickness and material reflector selection. Estimation of the dimensions of the reflected GFR core is given at the end of the section [7].

4.1 Reactor safety parameters

The safety parameters which were analysed were reactivity coefficients due to variations in fuel temperature and coolant density. The first parameter is Doppler coefficient, because it is related to the resonance broadening effect when temperature of the fuel increases. The calculations were done for fuel temperatures of: 300, 400, 500, 600, 800, 900 and 1200 K. The second parameter is important for postulated loss of coolant accident (i.e. pressure drop in a core) which results in a decrease of coolant mass density. The calculations were done for He density values of: 0.01, 0.005, 0.001, 0.0001 and 0.00001 g/cm^3. Monte Carlo parameters for this part of calculations were 5000 neutrons per cycle and 1000 cycles. These calculations were done for FA of 100 cm active height and 100 cm of axial reflector (ZrC). Reflection conditions (i.e. mirror boundary) were applied on the six lateral sides and escape conditions (i.e. vacuum boundary) were applied on the two axial sides.

4.2 Estimation of the axial reflector thickness

The FA with active height of 100 cm and ZrC reflector was used for criticality calculations for different axial reflector thickness: 25, 50, 60, 75 and 100 cm. The calculations were done for cold (300 K) and hot (1200 K) conditions, with reflective conditions on six lateral sides and escape conditions on two axial sides.

4.3 Reflector material selection

The desirable characteristics of any reactor reflector are: high scattering to absorption cross-section, high logarithmic energy decrement, thermal stability and radiation endurance. For the purpose of selecting optimal material of GFR reflector, we tested three materials. ZrC (Zr 90.5 w/o, C 9.5 w/o) is a ceramic material, good reflector, candidate to be used in generation IV reactors. SiC (Si 90.5 w/o, C 9.5 w/o) is a ceramic material, at present it is a proven industrial material with production on a large scale. Unat (natural uranium) is a metallic material, in fast reactor systems it has been used as reflector/blanket material. The FA model with active height of 100 cm and 60 cm of axial reflector was used with reflective conditions on six lateral sides and escape conditions on two axial sides.

4.4 Reactor core dimensions

In order to investigate reactor core dimensions several test-calculations were performed: core radial size, fuel active height, reflector radial and axial thickness. The core configuration is based on two zones: the inner zone with fuel and control elements, and the outer zone with reflective elements. Different core sizes were simulated by gradually increasing the number of fuel assemblies. Therefore, an equivalent diameter of the core was estimated: hypothetical circular area is the sum of the individual areas of each fuel assembly. Former analyses of FA reflector proposed ZrC with height of 60 cm, because at that height saturation of reactivity is reached. Hence, final full-core criticality calculations with different active height were performed, including 78 fuel elements, 7 control elements and 84 reflective elements. The reference value of the k_{eff} for estimation of the active height of the GFR core was selected from values proposed by other authors [8]: the value of 6000 pcm of excess reactivity conforms active height of 100 cm. Boundary conditions for the full-core model are vacuum for all sides. Monte Carlo parameters were 5000 neutrons per cycle and 1000 cycles, with 50 cycles skipped in order to spatial fission source to converge.

5 DISCUSSION OF THE RESULTS

5.1 Results for reactor safety parameters

Negative values of fuel temperature reactivity coefficient (Table 1 and 2) and reactivity coefficient due to the pressure drop (Table 3 and 4) are shown. The negative effect in Δk_{eff} produced by the increase of fuel temperature is greater than the positive effect produced by the coolant density loss. The total combined effect is thus negative, as required by safety directions.

Table 1 Doppler results for KENO-VI

T(K)	k_{eff}	1σ (pcm)	Δk_{eff}	ΔT(K)	$(\Delta k_{eff} / k_{eff}) / \Delta T$ (pcm/K)
300	1.27033	53	0.00000	*	*
400	1.26166	48	-0.00867	100	-6.872
500	1.25588	50	-0.00578	100	-4.602
600	1.25216	55	-0.00372	100	-2.971
800	1.24343	48	-0.00873	200	-3.51
900	1.24098	51	-0.00245	100	-1.974
1200	1.23313	49	-0.00785	300	-2.122

Table 2 Doppler results for MCNP5

T(K)	k_{eff}	1σ (pcm)	Δk_{eff}	ΔT(K)	$(\Delta k_{eff} / k_{eff}) / \Delta T$ (pcm/K)
300	1.26352	54	*	*	*
400	1.25507	54	-0.00845	100	-6.733
500	1.24862	54	-0.00645	100	-5.166
600	1.24515	52	-0.00347	100	-2.787
800	1.2386	53	-0.00655	200	-2.644
900	1.23612	53	-0.00248	100	-2.006
1200	1.22963	51	-0.00649	300	-1.759

Comparison of fuel assembly k_{eff} results for KENO-VI and MCNP5 to reference MCNPX results are depicted in Fig.2. Differences in obtained k_{eff} are depicted in Fig.3.

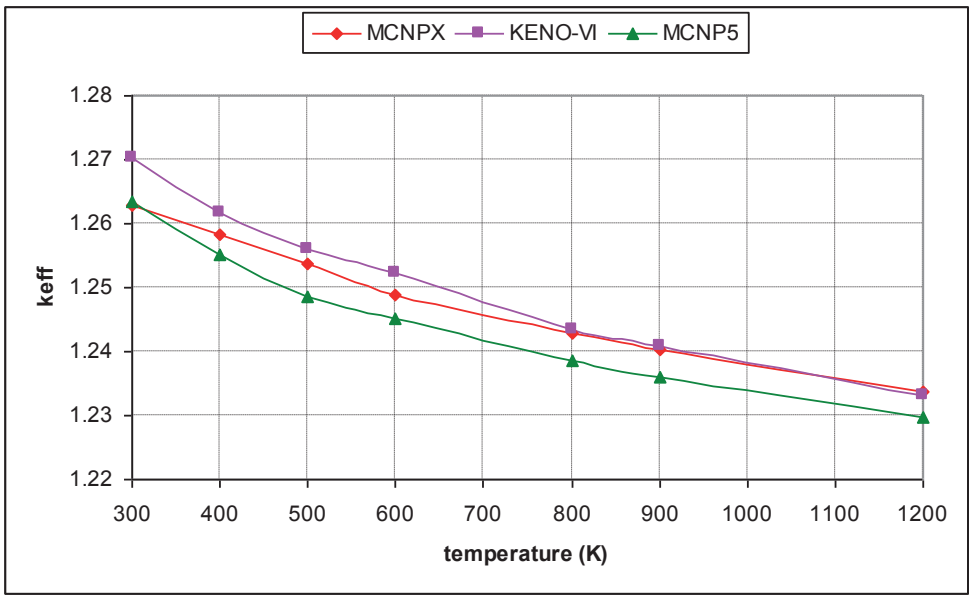

Figure 2: Comparison of KENO-VI and MCNP5 k_{eff} to MCNPX

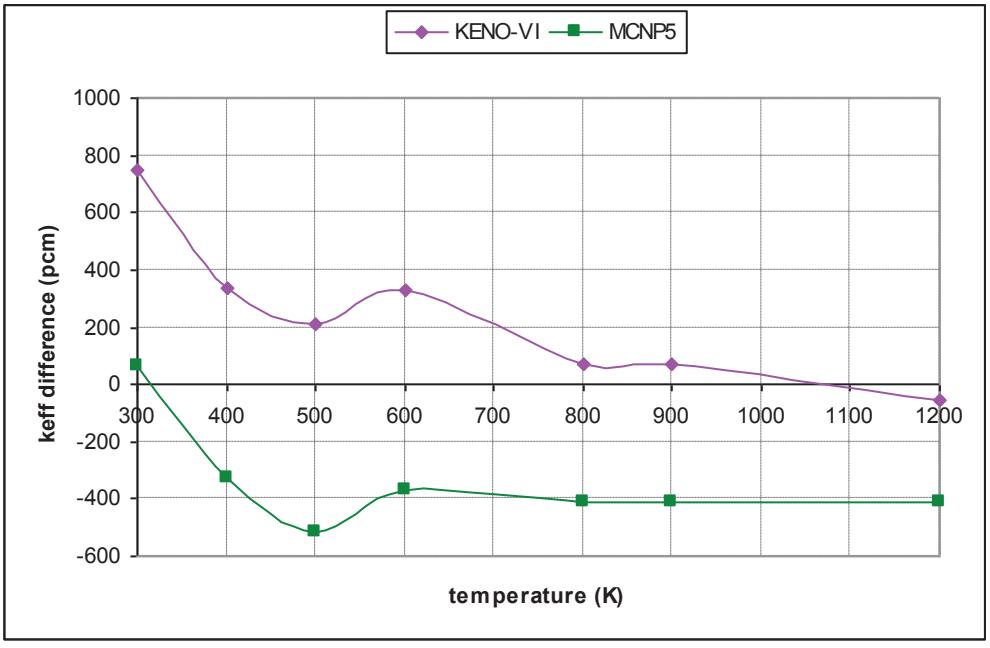

Figure 3: KENO-VI and MCNP5 k_{eff} differences to MCNPX

Table 3 Coolant density reactivity coefficient for KENO-VI

density He (g/cm^3)	k_{eff}	1σ (pcm)	$\Delta\rho$ (g/cm^3)	Δk_{eff}	(Δk_{eff} / k_{eff})/ $\Delta\rho$ (1/g/cm^3)
0.01	1.23376	22	*	*	*
0.005	1.23663	22	-0.005	0.00287	-0.574
0.001	1.23926	20	-0.004	0.00263	-0.6575
0.0001	1.24001	22	-0.0009	0.00075	-0.83
0.00001	1.2403	22	-0.00009	0.00029	-3.22

Table 4 Coolant density reactivity coefficient for MCNP5

density He (g/cm^3)	k_{eff}	1σ (pcm)	$\Delta\rho$ (g/cm^3)	Δk_{eff}	$(\Delta k_{eff} / k_{eff}) / \Delta\rho$ ($1/g/cm^3$)
0.01	1.22883	24	*	*	*
0.005	1.23203	22	-0.005	0.0032	-0.519
0.001	1.23472	24	-0.004	0.00269	-0.545
0.0001	1.23552	23	-0.0009	0.00080	-0.719
0.00001	1.23587	23	-0.00009	0.00035	-3.147

5.2 Results for axial reflector thickness

KENO-VI and MCNP5 results, for both cold (300 K) and hot (1200 K) conditions, are shown in Fig.4. Cold (300 K) and hot (1200 K) conditions are shown. One can observe high similarity between the two codes, i.e. small differences in k_{eff} are evident. Average Monte Carlo standard deviation of k_{eff} is ~ 50 pcm. Important result indicated by Fig.4 is saturation in reactivity gain [7] within reflector thickness of 60 cm. Thus, 60 cm of axial reflector thickness seems satisfactory for FA model with active height of 100 cm.

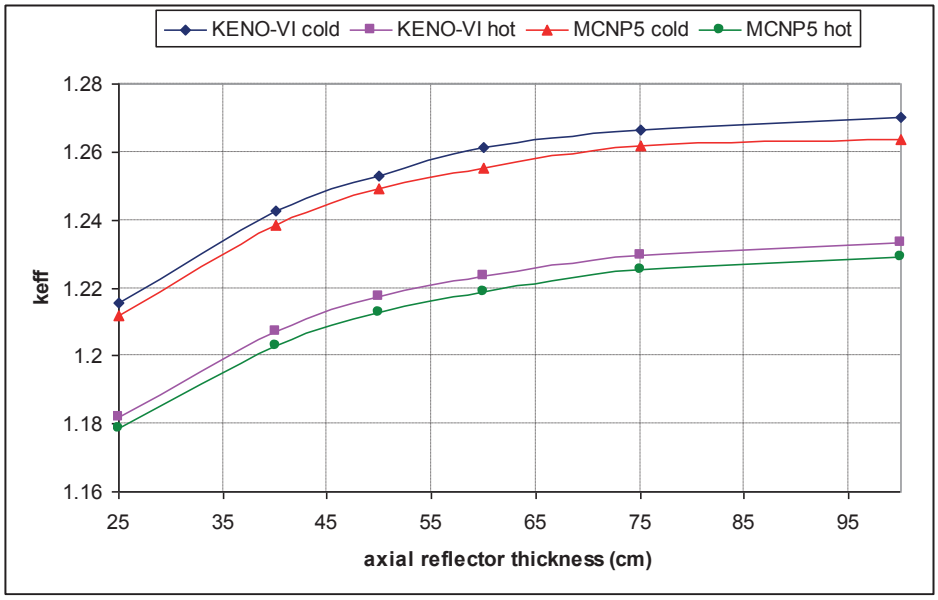

Figure 4: Axial reflector thickness results for KENO-VI and MCNP5 (300K and 1200K)

5.3 Results for reflector material

The results depicted in Fig.5 are for a model of FA with 100 cm of active height and an axial reflector thickness of 60 cm. Three reflector materials were tested (ZrC, SiC and Unat), but only ZrC and SiC reveal good reflector characteristics. Calculations for cold and hot conditions were done. In summary, ZrC is the material with the largest contribution to reactivity of the critical system and was selected as a reflector for full-core modeling.

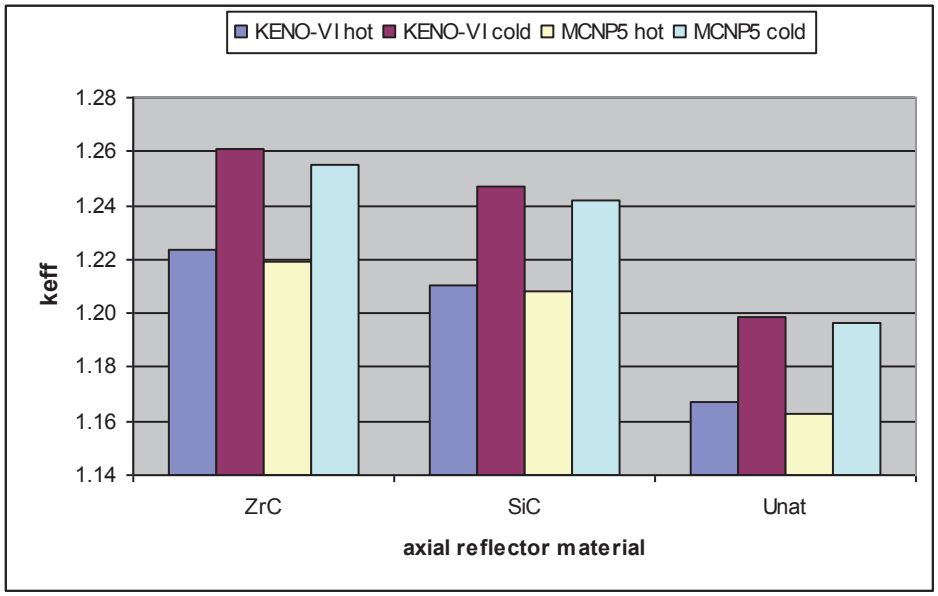

Figure 5: Reflector material results for KENO-VI and MCNP5 (300 K and 1200 K)

5.4 Results for reactor core dimensions

In order to investigate reactor core dimensions, several test-calculations were performed using KENO-VI and MCNP5 codes. Hot temperature condition (1200 K) was applied with escape conditions on all core sides. Initial calculations with bare and later reflected core suggested equivalent core diameter of 180-220 cm, which matches 61-91 FA in core. Again, saturation in reactivity is observed for equivalent diameter greater than 180 cm, so final proposed size of a reflected GFR core was 78 FA (eq.diameter of 207.04 cm). Additionally, seven preliminary locations of control assemblies were selected with control rods totally withdrawn from the core (He in active volume). The lateral core reflector comprises 84 reflective assemblies (ZrC in active volume). The GFR radial core configuration is shown in Fig.6.

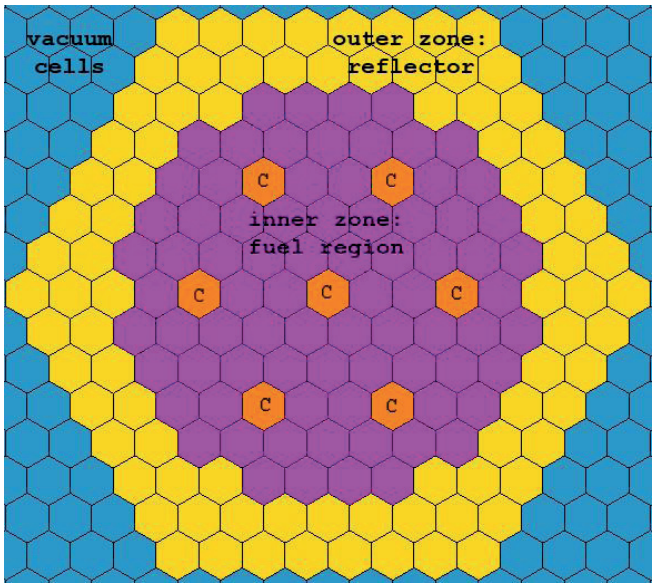

Figure 6: The GFR core axial midplane (C – control assembly)

Results for full-core criticality calculations with KENO-VI and MCNP5 with different core heights are shown in Table 5 together with reference results obtained with TRIPOLI-4. The

reference value of the k_{eff} for estimation of the active height of the GFR core was selected from values proposed by other authors: the value of 6000 pcm of excess reactivity conforms active height of 100 cm. It is evident that active height of 100 cm is a satisfactory value in terms of reactivity gain.

Table 5 Core criticality results for different active heights

core active height (cm)	***H/D***	**TRIPOLI-4**		**KENO-VI**		**MCNP5**	
		k_{eff}	1σ (pcm)	k_{eff}	1σ (pcm)	k_{eff}	1σ (pcm)
50	0.24	0.92998	29	0.94059	26	0.93571	25
60	0.29	0.97113	30	0.98006	25	0.97573	26
70	0.34	1.00451	32	1.01172	30	1.00674	26
80	0.39	1.03035	31	1.03524	28	1.03147	26
90	0.43	1.05181	33	1.05607	25	1.05155	25
100	0.48	1.07075	34	1.07255	29	1.06811	26

The parameter *H/D* (height-to-diameter) is related to the pressure drop inside the core [7], thus proposed core of 100 cm and *H/D* of 0.48 has a pressure drop of ~ 1 bar. Differences between KENO-VI and MCNP5 to reference TRIPOLI-4 results are shown in Fig.7. Constant offset of cca 500 pcm is observable for all core active height, although MCNP5 values are in better agreement to TRIPOLI-4. The values of k_{eff} for different core heights are shown in Fig.8. Typical CPU run time for full-core criticality calculation with KENO-VI and MCNP5 was about 4 h on average.

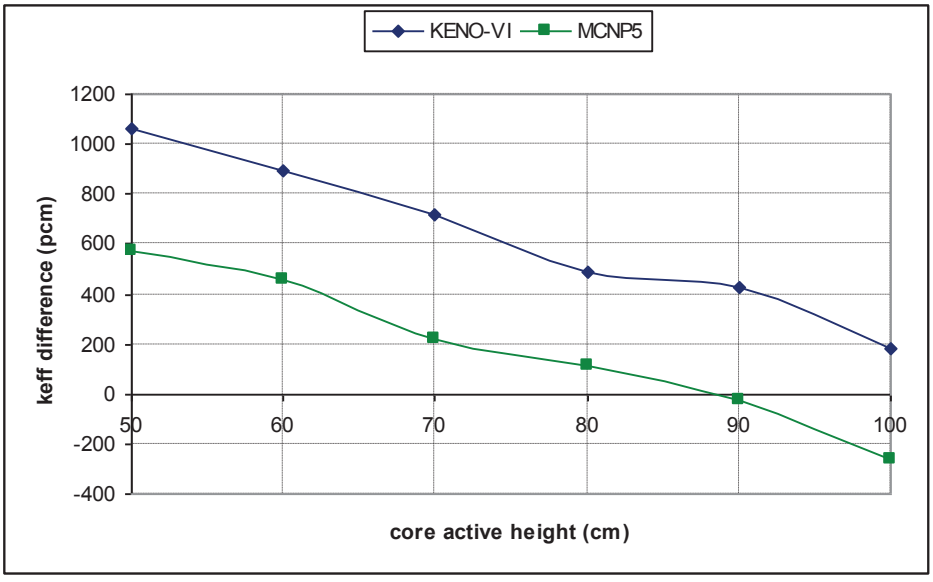

Figure 7: Differences of k_{eff} for KENO-VI and MCNP5 to TRIPOLI-4

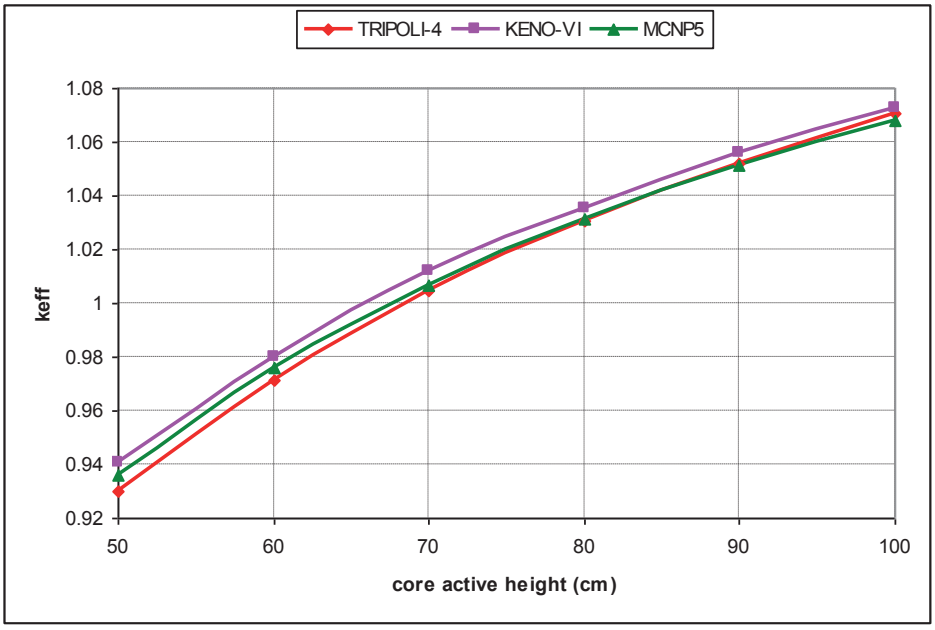

Figure 8: Values of k_{eff} for TRIPOLI-4, KENO-VI and MCNP5

Calculations of track length volume fluxes of GFR core were also done with MCNP5 (FMESH card) for criticality part, the tallies are for one fission neutron being born in the system at the start of a cycle. The user mesh was 100x100x100 cells over entire core with 100 cm height. The volume flux mesh tally is shown in Fig.9 for axial and radial midplane.

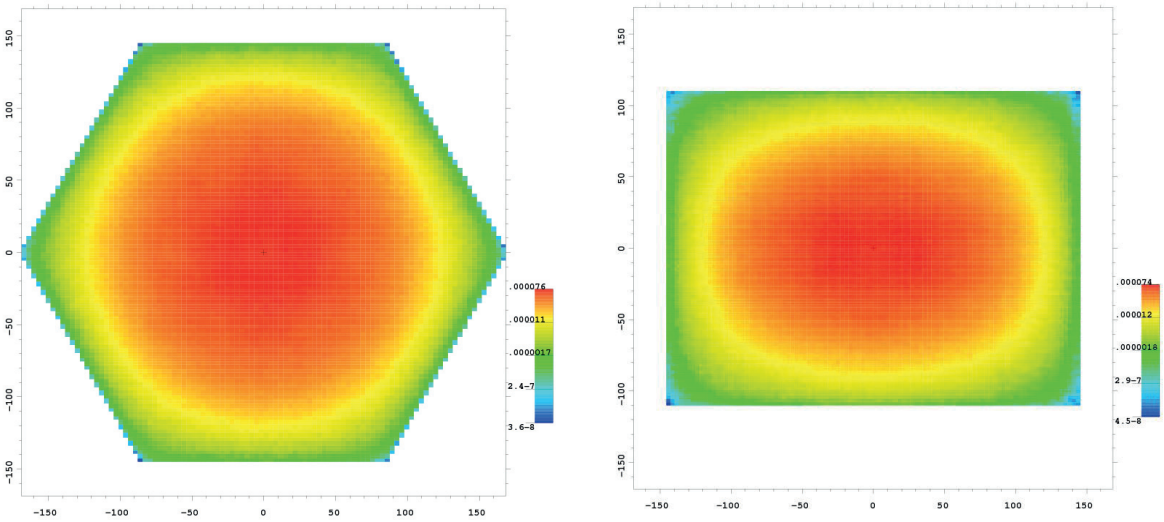

Figure 9: Track length volume flux for GFR core (MCNP5 results)

These tally quantities (i.e. user desirable results) are accumulated only after the inactive cycles are finished, after the spatial fission distribution attained eigenmode. To assist user in assessing the convergence of the fission source spatial distribution, MCNP5 computes a Shannon entropy[3,9] of the fission source distribution H_{src}. It is a well-known concept from information theory, and provides single cycle-wise number for convergence characterization. As the source distribution approaches stationarity the Shannon entropy converges to a single steady-state value. To calculate H_{src}, source distribution must be discretizied over 3D mesh grid with N_s elementary boxes to track a number of normalized fission sites P_j in it. Then, the Shannon entropy of a fission source distribution for every cycle is:

$$H_{src} = - \sum_{j=1}^{N_s} P_j \times \ln_2(P_j).$$

H_{src} varies between 0 for a point distribution to $\ln_2(N_s)$ for a uniform distribution. Plot of Shannon entropy vs. cycle number for core height of 100 cm is shown in Fig.10. Selected number of inactive cycles (50) in this paper was more than conservative, since stationarity of a source is reached about cycle 10.

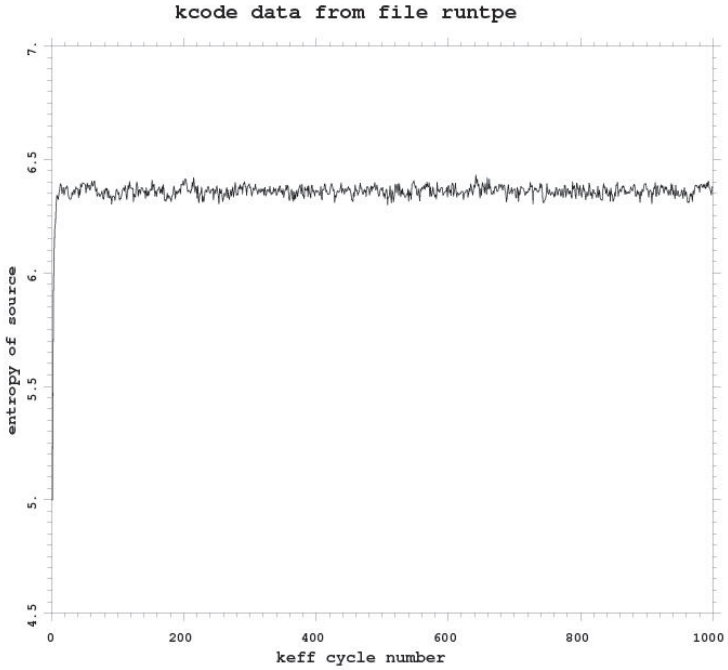

Figure 10: Shannon entropy of fission source distribution (MCNP5 results)

6 CONCLUSIONS

In this work we modeled a pin-type GFR heterogeneous FA (U+Pu carbide fuel, SiC clad, He coolant), and later full-core with KENO-VI and MCNP5 Monte Carlo codes. Calculational results of reactor safety parameters, axial reflector thickness and material reflector selection are first given and compared. The combined temperature reactivity effect is negative since Doppler effect is dominant over loss of coolant density case. A good value of axial reflector thickness was found to be 60 cm, since saturation in reactivity is observed. Zirconium carbide (ZrC) was selected as a best reflector material. Finally, the results of critical GFR core dimensions are given. Equivalent core diameter was found to be 207.04 cm, which corresponds to core of 78 fuel elements, 7 control elements and 84 reflector elements. Thus, proposed GFR core has an active height of 100 cm with ZrC axial reflector of 60 cm.

Overall, the obtained results are showing high similarity with reference results (MCNPX for FA calculations and TRIPOLI-4 for core calculations). Also, fission source distribution stationarity with Shannon entropy check in MCNP5 was found to be quite useful technique to determine number of inactive cycles in Monte Carlo criticality calculations.

REFERENCES

[1] J.C. Garnier et al., "Contribution to GFR design option selection", Proceedings of ICAPP06, Reno, USA, June 4-8, 2006.

[2] "SCALE: A Modular Code System for Performing Standardized Computer Analyses for Licensing Evaluation", ORNL/TM-2005/39 Version 6, Radiation Safety Information Computational Center at Oak Ridge National Laboratory.

[3] X-5 Monte Carlo Team, "MCNP – A General N-Particle Transport Code, Version 5 – Volume I: Overview and Theory", LA-UR-03-1987, Los Alamos National Laboratory (April, 2003).

[4] M.B. Chadwick, et al, „ENDF/B-VII.0: Next Generation Evaluated Nuclear Data Library for Nuclear Science and Technology", Nuclear Data Sheets, 107, 12, pp. 2931-3060, 2006.

[5] M.K. Meyer, Report on the Feasibility of GFR Fuel for Minor Actinide Management, Argone National Laboratory, University of Chicago, 2004.

[6] R.Reyes-Ramirez et al., „Comparison of MCNPX-C90 and TRIPOLI-4-D for fuel depletion calculations of a Gas-cooled Fast Reactor", Annals of Nuclear Energy, 37, pp. 1101-1106, 2010.

[7] C. Martin-de-Campo, et al., „Contributions to the neutronic analysis of a gas-cooled fast reactor", Annals of Nuclear Energy, 38, pp. 1406-1411, 2011.

[8] J. Krepel et al., „EQL3D: ERANOS based equilibrium fuel cycle procedure for fast reactors", Annals of Nuclear Energy, 36, pp. 550-561, 2009.

[9] F.B. Brown, „On the Use of Shannon Entropy of the Fission Distribution for Assessing Convergence of Monte Carlo Criticality Calculations", PHYSOR-2006, September 10-14, 2006.

Journal of Energy
VOLUME 62 Number 1–4 | 2013 Special Issue
journal homepage: http://journalofenergy.com/

Comparison of the SCALE, SERPENT and MCNP Criticality Safety Calculation of the NPP Krško Spent Fuel Pool

Marjan Kromar
"Jožef Stefan" Institute
Reactor Physics Division
Jamova 39, 1001 Ljubljana, Slovenia
marjan.kromar@ijs.si

Bojan Kurinčič
Nuclear Power Plant Krško
Engineering Division - Nuclear Fuel & Reactor Core
Vrbina 12, 8270 Krško, Slovenia
bojan.kurincic@nek.si

ABSTRACT

Criticality safety reanalyzes of the NPP Krško spent fuel pool has been performed. Limiting criticality cases at optimal moderation conditions are calculated using different SCALE code versions (SCALE-4.4a, SCALE-5.1 and SCALE-6.1) with 44-group ENDF/B-V and 238-group ENDF/B-VII.0 derived cross section libraries. Relative small discrepancies are observed. Additional verification is provided with SERPENT and MCNP5 codes, which are capable to take into account neutron continuous energy cross section library based on ENDF/B-VII.0 files. Comparison has shown that the results of the pool design calculations are conservative, precluding racks criticality even at optimum moderation conditions.

1 INTRODUCTION

Development of the computer hardware and improvements in the neutron cross-section libraries enables more and more accurate calculations of the neutron transport determined with the Monte Carlo codes. With the increased reliance on computational tools comes the need and requirement for redundant validation of performed criticality safety analyses by alternate criticality codes. Design calculations of the NPP Krško spent fuel pool have been performed almost 10 years ago [1,2]. SCALE [3] versions 4.4a and 5.0 with the 44-group ENDF/B-V derived cross section library 44GROUPNDF5 have been applied. Since then, new codes and neutron libraries have been developed. The limiting criticality calculations of the NPP Krško spent fuel pool are repeated using the latest SCALE versions and the ENDF/B-VII.0 library. Additional verification is provided with SERPENT [4,5] and MCNP [6] codes, which are capable to take into account neutron continuous energy cross section library.

2 METHODS AND MODELS

Criticality safety investigation of the NPP Krško wet spent fuel storage has been performed. NPP Krško is a 2-loop Westinghouse plant with a gross electrical output of 730 MW. The core consists of 121 fuel assemblies. Each assembly has 235 fuel rods arranged in a 16×16 array. The remaining 21 positions are intended for control rods and the central instrumentation channel. Used

fuel is stored in the storage pool, where two types of storage racks are implemented. Present analysis considers old racks configuration.

One storage cell with periodic boundary condition in the radial direction (representing infinite array of cells) has been applied in all cases. The radial and axial storage cell cross sections are presented in Figure 1. Water is represented in blue, UO_2 with red, cladding with light green. The stainless steel cell frame is in violet. Concrete structure of the pool is in light brown on the bottom of the right figure. It should be noted, that the aspect ratio of the axial slice is not preserved to allow reasonable geometrical presentation.

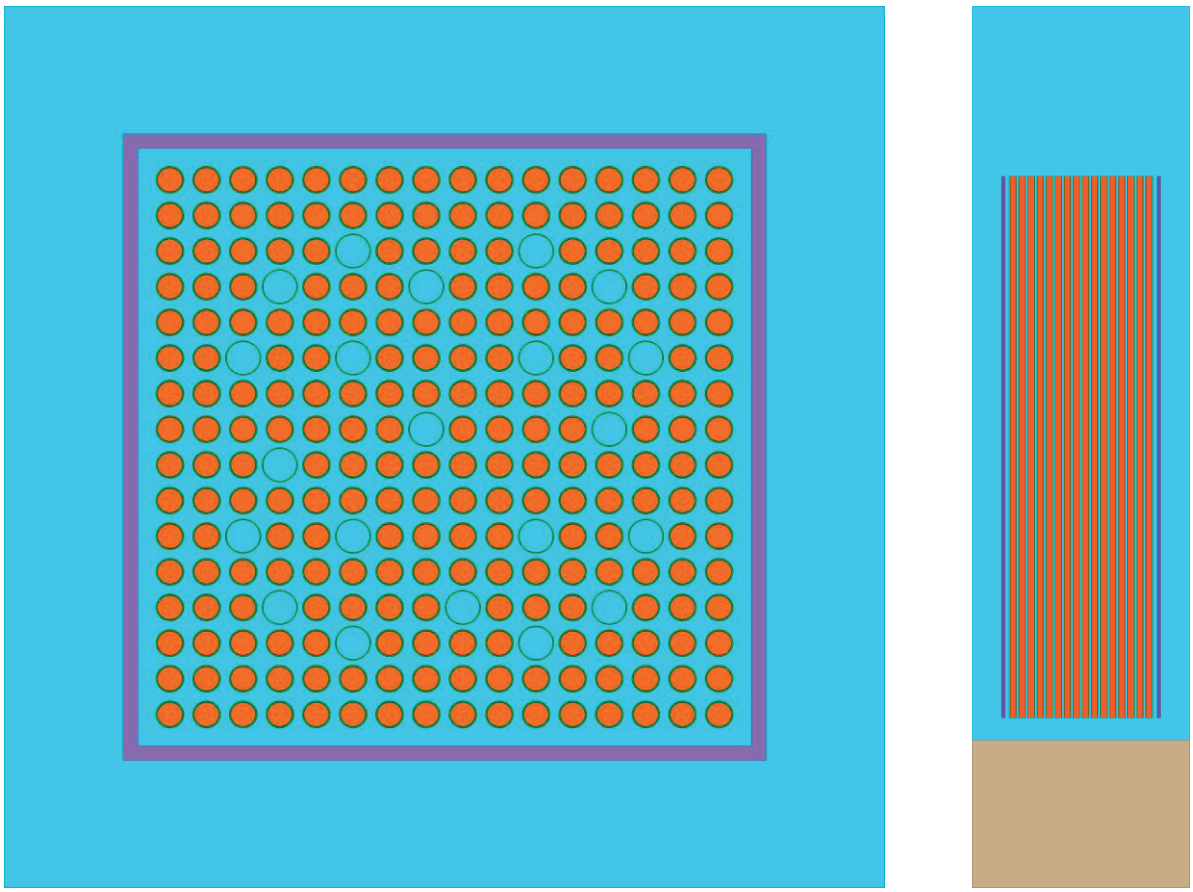

Figure 1: Geometrical layout of the NPP Krško storage cell, old racks

The design analysis [1,2] has shown that the limiting case (maximal k_{eff}) occurs at low water densities (optimal moderation). In such scenario with boiling pool water, fuel cooling is obstructed. Due to decay heat, temperature of the fuel could exceed temperature of the pool water. However, reactivity of the system would decrease with increasing fuel temperature due to the Doppler resonance broadening. At water temperature of 120 °C, water starts to boil at 2 bars. Such pressure corresponds to the depth of 10 m covering the storage of the fuel assemblies in the NPP Krško storage pool. Therefore, it is reasonably conservative to apply temperature level of 120 °C in the optimal moderation calculations. The highest possible fuel enrichment of 5 % has been considered in all cases.

The SCALE code package [3] is a comprehensive modeling and simulation suite for nuclear safety analysis and design that is developed and maintained by Oak Ridge National Laboratory (ORNL). It provides a verified and validated, user-friendly tool set for criticality safety, reactor physics, radiation shielding, radioactive source term characterization, and sensitivity and

uncertainty analysis. SCALE criticality calculations presented in the paper have been performed using the standard CSAS25 sequence. This control sequence activates the cross-section processing codes BONAMI, to provide resonance corrected cross sections in the unresolved resonance range, and WORKER, CENTRM and PMC, to provide resonance-corrected cross sections in the resolved resonance range. KENO V.a uses the processed cross sections and calculates the k_{eff} of three-dimensional (3-D) system models. The following code versions and neutron cross section libraries were used:

- SCALE-4.4a with 44-group ENDF/B-V derived cross section library 44GROUPNDF5 (updated 7/29/99).
- SCALE-5.1 with 44-group ENDF/B-V derived cross section library 44GROUPNDF5 (updated 3/25/2004).
- SCALE-6.1 with:
  - 44-group ENDF/B-V derived cross section library 44GROUPNDF5 (updated 3/25/2004) and
  - 238-group ENDF/B-VII.0 derived cross section library V7-238 (updated 12/17/09).

SERPENT [4] is a three-dimensional continuous-energy Monte Carlo reactor physics burnup calculation code, developed at the VTT Technical Research Centre of Finland. It uses a continuous energy neutron cross section library in an ACE format based on the ENDF/B-VII.0 evaluated nuclear data library [5]. The code is specialized for two-dimensional lattice physics calculations, but the universe-based geometry description allows the modeling of complicated three-dimensional geometries as well. SERPENT has the option to use a built-in Doppler broadening routine to adjust nuclide temperatures before the actual Monte Carlo calculation is performed.

MCNP [6] is a general-purpose Monte Carlo N–Particle code that can be used for neutron, photon, electron, or coupled neutron/photon/electron transport, including the capability to calculate eigenvalues for critical systems. The code treats an arbitrary three-dimensional configuration of materials in geometric cells bounded by first- and second-degree surfaces and fourth-degree elliptical tori. Pointwise (continuous energy) cross-section data are used. The calculations reported in this paper were performed with version 5.1.40 of the code and ENDF/B-VII.0 evaluated nuclear data library. An auxiliary processing code MAKXSF was used to provide case specific neutron cross section library at 120 °C.

3 RESULTS AND DISCUSSION

Two cases are examined. Nominal boron concentration in the pool water is limited by the Technical Specifications [7] to 2000 ppm. In addition, k_{eff} is determined also for a hypothetical case where no soluble boron is present in the pool. It should be mentioned here, that the pool has been designed to preclude criticality when at least 2000 ppm of soluble boron is present in the pool water [1,2,7]. The loading curve has been determined, which relates fuel assembly enrichment and discharged burnup. Only assemblies with sufficiently high burnup are allowed to be stored in the pool. Therefore, assemblies with 5 % enrichment and no burnup are not allowed to be stored in this configuration, since they exhibit too high multiplication factor. However, since only relative comparison has been performed in presented analysis, fresh fuel with highest possible 5 % enrichment was considered.

3.1 Comparison of different SCALE versions

Results obtained with different SCALE code versions are presented in Tables 1-2 and Figures 2-3. Uncertainties listed in the k_{eff} columns represent statistical error of 1 σ. Although the exact versions of the code and library used in the pool design calculations are not available, sample calculations on the several design input files have shown that the SCALE-4.4a with 44-group ENDF/B-V derived cross section library 44GROUPNDF5 replicates pool design calculations almost inside statistical error. Differences to this basic setup are shown in the tables and can be seen as differences to the design calculations. SCALE 5.1 gives slightly higher multiplication factor at low densities and lower k_{eff} at higher densities. SCALE 6.1 with the same 44GROUPNDF5 library is lower at entire range. Differences when 238-group ENDF/B-VII.0 library is applied are even more negative in the 2000 ppm case. Almost the same trend is observed when no soluble boron is present. Since it is reasonable to assume that the newer code and library versions with highest number of energy groups are more accurate, we can safely deduce that the design calculations have been performed in conservative manner.

Table 1: Comparison of the multiplication factors obtained with different versions of SCALE, 2000 ppm of boron

	SCALE 4.4a 44-group ENDF/B-V	SCALE 5.1 44-group ENDF/B-V		SCALE 6.1 44-group ENDF/B-V		SCALE 6.1 238-group ENDF/B-VII.0	
Density [g/cm3]	k_{eff}	k_{eff}	Difference	k_{eff}	Difference	k_{eff}	Difference
0.05	0.96581 ± 0.00007	0.96793 ± 0.00007	0.00212	0.95765 ± 0.00007	-0.00816	0.94580 ± 0.00007	-0.02001
0.08	1.00995 ± 0.00008	1.01148 ± 0.00008	0.00153	1.00402 ± 0.00008	-0.00593	0.99519 ± 0.00008	-0.01476
0.10	1.01778 ± 0.00008	1.01927 ± 0.00007	0.00149	1.01285 ± 0.00007	-0.00493	1.00552 ± 0.00008	-0.01226
0.12	1.01491 ± 0.00007	1.01620 ± 0.00008	0.00129	1.01070 ± 0.00008	-0.00421	1.00504 ± 0.00008	-0.00987
0.15	0.99819 ± 0.00008	0.99903 ± 0.00008	0.00084	0.99478 ± 0.00008	-0.00341	0.99085 ± 0.00008	-0.00734
0.20	0.95477 ± 0.00008	0.95464 ± 0.00008	-0.00013	0.95189 ± 0.00008	-0.00288	0.94977 ± 0.00009	-0.00500
0.30	0.86147 ± 0.00009	0.86035 ± 0.00009	-0.00112	0.85874 ± 0.00008	-0.00273	0.85932 ± 0.00008	-0.00215
0.40	0.79065 ± 0.00009	0.78868 ± 0.00008	-0.00197	0.78798 ± 0.00008	-0.00267	0.78923 ± 0.00009	-0.00142
0.50	0.74596 ± 0.00009	0.74321 ± 0.00008	-0.00275	0.74291 ± 0.00008	-0.00305	0.74479 ± 0.00009	-0.00117
0.60	0.72116 ± 0.00009	0.71792 ± 0.00008	-0.00324	0.71834 ± 0.00009	-0.00282	0.72014 ± 0.00009	-0.00102
0.70	0.71099 ± 0.00009	0.70742 ± 0.00009	-0.00357	0.70796 ± 0.00009	-0.00303	0.70985 ± 0.00009	-0.00114
0.80	0.70968 ± 0.00009	0.70598 ± 0.00009	-0.0037	0.70696 ± 0.00009	-0.00272	0.70849 ± 0.00009	-0.00119
0.90	0.71402 ± 0.00009	0.71019 ± 0.00009	-0.00383	0.71141 ± 0.00009	-0.00261	0.71290 ± 0.00009	-0.00112
0.943	0.71685 ± 0.00009	0.71309 ± 0.00009	-0.00376	0.71440 ± 0.00009	-0.00245	0.71578 ± 0.00009	-0.00107

Table 2: Comparison of the multiplication factors obtained with different versions of SCALE, no boron in the water

	SCALE 4.4a 44-group ENDF/B-V	SCALE 5.1 44-group ENDF/B-V		SCALE 6.1 44-group ENDF/B-V		SCALE 6.1 238-group ENDF/B-VII.0	
Density [g/cm3]	k_{eff}	k_{eff}	Difference	k_{eff}	Difference	k_{eff}	Difference
0.10	1.10277 ± 0.00008	1.10496 ± 0.00008	0.00219	1.09802 ± 0.00008	-0.00475	1.09135 ± 0.00008	-0.01142
0.15	1.13646 ± 0.00008	1.13822 ± 0.00008	0.00176	1.13336 ± 0.00008	-0.00310	1.13050 ± 0.00008	-0.00596
0.20	1.13904 ± 0.00009	1.14063 ± 0.00008	0.00159	1.13703 ± 0.00008	-0.00201	1.13709 ± 0.00009	-0.00195
0.25	1.12696 ± 0.00008	1.12797 ± 0.00009	0.00101	1.12546 ± 0.00008	-0.00150	1.12748 ± 0.00008	0.00052
0.30	1.10790 ± 0.00009	1.10850 ± 0.00008	0.00060	1.10658 ± 0.00008	-0.00132	1.10993 ± 0.00008	0.00203
0.40	1.06380 ± 0.00009	1.06360 ± 0.00009	-0.00020	1.06244 ± 0.00008	-0.00136	1.06809 ± 0.00009	0.00429
0.50	1.02413 ± 0.00009	1.02300 ± 0.00008	-0.00113	1.02262 ± 0.00009	-0.00151	1.02911 ± 0.00009	0.00498
0.60	0.99419 ± 0.00009	0.99230 ± 0.00009	-0.00189	0.99245 ± 0.00009	-0.00174	0.99944 ± 0.00009	0.00525
0.70	0.97498 ± 0.00010	0.97251 ± 0.00009	-0.00247	0.97293 ± 0.00010	-0.00205	0.98000 ± 0.00010	0.00502
0.80	0.96586 ± 0.00010	0.96300 ± 0.00010	-0.00286	0.96379 ± 0.00009	-0.00207	0.97080 ± 0.00010	0.00494
0.90	0.96494 ± 0.00010	0.96182 ± 0.00010	-0.00312	0.96280 ± 0.00010	-0.00214	0.96968 ± 0.00010	0.00474
0.943	0.96664 ± 0.00011	0.96326 ± 0.00010	-0.00338	0.96456 ± 0.00010	-0.00208	0.97106 ± 0.00010	0.00442

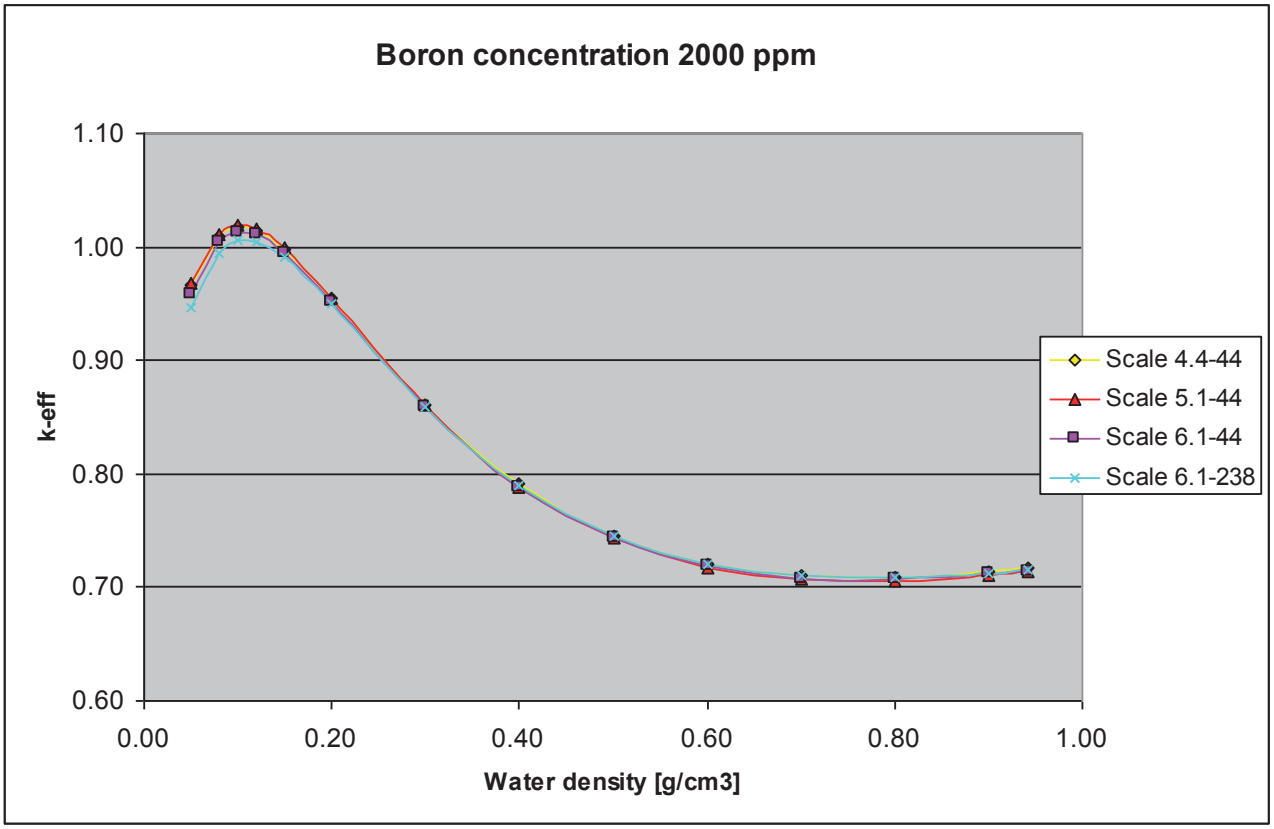

Figure 2: Comparison of the multiplication factors obtained with different versions of SCALE, 2000 ppm of boron

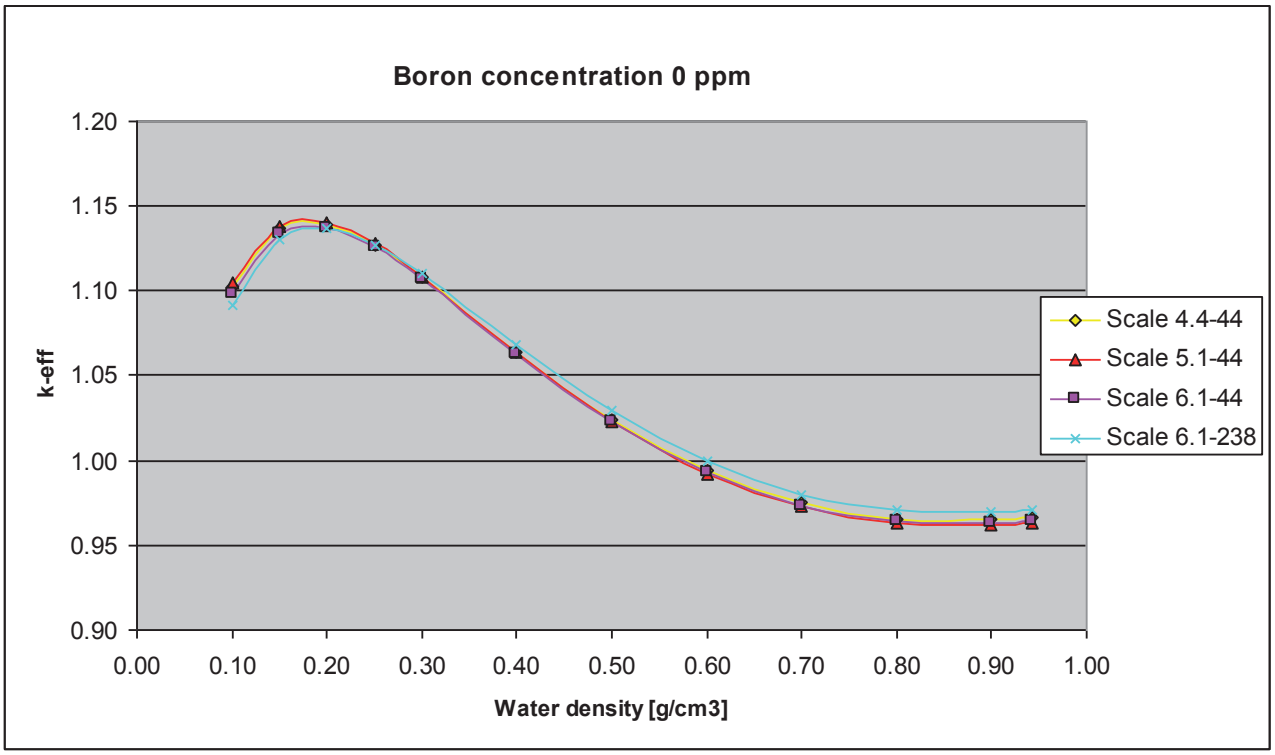

Figure 3: Comparison of the multiplication factors obtained with different versions of SCALE, no boron in the water

3.2 Comparison with the SERPENT and MCNP5

For additional verification calculations with the SERPENT and MCNP5 codes have been performed. Both codes are capable to take into account neutron continuous energy cross section library. Therefore, there is no need to perform additional spectral adjustments as in the multigroup case. Comparison is presented in Tables 3-4 and Figures 4-5. Discrepancies to the basic case are little larger than in previous SCALE comparison. However, both codes give significantly lower results again proving the conservative nature of the design calculations. SERPENT multiplication factors are slightly lower than MCNP5 results. That could be contributed to the internal temperature Doppler correction and lack of the temperature correction in the water energy dependent scattering kernel. Temperature corrections in the MCNP5 case have been done rigorously with the MAKXSF code.

4 CONCLUSION

Criticality safety reanalyzes of the NPP Krško spent fuel pool has been performed. Calculations of the pool racks with different water densities have been executed using the different SCALE code versions (SCALE-4.4a, SCALE-5.1 and SCALE-6.1) with the 44-group ENDF/B-V and the 238-group ENDF/B-VII.0 derived cross section libraries. Relative small discrepancies are observed. Multiplication factors are mainly under the basic setup consisting of SCALE-4.4a code with the 44-group ENDF/B-V library, which can be considered as a design setup. SCALE-6.1 with 238-group ENDF/B-VII.0 library gives lower values at low density range. Additional verification is provided with SERPENT and MCNP5 codes, which are capable to take into account neutron continuous energy cross section library. Cross sections based on the ENDF/B-VII.0 files have been used in both codes. Comparison has shown that the results of the pool design calculations are conservative, precluding racks criticality even at optimum moderation conditions.

Table 3: Comparison of the multiplication factors obtained with the SERPENT and MCNP5, 2000 ppm of boron

	SCALE 4.4a 44-group ENDF/B-V	SERPENT Continuous ENDF/B-VII.0		MCNP5 Continuous ENDF/B-VII.0	
Density [g/cm3]	k_{eff}	k_{eff}	Difference	k_{eff}	Difference
0.05	0.96581 ± 0.00007	0.91708 ± 0.00010	-0.04873	0.91825 ± 0.00008	-0.04756
0.08	1.00995 ± 0.00008	0.96456 ± 0.00010	-0.04539	0.96748 ± 0.00009	-0.04247
0.10	1.01778 ± 0.00008	0.97429 ± 0.00010	-0.04349	0.97824 ± 0.00009	-0.03954
0.12	1.01491 ± 0.00007	0.97348 ± 0.00010	-0.04143	0.97831 ± 0.00009	-0.03660
0.15	0.99819 ± 0.00008	0.95917 ± 0.00011	-0.03902	0.96495 ± 0.00009	-0.03324
0.20	0.95477 ± 0.00008	0.91920 ± 0.00011	-0.03557	0.92693 ± 0.00010	-0.02784
0.30	0.86147 ± 0.00009	0.83290 ± 0.00013	-0.02857	0.84195 ± 0.00010	-0.01952
0.40	0.79065 ± 0.00009	0.76850 ± 0.00015	-0.02215	0.77672 ± 0.00010	-0.01393
0.50	0.74596 ± 0.00009	0.72878 ± 0.00017	-0.01718	0.73611 ± 0.00010	-0.00985
0.60	0.72116 ± 0.00009	0.70843 ± 0.00017	-0.01273	0.71480 ± 0.00010	-0.00636
0.70	0.71099 ± 0.00009	0.70158 ± 0.00018	-0.00941	0.70667 ± 0.00011	-0.00432
0.80	0.70968 ± 0.00009	0.70311 ± 0.00018	-0.00657	0.70740 ± 0.00011	-0.00228
0.90	0.71402 ± 0.00009	0.70938 ± 0.00017	-0.00464	0.71273 ± 0.00011	-0.00129
0.943	0.71685 ± 0.00009	0.71283 ± 0.00017	-0.00402	0.71635 ± 0.00011	-0.00050

Table 4: Comparison of the multiplication factors obtained with the SERPENT and MCNP5, no boron in the water

	SCALE 4.4a 44-group ENDF/B-V	SERPENT Continuous ENDF/B-VII.0		MCNP5 Continuous ENDF/B-VII.0	
Density [g/cm3]	k_{eff}	k_{eff}	Difference	k_{eff}	Difference
0.10	1.10277 ± 0.00008	1.05388 ± 0.00010	-0.04889	1.05762 ± 0.00008	-0.04515
0.15	1.13646 ± 0.00008	1.08912 ± 0.00009	-0.04734	1.09500 ± 0.00009	-0.04146
0.20	1.13904 ± 0.00009	1.09305 ± 0.00009	-0.04599	1.10077 ± 0.00009	-0.03827
0.25	1.12696 ± 0.00008	1.08183 ± 0.00010	-0.04513	1.09162 ± 0.00009	-0.03534
0.30	1.10790 ± 0.00009	1.06384 ± 0.00010	-0.04406	1.07521 ± 0.00009	-0.03269
0.40	1.06380 ± 0.00009	1.02352 ± 0.00011	-0.04028	1.03639 ± 0.00009	-0.02741
0.50	1.02413 ± 0.00009	0.98831 ± 0.00012	-0.03582	1.00201 ± 0.00010	-0.02212
0.60	0.99419 ± 0.00009	0.96316 ± 0.00012	-0.03103	0.97695 ± 0.00010	-0.01724
0.70	0.97498 ± 0.00010	0.94892 ± 0.00013	-0.02606	0.96169 ± 0.00010	-0.01329
0.80	0.96586 ± 0.00010	0.94459 ± 0.00013	-0.02127	0.95579 ± 0.00011	-0.01007
0.90	0.96494 ± 0.00010	0.94743 ± 0.00014	-0.01751	0.95810 ± 0.00011	-0.00684
0.943	0.96664 ± 0.00011	0.95080 ± 0.00014	-0.01584	0.96054 ± 0.00011	-0.00610

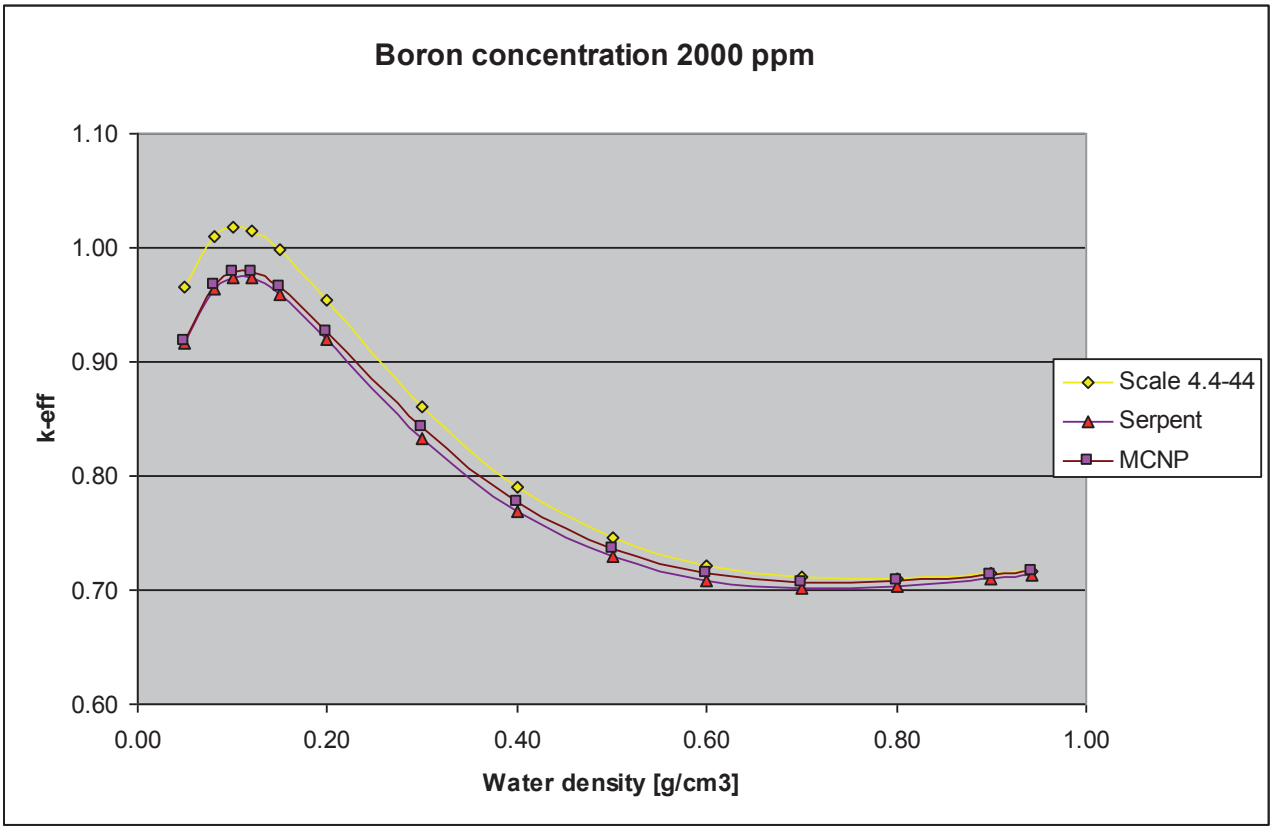

Figure 4: Comparison of the multiplication factors obtained with the SERPENT and MCNP5, 2000 ppm of boron

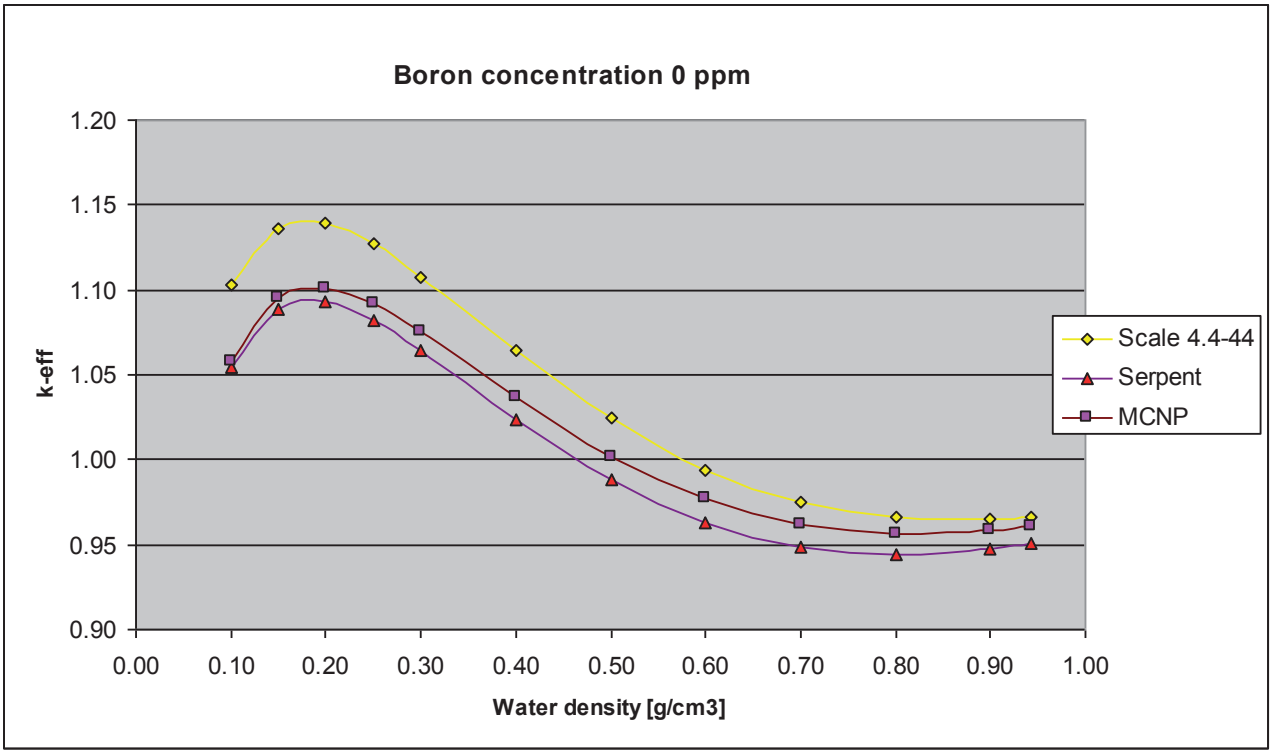

Figure 5: Comparison of the multiplication factors obtained with the SERPENT and MCNP5, no boron in the water

M. Kromar, B. Kurinčič, Comparison of the SCALE, SERPENT and MCNP Criticality Safety Calculation of the NPP Krško Spent Fuel Pool, Journal of Energy, vol. 62 Number 1–4 (2013) Special Issue, p. 200–208

REFERENCES

[1] J. C. Neuber, W. Tippl, "Criticality Safety Analysis of Old Spent Fuel Storage Racks", Framatome ANP GmbH, Work Report NGPM5/2003/en/0179, Rev. A, Offenbach, August 18, 2003.

[2] J. C. Neuber, M. Schmidt, "Determination of the Old Storage Racks Loading Curve Based on the Accident Condition - Boiling with Optimum Moderation", Areva NP GmbH, Work Report NEEA-G/2006/en/0152, Rev. A, Offenbach, August 01, 2006.

[3] S. M. Bowman, B. L. Broadhead, C. B. Bryan, J. A. Bucholz, K. W. Childs, A. L. Edwards, M. B. Emmett, P. B. Fox, S. K. Fraley, G. E. Gilels, N. M. Greene, O. W. Hermann, T. J. Hoffman, D. F. Hollenbach, W. C. Jordan, J. R. Knight, N. F. Landers, L. C. Leal, K. Lucius, C. V. Parks, L. M. Petrie, J. C. Ryman, J. S. Tang, J. C. Turner, J. T. West, R. M. Westfall, and P. T. Williams, "SCALE: A Modular Code System for Performing Standardized Computer Analyses for Licensing Evaluation", NUREG/CR-0200, Rev. 6 (ORNL/NUREG/CSD-2R6), Vols. I, II, III, May 2000. Available from Radiation Safety Information Computational Center at Oak Ridge National Laboratory.

[4] J. Leppänen, "PSG2 / Serpent – a Continuous-energy Monte Carlo Reactor Physics Burnup Calculation Code", VTT Technical Research Centre of Finland, November 6, 2009.

[5] NEA Data Bank, "ZZ SERPENT117-ACELIB, Continuous-energy X-sec lib., radioactive decay, fission yield data for SERPENT in ACE", NEA-1854/01, http://www.oecd-nea.org/tools/abstract/detail/NEA-1854/.

[6] X-5 Monte Carlo Team, "MCNP – A General Monte Carlo N-Particle Transport Code", Version 5, Los Alamos National Laboratory, 2003, USA.

[7] Nuclear power plant Krško, "Technical Specifications".

Journal of Energy

VOLUME 62 Number 1–4 | 2013 Special Issue

journal homepage: http://journalofenergy.com/

Impact of Limited Reprocessing Capacity on Nuclear Material Utilization in Advanced Fuel Cycles

Abiodun Adeniyi, Bojan Petrovic
Nuclear and Radiological Engineering, Georgia Institute of Technology
770 State St., Atlanta, GA 30332-0745, USA
aadeniyi3@gatech.edu, bojan.petrovic@gatech.edu

Bo Feng, Taek K. Kim
Argonne National Laboratory
9700 S Cass Ave., Argonne, IL 60439 USA
bofeng@anl.gov, tkkim@anl.gov

ABSTRACT

A nuclear energy scenario study was performed using VISION 3.4; to analyze three different fuel cycles: once through (open) cycle (OTC), full recycle with a transition through a modified open cycle (MOC), and direct introduction of full recycle without transition (FuRe) in terms of their impact on uranium resource utilization on both the front- and back-end of these fuel cycles, Both the MOC and FuRe show significant improvement (reduction) in the amount of uranium ore required to generate the same amount of energy for a 150-year period when compared to the OTC. The same conclusion also holds for the amount of used nuclear fuel (UNF) in storage (wet, dry and monitored retrievable (MRS)) in the back-end of the fuel cycle.

Findings suggest that under the analyzed deployment scenarios, amount of separation capacity deployed have impact on resource utilization. There is no clear advantage of either MOC or FuRe over one another in the front end of the fuel cycle as far as material utilization under both separation capacities analyzed. However, due to its potential for earlier deployment, MOC offers better UNF management in the back end at 2 kT/yr separation capacity: the amount of UNF for storage is smaller compared to OTC and FuRe, this advantage is not evident when the capacity was doubled. In terms of transuranic (TRU) consumption, FuRe is the better choice compared to MOC, under the lower separation capacity scenario, however at doubled capacity, both cycles consumed about the same amount of TRU. It can be concluded that the choice of either MOC or FuRe depends on the fuel cycle objectives, however both are better compared to OTC, in terms of uranium resources utilization.

1 INTRODUCTION

Current US nuclear policy of the once-through cycle implies that UNF (estimated at 42,616 metric tons in 2000 [1] and growing at an annual rate of ~2,000 metric tons) will continue to sit in above-surface storage sites across the country, and the UNF will not be recycled for further use. However, there are on-going efforts to explore the possibility of deploying advanced nuclear fuel cycles in the US that may further increase the utilization of uranium resources. Most of these efforts suggest that a full recycling policy will be the most adequate, but full-scale commercial deployment of this technology may not occur until much later.

Modified Open Fuel (MOC) cycle is a stop gap measure being proposed by the DOE. According to the DOE 2010 *Nuclear Energy Research Development Roadmap* [1], the MOC should achieve the following in terms of nuclear material utilization:

- *Improve uranium resource availability*
- *Improve uranium utilization*
- *Minimize waste generation, and*
- *Provide adequate capability and capacity to manage all waste produced.*

To investigate these requirements, nuclear energy scenario studies were defined and analyzed using VISION (VerifIable Fuel Cycle SimulatiON, version 3.4), which was benchmarked using data in [2, 3, 4], a dynamic nuclear fuel cycle analysis code developed for the Advanced Fuel Cycle Initiative (AFCI) studies through a collaboration between national laboratories and universities [5, 6]. The energy scenarios were setup using the information and parameters shown in Table 1.

Table 1: Nuclear Energy Scenario Parameters

Parameters		Unit	Values
General			
	Introduction of first full-recycling reactor (i.e., fast reactor)	Year	2050
	Electricity demand growth rate	% per year	1.0
	U.S. nuclear electricity capacity in 2010	GWe	100
	U.S. used nuclear fuel (UNF) inventory in 2010	ton HM	61482
	U.S. TRU inventory in 2010	ton	600
LWR – LWRMOX			
	Fuel form		UO_2, UO_2-MOX
	Electrical Power	MWe	1000
	Thermal Efficiency	%	34
	Average discharge burnup	GWd/t	50
	Average LEU enrichment	%	4.2
	Reactor capacity factor	%	90
	Life time	Years	60
	Cooling time in interim wet storage	Years	5
SFR – Full-recycling reactor			
	Fuel form		U-TRU-Zr alloy
	Electrical Power	MWe	380
	Thermal Efficiency	%	38
	Average discharge burnup	GWd/t	70 – 100
	Breeding ratio		1.0-1.2 (1.0 used in this study)
	Reactor capacity factor	%	90
	Life time	Years	60
	Cooling time in interim storage	Years	1
Reprocessing			
	Reprocessing start (depends on reactor)		Varied
	TRU recovery factor in reprocessing	%	99.9
	Reprocessing capacity	ton HM / year	Varied
	Total reprocessing time (including fabrication, transportation)	Years	2

All current thermal reactors in the US are modeled as LWRs without distinction between BWR and PWR, and every LWR reactor built after 2010 is assumed to be capable of operating with a full core of mixed oxide (MOX) fuel. The fast reactors deployed in the study were modeled as sodium cooled fast reactors (SFR) with a break even breeding ratio.

2 FUEL CYCLE SCENARIO SETUP

Three nuclear fuel cycles were considered for this study:

- Once Through Cycle (OTC also known as open cycle; current US option),
- Full Recycling (FuRe) fuel cycle, introduced without a transition
- Full recycle introduced via a transitional Modified Open Cycle (MOC), where MOX-capable LWRs are deployed first. This option will be denoted as MOC, although it ultimately transitions to FuRe.

In terms of nuclear material utilization, the OTC is the least efficient; close to 95% of usable nuclear material remains in the UNF designated for storage and disposal. FuRe is the best cycle in terms of material utilization; almost all of the extractable energy can be extracted from the fuel, however the commercial infrastructure for large-scale FuRe deployment is not yet in place.

2.1 Once Through (Open) Cycle Scenario

For the OTC scenario, it was assumed that the LWR capacity increased to meet the 1% growth in nuclear energy demand. As shown in Fig. 2.1, there is no separation or reprocessing of UNF. Instead, the discharged fuel (DF) is sent to interim storage (wet, then dry) and later to a permanent disposal repository.

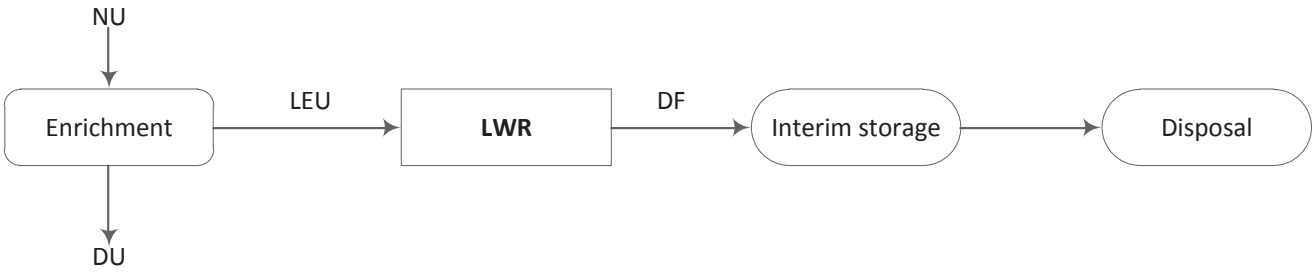

Figure 2.1: Once Through (Open) Cycle Scenario Setup

2.2 Full Recycling Cycle

In the FuRe scenario (Fig. 2.2), it was assumed that the LWR capacity increases until 2050 to fulfill the growing energy demand, after which only fast reactors are constructed. Consequently, all LWRs are out of service by 2110. Reprocessing of UNF inventory (legacy used fuel) and DF starts in 2048 using UREX+1 separation technology, while an electrochemical process is used for the separation of discharged SFR fuel. The recovered TRU from the UNF inventory is used for the startup SFR cores. The SFR breeding ratio (BR) is assumed to be break-even (BR = 1.0). This implies that there is no TRU limit to building new SFRs until the UNF inventory is completely exhausted. Except for the startup cycle, additional external TRU feed is not required due to the break-even breeding ratio. If TRU is not available for the new SFRs (due to exhausting of legacy UNF inventory), low-enriched uranium (LEU) was used as the contingent (or back-up) fuel for the SFRs. Otherwise, no SFRs will be built if there is insufficient TRU-based fuel.

A. Adeniyi, B. Petrovic, B. Feng, T. K. Kim, Impact of Limited Reprocessing Capacity on Nuclear Material Utilization in Advanced Fuel Cycles, Journal of Energy, vol. 62 Number 1–4 (2013) Special Issue, p. 209–220

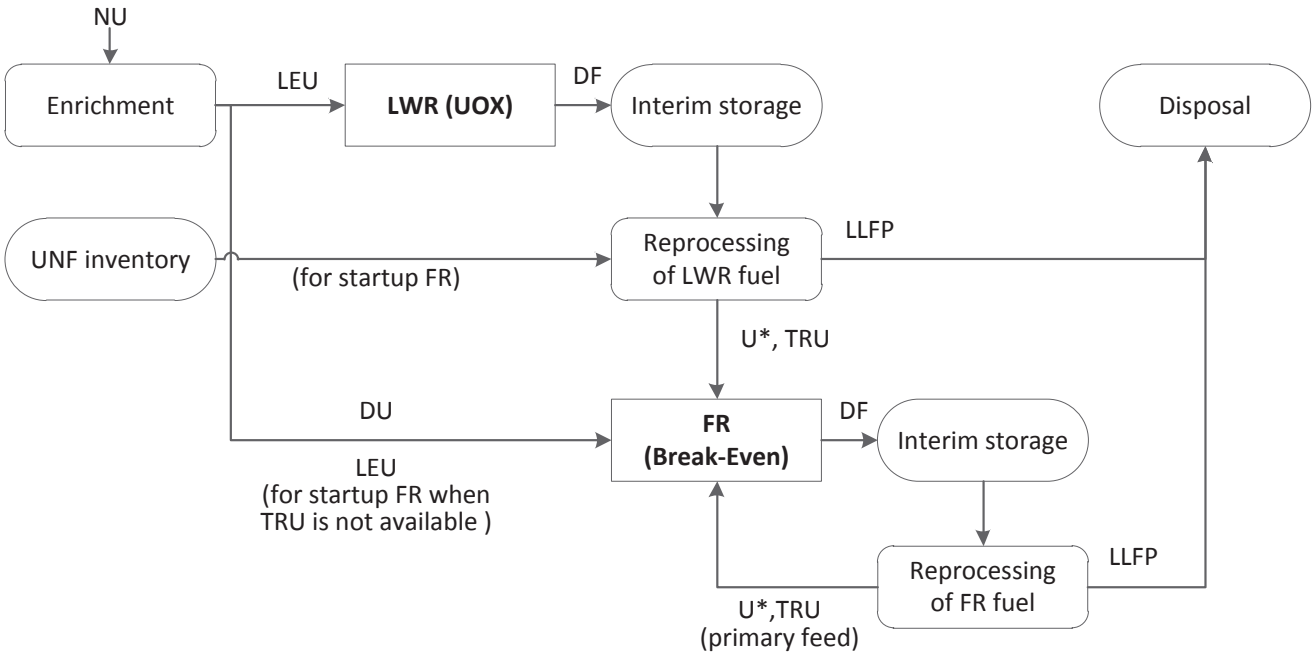

Figure 2.2: Full Recycling Cycle Scenario Setup

2.3 Modified Open Cycle (MOC: LWR-UOX / LWR-MOX / SFR) Scenario

In the MOC scenario (Fig. 2.3), a small amount of LWR-MOX reactors is introduced after 2025 along with the conventional LWR-UOX reactors, to meet the increasing energy demand.

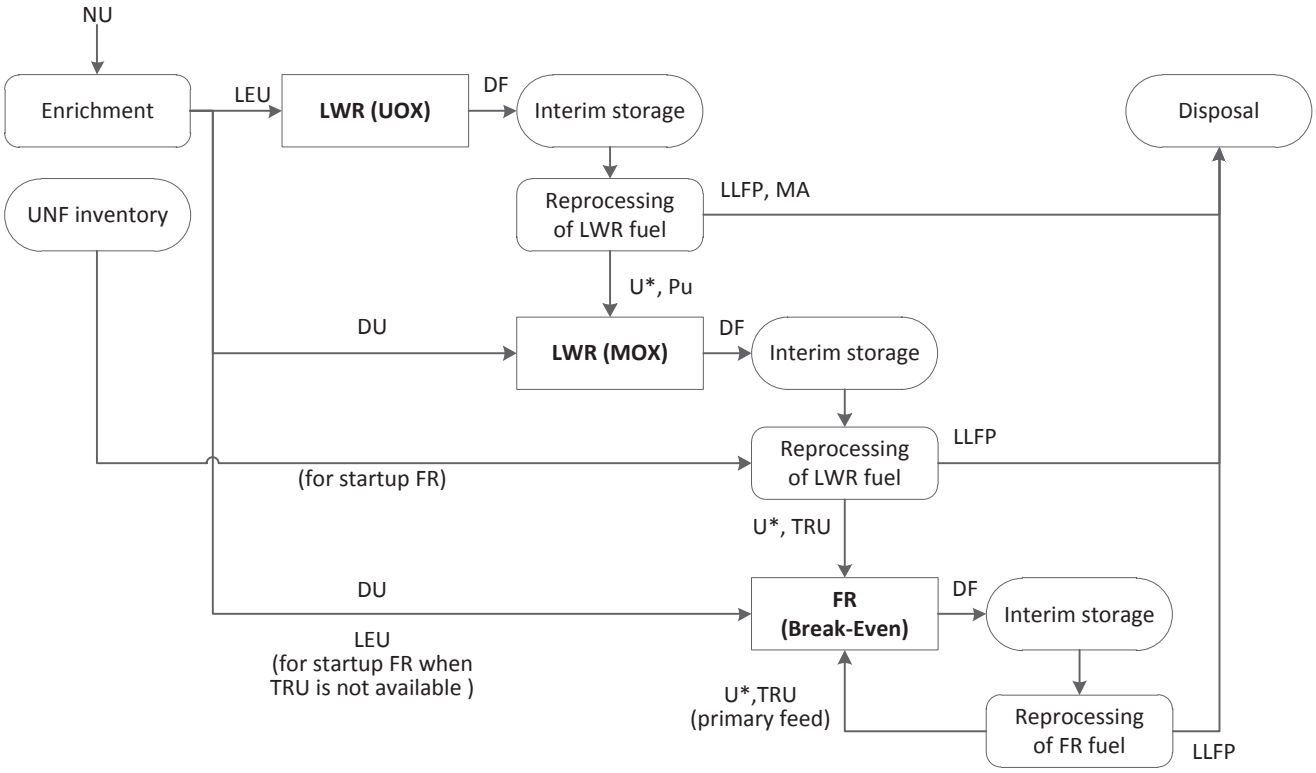

Figure 2.3: Modified Open Cycle Scenario Setup

A. Adeniyi, B. Petrovic, B. Feng, T. K. Kim, Impact of Limited Reprocessing Capacity on Nuclear Material Utilization in Advanced Fuel Cycles, Journal of Energy, vol. 62 Number 1–4 (2013) Special Issue, p. 209–220

Reprocessing of UNF inventory (legacy used fuel) and DF starts in 2020 by recycling U + Pu from discharged LWR-UOX fuel as well as from the legacy used fuel. Reprocessing of DF from LWR-MOX starts after the mandatory cooling time in temporary storage. After 2050, no new LWRs are constructed, only SFRs. Thus, all LWRs are completely replaced by full-recycling reactors after 2110. The recovered TRU/U from discharged LWR-MOX fuel is used as a makeup TRU feed for SFRs, if there is insufficient TRU/U from discharged LWR-UOX fuel. If there is insufficient TRU from any source, LEU is used to support FR deployment.

2.4 Other Scenario Parameters

All nuclear reactor types have a lifetime of 60 years with no assumed extensions. The separation capacity for LWR fuel is assumed to be 2000 metric ton per annum, the separation capacity for fast reactor DF is assumed to be unlimited, and all separation facilities have a lifetime of 40 years. LWR DFs (UOX and MOX) are recycled only once, while SFR DF is continuously-recycled.

3 RESULTS

As expected, both the FuRe and MOC scenarios showed better fuel utilization than the OTC scenario. The total amount of uranium ore consumed, shown in Figure 3.1, was reduced by about 45% (FuRe) and about 50% (MOC) at the end of the 150 years of simulation. The amount of energy generated is shown in Figure 3.2. The energy generated in the OTC and the advanced fuel cycles scenarios follows the energy demand. The assumptions for the analysis include a requirement that use of MOX fuel in LWR is limited to no more than 30%. The use of MOX fuel is limited by the LWR-UOX separation capacity, fixed at 2000 ton/yr; in reality this should increase as the number of LWRs increases. Although one may expect SFRs to counter this energy shortage starting from year 2050, this did not immediately happen because of the dependence of SFRs on reprocessed MOX fuel from LWR. It is important to note that there is no significant saving in required uranium ore until the deployment of SFRs in 2050, in both the FuRe and MOC. In the VISION model, both MOC and FuRe will operate on LEU (figures 2.2 and 2.3) if their primary fuels are not available (to run the reactor for their entire life cycle). Total separative work (in SWU units) required for uranium enrichment follows the same trends shown in Figure 3.1.

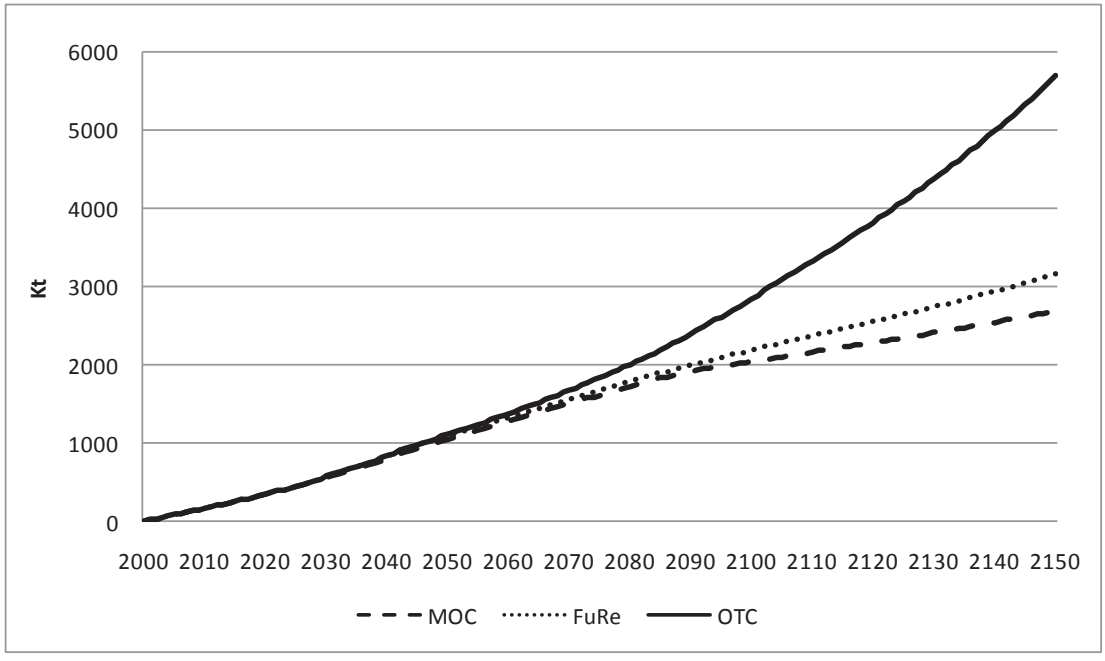

Figure 3.1a: Cumulative Uranium Ore Consumed in all Fuel Cycles @ 2 kT/yr Separation Capacity.

A. Adeniyi, B. Petrovic, B. Feng, T. K. Kim, Impact of Limited Reprocessing Capacity on Nuclear Material Utilization in Advanced Fuel Cycles, Journal of Energy, vol. 62 Number 1–4 (2013) Special Issue, p. 209–220

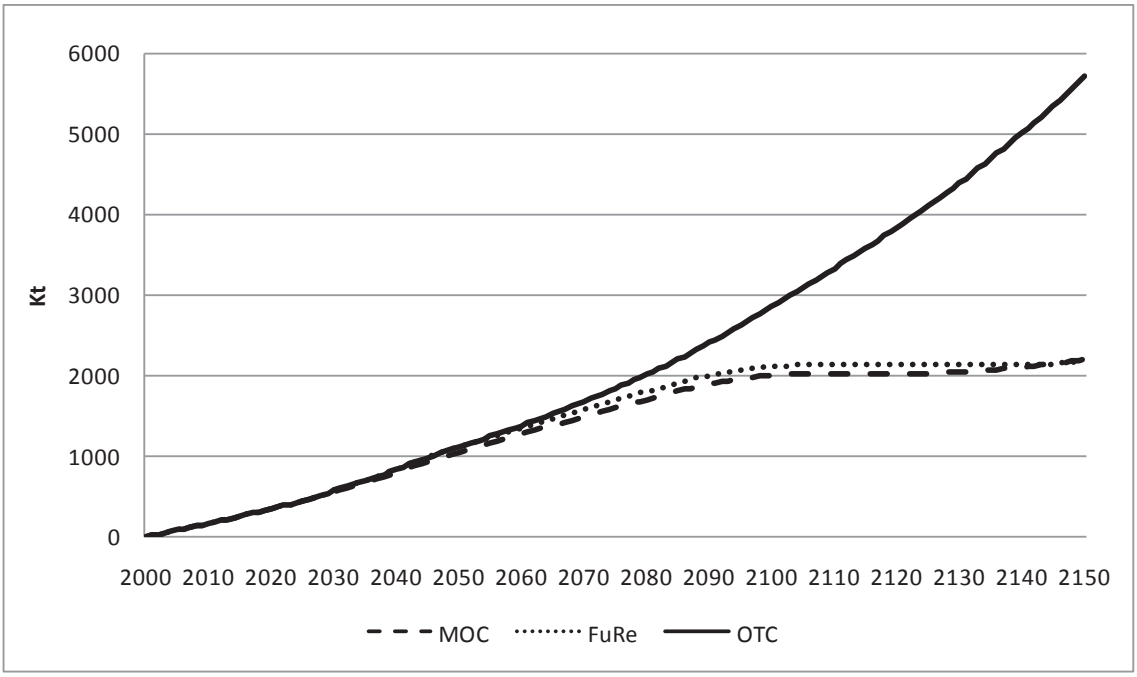

Figure 3.1b: Cumulative Uranium Ore Consumed in all Fuel Cycles @ 4 kT/yr Separation Capacity.

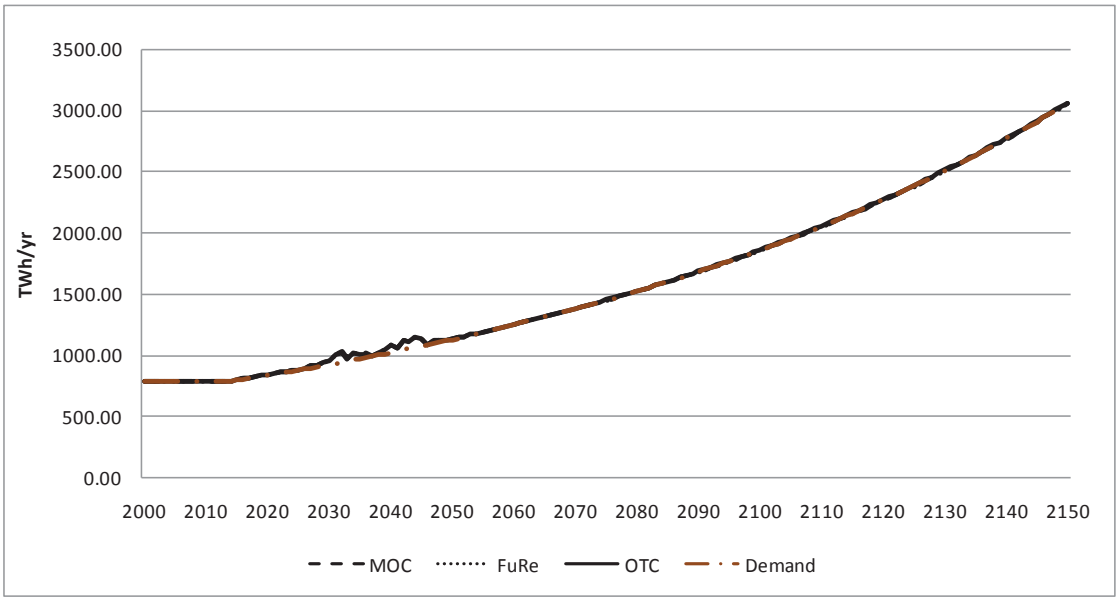

Figure 3.2a: Annual Energy Generated vs. Projected Demand @ 2kT/yr Separation Capacity.

The total reactor capacity (installed power) as a function of reactor type is shown in Figs. 3.3, 3.4 and 3.5 for the three scenarios considered. Most of the LWRs are out of service by the predicted year, 2110. Since the energy generated still meets the yearly predicted energy demand, it means LWRs can be phased out of MOC and FuRe scenarios. This may however be difficult to do in practice, when other factors and requirements are factored in. In Fig. 3.3 and 3.4, the LWR-MOX capacity only indicates that the reactors are capable of using MOX fuel, but no MOX fuel was actually used in either the OTC or FuRe scenarios. The impact of doubling the separation capacity is not noticeable in terms of installed reactor capacity as opposed to the impact shown on Uranium consumption (Fig. 3.1a and Fig. 3.1b) and in total amount of UNF in storage (Fig. 3.6a and Fig. 3.6b). Insufficient separation capacity will result in higher consumption of fuel resources and generate more UNF and other waste. Separation capacity should increase at approximately the same

rate as UNF generation. Although one could expect that FuRe would show the best performance, the possibility to deploy MOC earlier makes it also attractive.

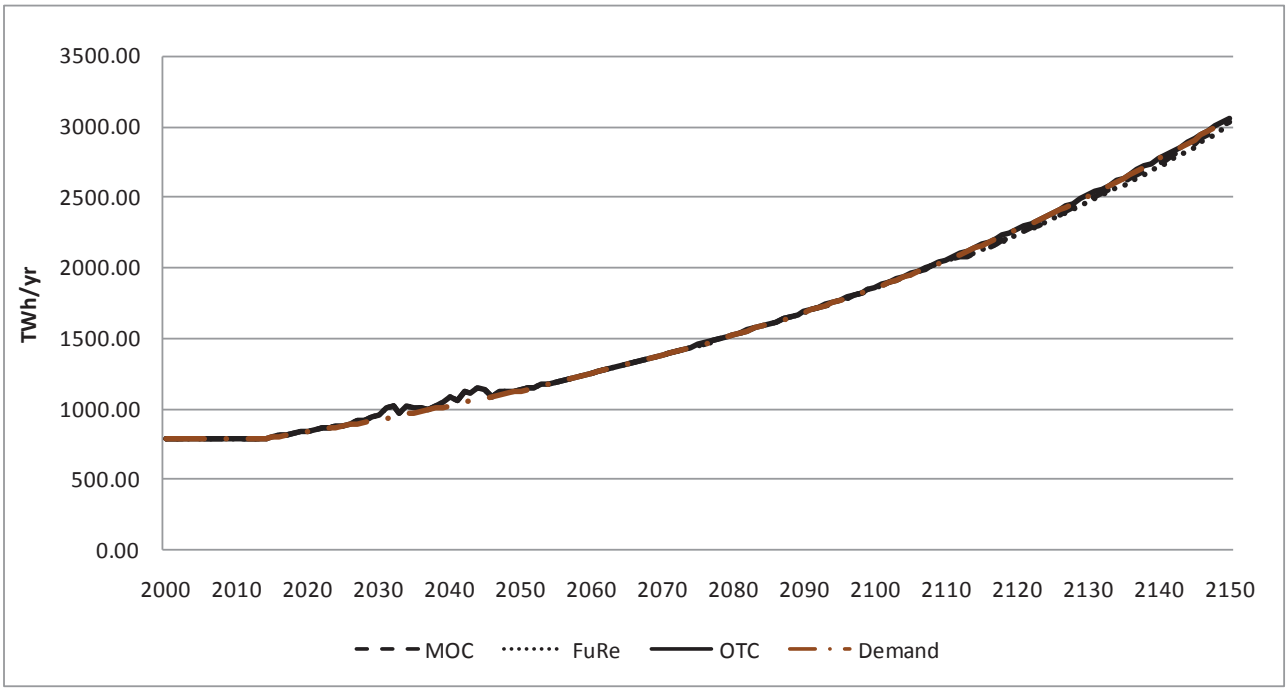

Figure 3.2b: Annual Energy Generated vs. Projected Demand @ 2kT/yr Separation Capacity.

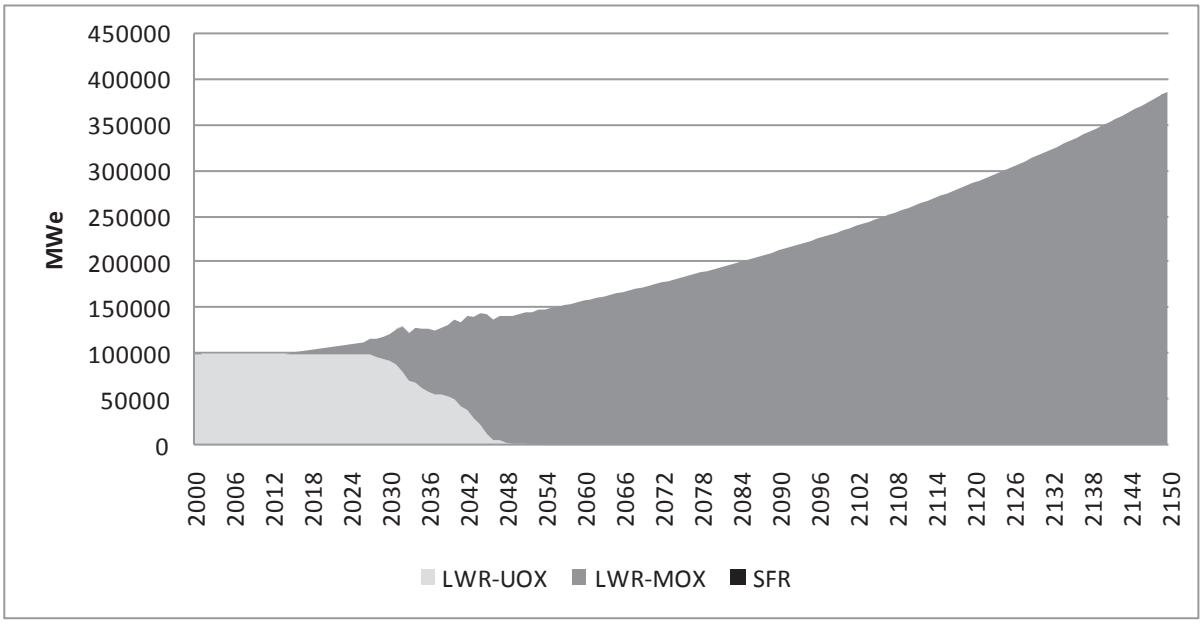

Figure 3.3: Reactor Capacity Deployed by Reactor Type in OTC

A. Adeniyi, B. Petrovic, B. Feng, T. K. Kim, Impact of Limited Reprocessing Capacity on Nuclear Material Utilization in Advanced Fuel Cycles, Journal of Energy, vol. 62 Number 1–4 (2013) Special Issue, p. 209–220

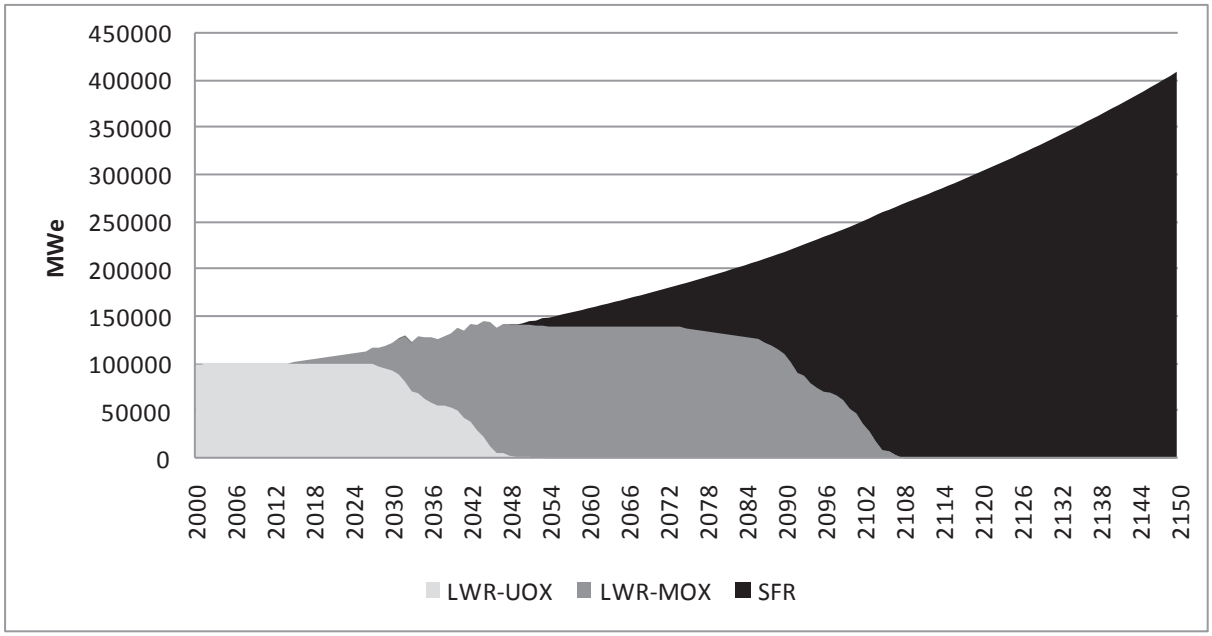

Figure 3.4a: Reactor Capacity Deployed by Reactor Type in FuRe @ 2 kT/yr Separation Capacity

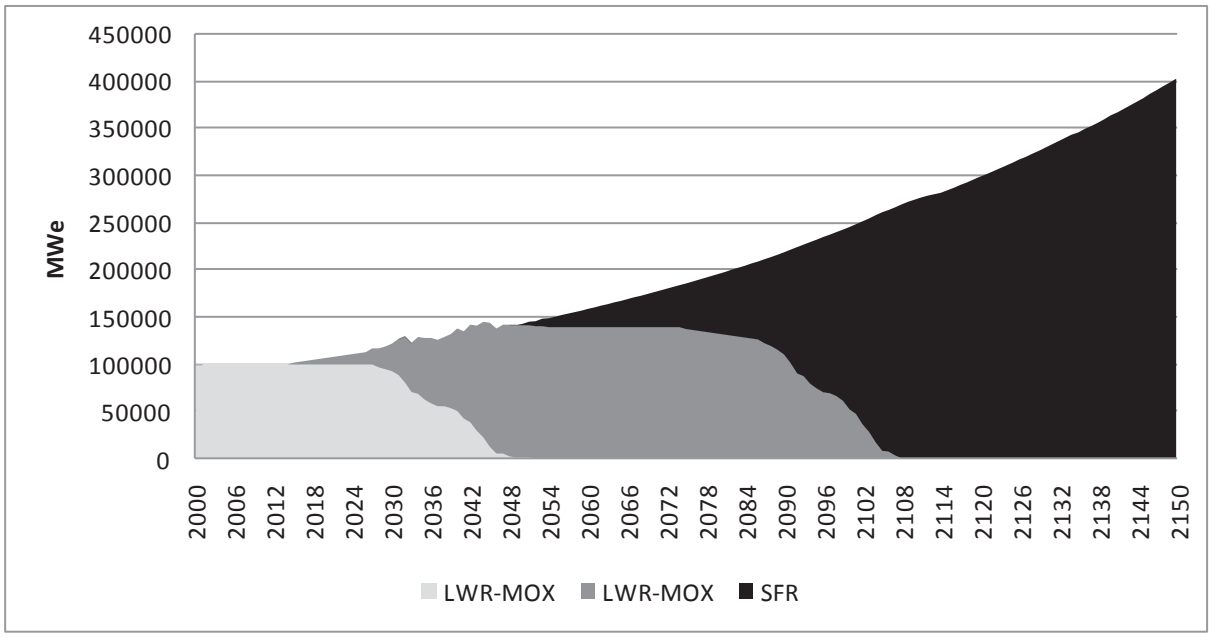

Figure 3.4b: Reactor Capacity Deployed by Reactor Type in FuRe @ 4 kT/yr Separation Capacity

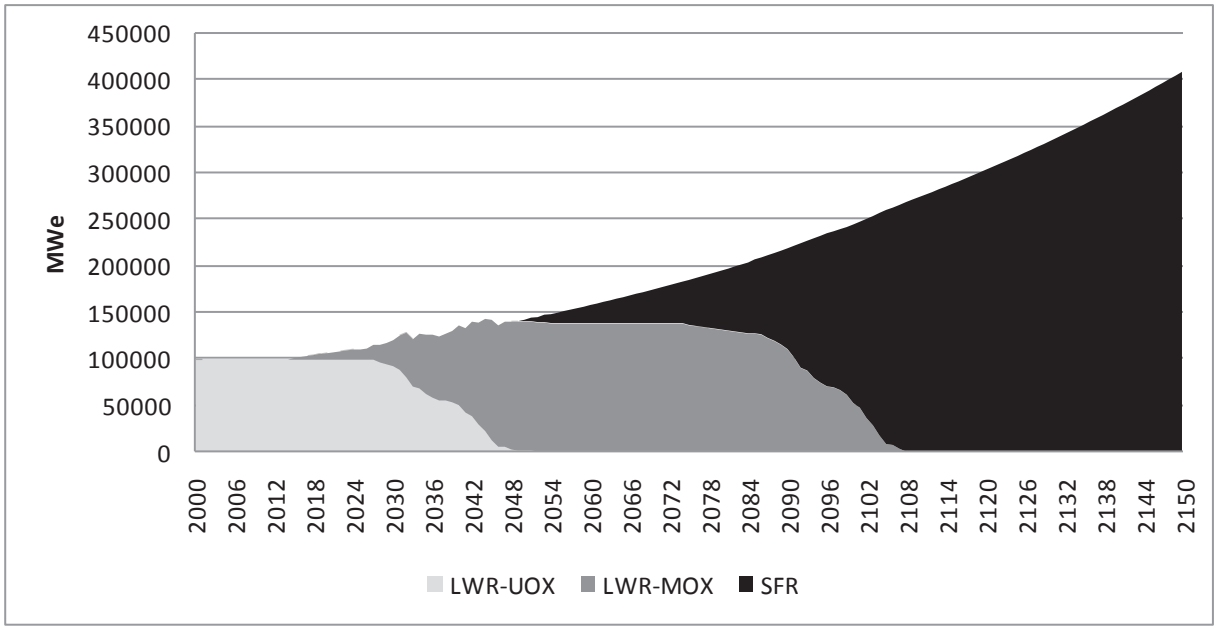

Figure 3.5a: Reactor Capacity Deployed by Reactor Type in MOC @ 2 kT/yr Separation Capacity

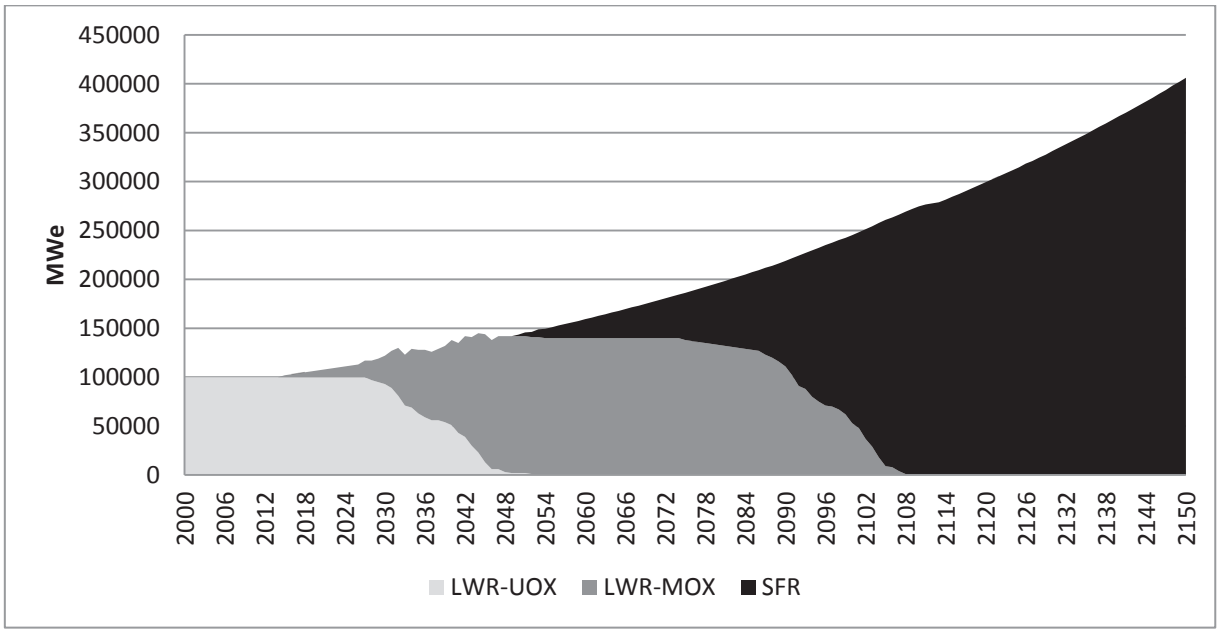

Figure 3.5b: Reactor Capacity Deployed by Reactor Type in MOC @ 4 kT/yr Separation Capacity

The results for the back end of fuel cycle did not give any clear superiority of either MOC or FuRe over one another. Figure 3.6 shows the amount of UNF in storage (wet, dry, and Monitored Retrievable Storage (MRS) in both MOC and FuRe, but defined as dry and wet in OTC): the decrease in trend after 2100 reflects phasing out of LWRs. The required energy demand is being met by break-even SFRs. There is a significant decline in the amount of UNF in storage. Note that un-used reprocessed uranium and fission products after separation are not included in this figure. Should these "separated elements" be included, the decline in total storage (used fuel and reprocessed fuel) is much more modest. The amount in storage is the same until reprocessing started in both MOC and FuRe, and the final amount in storage is about the same in both setup. Again, earlier deployment of MOC offsets the inherent theoretical advantage of FuRe.

A. Adeniyi, B. Petrovic, B. Feng, T. K. Kim, Impact of Limited Reprocessing Capacity on Nuclear Material Utilization in Advanced Fuel Cycles, Journal of Energy, vol. 62 Number 1–4 (2013) Special Issue, p. 209–220

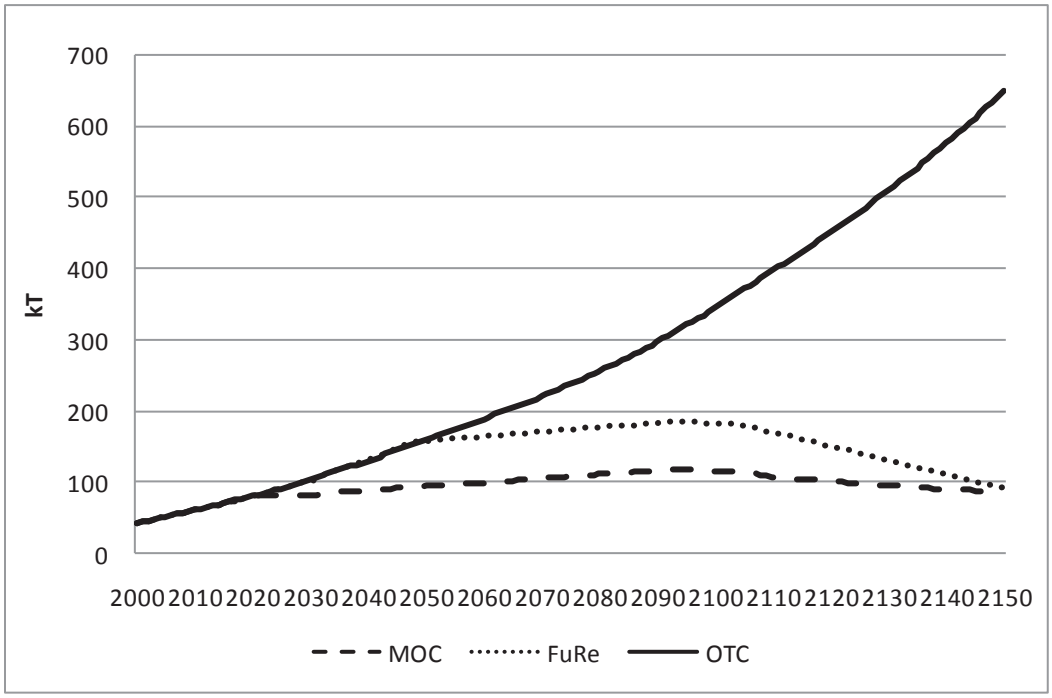

Figure 3.6a: Total Used Nuclear Fuel in Storage (Wet+ Dry + MRS) @ 2 kT/yr Separation Capacity

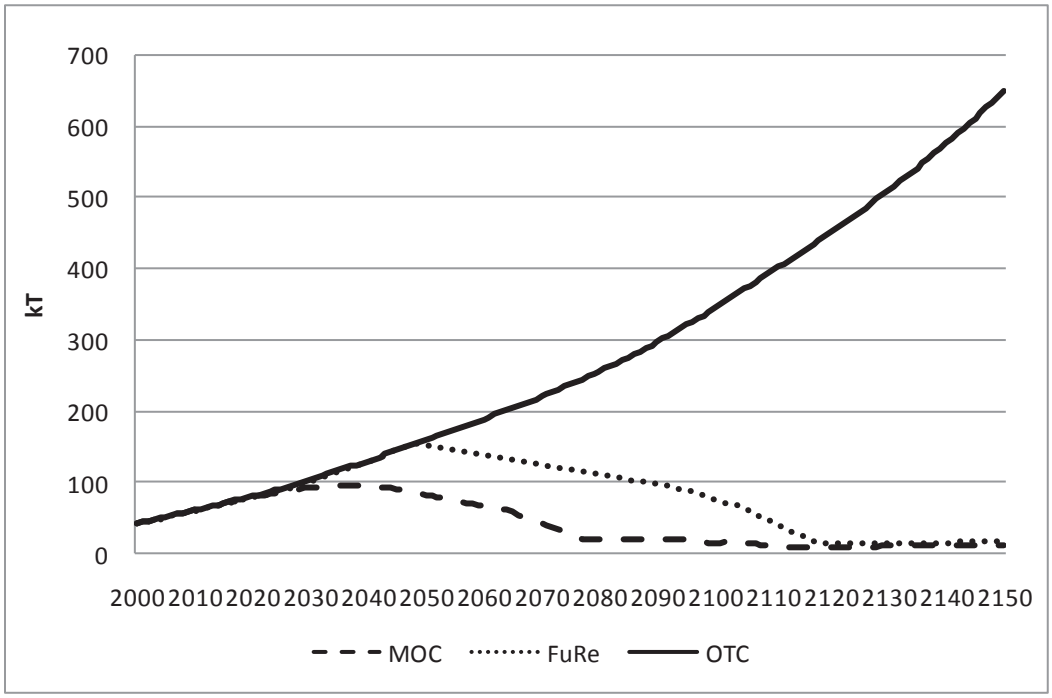

Figure 3.6b: Total Used Nuclear Fuel in Storage (Wet+ Dry + MRS) @ 4 kT/yr Separation Capacity

The total amount of TRU used in making new fuels in MOC and FuRe is shown in Figure 3.7a. The rate of TRU utilization is about the same for both of the advanced fuel cycles. However, because of the earlier deployment of reprocessing and recycling of UNF in MOC, the total TRU consumed is higher in MOC compared to FuRe at the end of the 150 years simulation. However under the 4 kT/yr separation capacity scenario (Fig. 3.7b), total TRU used was higher, and almost the same for both MOC and FuRe.

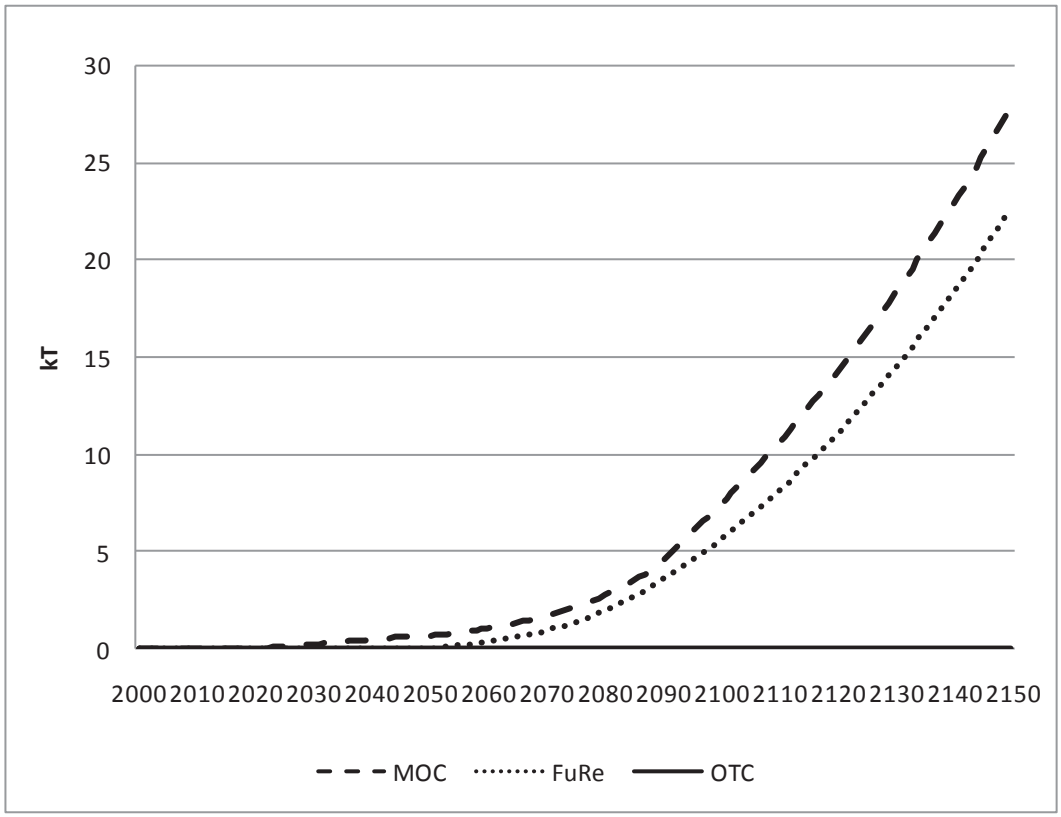

Figure 3.7a: Total Separated TRU Used for Fuel Fabrication (no TRU in OTC) @ 2 kT/yr Separation Capacity

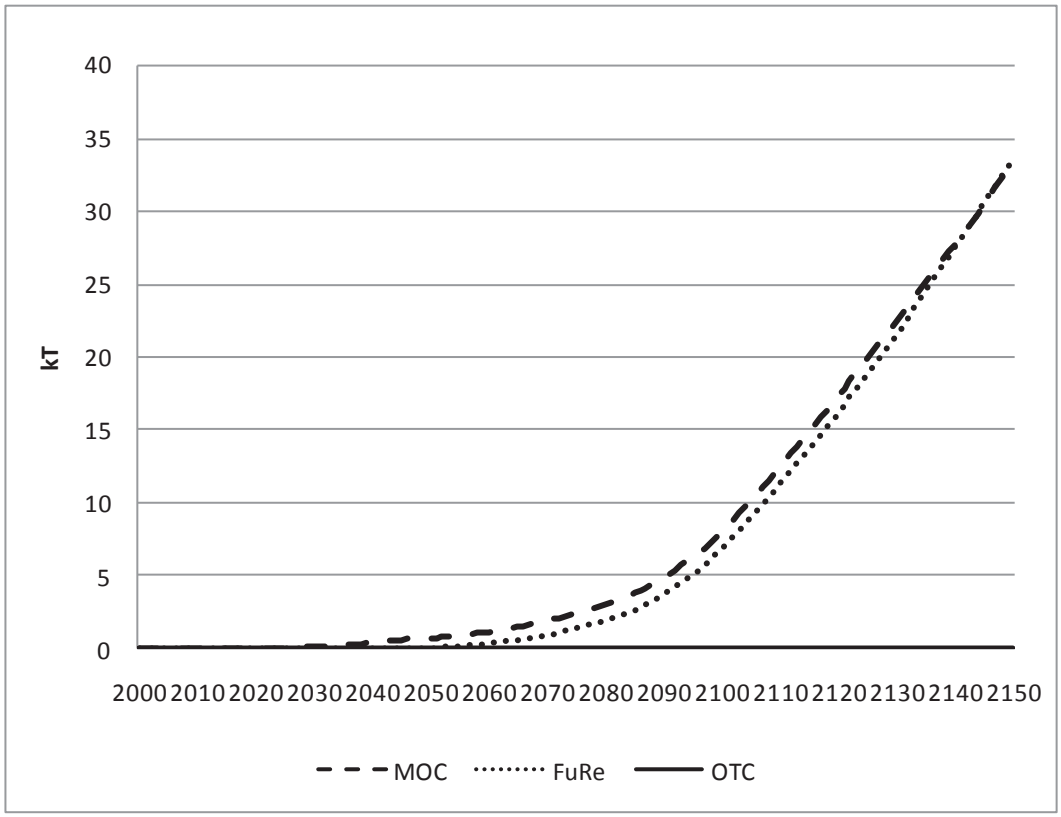

Figure 3.7b: Total Separated TRU Used for Fuel Fabrication (no TRU in OTC) @ 4 kT/yr Separation Capacity

A. Adeniyi, B. Petrovic, B. Feng, T. K. Kim, Impact of Limited Reprocessing Capacity on Nuclear Material Utilization in Advanced Fuel Cycles, Journal of Energy, vol. 62 Number 1–4 (2013) Special Issue, p. 209–220

4 CONCLUSIONS

A comparison study was performed on the OTC, MOC and FuRe scenarios with the constant external nuclear fuel cycle requirements and realistic deployment dates. From a nuclear material utilization perspective, the VISION results suggest that closing or modifying the OTC can greatly reduce the used fuel storage requirements. For a 2 kT/yr separation capacity, the MOC scenario results in a lower peak UNF storage requirement due to its earlier deployment of the recycling technology. When the separation capacity was doubled, there was about 30% improvement in the Uranium ore requirement in the FuRe scenario and about 18% in the MOC scenario (Fig. 3.1a and 3.1b). Also at this capacity, it is technically possible to eliminate all the UNF in storage (Fig.3.6a and 3.6b) because SFR dependence on LEU was eliminated (until after 2135 in MOC and 2145 in FuRe).

The amount of separation capacity deployed has a significant impact on the ability of any fuel cycle (as demonstrated above), to achieve any of the objective stated in the DOE 2010 *Nuclear Energy Research Development Roadmap*. Both the MOC and FuRe scenarios are better than OTC with respect to fuel cycle front and back end. This analysis underlines the importance of accounting for realistic, practical constraints, which may shift conclusions based on considering only inherent fuel cycle characteristics.

REFERENCES

1. DOE EIA "Nuclear Spent Fuel Data" http://www.eia.gov/cneaf/nuclear/spent_fuel/ussnftab3.html
2. DOE "*Nuclear Energy Research Development Roadmap"* Report to Congress, April 2010. http://www.ne.doe.gov/pdfFiles/NuclearEnergy_Roadmap_Final.pdf Accessed June 2010.
3. Kazimi M. S., et al., *The Future of the Nuclear Fuel Cycle.* Massachusetts Institute of Technology. 2011
4. Guerin, et al., *A Benchmark Study of Computer Codes for System Analysis of the Nuclear Fuel Cycle.* Nuclear Fuel Cycle and Technology Program. Massachusetts Institute of Technology. 2009.
5. Guerin, Laurent. *Impact of Alternative Nuclear Fuel Cycle Options on Infrastructure and Fuel Requirements, Actinide and Waste Inventories, and Economics.* Massachusetts Institute of Technology. 2007.
6. User Guide for VISION 3.4. Verifiable Fuel Cycle Simulation Model Idaho national Laboratory. INL/EXT-09-16645 Rev 3, June 2011.
7. Schweitzer T, *Improved Building Methodology and Analysis of Delay Scenarios of Advanced Nuclear Fuel Cycles with the **V**erifiable Fuel Cycle **Si**mulati**on** Model (VISION)*. Master Thesis. 2008.

Journal of Energy

ENERGIJA